An Investigation into Coking

on

Catalyst Support Materials

&

Supported Metal Catalysts

by

Michael A. O'Brien, B.Sc.(Hons.)

A Thesis presented to Dublin City University for the degree of
Doctor of Philosophy

This Work was carried out under the supervision of Dr. Odilla
Finlayson, School of Chemical Sciences, at Dublin City
University, Glasnevin, Dublin 9.

November 1997

Table of Contents

Supplementary study

I hereby certify that this material, which I now submit for assessment on the programme of study leading to the award of Ph.D., is entirely my own work and has not been taken from the work of others save and to the extent that such work has been cited and acknowledged within the text of my work.

Signed : _____

Michael O'Brien

ID No. : _____9370147 1_____

Date : __21 - 11 - '97__

Acknowledgements

I would like to extent my sincere gratitude to all those who throughout the past four years contributed to the successful completion of this research project. In particular a special word of thanks to my supervisor Dr. Odilla Finlayson for her support and guidance during the project and Dr. John Curley who kindly took of his own time to proof read and discuss this thesis. I would also like to thank my fellow post graduate students and the staff in the school of Chemical sciences.

I must also thank the members of Dr. Odilla finlayson's research group in lab AG20 for there interesting conversational topics; very few of which were related to chemistry. In particular a mention for Dominic Delicato, Mick Tiernan, Nick O'Hare and Michael Giles. Also to John, Paddy, Ultan and Niall who were the best flat mates I could have hoped to meet.

Finally I would like to convey my appreciation to friends and family who helped bring this phase of my career to a successful conclusion.

Abstract

The deposition of coke on oxidation catalysts leads to deactivation. For oxide supports this phenomena of coking has previously been identified with acidic sites. Measurement of coke formation on silica gel, α-, η- and γ-Al_2O_3 showed that the greatest amount of coke was formed on γ-Al_2O_3 followed by η-Al_2O_3 with no detectable coking occurring on either α-Al_2O_3 or silica gel. Titration results showed γ-Al_2O_3 to contain the highest concentration of acidic and Brönsted basic sites per gram followed by η-Al_2O_3, α-Al_2O_3 and silica gel.

The acidity of γ-Al_2O_3 was altered by treatment with HCl, NH_3 and NaOH. HCl treatment gave a reduction in coke deposition while NaOH treatment increased coking and NH_3 treatment had no effect on the level of coking.

The effect of doping γ-Al_2O_3 and 0.5%Pt/γ-Al_2O_3 with Sn, Ce and Zr on the amount of coke formed was investigated. It was found that the level and method of impregnation affected the amount of coke formed on each catalyst. Individual addition of Sn, Ce, or Zr to γ-Al_2O_3 brought about a large reduction in the level of coking relative to γ-Al_2O_3 with the greatest reduction being seen for addition of Zr. Doping Pt/γ-Al_2O_3 with Ce, Sn or Zr resulted in the lowest level of coking occurring on Pt–Sn/γ-Al_2O_3. No correlation between acidic and Brönsted basic sites was observed for the metal impregnated catalysts suggesting that these metals exert a much greater influence on coking than do acidic or Brönsted basic sites.

The effect of Sn, Ce or Zr addition on activity of Pt/γ-Al_2O_3 for oxidation of isobutane was investigated. Addition of Sn or Zr reduced activity while 0.3% and 3.0% Ce resulted in greater activity than that observed for Pt/γ-Al_2O_3.

Introduction

Richardson [1] defines a catalyst as a substance that increases the rate at which a chemical reaction approaches equilibrium without itself becoming involved in the reaction. In light of its economic importance, the study of catalysis is a very intensely pursued subject in physical chemistry. Many industrial reactions use catalysts and process improvements in these are often the result of using new and better catalysts.

Catalysts can be broadly divided into three categories (1) homogeneous, (2) heterogeneous and (3) enzymatic [1]. In the case of homogeneous catalysis the reactants and products are in the same phase as the catalyst. For heterogeneous catalysis the reactants and catalyst are in different phases e.g. solid catalyst used with liquid or gaseous reactants. Enzymes are protein molecules which catalyse biochemical reactions. They are present in life processes and are characterised by very high efficiencies and selectivity. This study will concentrate totally on heterogeneous catalysts.

Heterogeneous catalysis deals with the transformation of molecules at the interface between a solid (the catalyst) and the gaseous or liquid phase carrying these molecules. This transformation involves the following series of phenomena, which, if possible, must be controlled [2]:

1. how the catalyst is constituted both in its bulk and at its surface and the transformations that it experiences (chemical reactions, exchange of atoms between surface and bulk, sintering, etc.);
2. how the gaseous or liquid phase is modified (composition, kinetics, etc.);
3. the nature of the interface (adsorbed species and bonds between these species and the catalyst surface).

In almost all cases the catalyst is an inorganic material and generally is a d-electron transition metal. It is known that d-electrons and their orbitals, hybrid and otherwise, are responsible for the bonding within the metal and at the surface [1]. These surface bonds determine adsorption and surface mechanism which in turn determine the catalytic reaction. s–metals are unsuitable as they revert too easily to ionic states under catalytic conditions while f–metals are too difficult to prepare and too reactive to remain in the metallic state.

The catalyst material is often expensive so any procedure which increased the effective use or improved the mechanical strength of a physically weak catalyst has obvious advantages. Initially the concept of a support material was to do just that. In addition to these a support material should ideally have the following characteristics [3]:

1. inertness (should not interfere with the main reaction of the catalyst);
2. desirable mechanical properties, including attrition resistance, hardness and compressive strength;
3. stability under reaction and regeneration conditions;
4. surface area; High surface area is usually but not always desirable;
5. porosity, including average pore size and pore size distribution; High area implies fine pores (e.g. < 5nm) but these may become plugged in catalyst preparation, especially if high loadings are sought.
6. low cost.

Very few materials combine all these characteristics but of the more suitable ones are alumina, silica, activated carbon and zeolites. For the purpose of the literature review, most of the papers cited will deal with alumina as a support material and to a lesser extent silica gel, as the problem of coking is more prevalent on alumina.

Without exception, catalytic hydrocarbon reactions are accompanied by catalyst deactivation [1]. This deactivation results from either the

2

sintering of the catalyst, the presence of poisons in the reagents or the deposition of undesirable carbonaceous species. This study will concentrate on deactivation caused by the deposition of carbonaceous deposits commonly described as 'coking' of the catalyst.

The thesis itself is laid out in four chapters. The first part of Chapter One consists of a literature review on the formation, structure and chemistry of silica gel and various Al_2O_3 forms. In the second part the formation and chemistry of coke is discussed. Chapter Two details the results of coke quantification experiments on silica gel, α-, γ- and η-Al_2O_3. The γ-Al_2O_3 is modified by the addition of acids, bases, Sn, Ce and Zr and the effect of these on coke formation is again studied. The physical characteristics of modified γ-Al_2O_3 and Pt/γ-Al_2O_3 are given in Chapter Three in an attempt to correlate these physical characteristics with coking characteristics. The fourth chapter deals with a practical application of oxidation catalysts. A prototype catalytic heat exchanger is designed, constructed and tested. A short account of combustion catalysis is included in chapter four and this has relevance for both parts of this thesis.

Chapter

One

The bulk and surface structure of

alumina and silica

1 Introduction

In this literature review the crystal structure and surface characteristics of the support materials Al_2O_3 and silica will be examined. Initally support materials were used simply as a means of spreading out an expensive catalyst material, e.g. platinum, for its most effective use [1,2,3]. In addition to this, the support may actually contribute to catalytic activity depending on the reaction and reaction conditions. In 1935, Adadurove [4] proposed that metals would be polarised by the surfaces of oxides which contained highly charged cations. This was probably the first suggestion that the catalytic properties of a metal may be influenced by the support. Section 1.1 will examine in detail one such support which contains highly charged cations i.e. alumina (Al_2O_3). Silica will also be looked at briefly (Section 1.2). Methods which have been used to modify the support material's chemical and physical characteristics is reviewed in Section 1.3.

In the second section of the literature review (Section 1.4) coking of catalysts will be investigated. This includes the various methods of coke formation and the effect coke formation has on catalytic activity. Also methods for characterisation of coke will be reviewed along with procedures for coke inhibition and removal.

1.1 Alumina

1.1.1 Production of various alumina types

Alumina is usually obtained by precipitation from aqueous solutions of aluminium trihydroxides, the most common of which are bayerite (α-$Al(OH)_3$) and gibbsite (γ-$Al(OH)_3$) [5]. These are formed from boehmite gel which is the product of initial precipitation from aqueous solutions containing Al^{3+} ions, Fig. 1.1. The boehmite gel is normally heated between 40 and 80°C (aged), the

details of the ageing procedure being important in determining the properties of the final product. Once aged the precipitate is filtered, washed and dried. In the last stage of preparation the precipitate is heated at temperatures of up to 600°C.

Gibbsite is the more important of the two aluminium trihydroxides as it is an intermediate in the production of aluminium metal from bauxite ($Al(OH)_3$ & $AlOOH$) by the Bayer process [6]. In this process a concentrated sodium aluminate solution is slowly cooled in the presence of crystal seeds and the gibbsite obtained consists of almost spherical crystal conglomerates which can be easily filtered. Bayerite does not occur in nature and is usually obtained as an intermediate during the preparation of gibbsite from aluminate solutions [6]. Most investigators prepare bayerite by treating precipated gelatinous aluminium hydroxides with ammonia solutions [6].

Fig. 1.1 *{Ref. 5}* Schematic representation of formation of various Al_2O_3 -hydrates
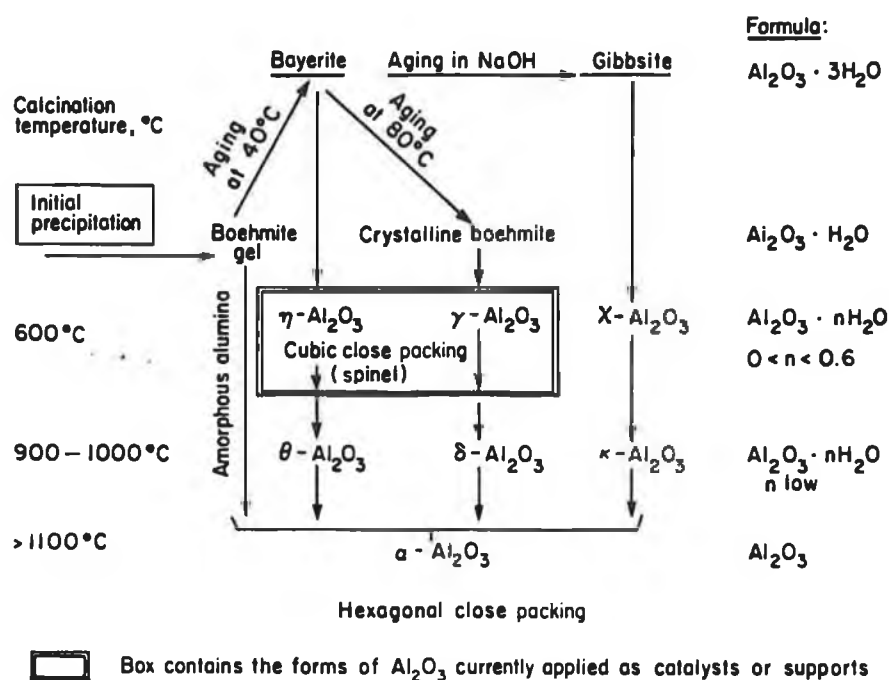
As can be seen from Fig. 1.1 the temperature of ageing can determine the type of Al_2O_3 obtained. The diagram also outlines how the various phases are formed from each other. Initial precipitation from aqueous solutions containing Al^{3+} ions leads to the formation of a gel containing minute crystals of boehmite ($AlO(OH)$). If filtered

and calcined at this stage none of the identifiable intermediate compounds with $0 <$ $n < 0.6$ (where n is the number of water molecules associated with the hydrated Al_2O_3) are formed. This material remains amorphous until after heating to $1100°C$ where α-Al_2O_3 is formed. However, when the boehmite gel is aged at $40°C$, it is converted into bayerite. If the bayerite is filtered, dried and then calcined a compound called η-Al_2O_3 is formed. When the η-Al_2O_3 is calcined at 900–$1000°C$, θ-Al_2O_3 is formed and this in turn is converted to α-Al_2O_3 at temperatures over $1100°C$.

Alternatively, if the bayerite slurry is further aged at $80°C$ it is converted into a more crystalline form known as *crystalline boehmite*. After the crystalline boehmite is filtered, washed and heated it is converted to γ- and δ-Al_2O_3 which are similar but not identical to η- and θ-Al_2O_3. When heated to temperatures higher than $1100°C$, δ-Al_2O_3 is converted to α-Al_2O_3.

The bayerite may be converted into gibbsite if it is aged in aqueous NaOH. Upon heating the gibbsite is converted into dehydrated forms, namely χ– and κ–Al_2O_3 and finally α-Al_2O_3.

While Fig. 1.1 outlines how the various forms of Al_2O_3 are formed from each other, it is important to realise that investigators differ over the reaction paths leading to the formation of each Al_2O_3 type [3]. Also, it is quite common for mixtures of the different types to be formed since the structures obtained are determined by kinetic considerations rather than thermodynamics. This is why it is not surprising that various aluminas supplied by different manufactures may be found to vary in their behaviour as catalyst supports, and in ways which may be difficult to relate to identifiable differences [3].

Of the various phases mentioned the more important ones for use as catalyst supports are η- and in particular γ-Al_2O_3. These materials have high surface area, relatively high thermal stability, and their surface acidity can be controlled [3].

1.1.2 Crystal structure of Al_2O_3

The crystal structure of Al_2O_3 has been closely studied by Lippens et al. [6] and they point out that both γ- and η-Al_2O_3 have lattice structures which are very similar to that of spinel ($MgAl_2O_4$). In a typical spinel structure (Fig. 1.2) eight metal atoms (A) occupy tetrahedral sites and sixteen metal atoms (B) occupy octahedral sites. The unit cell contains thirty two oxygen atoms in an almost perfect cubic close packed (CCP) array. CCP is one type of oxygen ion packing arrangement displayed by many oxide structures, the other being hexagonal close packing (HCP).

Fig. 1.2 *{Ref. 7}* Spinel structure of AB_2O_4

●A ⊘B ○O
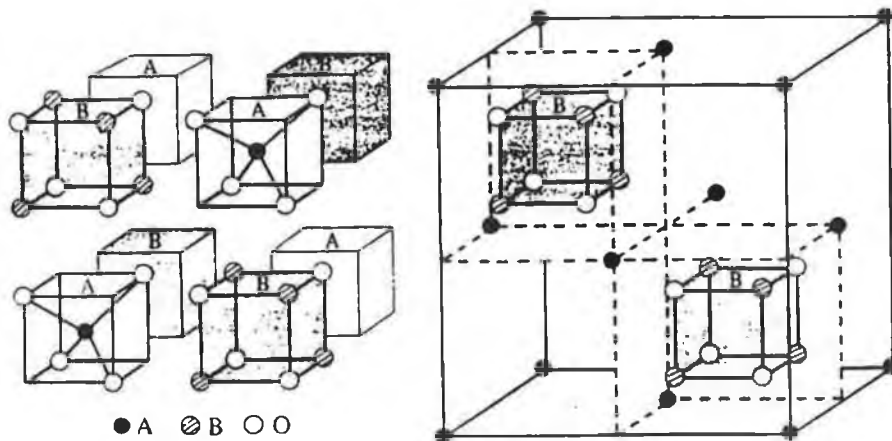
The structure can be considered as eight octants of AO_4 tetrahedra and B_4O_4 cubes as outlined in the left-hand part of Fig. 1.2. In all eight octants the 4O atoms have the same orientation and so build up into a fcc lattice of 32 ions which coordinate A tetrahedrally and B octahedrally. The 4A ions and the 4B octants contain a total of 16B ions. In the right-hand diagram it can be seen that the unit cell is completed by an encompassing fcc of A ions (●) that is shared with adjacent unit cells and makes up the remaining 4A ions in the complete unit cell $A_8B_{16}O_{32}$.

8

One of the most important structural characteristics of the catalytically useful forms of Al_2O_3, i.e. γ- and η-, is CCP of oxygen [5]. Gates et al [5] gave a good outline of close packing in metal oxide structures by considering the oxygen anions as hard spheres. The model considered a layer of close-packed spheres and from this the Al_2O_3 structures was derived. As can be seen from the diagram of this layer (Fig. 1.3) it has triagional symmetry with each oxygen ion located in the positions assigned 1. On top of this layer a similar layer is positioned with each sphere of the second layer positioned above a hole in the first layer, denoted as position 2 in Fig. 1.3. When placing the third layer on top of the previous two there are two options. If the third layer is placed in the position of the first it is referred to as HCP and the sequence is 1,2,1,2,1,2....... . For CCP the third layer is packed above another set of holes in the first layer, indicated as position 3 in Fig. 1.3. This leaves all the possibilities exhausted and so the fourth layer is equivalent to the first layer. The sequence for CCP is represented as 1,2,3,1,2,3, ...

Fig. 1.3 *{Ref. 5}* Single layer of close-packedspheres; 2 and 3 indicate sites of additional layers.
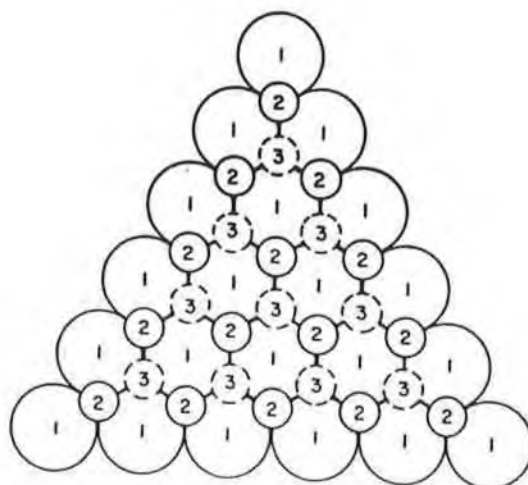
Cations, in this case the Al^{3+} ions, in a close-packed anion structure must be located between the close-packed anion layers [5]. The only positions which have sufficient room for the Al^{3+} ions are between the two layers and so they are located there. The Al^{3+} ions can be placed in the sites just above the triangularly formed holes in Fig. 1.3; the second oxygen layer in the 2 position then

9

placed over them. This results in the Al^{3+} ion being surrounded by six oxygen atoms and is refereed to as being in an octahedral position, Fig. 1.4.

Fig 1.4 *{Ref. 5}* Octahedral position of Al^{3+} ion.
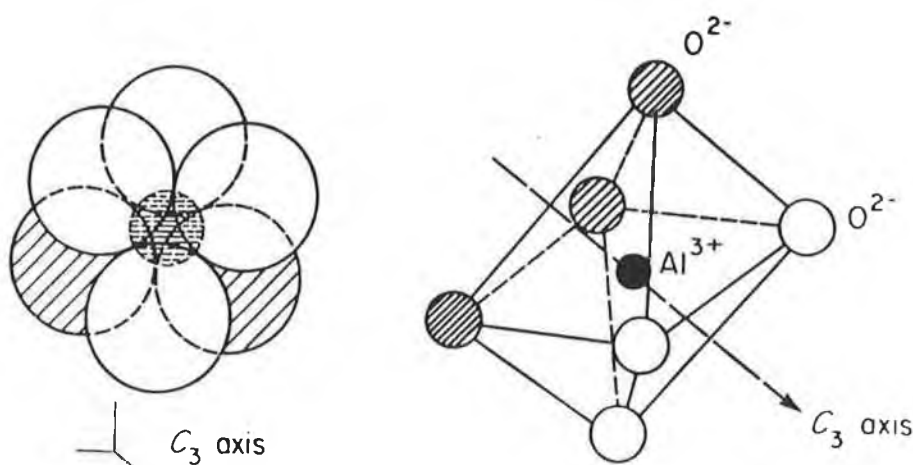
If this method of stacking O^{2-} and Al^{3+} is continued for hexagonal close packing it is found that there are just as many sites for the cations in the cation layer as sites for O^{2-} in the anion layer. This would fail to meet the requirement of electrical neutrality and so in order to satisfy this requirement, one in every three cation sites must be vacant. These vacancies lead to several possibilities for symmetry of the Al^{3+} ions. When the position of the cations is viewed diagonally the vacancy in every third cation site can be seen, Fig. 1.5. According to Lippens et al. [6] γ-Al_2O_3 only possesses $21\frac{1}{3}$ Al-atoms which have to be distributed over the 24 cation positions. For this reason the γ-Al_2O_3 structure is often regarded as a 'defect' spinel structure [9]. Essentially, any irregularity in charge distribution in the surface layer constitutes a 'defect' [10].

Fig. 1.5 *{Ref. 5}* Positions of cations in α-Al_2O_3 and aluminium trihydroxides.

○ Oxygen
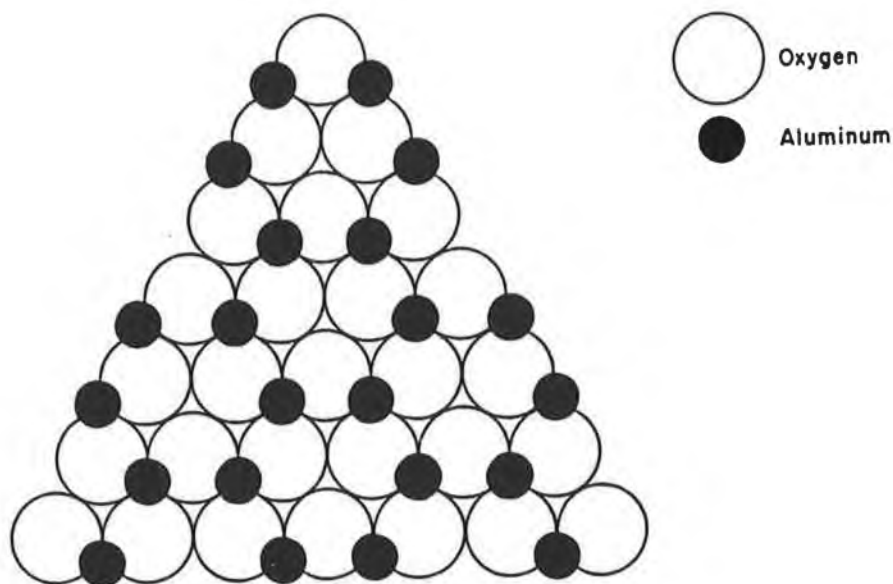
● Aluminum

The η- and γ- forms of Al_2O_3 differ in their ratios of octahedral to tetrahedral Al^{3+} ions [5]. It has been deduced by Verway [11] that the unit cell of γ-Al_2O_3 has two and two-third vacancies ($\square$) on the octahedral positions and that eight aluminium atoms are distributed over the tetrahedral holes. This corresponds to the notation $Al[Al_{13\frac{1}{3}}\square 2\frac{2}{3}]O_{32}$. Further work carried out by Jagodzinski et al. [12] on mixed crystals of γ-Al_2O_3 also concluded that the two and two-thirds vacant cation positions in γ-Al_2O_3 were probably octahedral.

While it was once generally believed that η-Al_2O_3 contained relatively more tetrahedral Al^{3+} ions than γ-Al_2O_3 [5], it has been shown by Leonard et al. [13] that the fraction of cations in tetrahedral positions is marginally higher in γ-Al_2O_3 than in η-Al_2O_3.

Gates et al. [5] have proposed the models for γ- and η-Al_2O_3 shown in Figs. 1.6 and 1.7 respectively. In the case of η-Al_2O_3 it starts with the

close packed oxygen layer already outlined in Fig. 1.3 . The first layer (B) has Al^{3+} ions in octahedral positions only, as shown in Fig. 1.6.

Fig. 1.6 *{Ref. 5}* Structure of η-Al_2O_3 showing tetrahedral and octahedral Al^{3+} ion positions.
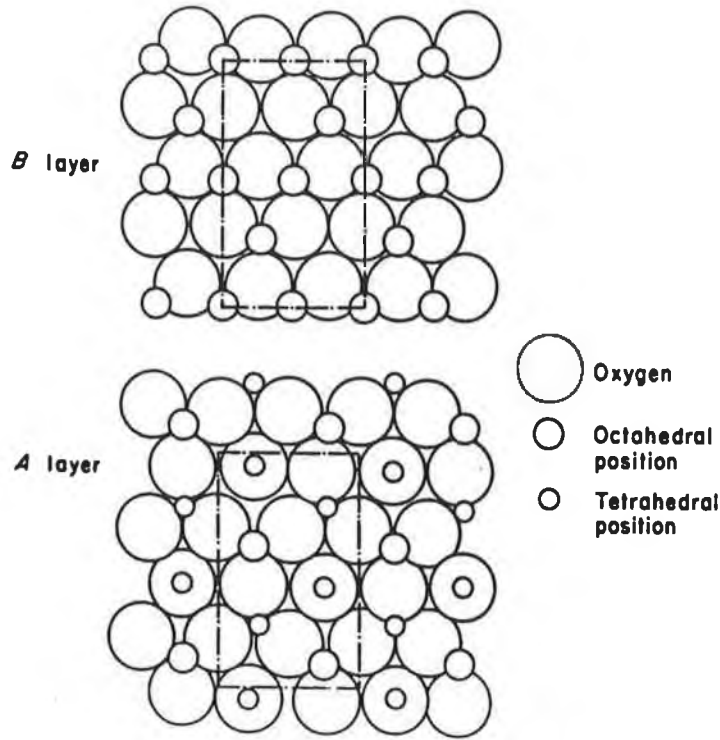
The second arrangement (the A layer) is obtained from the first by transferring two-thirds of the cations from octahedral to tetrahedral positions. This results in a stacking of the layers ABAB...... .

In the case of γ-Al_2O_3 (Fig. 1.7) the structure is easier to visualise by considering the (110) crystal plane which is orientated at an angle to the (111) plane [5]. There are two layers, nominated as C and D. The D layer possesses only octahedrally located Al^{3+} ions and the C layer has equal amounts of tetrahedral and octahedral sites. The packing of the structure is CDCD ....

Fig. 1.7 *{Ref. 5}* Structure of γ-Al_2O_3 showing tetrahedral and octahedral Al^{3+} ion positions.

C layer   *D* layer

Boehmite

○ Oxygen

○ Octahedral position

○ Tetrahedral position

C layer
D layer
C layer
D layer
C layer
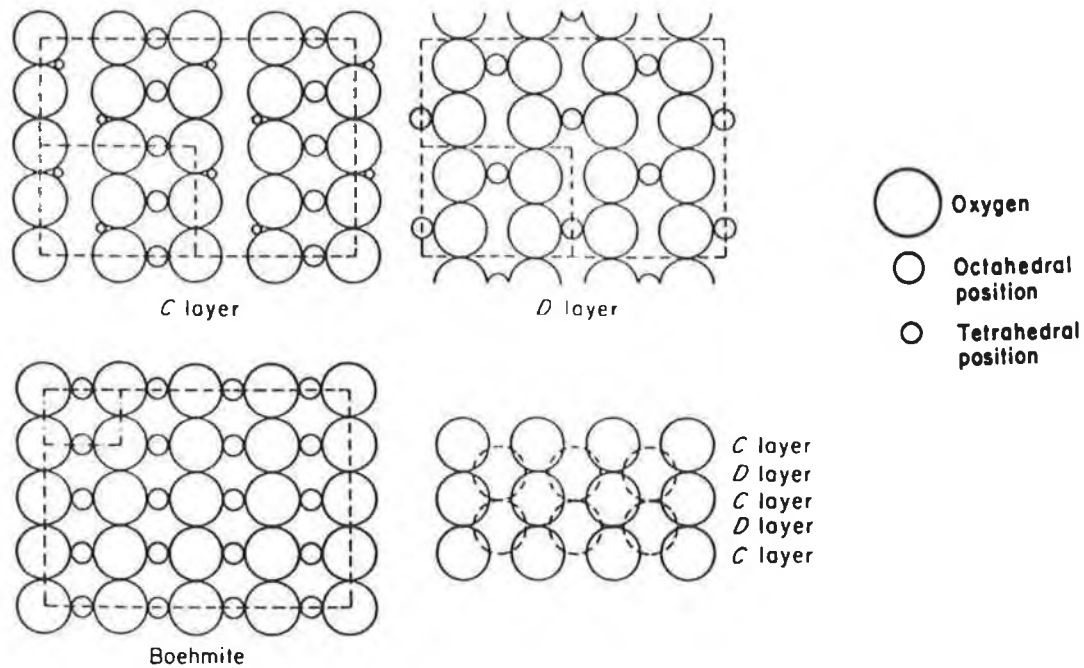
Stumpf et al. [14] established the existence of the seven nearly anhydrous crystalline Al_2O_3 forms namely α-, γ-, δ-, η-, θ-, κ-, and χ-Al_2O_3, using x-ray powder diffraction. They also studied the transformation sequences of Al_2O_3 hydrates heated both in dry air and in steam. It was found that the same crystalline transformations were observed for both short and long heating periods with the effect of holding the sample at a certain temperature for a long time being to lower the transformation temperatures. Heating in steam was seen to promote the formation of phases with more perfect crystallinity.

Fig. 1.8 shows the x-ray powder diffraction patterns for the seven forms of nearly anhydrous crystalline Al_2O_3 identified by Stumpf et al. [14]. The authors [14] found that α-Al_2O_3 was the only one of the seven forms which had an established crystal structure and the patterns for γ- and η-Al_2O_3 contained sharp and diffuse lines which suggested that the lattices were strongly disordered.

Fig. 1.7 *{Adapted from Ref. 231}* X-ray diffraction patterns of Al_2O_3 forms

2θ
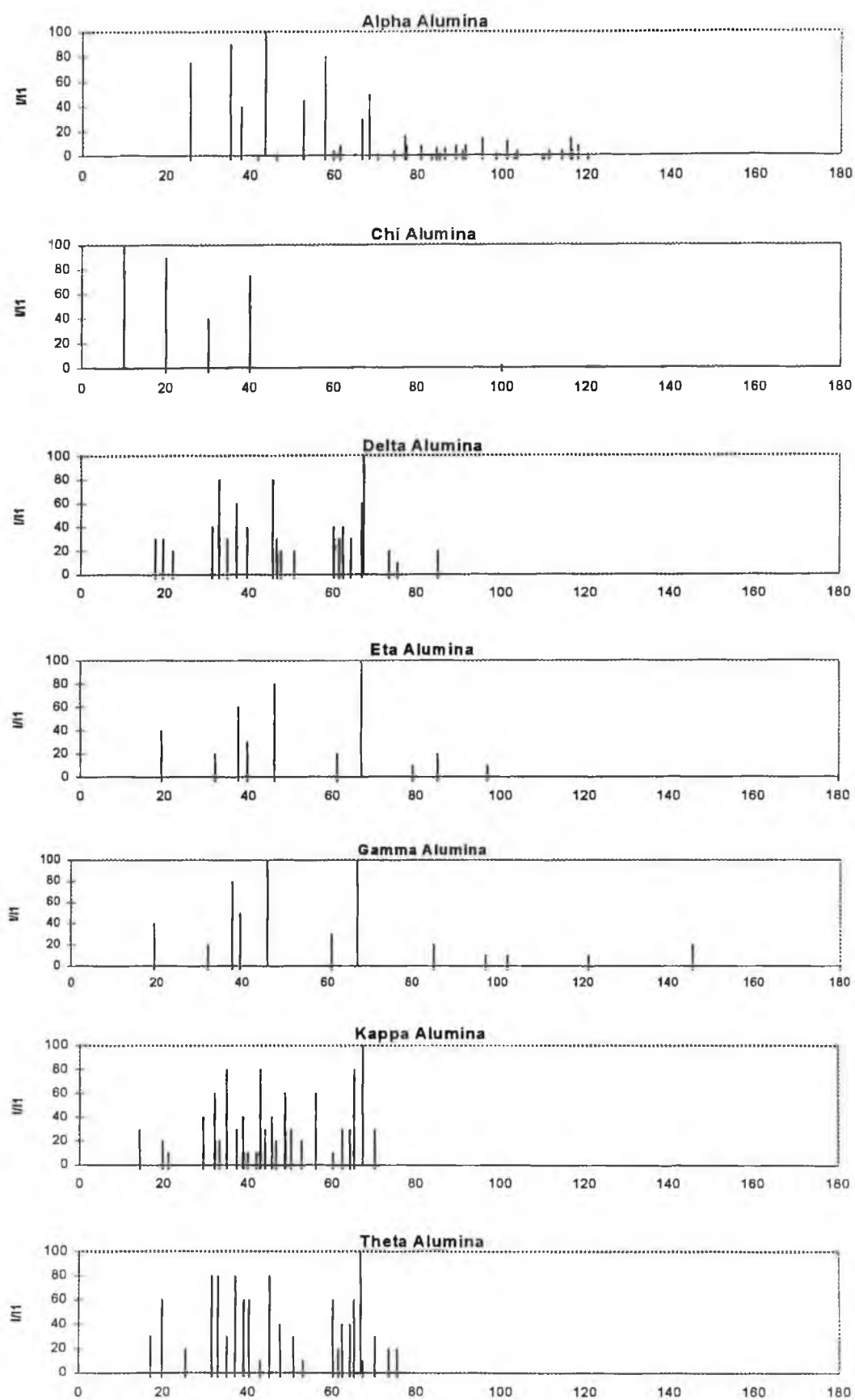
Lippens and de Boer [15] found that η- and γ-Al_2O_3 have spinel lattices that differ in disorder. η-Al_2O_3 has a strong one-dimensional disorder of the CCP stacking while γ-Al_2O_3 has a fairly well ordered oxygen sublattice but its tetrahedral Al lattice is strongly disordered. The authors [15] also suggest that differences in dehydration mechanisms may explain the differences in crystallographic texture of η- and γ-Al_2O_3.

The representations of γ-Al_2O_3 as a defect spinel structure however ignore the nature of the surface hydroxyl groups [16]. The nature of the surface hydroxyl groups are reviewed in the next section.

1.1.3 Surface structure of γ- and η-Al₂O₃

In this section the surface chemical nature of η- and γ-Al₂O₃ surface will be reviewed as it is what determines the alumina's catalytic and adsorptive properties [6].

Active Al₂O₃ (i.e. high surface area Al₂O₃) is not pure Al₂O₃, but depending on the temperature and water vapour pressure, it can contain from a few tenths to about 5% water [6]. Water adsorbed onto active Al₂O₃ can be in the form of either hydroxyl ions or as water molecules on the surface depending on the temperature. Alumina exposed to water vapour at room temperature adsorbs water as undissociated molecules bonded with strong hydroxyl bonds to the surface beneath [6]. Stumpf et al. [14] state that a 1% water content would cover an area of $30m^2$ to a monolayer thickness. According to Tamale [17] aluminium ions provide the electrophilic centres by which water is held on the surface. In the same paper it is claimed that hydration occurs dissociatively when the electron pair of the hydroxide is positioned over the aluminium ion while the dissociating proton forms a hydroxyl by binding to lattice oxygen. Dabrowski et al. [18] suggest that there may be differences in the energies of interaction for octahedrally and tetrahedrally co-ordinated aluminium ions but they do not have any experimental data to support this.

Removal of hydroxyl groups from Al₂O₃ is accomplished by the reaction between two surface Al-OH groups to form Al-O-Al and water as shown in Fig. 1.9 [19].

Fig. 1.9 *{Ref. 19}* Dehydration steps on Al₂O₃ surface
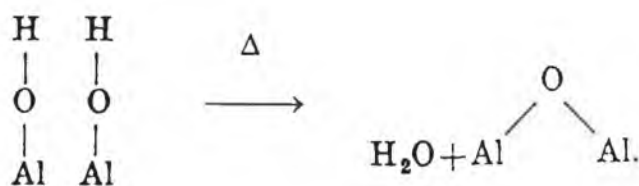
In the early stages of dehydration, neighbouring Al-OH groups can form Al-O-Al quite easily but as dehydration proceeds the remaining surface Al-OH groups are not situated close enough together to form Al-O-Al with normal crystallographic distances and consequently lattice distortion occurs. With extensive dehydration of oxides, a solid with a high surface strain is produced. The strain will extend through a number of ions, both along the surface and beneath it [19]. According to Cook et al. [20] a strained surface is important as a catalytic centre since it can react chemically with certain molecules to relieve surface strain. In order for this reaction to be useful catalytically the surface strain must be able to react chemically with the molecules to be activated in a reversible manner and neither the reactants or products should form stable compounds with the surface [19].

A statistical model has been proposed by Peri [10] to account for the surface hydration and catalytic properties of γ-Al_2O_3. This model is based on the assumption of preferred exposure of a single plane i.e. the (100) plane. On 'ideal' dry Al_2O_3 the top layer has only oxide ions which are regularly arranged over aluminium ions in octahedral sites in the next lower layer, Fig. 1.10(a).

Fig. 1.10 *{Ref. 10}* Ideal (100) surface of the Al_2O_3 containing the spinel structure.

(a) Dry surface

(B) Hydrated surface

Surface lattice of oxide ions remaining
after removal of H_2O

Surface layer of hydroxyl ions.

Next lower plane - alternate Al^{3+} ions ●
lie beneath oxide ions of surface lattice

Next lower plane (Al^{3+} ions ● lie directly below
OH⁻ ions of surface layer)

17
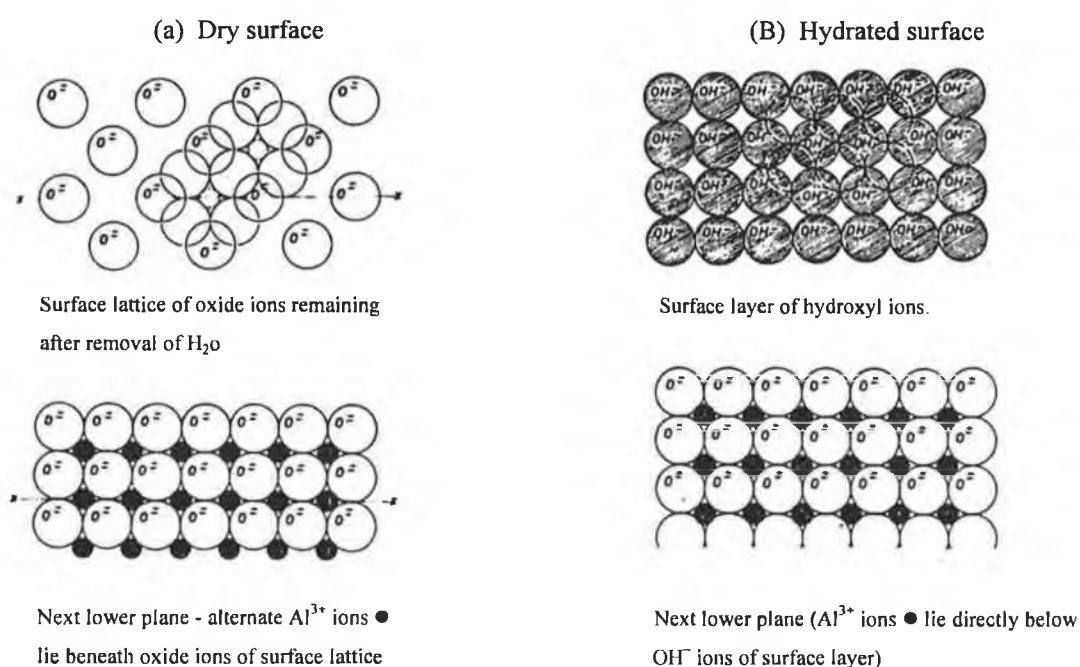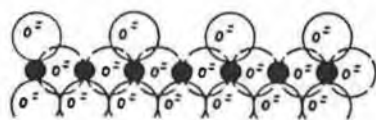
Section perpindicular to surface at x – x
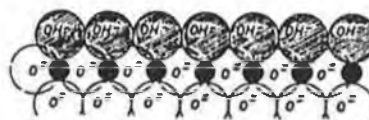
Section perpindicular to surface

The amount of oxide ions present in the top layer is only half that present in the lower layer which represents the (100) plane of a cubic close-packed oxide lattice. At $100^{\circ}C$ (or higher depending on the method of rehydration) enough chemisorbed water is held to convert the top layer to a filled, square lattice of hydroxyl ions (Fig. 1.10(b)). As can be seen from Fig. 1.10(b) each hydroxyl ion is directly over an aluminium ion in the next lower layer. Peri [10] proposes that during dehydration of the surface adjacent hydroxyl ions combine to form water molecules which are desorbed leaving one oxide in the top layer and one aluminium ion in the incomplete octahedral site of the next lower layer. This mechanism disagrees with the formation of a 'strained oxygen bridge' as suggested by Cornelius et al. [19] but is now accepted as being correct [6].

To reduce the disorder that would result from a totally random dehydration process, an assumption is made which allows local order to be retained in the residual oxide lattice [10]. This assumption is that water must initially be removed in such a way that two (or more) oxide ions are not left on immediately adjacent sites, and two or more immediately adjacent sites are not left vacant. This system only allows for removal of two-thirds of the OH⁻ ions. In order to get further dehydration Peri [10] removed the restriction for preservation of local order. With this restriction gone the computer model was able to proceed to 90.4% removal of hydroxyl pairs. The surface remaining had many defects which lie in the boundaries between oxide domains as shown in Fig. 1.11. As can be seen the hydroxyl ions remaining are found on five types of sites and they have from zero to four nearest oxide neighbours.

18

In order to get dehydration levels of greater than 90.4%, migration of surface ions must occur. Peri et al. [21] have shown that at temperatures between 400 and 600°C, some mobility of surface ions occurs and at temperatures above 600°C protons migrate readily on the surface of γ-Al$_2$O$_3$. This would suggest that drying temperatures in excess of 600°C are required to reduce the surface hydroxyl concentration below 9.6%. At this last stage of dehydration there is a large increase in the number of defects on the surface, the major ones being where the hydroxyls have two and three directly adjacent vacancies and two and three directly adjacent oxide ions.

Fig. 1.11 *{Ref. 10}* Types of isolated ions on spinel type Al$_2$O$_3$ surface (+ denotes Al-ion in lower layer)
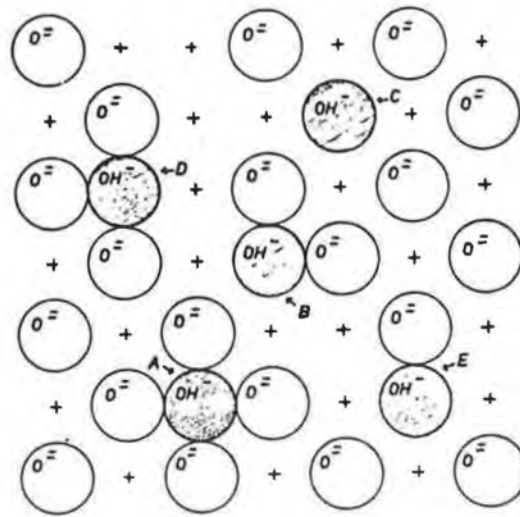
One serious limitation of Peri's model is the assumption that a spinel type Al$_2$O$_3$ exposes only the (100) planes on its surface [10]. Although Lippens & Steggerda [6] found strong evidence to suggest that this was the case for γ-Al$_2$O$_3$ formed by dehydration of crystalline bohemite, Soled [16] believes that it is the (111) faces which are exposed. Peri [10] however acknowledges that crystal faces other than the (100) may be exposed to a major extent and states that his model

is very speculative since the surface may be very different to that depicted and possibly much more complex. The model should however prove applicable to other faces which can be approximated by a square lattice but cannot be readily applied, for example, to a (111) face. In addition to this the crystal lattice of transition Al_2O_3 is probably indistinct at very high temperatures with ions vibrating strongly about regular sites of attachment and often moving to adjacent vacant sites. This may result in surface strains beginning to 'heal' at higher temperatures [22].

The model proposed by Knözinger and Ratnasamy [23] has assumed that the η-phase preferentially exposes the (111) face and the γ-phase the (110) face. This differs from earlier models [10,18] in that both octahedral and tetrahedral ions are at the surface since (110) and (111) planes are used.

Both the (111) face of η-Al_2O_3 and the (110) face of γ-Al_2O_3 can expose two different layers of ions [24]. These are designated A– and B–layers and are shown in Figs. 1.12(a) and 1.12(b) respectively.

Fig. 1.12 *{Ref. 23}*
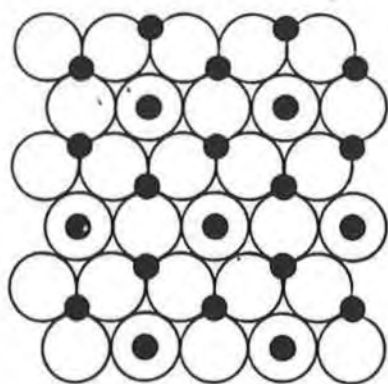
(a) (111) - Face of η-Al_2O_3, A-layer.　　　　　　(b) Face of η-Al_2O_3, B-layer.
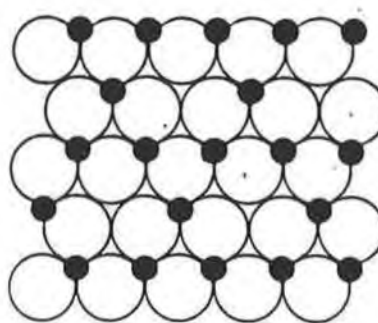
The B-layer contains 24 octahedral cation positions. The A-layer also possesses 24 octahedral cation positions but eight of them are distributed in octahedral and the remaining 16 in tetrahedral interstices. Two cation arrangements are also present in

the spinel lattice parallel to the (110)-plane, the C– and D–layers, Figs 1.13(a) and 1.13(b). Equal numbers of cations are aligned in tetrahedral and octahedral interstices in the C-layer, whereas in the D-layer only cation positions in octahedral interstices occur. As has been mentioned earlier [10,18] the (100) face is represented by a square lattice of oxygen atoms where only octahedral cations are possible.

Fig. 1.13 *{Ref. 23}*
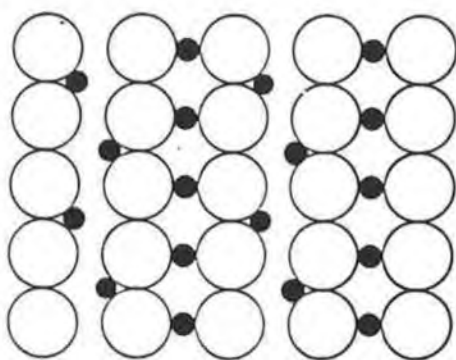
(a) (110) – Face of γ-Al_2O_2, C–layer.   **(b)** (110) – Face of γ-Al_2O_3, D–layer
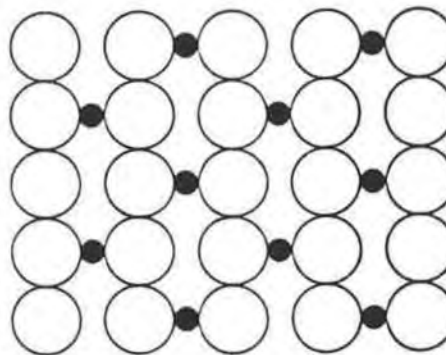
It has been shown that the surface of Al_2O_3 is normally covered by OH groups [25] as these minimise the surface energy [23]. The OH layer on top of the A-layer for a surface layer parallel to the A-plane (111) of the spinel lattice is shown in Fig. 1.14. In this diagram two types of OH configuration can be seen within the layer.

Fig. 1.14 *{Ref. 23}* Anion layer on top of (111) – face of η-Al_2O_3, A layer.

21
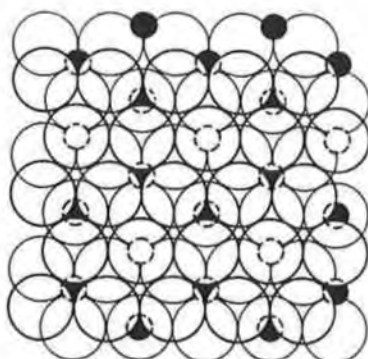
The first one referred to as a 'type Ia' (Fig. 1.15(i)) is formed where a terminal OH group is co-ordinated to a single tetrahedral Al^{3+} cation.

Fig. 1.15 *{Ref. 23}*

(i)

Type Ia:

$$
\begin{array}{c}
OH \\
| \\
Al \\
\diagup | \diagdown
\end{array}
$$

(ii)

Type IIa:

$$
\begin{array}{c}
H \\
O \\
\diagdown | \diagup \quad \diagdown \\
Al \quad\quad Al \\
\diagup | \diagdown \quad \diagup | \diagdown
\end{array}
$$
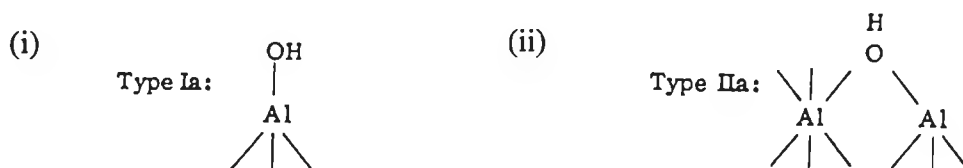
In the second configuration (type IIa), the OH group is in a bridging structure which links a tetrahedral and an octahedral cation.   This configuration occurs thrice as frequently as type I(a) [23].

In the OH layer on top of a B-layer, two OH configurations occur as shown in Fig. 1.16.

Fig. 1.16 *{Ref. 23}* Anion layer on top of (111) – face of $\eta\text{-}Al_2O_3$, B–layer.
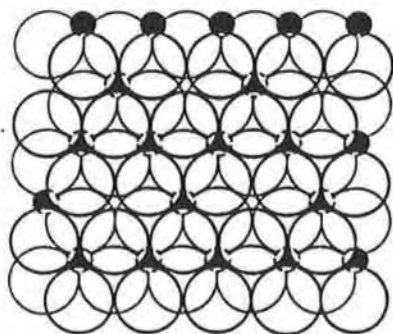
In both cases the configuration consists of bridging OH groups. In type IIb (Fig. 1.17(i)) the OH group links two cations in octahedral positions. The type III (Fig. 1.17(ii)) has the OH co-ordinated to three cations in octahedral interstices. In the B-layer type IIb configurations occur three times more often than type III configurations [23].

Fig. 1.17 *{Ref. 23}*

(i)

Type IIb

(ii)

Type III
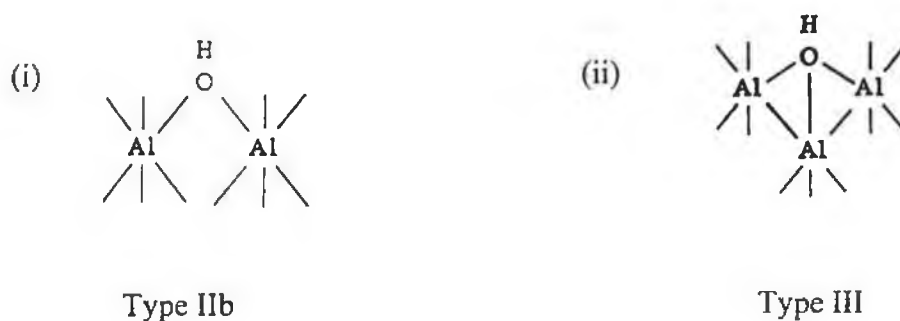
When vacant cation positions are taken into consideration a fifth configuration referred to as a type Ib can occur in either the A– or B–layer, Fig. 1.18. In this configuration the OH group is co-ordinated to a single cation in an octahedral interstice. The Ib configuration is obtained from configuration IIa if the tetrahedral cation is removed or from configuration IIb if one of the octahedral cations is removed.

Fig. 1.18 *{Ref. 23}*
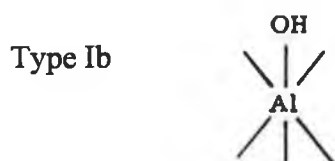
Type Ib

With regard to the C- and D-layers parallel to the (110)-plane of the spinel lattice, OH groups type Ia and IIb occur on top of the C-layer. The only OH configuration which can occur on top of a layer parallel to the (100)-plane of the spinel lattice is type Ib.

The five possible OH configurations are sumarised in Table 1.1 [23].

Table 1.1 {Ref. 23} Possible OH configurations

Crystal face	Configuration[a]	Coordination numbers of surface anion		Net charge at O	Net charge at OH	$\nu(OH)$ cm^{-1}
		Al(VI)	Al(IV)			
(111)	III	3	-	-0.5	+0.5	3700-3710
	IIb	2	-	-1.0	0	3740-3745
	IIa	1	1	-0.75	+0.25	3730-3735
	Ia	-	1	-1.25	-0.25	3760-3780
	Ib	1	-	-1.5	-0.5	3785-3800
(110)	IIb	2	-	-1.0	0	3740-3745
	Ia	-	1	-1.25	-0.25	3760-3780-
	Ib	1	-	-1.5	-0.5	3795-3800
(100)	Ib	1	-	-1.5	-0.5	3785-3800

○ = oxygen atoms or hydroxyl groups; ● = Al(VI); ⵔ = Al(IV)

The values for the net charge at a surface oxygen and a surface OH group, given in columns 5 and 6, of Table 1.1 respectively, are the sum of the negative charge of the anion and the sum of the strengths of the electrostatic bonds (cation charge divided by co-ordination number) to the anion from adjacent cations. The strength of an electrostatic bond between an anion and an Al^{3+} cation in an octahedral position is therefore equal to +0.5, whereas that between an anion and an Al^{3+} cation in a tetrahedral position is +0.75 [24]. Pauling's electrostatic valence rule states that the net charge in a stable ionic structure should be equal or nearly equal to zero [26]. From the values in columns 5 and 6 of Table 1.1, it can be clearly seen that this requirement is better approximated when OH groups are the surface ligands rather than oxygen. The only exception to this is configuration III where the absolute values for the net charge of O^{2-} and OH^- are equal (i.e. 0.5).

An important deduction from the above is that a maximum of five different OH configurations can exist on the surface of Al_2O_3. In these various configurations the OH groups bear slightly different net charges and hence should posses different properties [23]. Knözinger et al. [23] suggest that the OH configuration of type III is the most acidic since it has a positive charge of +0.5 and abstraction of a proton would produce an oxygen bearing a net negative charge of only -0.5 which is still close to the value of zero necessary for electroneutrality. This argument implies that the protonic acidity of the OH groups will decrease as the net charge on them becomes more negative and consequently their basicity will increase at the same time. The ease with which OH groups can be removed should parallel their basicity since the remaining net positive charge at the 'hole' or anion vacancy is lower the higher the net negative charge of the leaving OH group. Bond et al. [24] have recognised that a problem associated with Knözinger's model is the assumption that bonds at the surface are purely ionic. Infrared studies of chemisorbed pyridine and CO_2 seem to indicate the presence of a co-operative effect between nearest neighbours i.e. some degree of covalency. Bond et al. [24] however acknowledge that the merit of Knözinger's model is relevant.

Van Cauwelaert et al. [27] have demonstrated that the removal of water and/or hydroxyl groups from Al_2O_3 surfaces is essential for the development of catalytic activity. The authors [27] showed this by monitoring the rate of ortho-para H_2 conversion and H_2-D_2 exchange reactions over a transition Al_2O_3 dehydroxylated at different temperatures. It is also known that the proton acidity and ease of removal of an OH group are important factors which govern the dehydroxylation process, at least initially, at low temperatures when proton mobility is slow [23]. The surface acidic properties of Al_2O_3 will be reviewed in the next section.

1.1.4 Acidity of Al_2O_3

The surface constituents of Al_2O_3 which have been discussed in the previous section determine the surface acidic and basic properties. Coordinatively unsaturated Al^{3+} sites have Lewis acid (electron pair acceptor) character whereas the surface oxide sites should function as Lewis base (electron pair donor) sites [28]. The surface hydroxide species may develop basic or proton acidic properties. When the negative charge density on the OH group is high it will behave like a hydroxide ion [28], but OH groups with high positive charge densities will behave more like Brönsted acids (proton donors). Tanabe et al. [29] have found that the protonic (Brönsted) or aprotic (Lewis) acid and base centres on metal oxides are of varying acid or base strengths distributed more or less widely around the mean. Experiments by Boehm [30] on surface hydroxyl groups of metal oxides have shown that half of the hydroxyl groups are acidic in character while the other half are basic and can be exchanged for other anions.

Undissociated water molecules on the surface of Al_2O_3 are completely removed by heating to 200°C [31] and when γ-Al_2O_3 is calcined above 300°C, the following sequence occurs, Fig 1.19 [1].

Fig. 1.19 *{Ref. 1}* Effect of calcining γ-Al_2O_3 above 200°C
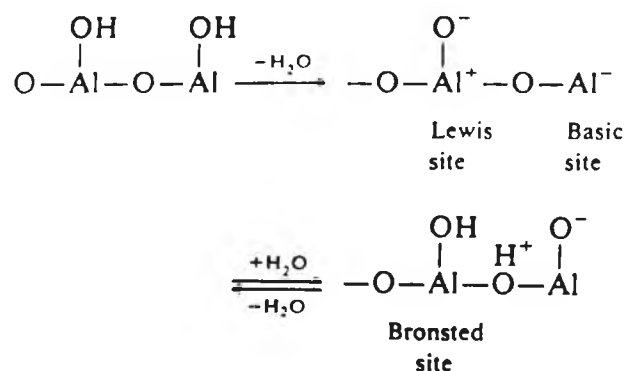
The Brönsted acid sites, in large concentrations at high water contents, are gradually converted into Lewis acid sites upon dehydration [6]. It can be seen from Fig. 1.19 that dehydration of the hydrous oxide gives a surface containing both Lewis acidic and basic sites. Sufficient water however is always present to generate Brönsted sites [1]. Peri [10] has proposed the creation of active sites through this dehydration process which exposes aluminium ions (Lewis acids) and adjacent O^{2-} ions (Lewis bases) as shown in Fig. 1.19. In H_2-D_2 exchange experiments over Al_2O_3, Pines et al. [32] discovered that Lewis acid sites were responsible for the catalytic action. They also found that moisture was a poison for the reaction due to the acidic sites becoming covered with hydroxyl groups.

In a subsequent study on the exchange of hydroxyl groups on Al_2O_3 with deuterated methane, Larson et al. [33] found that Al_2O_3 contained $3 \times 10^{12}/cm^2$ active sites. According to Peri's model [10] a completely hydroxylated Al_2O_3 surface would contain $1.3 \times 10^{15}/cm^2$ of OH and when 90% dehydroxylated $5 \times 10^{14}/cm^2$ of aluminium ions would be exposed and an equal number of O^{2-} ions formed. This leaves a hydroxyl concentration of $1.3 \times 10^{14}/cm^2$, most of which would have adjacent exposed aluminium ions with O^{2-} nearest neighbours and it is these configurations that are considered active for the exchange of hydrogen with methane [33]. As can be seen from the figures above, the surface density of such configurations is however at least an order of magnitude higher than the number of active sites calculated from the experimental results. This has led Larson et al. [33] to conclude that not all hydroxyl groups having adjacent exposed aluminium ions and O^{2-} nearest neighbours are catalytically active and that only high energy sites created at the domain boundaries are strong enough to dissociate methane. This view is held by Knözinger [34] who found from specific poisoning experiments that the number of Lewis acidic and basic sites are one to two orders of magnitude higher than the number of active sites. In addition to this Knözinger [34] found that catalytic activity of Al_2O_3 was only developed after dehydration at temperatures above 300°C to 400°C although 3.7×10^{14} vacancies (Lewis acid sites) and co-ordinately unsaturated (CUS) oxygen atoms (Lewis basic sites) have already formed at 300°C. The author [34] conclude that Lewis acidic and basic sites produced

during the regular dehydration process are unlikely to be involved in catalytic reactions as active sites. It may also be possible that at temperatures between 300 and 400°C special site configurations of low probability begin to develop which posses the structural and energetic properties required for an active site [23].

With regard to Brönsted sites, the strength with which the proton is hydrogen bonded to the hydroxyl group is related to the electronic environment of the Al^{3+} ion [1]. This would suggest that factors which shift the electron distribution in the Al–OH bond toward the Al^{3+} ion weaken the OH–H^+ bond and increase the acidity of the proton. As has been stated in section 1.1.3 Al^{3+} ions in Al_2O_3 occupy both tetrahedral and octahedral sites with neighbouring oxygens, the surface co-ordination depending on crystal face exposed.

In Fig. 1.11 five different types of isolated hydroxyl ions were outlined with their relationship to the O^{2-} and Al^{3+} ions in the layer below the surface. It can be seen that site A has a weaker OH–H^+ bond, due to the four adjacent O^{2-} ions, and therefore greater acidity than the other sites. The other sites have varying degrees of acidity which explains the acid strength distribution found on Al_2O_3 by Tanabe et al. [29].

Peri [10] has proven the existence of these five types of OH groups by the presence of five isolated bands observed in the infrared spectra of dry Al_2O_3. NH_3 adsorption has been followed by infrared [35] and pressure variations as a function of temperature [36] to clearly demonstrate the presence of various acid sites. In Peri's study [35] the Al_2O_3 was predried at 800°C and then exposed to NH_3 at 50°C. At this temperature roughly 30% monolayer of ammonia chemisorbs on the Al_2O_3. The author [35] found that the hydroxyl groups already present on the Al_2O_3 were all affected by the NH_3 and that new hydroxyl groups were formed. The infrared spectra indicated the presence of NH_4^+, NH_3, NH_3^+, and NH_2^-, bonded on Brönsted sites, Lewis sites, very strong Lewis acid sites (triple vacancies) and dissociatively adsorbed as NH_2^- and OH^- on adjacent acid–base sites respectively.

The position of the infrared band of adsorbed NH_3 can be related to the acid strength of adsorption centres allowing the acid strength of surface Brönsted centres to be determined by measuring the OH band shift caused by NH_3 adsorption [37]. The higher the acid strength of the surface site the greater is the shift of the infrared band to lower frequencies (higher wave-number).

An advantage of methods using adsorption/desorption of gaseous bases is that the number of acid sites which a solid catalyst possesses under actual working conditions, can be determined [29]. Also these techniques, unlike titrimetric techniques which use indicators to determine end-points, are applicable to all samples regardless of colour [36]. However, they suffer from the disadvantage that it is difficult to distinguish between chemical and physical adsorption and to differentiate the number of acid sites of various acid strengths [29]. Barth et al. [36] also admit that with certain types of catalysts there is a possibility of ammonia decomposition during desorption at elevated temperatures.

Parry [38] drew attention to problems of extraneous physical adsorption and diffusion limitations that give rise to difficulties in interpretation of IR spectra of chemisorbed NH_3 on solid acids. Also he found that the ammonia band used to describe co-ordinately bonded ammonia was subject to some interference. In addition to this, ammonia is such a strong base ($pK_b \sim 5$) that it will react with extremely weak acidic sites. Parry examined the infrared spectrum of pyridine chemisorbed on various solids including η-Al_2O_3. Since pyridine, while still being a relatively strong base (pK_b pyridine ~ 9), is significantly weaker than ammonia it will not react with some of the weaker sites that would react with ammonia [38]. The results of his work indicate that the strong acid sites of η-Al_2O_3 are of Lewis acid type. No Brönsted acid sites strong enough to react with pyridine were found on the surface of dehydrated η-Al_2O_3. Even after the addition of excess water vapour no Brönsted acid sites were detected which led Parry [38] to conclude that any protons present on the η-Al_2O_3 are too weak to react with pyridine.

Infrared studies of n-butylamine adsorption has been used by Morimoto et al. [39] to determine acid types on surfaces. Since n-butylamine is a stronger base (pK_B = 3.38) than either pyridine (pK_B = 8.75) or ammonia (pK_B = 4.75) it should react with the weak acidic sites [39]. When this technique was applied to Al_2O_3 which had been pre-treated at 500^oC *in vacuo* no band which corresponded to protonic acid sites was observed. In agreement with the results obtained by Parry [38], spectroscopic evidence was found which suggested the presence of aprotonic acid sites. Adsorption of n-butylamine on Al_2O_3 which has been pre-treated at 100^oC in air was also carried out [39]. The infrared spectra for this sample on which a considerably large amount of water remained, possibly physisorbed, revealed the existence of Brönsted acid sites. This result led the authors [39] to conclude that part of the Lewis acid sites were converted to Brönsted acid sites through reaction with water which is also the view held by Parry [38].

When a hydroxyl containing compound is placed in solution the infrared band due to the OH vibration is moved to lower frequencies due to the H-bonding interaction between solute and solvent [40]. This OH band frequency shift is a direct function of both acidity of the OH group and basicity of the solvent and allows calculation of the acidity of OH groups on metal oxide surfaces including silica and silica-alumina. The authors achieved this by adding the oxides to a solution of methanol, phenol and trichlorophenol in carbon tetrachloride. Since the acidity values (pK_a) of the OH groups on the methanol and two phenols are known the position of the perturbed hydroxyl band(s) on addition of the donor oxides can be used to calculate the acidity of OH groups on the oxides [40].

The acidic properties of Al_2O_3 have also been studied using Nuclear Magnetic Resonance (NMR) spectroscopy. Pearson [41] suggested an NMR method to measure the Brönsted acid sites on Al_2O_3 which was based on the reaction of deuterated pyridine with the Al_2O_3 surface, Fig. 1.20.

Fig. 1.20 *{Ref. 41}*   Deuterated pyridine on Al₂O₃ surface
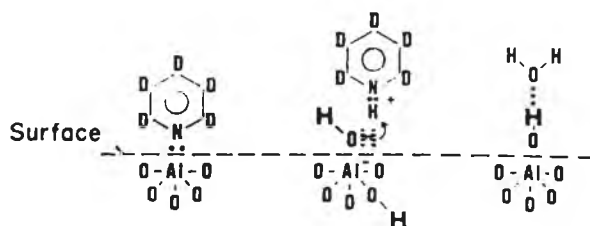
It was found that under certain conditions the pyridium ion formed when a deuterated pyridine molecule reacted with a Brönsted acid site could be quantitatively measured with proton NMR [41]. The method was used to study the effect of evacuation temperature on the water content and Brönsted acidity of Al₂O₃ over the temperature range 100 – 700°C. The results of his work are summarised in Table 1.2. The results obtained by Pearson in Table 1.2 are in agreement with those obtained by Peri et al. [21] who also found that there was an increase in Brönsted acidity as a function of activation temperature. Inconsistencies however arise when Pearson's results [41] are compared with those of Parry [38] who did not find evidence for the existence of Brönsted acid sites on η-Al₂O₃ by infrared analysis of adsorbed pyridine. When these results are viewed in conjunction with those obtained by Morimoto et al. [39] who used infrared analysis of adsorbed n-butylamine, which is a much stronger base than pyridine, to detect Brönsted acid sites, it would appear that the discrepancy is due to the weakness of the protonic acidity on the Al₂O₃ surface. According to Pearson [41] the NMR method is undoubtedly the most sensitive.

Table 1.2. *{Ref. 41}* Number of Brönsted acid sites vs evacuation temperature

Evacuation temperature	$H^+/g\ Al_2O_3$		Brönsted sites/g	H^+ Acidic	
(°C)	Total × 10^{20}	Surface ×10^{20}	Al_2O_3 ×10^{19}	% Total	% surface
100	19.20	11.1	3.48	1.81	3.14
200	11.32	6.56	5.32	4.71	7.18
300	9.76	5.71	6.00	6.12	10.6
400	5.94	3.99	5.89	9.98	14.8
500	6.18	3.86	7.18	11.6	18.6
600	2.11	1.47	7.32	34.9	49.8
700	0.58	0.41	3.28	56.6	80.0

Investigation of surface acidity using ^{13}C NMR has been carried out by Gay et al. [42]. The technique was based on the fact that relatively large chemical shifts occur upon protonation of aromatic and heterocyclic amines in aqueous solutions which can be measured using ^{13}C NMR. Using aniline, no evidence of large upfield shift was seen on exposure to the Al_2O_3, which was found on protonation in acid solution. This at first hand would suggest that no acidic sites were detectable using the ^{13}C NMR but using N,N-diethylaniline, which is a much stronger base than aniline, it was found that there was a pronounced steric effect on γ-Al_2O_3 with the strong acid sites being relatively inaccessible.

Knözinger et al. [43] has reported on the effect observed on the electronic spectra of substituted pyridines after adsorption onto η-Al_2O_3. Their results show that the π–π^* transitions of the pyridines appear to be slightly shifted towards longer wavelengths after adsorption on Al_2O_3 compared with their position in the liquid phase. The authors suggests that the shift in the π–π^* bands towards longer wavelengths is due to co-ordination of the substituted pyridines onto Lewis acid sites but admit that their deductions are speculative [43].

Interaction of an acid centre with a basic molecule is accompanied by heat evolution and the stronger the acidic centre the more pronounced the thermal effect [37]. Microcalorimetry can detect some heat changes due to reaction and therefore can be used in the characterisation of acidity and basicity on solid oxide surfaces. This is achieved by measuring the differential heat of adsorption of probe molecules which can be acidic or basic in nature [44]. Maciver et al. [45] have used ammonia adsorption to study the acidic properties of η- and γ-Al_2O_3 as a function of dehydration. This technique involved adsorbing ammonia on dried samples of Al_2O_3 which had been pre-treated at various temperatures. After evacuation at elevated temperatures the amount of ammonia remaining was measured. High desorption temperatures for ammonia were found to correlate to strong acid sites. Taniguchi et al. [46,47] have demonstrated that there is in fact a close relationship between the values of differential heats of ammonia adsorption on different catalysts and their acid strengths, Table 1.3.

Table 1.3 *{Ref. 47}* Comparison of differential heat of NH_3 adsorption with acid centre strength.

Acid strength (H$_o$)	Differential heat of NH$_3$ adsorption (kJ mole^{-1})
-14.52	-137.0
-5.6	-76.1
-3.0	-65.6
+1.5	-61.8
+3.3	-55.1

Nelson et al. [48] have outlined a temperature – programmed desorption technique which used adsorption of t-butylamine to estimate surface acidity on solid oxide catalysts. In this technique the area of the desorption curve for chemisorbed t-butylamine was taken as a measure of the amount of 'strong' acidity while the peak maximum was an index of acid strength. When combined with

surface area measurements this allows the calculation of the acid site density (acid area/surface) in a catalyst [48].

CO_2 and NH_3 have been used as microcalorimetry probe molecules to analyse for the presence of both acidic (relating to Al^{3+} ions) and basic (relating to O^{2-} ions) sites on Al_2O_3 by Auroux et al. [44]. The authors concluded that microcalorimetry allowed information to be gained about the strength and distribution in strengths of acidic and basic sites but gave no information about the nature of the sites and contrary to them being familiar with the work of Taniguchi et al. [46,47], they saw that no direct relationship but only a reasonable proportionality between the heat of adsorption and the acidic or basic strength of the sites.

A differential scanning calorimeter (DSC) was used in studying acid strength distribution in catalysts by Aboul–Gheit et al. [49]. According to the authors this procedure offers some advantages over temperature programmed desorption (TPD) techniques. Due to the comparatively small samples used for the DSC technique peak overlap is reduced which results in well resolved peaks for ammonia desorption where only one peak may be observed with TPD. The DSC peaks can be used to distinguish acid site strengths with the highest temperature peak representing the highest acid site strength [49]. In addition to being more sensitive than TPD the DSC detection system, unlike the TPD method, can differentiate between physically and chemically adsorbed phases of a base as they give rise to endothermic and exothermic peaks respectively.

Benesi [50] states that in order for an acidity measurement of solid catalysts to be useful it must first fulfil two requirements: (a) it should be simple to carry out; and (b) it should determine the source of catalytic activity. If catalytic activity of Al_2O_3 is due to protonic acids on the surface then the work carried out by Pearson [41] and Peri et al. [21] would suggest that Al_2O_3 is a strong acid only at high temperature and not at room temperature where titrations are performed [22]. Pines et al. [22] found that Lewis acidity could be detected at room temperature using indicator based techniques. Subsequent to this Tanabe et al. [29]

found that amine titrations could be used to measure the sum of both Brönsted and Lewis acids since both proton donors and electron pair acceptors on the surface will react with either the electron pair $(-N=)$ of the indicator or that of amine $(\equiv N:)$ to form a co-ordination bond.

As far back as 1956, Benesi [51] stated that a measure of the acid strength of a catalyst surface can be obtained by noting the colours of suitable Hammett indicators. The Brönsted acid strength of a solid surface was defined quantitatively by the Hammett acidity function, H_0.

$$H_0 = -\log a_{H^+} \frac{f_I}{f_{IH^+}} \qquad \{Ref.\ 2\}$$

where

$\qquad$ $\mathbf{H_0}$ $\quad$: is the Hammett Acidity function;

$\qquad$ $\mathbf{a_{H^+}}$ $\quad$: is the hydrogen ion activity of the surface acid;

$\qquad$ $\mathbf{f_I}$ $\quad$: activity coefficient of indicator in basic form;

$\qquad$ $\mathbf{f_{IH^+}}$ $\quad$: activity coefficient of indicator in conjugate acid form.

Benesi [51] reasoned that the Hammett acidity function could not be applied to Lewis acid sites since the relative strengths of generalised (Lewis) acids depend not only on the solvent medium but also on the particular base used for reference. Therefore indicator colour changes for Lewis acids on a solid surface could not be expressed in terms of a single H_0 function and each Lewis acid would have to be treated as an individual case. In spite of this however, most authors assume that proton and Lewis acid centres react in the same way with both proton and Lewis acid sites, and use the H_0 function for Lewis acid sites [37]. Benesi [51] also remarked that generally, only a small fraction of the catalyst surface is occupied by acid centres and so the colour of the acid form of the indicator must mask the colour of the basic form.

Later, Benesi [52] outlined a method for determining the number of acid sites on a solid acid. The method consisted of titrating a solid acid, suspended in benzene, with n-butylamine using an indicator. By using various indicators with different pK_a values a determination of the amount of acid at various acid strengths is possible [29]. The use of n-butylamine as a titrant is appropriate since it is not too volatile, and yet not too large a molecule to enter the small pores of the catalyst [17]. For all titrations using n-butylamine on solid surfaces it was assumed that both amine and indicator molecules attained adsorption equilibrium [52,29]. However it was found by Take et al. [53] that amine molecules approach surfaces irregularly and then remain, without reaching adsorption equilibrium, on the adsorption sites at which they first arrived. The authors concluded that under normal titration conditions, performed at room temperature with agitation, the indicator and amine are far from equilibrium and this can lead to overestimation of the acid content.

Another problem associated with amine titrations is the large size of indicator molecules which prevents them migrating into micro pores of porous materials [2,46]. This point however has been argued against by Barthomeuf [54] who asserts that only a small fraction of the acid sites must react with the indicator which is only a 'probe' of the acidity. In fact one indicator molecule in every ten cavities or less may be sufficient [54]. The author concludes by saying that even when pore size is small, acidity is still titratable, at least partly, as long as the base enters the pores [54]. It would seem therefore that the size of the basic molecule is more critical than that of the indicator. There can also be problems recognising colour changes of indicators with the naked eye [46] since the acidic centres only occupy a small, fraction of the total catalyst surface [51]. Also, the indicator concentration has to be maintained low so that only a small fraction of the acid sites react with the indicator while the majority are neutralised by the basic titrant molecules. The amine method makes it difficult to measure surface acidity on coloured or dark samples but this shortfall can be minimised by mixing a white substance of known acidity with the sample [29].

A comparison of the calorimetric titration method with the amine titration method for the determination of acid strength on solid catalysts has been made by Taniguchi et al. [46]. They found that if one ammonia molecule is adsorbed on one acid site, one butylamine molecule seems to occupy about two sites. This is interesting when it is considered that the cross sectional area of an ammonia molecule is $16\mathring{A}^2$ and that of a butylamine molecule is $32\mathring{A}^2$ [46]. Also the authors [46] found that adsorption equilibrium of ammonia was attained within one or two hours which is much faster than for butylamine which according to Take et al. [53] had not achieved adsorption equilibrium after twenty five days. However, Tamale [17] states that the adsorption of ammonia on catalysts is a very complex phenomenon since besides chemisorption, physical adsorption and capillary condensation may occur simultaneously.

Maciver et al. [45] noted that apart from textural differences the most obvious difference between the η- and γ-Al_2O_3 was that after removal of any weakly bound, physically adsorbed water by evacuation at $25^{\circ}C$, γ-Al_2O_3 contained 7% water as compared to 4.5%wt. in the case of η-Al_2O_3. Most of this 3.5% 'excess' water could be desorbed by heating below $300^{\circ}C$. The authors [45] found that the acidity of η-Al_2O_3 increased continually with dehydration temperatures up to $500^{\circ}C$ while γ-Al_2O_3 did not develop appreciable acidity until 200–$300^{\circ}C$ at which point the excess water was eliminated. The water content for η-Al_2O_3 can be accounted for on the basis of surface hydroxyl groups while it is suggested that the 'excess' water of γ-Al_2O_3 may exist as molecular water strongly bound to the surface [45]. It has been shown by Peri et al. [21] that Al_2O_3 may contain several types of surface hydroxyl groups of varying degrees of polarity. The more polar types predominate on γ-Al_2O_3 as opposed to η-Al_2O_3 and these strongly polar groups may be responsible for the adsorption of 'excess' water on γ-Al_2O_3 [45]. The second major difference detected between η- and γ-Al_2O_3 was that while total acidity, as measured by ammonia adsorption, was about the same in both cases, the average strength of the acid sites was greatest for η-Al_2O_3 [45]. Also as the temperature of dehydration is increased the acid strength distribution of the two aluminas change relative to each other. The authors [45] suggest that some of the

observed differences in ammonia adsorption of the two aluminas may be due to the fact that the surface of η-Al_2O_3 is mainly formed by the (110) plane. In conclusion it is stated that not only the texture but also the basic surface chemistry of Al_2O_3 is to some extent a function of the structure or 'form' of the Al_2O_3 [45].

Table 1.4 summarises the main methods reviewed to determine the acidity of metal oxides.

Table 1.4 Summary of Techniques used to determine acidity of metal oxides

Technique	Ref.	Sample used	Description
Infrared of adsorbed NH_3	35	γ-Al_2O_3	NH_3 chemisorbed immobily on γ-Al_2O_3 predried at 800°C which shows the presence of acid sites
Infrared of adsorbed NH_3	37	oxide type not specified	Position of adsorbed NH_3 band can be related to acid strength of adsorption centres i.e. higher the acid strength of the surface the greater is the shift of the IR band to lower frequencies.
Measure amount of adsorbed NH_3 by drop in pressure	36	alumina, silica/alumina, silica.	Volume of gas adsorbed is measured as a function of the temperature, a relationship which depends on the strength of the bond between the NH_3 molecule and the catalyst active site.
Infrared of adsorbed pyridine	38	η-Al_2O_3	Strong acid sites are of Lewis type and no Brönsted sites detected
Infrared of n-butylamine	39	Silica/alumina η-Al_2O_3	Aprotic acid sites detected and Brönsted acid sites detected on η-Al_2O_3 containing a large amount of water, possibly physisorbed.
Infrared of oxide suspended in basic solution	40	silica, magnesia, phosphorous, Boron, silica/alumina	When hydroxyl containing compound is placed in solution, OH band shifts to lower frequencies which is a direct function of OH acidity and basicity of solvent.
NMR of deuterated pyridine on surface	41	aluminas (transition)	Under certain conditions the pyridium ion formed when a deuterated pyridine molecule reacts with a Brönsted acid site can be quantitatively measured with proton NMR.
^{13}C NMR of aniline & N,N-diethylaniline on oxide surface	42	silica silica/alumina alumina	Relatively large chemical shifts occur upon protonation of aromatic and heterocyclic amines in aqueous solution which can be measured using ^{13}C NMR
UV spectra of substituted pyridines on oxides	43	η-Al_2O_3	The π-π transitions of substituted pyridines appear to be slightly shifted towards longer wavelengths after adsorption on alumina compared with their position in the liquid phase
Microcalorimetry	44,45, 46,47, 48	η-Al_2O_3 γ-Al_2O_3	The interaction of an acid centre with a basic molecule is accompanied by heat evolution which is directly related to the strength of the acid centre
DSC of adsorbed triethylamine	49	metal impregnated γ-Al_2O_3	Chart containing peaks is obtained where the position of these peaks distinguish acid strength
Titrimetry	22,29, 51,52, 37	alumina silica silica/alumina	Metal oxides are suspended in solvent and titrated with suitable acids/bases, the end point being determined by indicator colour change

1.1.5 Basicity of alumina.

Alumina is typically considered an acid catalyst and therefore much less information is available in the literature on its basicity [55]. As has been stated in section 1.1.4, the surface OH group on Al_2O_3 will behave like a hydroxide ion when the negative charge density on it is high. Therefore type Ia and type Ib co-ordinated OH groups will possess most hydroxide character, Table 1.1.

On oxide surfaces the species responsible for the basic properties are hydroxyl groups and oxygen ions [37]. The surface hydroxyl group can have acidic, basic or neutral character [27,30] depending on its polarisation as a result of being bonded to a metal cation and its proximity to other (a) hydroxyl groups, (b) exposed oxygen atoms and (c) cation and anion vacancies. The co-ordination number of the metal atom and neighbouring oxygen atoms can also affect the properties of the hydroxyl group. Malinowski et al. [37] state that oxygen ions on metal oxide surfaces such as Al_2O_3 can be in different co-ordination depending on their position on the surface and on their position in the vicinity of a cation vacancy. The level of Lewis basicity due to the oxygen ions varies with the co-ordination number of the oxygen. Che et al. [56] have noted that the reason for this is that the ionisation potential of oxygen changes with co-ordination number. Oxygen in low co-ordination has the lowest ionisation potential and hence strong Lewis basicity.

Tanabe et al. [29] define the basic strength of a solid surface as its ability to convert an adsorbed electrically neutral acid to its conjugate base i.e. the ability of the surface to donate an electron pair to an adsorbed acid.

Scokart et al. [57] have investigated the frequency shift of the NH stretching mode of pyrrole adsorbed on Al_2O_3 surfaces. This shift in frequency was considered by Pearson [41] as a measure of the basicity of the H−bond acceptor site on the surface with low NH stretching wavenumbers indicating a strong H bond

and consequently strong basic sites on the surface. Results from this analysis showed wavenumbers for Al_2O_3 which were similar to those of pyridine suggesting that their basic strengths are comparable. The usefulness of this technique is limited by the fact that surface OH and surface O^- groups are not distinguishable. Strong basic sites were found on both η- and γ-Al_2O_3 with no clear difference detected between the two.

In order to distinguish between the two types of basic sites Paukshits et al. [58] have proposed the use of deuterochloroform as a probe with the position of the C–D stretching band being considered as a measure of the base strength. When $CDCl_3$ was adsorbed onto Al_2O_3, which had been calcined at $450^{\circ}C$ for one hour, infrared bands in the region 2210–$2220cm^{-1}$ and 2245–$2250cm^{-1}$ were detected [58]. Paukshits et al. [58] associated the band between 2245 and $2250cm^{-1}$ with weak basic sites (considered to be surface O^- species). The basic strength of Al_2O_3 was found to be no more than +7 i.e. ($pK_a = +7$) [58].

In the previous section (1.1.4) the use of indicators for acid strength determination was reviewed. A similar technique can be used to determine the basic strength of solid bases [29]. When an electrically neutral acid indicator is adsorbed on a solid base from a nonpolar solution, the colour of the acid indicator is changed to that of its conjugate base if the solid has the necessary basic strength to impart electron pairs to the acid [29]. By using a suitable selection of acid indicators the basic strength over a wide range of $pK_a = pK_{BH}$ can be calculated.

The reaction of an acid indicator BH with a solid base ($\bar{B}$) is

$$BH + \bar{B} \rightleftharpoons B^- + \bar{B}H^+ \qquad \textit{\{Ref. 29\}}$$

and the basic strength H_o of $\bar{B}$ is given by the following equation

$$H_o = pK_a (= pK_{BH}) + \log_{10} \frac{[B^-]}{[BH]} \qquad \textit{\{Ref. 29\}}$$

where

[BH] : concentration of acidic form of indicator;

[B⁻] : concentration of basic form of indicator.

The number of basic sites on a solid can be measured by suspending the solid, on which an indicator has been adsorbed in its conjugate basic form, in benzene and titrating with benzoic acid dissolved in benzene. This gives a measure of the number of basic sites having a basic strength corresponding to the pK_{BH} value of the indicator used [59].

Conventionally acid strength (H_o) was expressed by the pK_a values of the conjugate acids of basic indicators, while basic strength (H_o) was expressed by the pK_a values of acidic indicators [29]. The indicators used for both determinations were different so it was not possible to determine the acid–base strength on a common scale. In 1975 Yamanaka et al. [60] presented a method which allowed both acidic and basic properties to be determined on a common H_o scale. On this scale the strength of basic sites is expressed by the H_o of the conjugate acidic sites. The technique involves adding a Hammett basic indicator to a solid suspended in benzene. If the solid has no acid sites for which $H_o \leq pK_{IH^+}$, the colour of the basic indicator does not change. A standard Brönsted acid in benzene is then added gradually until the colour of the indicator changes to that of its conjugate acid which defines the end-point. At the end-point, acid strength H_o of the resultant solid, which was formed by the addition of Brönsted acid to the original solid, is equal to the pK_{BH^+} of the indicator used. The volumes of standard Brönsted acid required for neutralisation give a measure of the number of basic sites (basicity) on the surface [29]. Thus, 'basic strength H_o' of basic sites is defined as the acid strength, H_o, of conjugate acids of the basic sites [60]. It is worth noting however that this technique of measuring basicity, when the basic strength H_o is equal to or greater than a pK_{BH^+} value, is only possible when there are no acid sites present whose acid strength is equal to or less than the same pK_{BH^+} value [60].

The adsorption of gaseous acids, which is based on the same principle as that of the gaseous base adsorption method mentioned in 1.1.4 can be

used for the measurement of basic properties on solid acids [29]. Tanabe et al. [29] state that the amount of CO_2 irreversibly adsorbed is a good measure of the number of basic sites on solid surfaces. Auroux et al. [44] used the differential heat of CO_2 adsorption to characterise the basic properties of metal oxides including SiO_2 and Al_2O_3. This analysis assumes that the stronger the basic sites present the higher the temperature required to desorb CO_2 [29]. In conclusion Auroux et al. [44] stated that microcalorimetry using CO_2 could be used to gain information about the number, strength and distribution in strengths of basic sites. It is limited however in that no information is obtained about the nature of the sites [44].

Esumi et al. [61] has compared the basicity of Al_2O_3 determined by titration and electron acceptor adsorption. The theory behind the electron acceptor method is that when an electron acceptor with high electron affinity is adsorbed on the surface of metal oxides, the corresponding anion radicals are formed. These anion radicals are a result of electron transfer from electron donor sites i.e. basic sites, on the surface to the adsorbed electron acceptor. The titration method used was the one devised by Yamanaka et al. [60], already mentioned. Esumi et al. [61] report that the characteristics of basic sites estimated by the two methods are different due to the fact that basic sites estimated using the adsorption of electron acceptors are associated with Lewis sites while those estimated by titration are associated with Brönsted sites.

Vit et al. [62] have demonstrated that the basicity of Al_2O_3 is significantly influenced by calcination in air at temperatures up to $1000^{\circ}C$. A maximum in basic site concentration was observed after calcination at $500^{\circ}C$. In addition to this, calcination temperature was found to change the strength of basic sites on Al_2O_3. The basicity of Al_2O_3 was determined by measuring the rate of 2–(1–hydroxycyclohexyl)–cyclohexanone retroaldolisation to cyclohexanone which is a very fast and selective base catalysed reaction.

1.2 Silica

Unlike α-, γ- or η-Al_2O_3 silica is amorphous [16]. It is used extensively as a catalyst support and here its behaviour as a support will be reviewed.

1.2.1 Formation of silica

In 1940 Carman [62] proposed that formation of silica gel occurred in three stages. In the first stage silic acid [$Si(OH)_4$] condenses to form colloidal particles of silica. The silic acid is usually formed by mixing an acid with a solution of 'water glass' which consists mostly of orthosilicates (Na_4SiO_4) and metasilicates (Na_2SiO_3) [3]. The second stage consists of growth of particles and depends on the concentration of the silica [63]. In dilute solution, a slow increase in particle size occurs but at a concentration of about one percent silica the colloidal particles are able to condense together to form an ill-defined polymer where the primary bonds are of the siloxane type (Si – O – Si). The final stage in the formation of silica gel involves linking of particles into branched chains, then networks, which finally extend throughout the liquid medium and thicken it to a gel. This polymerisation is believed to be due to the condensation of silanol groups and occur as follows [63]

$$-SiOH + HOSi - \; = \; - SiOSi - + H_2O$$

Iler [63] outlines diagramatically the polymerisation process as shown in Fig. 1.21. The first step in the polymerisation involves conversion from a monomer to a dimer and occurs when a solution of monomer, $Si(OH)_4$, is formed at a concentration greater than about 100–200ppm. When the concentration of SiO_2 is greater than the solubility of the solid phase of amorphous silica and there is no solid phase present the monomer polymerises by condensation to form dimers and higher molecular weight species of silic acid. In the second step, polymerisation by condensation leads to ring structures since silicic acid has a strong tendency to polymerise in such

45

a way that there is a maximum of siloxane bonds and a minimum of SiOH groups. The ring structures link together to form large three dimensional molecules which condense internally to the most compact state with SiOH groups on the outside. This results in the formation of spherical units which form the larger particles in step 3. Since the small particles are more soluble than larger ones and since not all the three dimensional particles are the same size, the particles grow in average size and diminish in number as the smaller ones dissolve and the silica is deposited upon the larger ones [63]. The early stages in polymerisation have been studied by Vysotskii et al. [64]. Particle growth processes for silica in an aqueous system occurs by two processes. In the first process there is growth of particles from silic acid, present in the solution from the moment of its preparation. The second stage consists of further growth of larger particles by desorption of silic acid dissolving from the smaller particles. This method is in good agreement with that proposed by Carman [62].

Fig. 1.21 *{Ref. 63}*   Polymerisation of silica to silica gel.
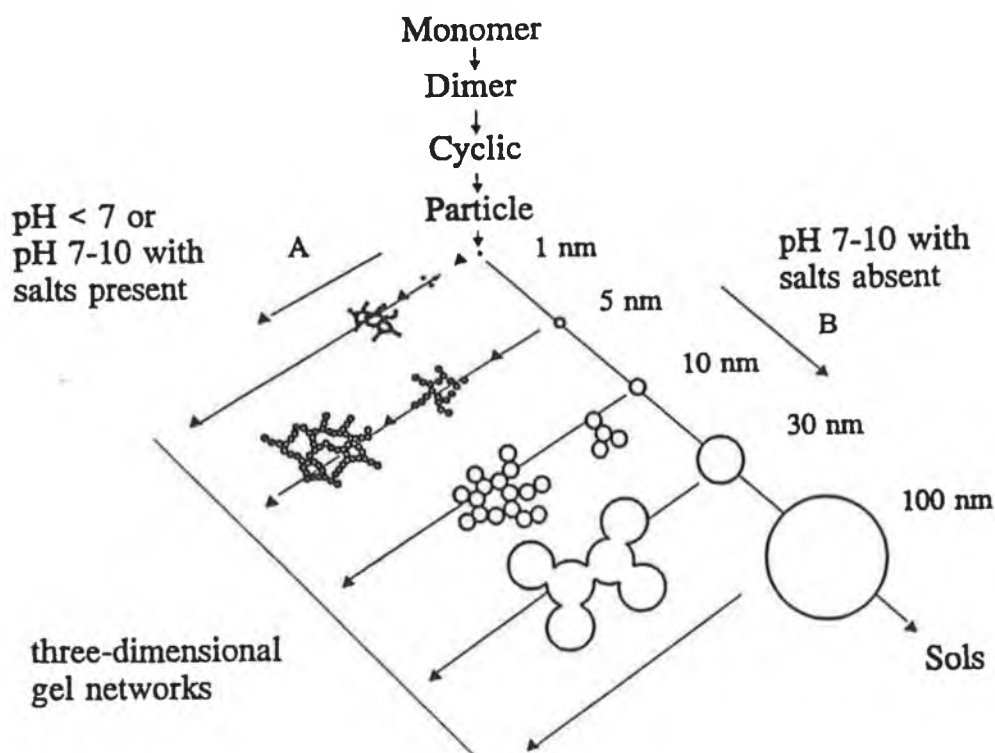
Unlike other metal oxides the process of aggregation and gelling in the silica system is unique because the solid phase remains completely amorphous, appreciably soluble in water and is generally in solubility equilibrium with the monomer [63].

By controlling the reaction for formation of silica gel it is possible to produce silica gel with surface areas as high as $700m^2/g$ [3]. These high area silicas, however, only contain micropores which can lead to diffusion problems. The manufacturing and ageing procedures can be varied to produce silica gels with higher pore diameters and correspondingly lower surface areas.

1.2.2 Surface chemistry of silica.

Iler [63] quotes Kiselev as having said in 1936 that the surface of silica gel is covered by OH groups bound to the SiO_2 skeleton. Four years later Carman [62] discovered that water adds to the surface of anhydrous SiO_2, to create silanol groups (SiOH). As the surface of amorphous silica is not an exactly geometrical arrangement, the OH groups attached to the silicon atoms will not be equal distance from each other as shown in Fig. 1.22 [63]. Therefore the OH groups are not all equivalent.

Fig. 1.22 *{Ref. 63}* Postulated types of hydroxyl groups on the surface of amorphous silica.
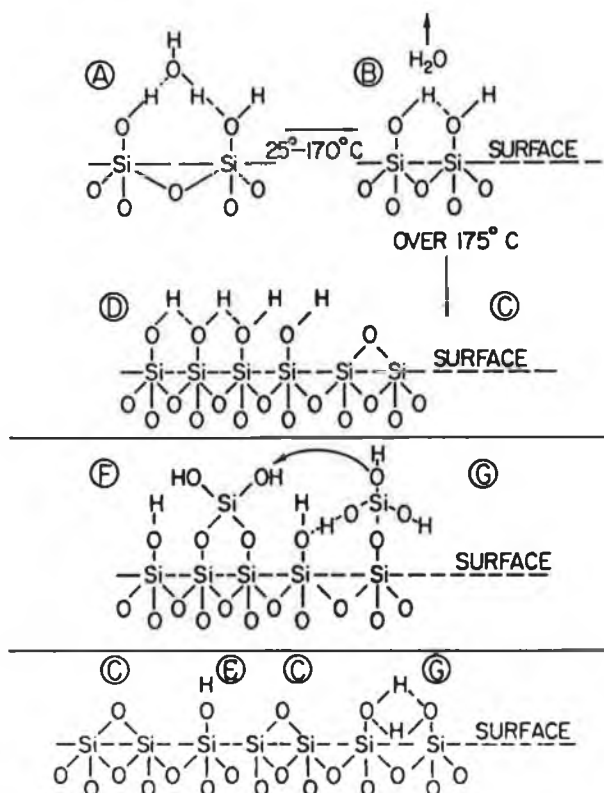
A : Vicinal hydrated

B : Vicinal anhydrous

C : Siloxane – dehydrated

D : Hydroxylated surface

E : Isolated

F : Geminal

G : Vicinal, hydrogen bonded

Note : F and G types probably do not actually exist on a dried surface.

In aqueous solution more monosilic acid molecules may condense on the surface to give attached silicon atoms with two or even three attached hydroxyl groups as represented by F and G in Fig. 1.22. These groups most likely condense further leaving only SiOH groups on the dried surface [63]. Also hydrogen-bonded water molecules found on silica which has been in water can be removed by heating to $150^{\circ}C$ in air.

The number of OH groups on silica formed in water can be affected in several ways as outlined in Fig. 1.23 [63].

Fig. 1.23 *{Ref. 63}* Factors affecting the number of hydroxyl(silanol) groups in and on a silica particle formed in water
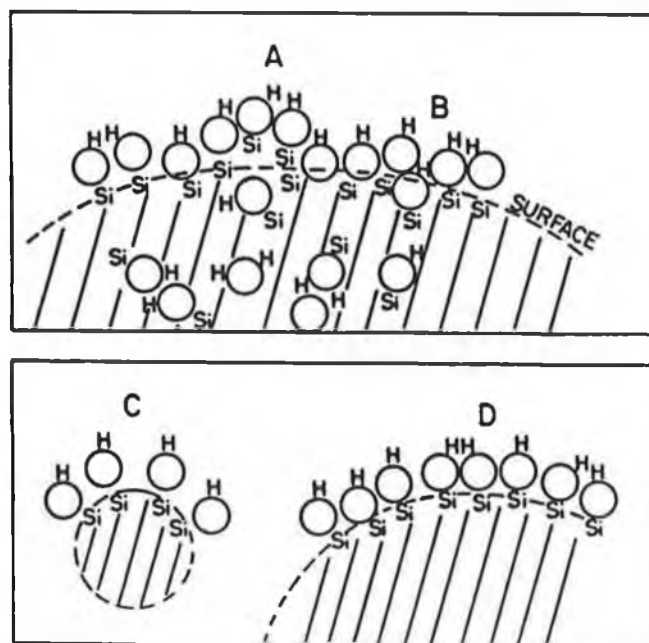
Some SiOH groups are below the surface of the siloxane network. These give rise to distortions at the surface and may require high temperature to be removed (Fig 1.23 (A)). In the case of B (Fig. 1.23) the SiOH groups are located within the surface and increase the average packing density of OH groups per unit surface area. If the particles have a small radius then the convex surface tends to hold SiOH groups further apart. This means that fewer hydrogen bonds can form between them and so

49

they are more easily removed at high temperatures i.e. C as compared to D (Fig. 1.23). This phenomena also occurs in concave areas such as micropores where the surface OH groups are brought closer together due to the curvature and consequently dehydration is more difficult [63].

It has been demonstrated by Brunauer et al. [71] that small particles of SiO_2 (e.g. diameter 3.7nm) are surface dehydrated at lower temperature than larger ones (e.g. diameter 6.4nm). This result was confirmed by Whalen [72] who found that silica with an area of $330m^2g^{-1}$ held 7 OH/nm^2 at 110°C and one with $650m^2g^{-1}$ held 5.5 OH/nm^2. The effect of particle size where the radius of curvature is positive and of pore diameter where it is negative can be seen in Fig. 1.24.

Fig. 1.24 *{Ref. 63}* Effect of curvature of the silica surface on dehydroxylation.
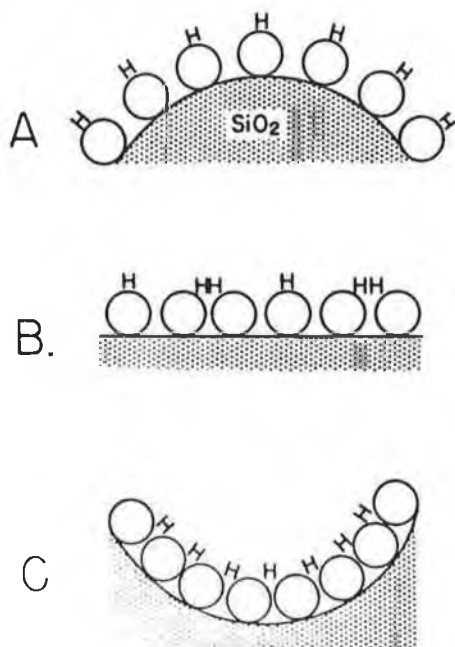
Surface hydroxyls are more tightly hydrogen bonded on large radius particles (B) due to the relatively flat surface and as such are more stable toward removal at high temperature. In small pores (diameter < 100Å) the curvature brings the silanol groups closer together (C) so there can be more mutual hydrogen bonding leading to greater stability [63]. On silica surfaces of small positive radius of curvature (A) there are fewer hydrogen bonds which makes it easiest to dehydroxylate.

In a study on the behaviour of water at the silica surface, Klier et al. [65] have shown that water sits 'oxygen down' on the SiOH groups, at least at the early stages of adsorption. This allows for hydrogen bonded clusters of H_2O molecules to be formed even before all the SiOH groups have adsorbed H_2O molecules to form $Si_sOH:OH_2$ groups. (Si_s represents a silicon atom at the surface). As a consequence of this, water on isolated SiOH groups is less strongly adsorbed than on top of other water molecules already adsorbed. Iler and Dalton [66] have used viscosity measurements to show that when colloidal particles of SiO_2 are in water and fully hydroxylated there is a monolayer of water molecules more or less immobilised on the SiOH surface by hydrogen bonding. Lange [67] claims that there are two types of adsorbed water on hydroxylated silica; the first which he refers to as 'physically adsorbed' is desorbed during drying at 25-105°C and the second type referred to as 'hydrogen bonded' is removed at 105-180°C.

Heating of hydroxylated silica not only removes adsorbed water but results in condensation of hydroxyl groups to form siloxane bonds and water is evolved [63]. This dehydration is a non-equilibrium process so the rate at which water is lost at any stage is a function of temperature and the concentration of remaining silanol groups. Above 170°C silanol groups start to condense and water is evolved. Just under half the hydroxyl groups have been removed at 400°C so that most of the remaining hydroxyl groups are still adjacent to one other. These hydroxyl groups can readily undergo rehydration at this stage by adsorbing water. At temperatures in excess of 400-450°C more hydroxyl groups are removed which leaves larger siloxane areas that are less readily rehydrated [70]. Thorp [70] has shown that at about 750°C only free unpaired SiOH groups are present at a concentration of 1.3 OHnm^{-2}. Curthoys et al. [68] have measured the concentration of residual SiOH groups in the 700 – 1000°C temperature range and the results obtained are presented in Table 1.5.

Table 1.5 *{Ref. 63}* Number of OH groups on surface of silica gel as it is heated

Temperature (^{o}C)	Number OH/nm^2
700	1.2
800	0.9
900	0.65
1000	0.4

With regard to rehydration Mc Donald [73] has shown by infrared spectroscopy that it most likely begins next to a free hydroxyl group on a highly dehydrated silica surface. The hydroxylated area grows in patches along the boundary between hydroxylated and siloxane areas [73].

Work by Shapiro et al. [74] and Trouton [75] suggests that the dehydrated silica surface is hydrophobic with the electrons of the strained siloxane oxygen not free to enter into hydrogen bond formation. Shapiro et al. [74] found that methyl red adsorbed on SiOH groups but not Si-O-Si while Trouton [75] discovered that water adsorbed readily on partially dehydrated silica but with great difficulty on highly hydrated silica.

1.3 Modification of acid/base properties of Al₂O₃ & SiO₂

The effect of ion addition on silica and Al_2O_3 has been widely studied. Since γ-Al_2O_3 is the most important carrier used in catalysis the vast majority of literature on modification of supports refers to work done on γ-Al_2O_3 in an attempt to stabilise it or modify its surface characteristics [76]. The reactions catalysed by Al_2O_3 such as dehydration of alcohols and skeletal isomerisation of cyclohexene are acid catalysed [22]. This would suggest that the addition of a substance to Al_2O_3 which affected its acidity may also affect its behaviour as a catalyst or a support material.

Pines et al. [22] found that Al_2O_3 impregnated with up to 1.5 wt.% Na using solutions of sodium hydroxide and sodium chloride had reduced activity for alcohol dehydration and olefin isomerisation compared to untreated Al_2O_3. The NaCl was adsorbed on strong acid sites. This was reflected in its higher poisoning efficiency for cyclohexane and also it increased the selectivity of Al_2O_3 for certain isomerisations. The authors [22] also concluded that at least for addition of NaCl the adsorption of Na ions was not due to ion exchange with protons on the surface,

$$Cat^- H^+ + Na^+ Cl^- \longrightarrow Cat^- Na^+ + H^+ Cl^- \qquad [22]$$

but occurred on incompletely co-ordinated aluminium ions at the surface (Lewis acid sites = −Al) as shown in Fig. 1.25. The reason for the more selective adsorption of NaCl as compared with NaOH may be a result of the lower basicity of the chloride anion relative to the hydroxide anion [22].

$$—Al + :\ddot{Cl}:^-Na^+ \longrightarrow [—Al—Cl]^-Na^+$$

$$—Al + :\ddot{O}:H^-Na^+ \longrightarrow [—Al—OH]^-Na^+$$

$$—Al\cdots O\!\!\begin{array}{c}{}^H\\{}_H\end{array} + Cl^-Na^+ \longrightarrow [—Al—Cl]^-Na^+H_2O$$
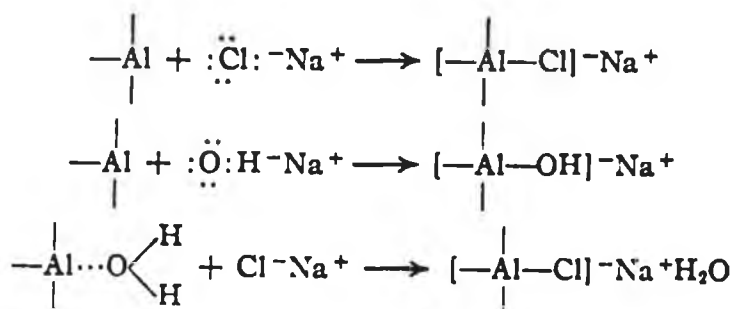
In their investigation into the effect of NaCl on the selectivity of γ-Al_2O_3 for the decomposition of ethyl alcohol, Ross et al. [77] discovered that the percentage ether formed increased with increase in catalyst Na content up to 2.87 wt.% while the percentage of ethyl alcohol decomposed to ethylene decreased. The authors [77] did not find any evidence for the acid/base surface complex postulated earlier by Pines et al. [22] but suggested that it was the Brönsted acid sites that were the alcohol dehydration initiation centres. If Na ions exchanged with protons from surface hydroxyl groups (Brönsted acid sites) then the decrease in total activity of the catalyst corresponding with an increase in sodium content can be explained by a fall in the concentration of these reaction initiation centres

Deo et al. [78] has used infrared spectroscopy to study the adsorption mechanism of 1–propanol at different temperatures on γ-Al_2O_3 (Fig. 1.26) and γ-Al_2O_3 doped with 2.0% NaOH (Fig. 1.27). The base line (Fig. 1.26) shows three broad bands at 3785, 3720 and 3680 cm^{-1} which are attributed to the three different types of surface hydroxyl groups reported by Peri et al. [21].

The spectrum for the NaOH treated γ-Al_2O_3 (Fig. 1.27, base line) shows only two well separated hydroxyl bands at 3740 and 3680cm^{-1}. Peri [10] has reported that the band at 3680cm^{-1} appears to be the more acidic of the three hydroxyl groups which makes the disappearance of the 3785cm^{-1} and not the more acidic 3680cm^{-1} band quite surprising. The disappearance suggests that NaOH reacts with the high frequency surface hydroxyls to form Al-O-Na [78]. It has

however been found by Paukshtis et al. [82] that the OH bands at 3680cm^{-1} and at 3785cm^{-1} decrease in intensity on Al$_2$O$_3$ doped with 3% NaOH.

Fig. 1.26 *{Ref. 78}* 1-Propanol on γ-Al$_2$O$_3$. Heated in 1cm of PrOH at T° for 1hr and pumped off at T° for 1 hr.
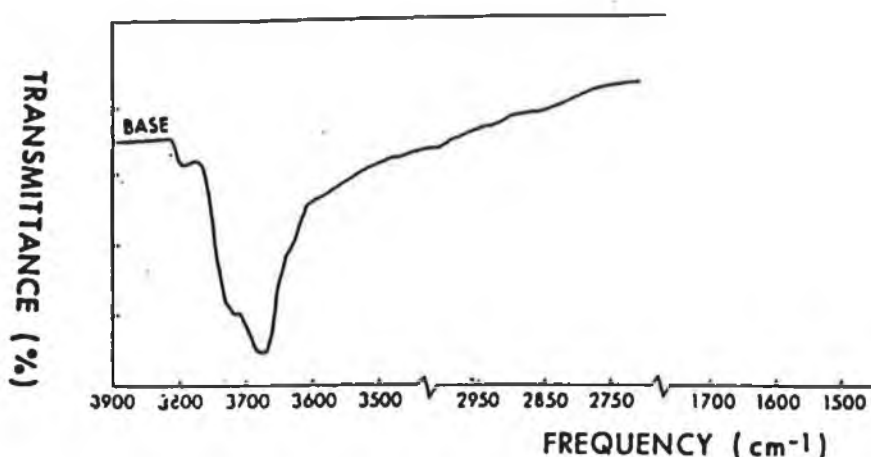
Fig. 1.27 *{Ref. 78}* 1-Propanol on NaOH treated γ-Al$_2$O$_3$. Heated in 1 cm^3 of PrOH for 1 hr. and pumped off at T° for 1 hr.
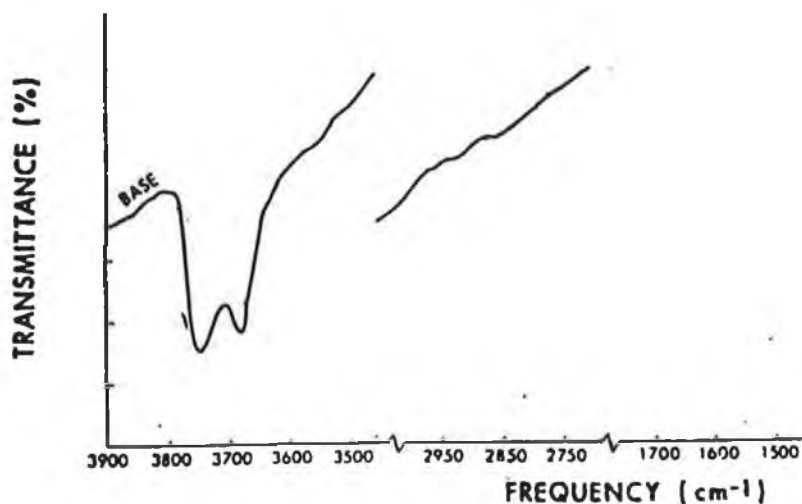
Based on their results, Deo et al. [78] suggested that the surface hydroxyl groups compete successfully with the aluminium ions as active sites for the dehydration of 1-propanol. When this tendency is suppressed by doping with NaOH, the main reaction involves aluminium ions and so dehydrogenation reactions become dominant. The NaOH itself does not appear to take part in the dehydration of 1-

propanol but suppresses one type of active site on the γ-Al$_2$O$_3$ and leaves the other unaffected.

The catalytic activity and selectivity of γ-Al$_2$O$_3$ doped with increasing amounts of NaOH up to 15 wt.%, has been studied by Chuang & Dalla Lana [79]. Using pyridine adsorption, they showed that only the two Brönsted-acid sites (hydroxyl groups) with bands at 3680cm^{-1} and 3785cm^{-1} could be doped with NaOH and not the Lewis-acid sites (aluminium ions). This disagrees with the reaction between a Lewis acid site and NaOH proposed by Pines et al. [22] (Fig. 1.25). It was also pointed out by Chuang et al. [79] that if Brönsted acid strength is considered in terms of reactivity with NaOH solutions then it is the 3785cm^{-1} band which is most acidic as opposed to the 3680cm^{-1} band which was considered most acidic by Peri [10]. For the dehydration of secondary alcohols the authors [79] found that aluminium ion sites do not compete favourably with the hydroxyl sites for reactant molecules. However, when the 3785cm^{-1} hydroxyl sites are doped with adequate amounts of NaOH the aluminium ion sites do compete with the remaining 3680cm^{-1} hydroxyl sites. The saturation level for doping of Brönsted acid sites on γ-Al$_2$O$_3$ was found to correspond to an NaOH content slightly in excess of 5 wt.% [79].

Fledorow & Dalla Lana [80] have studied the effect of 2 and 5 wt.% additions of NaOH and LiOH on the Lewis-acid centres of Al$_2$O$_3$. Their technique involved the IR of γ-picoline whose adsorption, under appropriate conditions, on Al$_2$O$_3$ is confined to Lewis-acid sites. Results showed that the elimination of Lewis-acid centres by reaction with LiOH is almost linear up to 0.7 wt.% Li. Much less NaOH was required to remove an equivalent number of moles of surface hydroxyls. If a stoichiometric relationship exists between Li ions and Lewis-acid centres, then the greater interaction seen between Na ions and Lewis-acid centres probably involves an additional mechanism for eliminating Lewis-acid sites, possibly steric [80]. When only one fully accessible type of Al^{3+} surface cation is considered the poisoning with LiOH can be represented as shown in Fig. 1.28.

Fig. 1.28   *{Ref. 80}*   Poisoning of Lewis acid sites on Al_2O_3 with LiOH.
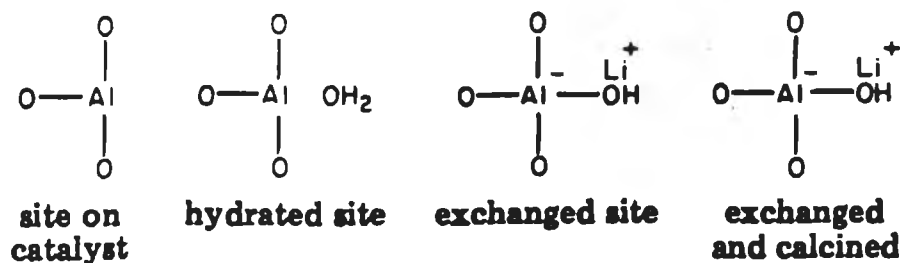
The authors [80] conclude from their results that the addition of metal alkali hydroxides to Al_2O_3 eliminates Lewis acid centres.

Introduction of sodium at concentrations as low as 0.03 wt.% decreased both the strength and number of acid sites (especially strong Lewis acid sites) on γ-Al_2O_3 while increasing the concentration of Na from 0.03 to 0.10 wt.% only marginally decreased the number of Lewis acid sites. It was also proposed by Saad et al. [84] that the 0.03 wt.% Na^+ ions are localised in the cation vacancies of the defect spinel structure of Al_2O_3. Contescu et al. [88] agree with Saad et al. [84] regarding the incorporation of Na^+ ions into the vacant cationic positions in or near the surface of γ-Al_2O_3. While it can be argued that Na^+ (ionic radius 0.98Å) being twice as big as Al^{3+} (ionic radius 0.45Å) is to big to fit into the spinel lattice, the near surface can undergo distortions which would be unlikely in the bulk [88].

The results of Fledorow et al. [80] and Saad et al. [84] conflict with those obtained by Chuang et al. [79]. A possible solution to these conflicting views is offered by Marczewski et al. [81]. They found that NaOH can both decrease and increase the acidity of Al_2O_3 depending on the concentration. With increasing NaOH content up to 0.8 wt.% the strong Lewis acid centres increased in number and for the weaker acid centres there was a maximum in acidity at 4 wt.% NaOH. After 4 wt.% NaOH there was a continuous decrease of surface acidity with complete disappearance at 40 wt.% NaOH. Since Chuang et al. [79] did not exceed 15 wt.% NaOH on their Al_2O_3 samples it would suggest that higher concentrations are required before the Lewis acid sites are eliminated.

Addition of Na^+ to Al_2O_3 can affect the basicity as well as the acidity. Saad et al. [84] suggested that small amounts of sodium poison acid sites, in particular the strongest ones, while in larger quantities sodium could create new basic sites. Paukshtis et al. [82] found that Na^+ led to an increase in concentration and strength of strong basic centres with a consequent decrease in concentration of weak basic centres. The authors [82] concluded that the presence of sodium ions in Al_2O_3 changes the strength of aprotic centres due to the effect of the sodium ions oxygen atoms which in turn affect the properties of Al^{3+} ions.

γ-Al_2O_3 in aqueous suspensions can be treated as a diprotic acid as shown in Fig. 1.29 [83].

Fig. 1.29 *{Ref. 82}* γ-Al_2O_3 in an aqueous solution

$$\overline{Al}OH_2^+ \xrightleftharpoons{K_1^{int}} \overline{Al}OH + H^+_{(s)}$$
$$\quad (I) \qquad\qquad (II)$$

$$\overline{Al}OH \xrightleftharpoons{K_2^{int}} \overline{Al}O^- + H^+_{(s)}$$
$$\qquad\qquad (III)$$

$$H^+_{(s)} \rightleftharpoons H^+$$
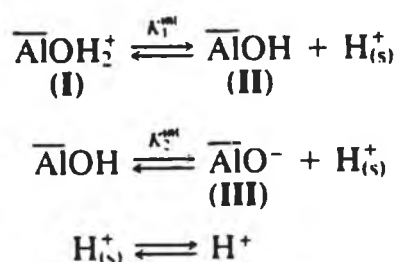
$$\overline{Al} : \text{Surface } Al_2O_3$$

From the equilibria in Fig. 1.29 Vordonis et al. [76] proposed that the relative concentration of I, II, and III depend on the pH of the impregnating solution. The authors [76] found that doping γ-Al_2O_3 with 0.2 wt.% sodium ions using aqueous solutions of $NaNO_3$, caused a large increase in concentration of the diprotic acid $\overline{Al}OH_2^+$, in the pH region 5-8. The Na^+ doping also resulted in a disappearance of the negative surface groups (basic sites) in this region. Since only low concentrations of sodium were required, this agrees well with the results obtained by Fledorow et al. [80]. A practical consequence of the sodium doping mentioned is that the pH range in which γ-Al_2O_3 can adsorb negatively charged species is

extended from pH 1–5 to pH 1–9 [76]. This allows for the selective adsorption of negative species.

Fledorow et al. [80] state that the type of alkali metal involved can affect the stoichiometric equivalence of alkali : Lewis-acid centres which suggests that steric factors may be involved for alkali metals with radii larger than that of Li. The ionic radii of Na, Li and Al ions are 0.97Å, 0.68Å and 0.45Å respectively so an NaOH-Lewis-acid interaction may be able to block access of probe or reactant molecules to adjacent Lewis-acid centres also.

Shen et al. [85] have studied the acid/base properties of γ-Al_2O_3 modified by K^+ oxide, Mg^{2+} oxide and La^{3+} oxide. The atomic radius of K (1.52Å) is larger than for Li or Na. Addition of the metal oxides at loadings of 0.43 wt.% K, 1.53 wt.% La and 0.26 wt.% Mg caused a decrease in the number of strong acid sites and an increase in the number of intermediate strength acid sites. Above 0.78 wt.% K^+, 2.78 wt.% La^{3+}, and 0.48 wt.% Mg^{2+} the number of sites having intermediate strength decreases with increasing amounts of the metals. This would suggest that the addition of basic metal oxides first converts the strong acid sites on γ-Al_2O_3 to sites of intermediate strength, followed by neutralisation of the sites having intermediate strength and formation of weak acid sites. The authors [85] found that γ-Al_2O_3 had few strong basic sites and a relatively larger number of intermediate and weak basic sites for CO_2 adsorption. A large increase in all basic sites was observed with the addition of 11.7 wt.% K^+, 41.7 wt.% La^{3+} and 7.2 wt.% Mg^{2+}, but low loadings of Na^+ and Mg^{2+} oxides were not effective in generating strong basic sites [85]. The authors [85] state that this is because the oxides act to neutralise strong acid sites at low loadings. In conclusion they say that the effectiveness of basic metal oxides at neutralising acid sites and generating basic sites on Al_2O_3 can be related to the electronegativities of the three oxides.

Berteau et al. [86] also found that Na^+ and Mg^{2+} increased the number of weak basic sites, created a certain number of intermediate basic sites and increased the overall basicity. They did not detect an increase in the number of

strong basic sites using concentrations of 1.0 wt.% and 0.2 wt.% Mg and Na respectively [86].

Results by Malinowski [87] on addition of NaOH to Al_2O_3 showed that addition of 0.58 wt.% Na^+ brought about small changes in the number of basic centres and their basicity while addition of 5.75 wt.% Na decreased the number of strong acidic centres while the number of low acidity centres increased considerably and the number of basic centres increased slightly. These findings again appear to add validity to the theory of Shen et al. [85] which stipulates that basic oxides at low loadings act to neutralise strong acid sites.

The effect of electronegative ion addition on the acid/base characteristics of Al_2O_3 have also been examined. Contescu et al. [88] have studied the effect of doping Al_2O_3 with F^- on the proton affinity distribution (PAD) of surface hydroxyls at the Al_2O_3/water interface. They found that doping with F^- at levels below 1% caused replacement of terminal −OH by F^- which has an inductive effect on neighbouring hydroxyls, pulling electron density off the H and hence increasing its acidity. At higher F^- content (2–4%) it was found that F^- replaces −OH in a 1:1 stoichiometry giving a new phase of fluoride. Corma et al. [89] have found that doping of γ-Al_2O_3 with fluorine affected both Lewis and Brönsted acid centres. Fluorine addition resulted in a decrease in total number of Lewis acid sites per square meter while the number of those with strong acidity reached a maximum for samples with 2–4% fluorine content. In the case of Brönsted sites their total number increased with fluorine content and again the number of them with strong acidity reached a maximum with 2–4% fluorine content [89].

Addition of F^- to γ-Al_2O_3 increased Lewis acidity and produced a small increase in the concentration of Brönsted sites [95] which agrees with the results obtained by Corma et al. [89].

Garbowski et al. [90] investigated the effect of Cl^- (from CCl_4) on γ-Al_2O_3 for isomerisation of n-butane. Results showed that the chlorinated

Al$_2$O$_3$ was a very active isomerisation catalyst compared to the untreated γ-Al$_2$O$_3$, on which no isomerisation was detected. During the surface chlorination process one atom of oxygen is removed from the surface and replaced by two atoms of chlorine. In a later study, Melchor et al. [92] investigated the isomerisation of n-butane on γ-Al$_2$O$_3$ that had been modified by Cl from CCl$_4$ and HCl. The HCl treated Al$_2$O$_3$ had a greater number of stronger Lewis acid sites but activity was not substantially enhanced. This suggests that the strength of sites is not sufficient to account for activity and there seems to be other factors that affect activity of the sites [91]. The Al$_2$O$_3$ chlorinated by CCl$_4$ was more active than Al$_2$O$_3$ chlorinated with HCl although the number of Lewis acid sites were similar for both. Adsorption of mineral acids on Al$_2$O$_3$ is usually described in terms of the equivalent exchange of aqueous electrolytes with H$^+$ and OH$^-$ ions at the surface [94]. The occurrence of a charged or neutral surface has been attributed by Jacimovic et al. [93] to the formation of metal-aquo complexes of the type shown in Fig. 1.30.

Fig. 1.30 *{Ref. 93}* Adsorption of mineral acids on Al$_2$O$_3$.

$$[Al(H_2O)_2OH]^+ \underset{(pH<7.0)}{\overset{H^+A^-}{\rightleftharpoons}} [-Al(H_2O)(OH)_2]^0 \underset{(pH>7.0)}{\overset{B^+OH^-}{\rightleftharpoons}}$$

$$[-Al(H_2O)(OH)O]^- + H_2O$$

Impregnation of silica with alkali metal hydroxides can lead to surface modification [96]. The method most commonly used for the deposition of an alkali metal ion on silica is saturation of the silica with an aqueous solution of the alkali metal hydroxide followed by calcination at different temperatures. Using sodium as an example, the first step is the gradual exchange between sodium cations and protons of the OH groups on the surface of silica leaving −ONa groups on the surface. Simultaneously, hydrolysis of Si-O-Si takes place which gives new OH groups with different properties. This in turn leads to new −ONa groups being generated and so a 'chain reaction' is set up [96]. Melchor et al. [92] found that, unlike Al$_2$O$_3$, silica could not be chlorinated by CCl$_4$ due to the relatively inert

nature of its hydroxyl groups. They did however find, using infrared spectroscopy, that AlCl$_3$ reacted with the surface hydroxyl groups of silica.

1.4 Coking

This section will examine how the structure and surface chemistry of silica and Al_2O_3 can lead to the production of carbonaceous residues, referred to as 'coke', on the surface. Coke formation on metals and supported metal catalysts will also be reviewed. The word coke is used to describe all carbonaceous deposits formed on heterogeneous catalysts even though the nature of these deposits can vary greatly depending on their chemistry of formation [97].

In their review of catalyst deactivation by coking, Wolf et al. [97] use the term '*deactivation*' to define the phenomenon whereby activity of a catalyst decreases due to the interaction of carbon-containing molecules with active sites. Many petrochemical and petroleum refining processes are accompanied by side reactions leading to coke, which affects the catalyst activity and selectivity [153]. Coke can vary in structure from hydrogen-deficient aromatic type polymers to graphitic carbon and may be found in amounts of up to 20 wt.% whenever carbon-containing feeds are exposed to catalytic surfaces [97]. Formation of coke is an important reaction because it can accumulate on the catalyst, plugging the support porosity and may lead to catalyst inactivity [98]. Coking from hydrocarbons can occur on both acid and metal sites and each type will be reviewed.

1.4.1 Formation of coke

Coking has been defined as 'a balance between coke formation and removal which depends on the operating conditions and on the natures of the catalyst, gases present and coke formed' [125]. The coke or carbonaceous deposits can consist of high molecular weight polycyclic aromatics and carbon. The routes to coke formation are outlined in Fig. 1.31 [125].

Fig. 1.31 *{Ref. 125}* Routes to coke formation. Gasification of coke or intermediates leading to coke can take place at any point.

(i) Gas phase free radical intermediates → Gas phase tars / Gas phase carbon

(ii) Surface

Feed Hydrocarbons or impurities → Surface intermediates → Non-catalytic surface tars / surface carbon

Catalytic surface → Catalytic intermediates → Catalytic carbon

(iii)

Gas phase intermediates, may be free radicals
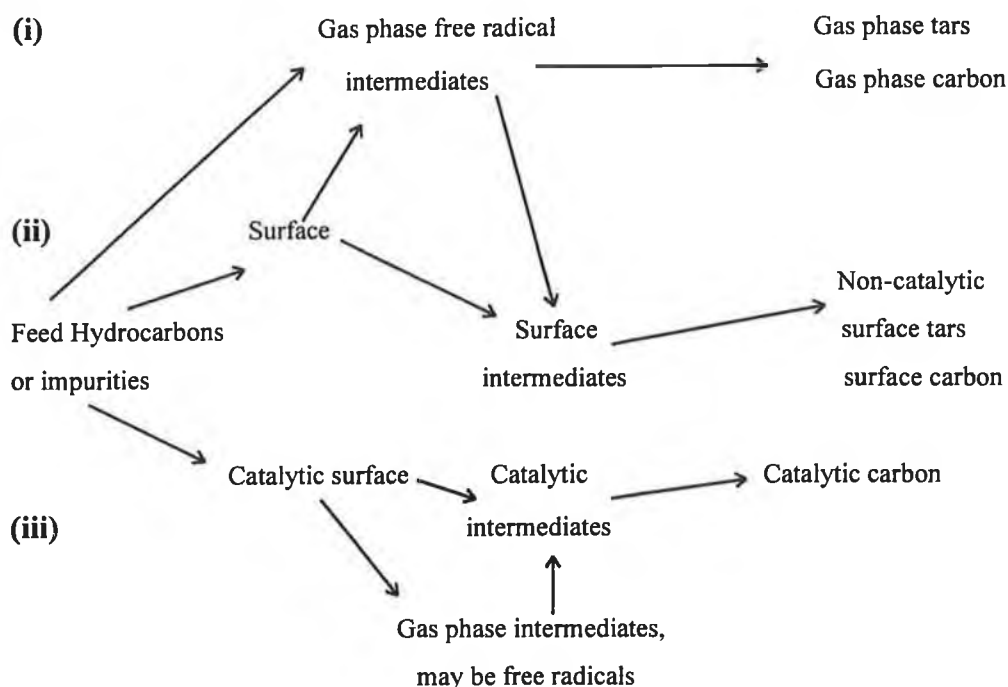
As can be seen from Fig. 1.31, there are three major processes in coke formation which are interconnected. Coke can be formed by free radical reactions in the gas phase (i) which in turn may be influenced by the physical or chemical nature of the surface. Both catalytic (iii) and non-catalytic (ii) surfaces can lead to coke formation, with the surface influencing the nature of the intermediates and hence the nature of the coke.

Baird et al. [104] have proposed the formation of three distinct types of carbon on Fe and Ni foils, namely, (i) platelet graphite (ii) non-orientated graphite (a less well-defined graphite deposited in random orientation) and (iii) filamentous carbons. Platelet graphite and the filamentous carbon are formed by a catalytic process involving the surface diffusion of metal-metal hydrocarbon species across the edges of the layer planes where growth occurs. Metal atoms can diffuse either from the metal foil surface or from the filamentary bead to the layer planes bringing with them hydrocarbon species. At the edges of

64

the layers dissociation occurs giving carbon and metal. Baird et al. [104] suggest that the reason for this enhanced growth at grain boundaries is because grain boundaries contain edge atoms that are less strongly bound than plane surface atoms. The amount of growth on particular exposed crystal faces is a function of the ease of abstraction of an atom from that face. In conclusion the authors [104] state that the nature of the carbon deposition is essentially dependent on the rate of surface diffusion of a metal or organometallic species from the metal catalyst to the growing edges of graphitic layer planes. This rate is in turn dependent upon the ease of formation of the organometallic species that precedes the deposition of elemental carbon [104].

Three forms of carbonaceous deposit were also observed by Baker et al. [99] during Ni catalysed decomposition of acetylene; namely, amorphous, filamentous and graphitic. The mechanism for growth of filamenteous carbon was proposed to occur in three stages (i) an initial growth period, (ii) a region of constant growth rate, and (iii) a tailing off period. Initially acetylene decomposed on the exposed surfaces of the nickel particle releasing a considerable amount of heat. Since the acetylene is unlikely to decompose as rapidly on the region surrounded by the flocculent carbon, a temperature gradient will be set up within the particle which is steepest in the regions immediately adjacent to those covered by the flocculent deposit, Fig. 1.32b.

Fig. 1.32 *{Ref. 99}* Stages in the growth of filaments.

65
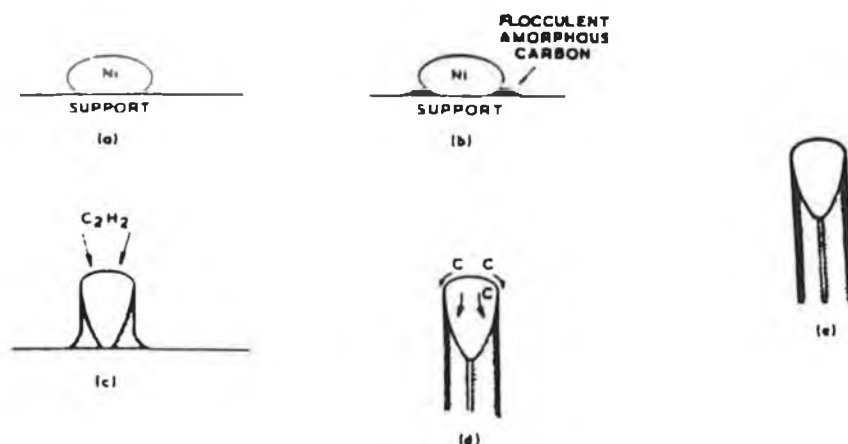
The carbon resulting from decomposed acetylene is taken into solution, diffuses down the thermal gradient and deposits in the protected regions producing the situation shown in Fig. 1.32(c). The carbon builds up at the rear of the particle and eventually forces the particle away from the support. Oxidation experiments showed that the filaments had an outer sheath of relatively oxidation resistant material, proposed to be graphitic in nature, while the region within consisted of more readily oxidazable material. This difference between the surface and bulk composition of the filament would suggest that these two phases are produced by different processes [99], namely that the bulk material arises from carbon transported through the catalyst particle and the surface material by carbon transported around its peripheral surface as depicted in Fig. 1.32(d). Termination of filament growth begins when excess carbon on the surface does not move away to form the filament skin rapidly enough. This results in a reduction in the fraction of free particle surface available for adsorption and decomposition of acetylene and consequently a decrease in heat input to the particle which leads to a decrease in the rate of diffusion through the particle. Eventually the particle is completely encapsulated by surface carbon and filament growth ceases as shown in Fig. 1.32(e). Walker et al. [100] however, repute blocking of the catalyst by carbon as a reason for termination of carbon formation since the surface carbon produced is highly porous and consequently, should not prevent reacting gas molecules from reaching the catalyst.

In a later paper Baker et al. [105] proposed a mechanism of carbon deposition on platinum-iron alloy supported on silica. In this case, growth of carbon occurred by extrusion from the metal alloy particle on the support surface. Before filament growth occurred in the Pt-Fe/C_2H_2 system, separation of the Pt/Fe alloy occurred with Pt forming an 'apron' around a core of Fe as shown in Fig. 1.33(a). Decomposition of adsorbed acetylene occurs on the surface of the particle containing Pt and some of the carbon produced from the hydrocarbon decomposition is taken into solution by Pt and diffuses down the temperature gradient created in this metal by the acetylene decomposition [105].

Fig. 1.33 *{Ref. 105}* Stages in growth of filaments.
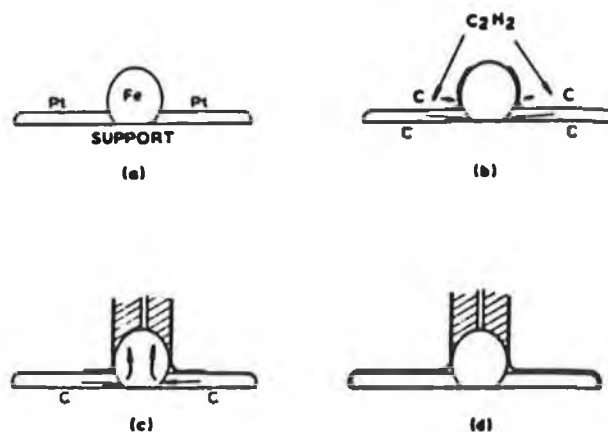
The carbon moves to the cooler Pt-Fe interface to build up there and be steadily transferred into the Fe as shown in Fig. 1.33(b). Fig. 1.33(c) shows carbon filament formation which occurs as the diffusion rate increases when heat is transferred to the Fe surfaces in contact with Pt. This type of carbon filament formation also occurs as the upper surface of the Fe core is cooled when carbon is endothermically precipitated on it. The Pt surface can become blocked rapidly if the carbon at the particle surface is not removed quickly enough to form the filament skin. This results in removal of the source of the temperature gradient and so the passage of carbon through the particle ceases abruptly.

Kim et al. [128] noted that before growth of filaments occurred on Cu–Ni catalysts the Cu–Ni particles underwent a structural transformation from globular to a thin flat structure. For the major part of the growth process the filaments were relatively smooth and tended to form into large loops but over a period of time many of the loops slowly decreased in width. This was due to catalyst material being dissipated within the structure and this behaviour often resulted in the formation of secondary smaller filaments on the parent growth [128]. When the particle had reached approximately one third of its original size a change in shape occurred and it started to rotate on its axis perpendicular to the direction of filament growth causing the filament to acquire a spiral form. This

67

occurred for a short period of time prior to catalyst deactivation and occurred at all growth temperatures, Fig. 1.34. Activity of the catalyst particles decreased at 700°C and above 740°C almost all filament growth ceased.

Fig. 1.34 *{Ref. 128}* Schematic representation of the change in morphology of filaments produced from Cu–Ni (1:1) catalysed decomposition of acetylene at 500°C.
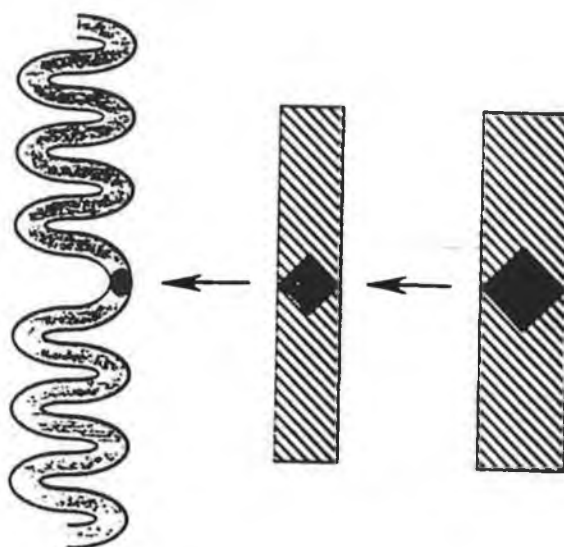
Carbon deposition on nickel-copper alloy catalyst resulting from the decomposition of methane has been studied by Alstrup et al. [114]. The type of carbon formed was referred to by the authors as 'octopus' carbon due to its shape where several filaments developed from an alloy particle. It was found that carbon inside the filaments of this structure was much less structurally ordered than that in the outer shell of the filaments.

Carbon in the form of twisted filament, double or triple helices and tubes as well as straight strands were seen after reaction of CO on Ni and Fe catalysts [101]. Boehm [101] deduced that the carbon filaments were built of shallow domeshaped layers stacked like saucers with planes orientated parallel to the

surface of the fibres. The paracrystalline carbon formed from disproportionation of CO or hydrocarbon decomposition has a relatively low degree of organisation. Iron carbides catalytically recrystallize this carbon but are unstable above $450^{\circ}C$ and decompose giving iron and carbon [99]. It has been proposed by Ruston et al. [102] that carbon filaments grow only from certain crystal faces of the metal carbide and Fig. 1.35 depicts the types of filament formed on rectangular and angular shaped catalyst particles. Boehm [101] suggests that disorganised or poorly crystalline carbon is more soluble in the carbide phase than graphitic carbon.

Fig. 1.35 *{Ref. 101}* Schematic representation of growth mechanism of filamentary carbon on iron carbide. (a) on rectangular carbide particle, (b) on carbide particle with two active faces at oblique angles.
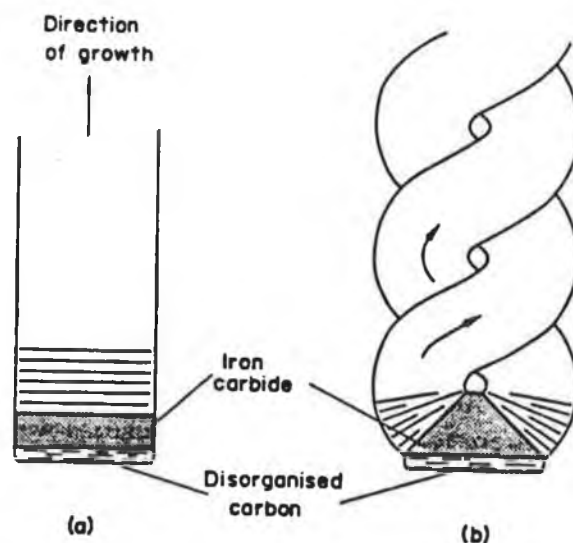
Boehm [101] states the mechanism for formation of graphitic carbon appears to be the same whether CO or hydrocarbons are used as the starting material. This mechanism is most likely precipitation from supersaturated solutions in the catalyst [103].

In a situation where well-crystallised carbon is nucleated on a crystal face, the carbide phase is supersaturated in carbon with respect to this crystalline carbon [101]. This results in graphitic carbon growing at the expense of

carbon dissolved in the carbide lattice. Growth rate is therefore controlled by diffusion of carbon atoms in the carbide. Diffusion also transports disorganised or poorly crystalline carbon in contact with other crystal faces to the thermodynamically more favoured and better crystallised carbon phase.

Transmission electron microscopy was used to examine carbon deposits on Cu–Ni and Ni catalysts [126]. These deposits were found to consist almost entirely of filamentous carbon with diamond-shaped catalyst particles inside the filament structure. By comparison of the size of the active catalyst particles before and after reaction, it was found that the particles were considerably smaller after reaction indicating that during the reaction fragmentation of the starting material occurred prior to carbon filament formation. Carbon deposition appeared to take place in a sequential fashion starting with prolific filament growth on the exposed metal surfaces resulting in removal of a small fraction of particles from the catalyst surface [126]. This led to fresh catalyst particles below the carbon layer becoming activated and the chain of events was repeated until all the catalyst was consumed. Kim et al. [126] also found that the orientation of a particle is a key factor in determining its ability to decompose a hydrocarbon molecule and to initiate and sustain carbon filament growth. Bimetallic Cu–Ni systems were found to have higher activity than nickel for both carbon deposition and hydrogasification of carbon. This agrees well with data reported by Nishiyama et al. [127] who suggested that the enhanced activity of the bimetallic system was due to the creation of lattice defects in the metal crystallites. These defects play an important role in promoting the growth of filamentous carbon since they facilitate the diffusion of carbon through the catalyst particles.

Chang et al. [124] have used a combination of electron microscopy and thermogravimetric techniques to examine the nature of carbonaceous deposits and the characteristics of the metal particles on Al_2O_3 supported platinum particles. Platinum particles of 10–20nm diameter were supported on γ-Al_2O_3 and heated in an atmosphere of 2 torr acetylene, Fig. 1.36a. At 480°C the metal particles were observed to wet and gradually spread on the support

in regions where carbon was deposited, Fig. 1.36b. Following this, carbon at the metal interface gasified as the edge of the Pt receded resulting in the formation of 'clean islands' around the platinum. Once the gasification reaction stopped small metal particles reappeared which ranged from 2.5 to 5.0nm in diameter, Fig. 1.36c.

Fig. 1.36 *{Ref. 124}* Schematic representation of the observed changes in appearance of platinum particle supported on Al_2O_3 when heated in 2 Torr of acetylene at 480°C : (a) platinum particle on γ-Al_2O_3. (b) spreading of platinum at the carbon deposit interface, and (c) eventual redispersion and creation of apparently clean islands around each particle.
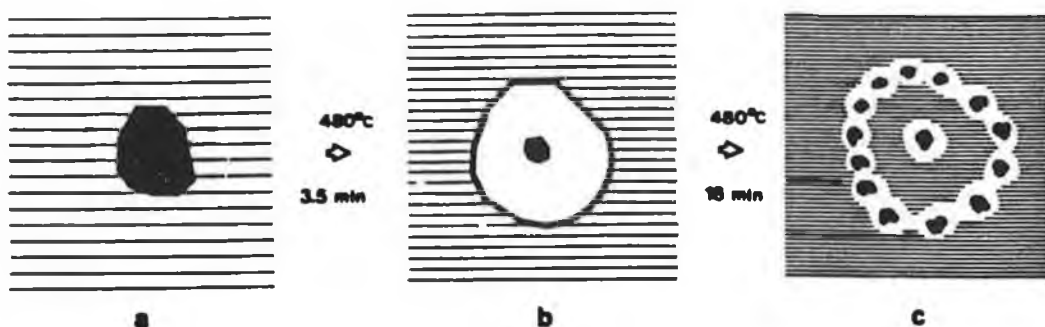
Above 600°C the rate of carbon accumulation increased significantly resulting in loss of clean regions around the metal particles. The filament growth for this system involved removal of the metal particle from the support to the tip of the filament. It was noted that when a gasification step was performed in an oxygen environment at 600°C metal particles on the surface, not associated with filaments, catalysed the removal of the carbon overlayer. This occurred by the development of channels through the deposit and resulted in an increased rate of sintering due to platinum particle mobility and collisions between particles [124]. Also, under these conditions platinum particles located at the tips of filaments catalysed oxidation of the filaments and retracted back to their original location on the Al_2O_3 support. These results explain why platinum particles maintain their catalytic activity in systems where carbon deposition is appreciable. It was seen that carbonaceous

71

deposits tended to collect at specific sites on the Al_2O_3 support, leaving the metal particles relatively free of coke [124]. The coke formed was non graphitic in nature.

Specific step and kink sites may be important in coking [108]. The reaction probability for a H-D exchange reaction was four orders of magnitude higher on a highly stepped platinum surface to that on the Pt(-111) surface [112]. Also dehydrogenation of cyclohexane and cyclohexene to benzene occurred at a higher rate on the stepped platinum surfaces [112]. These results suggested that steps were effective for C–H and H–H bond breaking while kinks were effective in breaking C–C bonds as well as C–H and H–H bonds. During the experiments with hydrocarbons, the catalyst surfaces were always covered with a carbonaceous overlayer which consisted of partially dehydrogenated hydrocarbon species, formed from the dissociation of the reactants, Fig. 1.37.

Fig. 1.37 *{Ref. 112}* Model of active platinum catalyst surface with a full carbonaceous overlayer showing exposed catalytic sites.
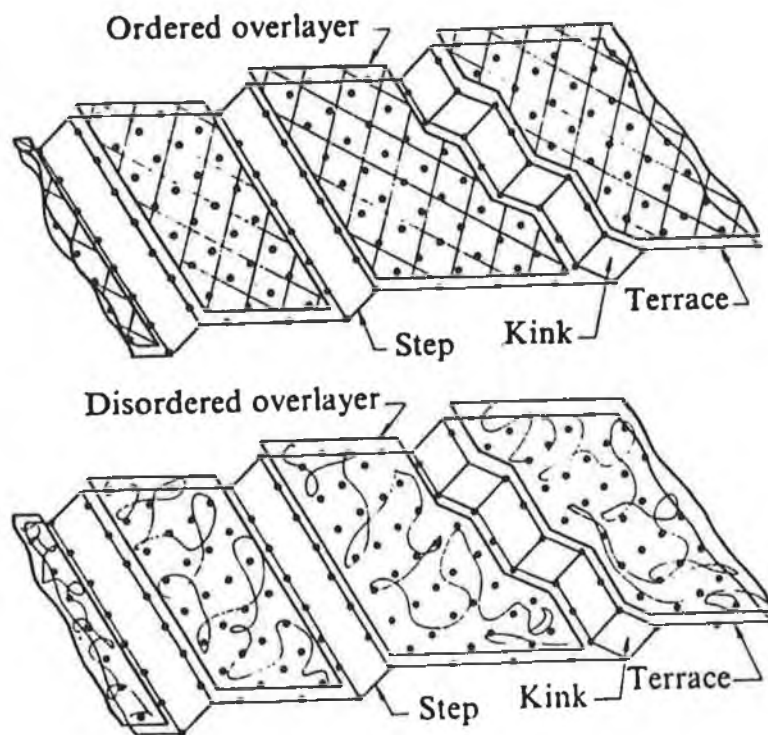
Although the step and kink sites exhibit higher binding energy for both hydrogen and hydrocarbons the higher rate of hydrogen dissociation may keep these sites active [112]. On the basis of the experimental observations, Somorjai et al. [112] proposed an atomic model of the platinum surface active in the catalysis of hydrocarbon reactions. Diffusion and desorption of the products probably occurs on areas covered by the carbonaceous overlayer since the binding energy of products is lower there. The carbonaceous overlayer may be ordered or disordered depending on the platinum surface structure, nature of the reactant and hydrogen-hydrocarbon ratio used in the experiment. Structure of the carbonaceous overlayer is important as some reactions are very sensitive to the presence of ordering on the overlayer, e.g. cyclohexene conversion to benzene. This model does not take into account the effect of porous materials used to support and disperse platinum. However the authors feel that since most catalytic reactions which are attributed to platinum supported catalysts can be reproduced on single crystal surfaces, their model of the platinum catalyst should not be markedly changed when support effects are taken into account [112].

In a later paper, Blakely and Somorjai [119] found that higher molecular weight reactants and products yielded greater carbonaceous overlayer coverage than low molecular weight hydrocarbons which did not readily react on platinum surfaces at low pressures. The authors [119] recognised two types of structural features on platinum surfaces that influence the catalytic surface reactions (a) atomic steps and kinks i.e. sites of low metal co-ordination number and (b) carbonaceous overlayers which can have an important effect in both the catalytic activity and selectivity of a metal surface. In fact it has been postulated by Weinberg et al. [120] that the carbonaceous overlayer is the catalytic site for hydrogenation of ethylene on Pt (111) surfaces.

A review of carbon formation mechanisms on nickel-containing catalysts was carried out by Rostrup-Nielsen and Trimm [107]. They noted that agreement existed for nucleation of carbon occurring on specific steps and kinks of the nickel surface [104,107]. Evidence against adsorption followed by

decomposition and diffusion of carbon to the growing fibre as proposed by Grenga et al. [108] is given by Massaro et al. [109] who found that the surface diffusion of carbon on nickel foil is negligibly small in the temperature range 350–700°C. The authors [107] disagreed with the temperature driven dissolution-precipitation mechanism of Baker et al. [99] because carbon filaments have been formed on nickel crystallites where decomposition of the gases being used was endothermic. Therefore in these situations, diffusion of carbon through nickel driven by a temperature gradient is not possible and the only remaining driving force is concentration. The carbon growth should then involve a fast gas phase reaction resulting in carbon atoms on the surface [107]. These dissolve in the metal and precipitate out through a dislocation at the rear of the particle to form a graphite whisker as shown in Fig. 1.38.

Fig. 1.38 *{Ref. 107}* Model of carbon transportation.
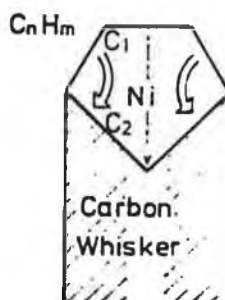
The authors [107] conclude that transportation of nickel at the surface of growing carbon cannot be totally explained by the temperature driven dissolution-precipitation mechanism and is probably not due to surface migration of carbonaceous species either. Diffusion of carbon through the nickel under a concentration gradient appears to be the most probable explanation. Eight years later Yang et al. [110] found evidence to support the temperature driven dissolution-precipitation mechanism proposed by Baker et al. [99]. They studied the coke deposition from four hydrocarbons on Ni, two of which were exothermic when combusted and two which were endothermic. It was found that for the exothermic

reactions coke was deposited on the exposed face of the catalyst metal while no coke was found on the exposed face of the catalyst metal for the endothermic reaction.

Amorphous carbon deposits are not dependent on the support material since similar materials can be formed on Ni/silica and Ni/graphite supports [99]. The deposits were most likely formed by gas phase polymerisation of acetylene, with the nickel particles merely acting as nucleating centres for physical accumulation of coke on the surface [99]. Graphitic platelet formation was seen to occur only on isolated nickel particles, with diameters of at least 300nm, and appeared to coincide with loss of mobility of these particles suggesting that the platelets are formed due to surface diffusion of carbon from either the graphite support or the amorphous deposit to catalytically active sites near nickel particles [99].

According to Richardson [1], coke formation on silica-alumina cracking catalysts is directly related to acidic strength and density. Two major types of carbon structure exist as highly dispersed phases in the silica-alumina pores, namely (a) pseudographitic or turbostratic coke existing as random-layer lattices, similar to graphite with a composition of $CH_{0.4}$ to $CH_{0.5}$ and (b) coke consisting of poorly organised polynuclear aromatic macromolecules [1]. In the case of dehydrogenation catalysts, Richardson [1] states that the type of coke formed is different to that formed on acidic sites. The process whereby dehydrogenation and associated hydrogenolysis lead to carbon fragments is outlined in Fig. 1.39. On acid supports, these fragments migrate from the dehydrogenation sites and provide precursors for acid coking. It has been suggested by Richardson [1] that acid coke originates from aromatic and olefinic hydrocarbons. These molecules can form ion radicals quite easily with acid sites, polymerise with other unsaturates, and then dehydrogenate to form coke.

Fig. 1.39 *{Ref. 1}* Carbon formation on dehydrogenation catalysts.
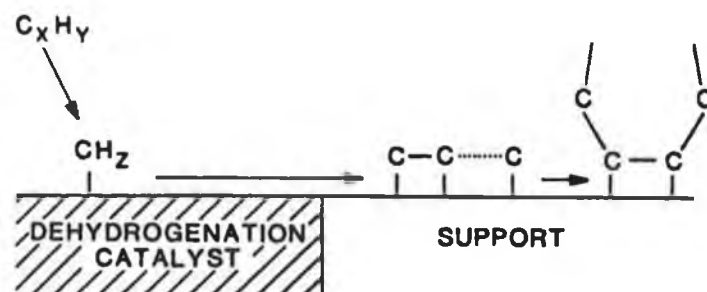
It was found by Scelza et al. [131] that the sites on Al_2O_3 which retains chlorine are not those which are involved in coke formation. Also it is known that in a bifunctional catalyst the coke is deposited both on the metallic and on the acidic function although the amount of coke is normally higher on the acidic function [132]. Peña et al. [133] have suggested that the sites for dehydrogenation reactions may be the same as those for coking. Based on the dehydrogenation of n-butene to butadiene over fresh and thermally aged Cr_2O_3/Al_2O_3 catalysts it was found that thermal ageing of the catalyst reduced butadiene production and the rate of coking. Since conversion of n-butadiene involves dehydrogenation it seems plausible that the formation of coke may also involve the same dehydrogenating sites [133].

Sn acts to moderate the activity of Pt for hydrocarbon conversion, thereby, improving stability and probably reducing the rate of coke formation [135]. It was found by Afonso et al. [134] that coke formation during dehydration of n-alkanes on Pt–Sn was attributed to a combination of several processes, namely, successive dehydrogenation reactions, oligomerization of n-alkanes, and probably Diels-Alder type reactions. The formation of polycondensed aromatic rings was found to predominate over the formation of isolated rings. Also it was found that olefins were the primary precursors for coke formation [134].

The build-up of coke with time and conditions of reaction can be related by the *Voorhies equation* [123].

$$C_c = At^n$$

where,

C_c is the coke formed at process time t

A   is a constant that correlates with aromatic content

n   is a constant with values between 0.3 and 0.5

Carbon deposition from methane on bulk Fe showed an 'incubation period' initially where carbon dissolved in the metal until its saturation solubility has been exceeded [121]. The initial solid product formed was found to cause no disruption of the metal surface and the growth rate remained low. As parts of the main catalyst metal were extracted and became incorporated in the deposit, disruption of the catalyst structure began to occur leading eventually to its complete breakdown. Most of the carbon deposit was formed during this period and the reaction eventually slowed down due to formation of inert products e.g. Fe + CO [100] or by encapsulation of the active metal particles in carbon [99]. In a study of catalyst stability in naphtha reforming catalysts, Figoli et al. [122] found that the greatest rate of coke deposition occurred during the first two hours of operation. The authors [122] suggest that this may be due to the presence of very active sites in the catalyst which are then passivated by the carbon deposition. It was also noticed that coke deposition was greater at lower pressures [122].

Billaud et al. [130] have reviewed coke formation during the thermal cracking of methane. They concluded that operating conditions affect the amount and most of the properties of the carbon deposit. Severe pyrolysis conditions (high temperature and pressure or lower flow rate) accelerated the formation of coke. The formation of surface carbon was enhanced by conditions that improved the diffusion of coke precursors such as, (a) high surface-to-volume ratio, (b) high temperature and (c) turbulent flow. Also, low partial pressure promoted the formation of surface carbon which is basically pyrolytic carbon deposited on the surface. With regard to dispersed carbon, which is fine spherulitic pyrolytic carbon, its formation is enhanced by high partial pressure of methane, low

surface-to-volume ratio and high temperature. The rates of formation of dispersed carbon are greater than those of surface carbon and coke is mostly a mixture of these two different types of carbon [130].

Coking of Pt/Al_2O_3 with C_6 hydrocarbons has been studied by Cooper et al. [111]. They found that olefins gave higher coking rates than saturated hydrocarbons which agrees with results obtained by Baird [106]. It was also noticed that after varying the acidity by addition of Cl^-, the amount of coke formed by the high coking hydrocarbons was greatly reduced but that of low coking feeds remained approximately the same. Barbier et al. [98] also studied coke formation on Pt/Al_2O_3 catalysts and found that the amount of carbon deposited on the support was directly related to the number of exposed Pt atoms on the surface. They also found that the number of carbon atoms deposited per platinum surface site decreased as platinum dispersion increased. This agrees with the findings of Somorjai et al. [112] who showed that Pt atoms located at the edges and on the corners of the platinum crystallites are more resistant to coke deposition than the atoms placed on the faces of the crystallites. Rivera-Latas et al. [113] showed that approximately 50% of the platinum surface remained free of carbon deposits following hexane hydrogenolysis.

On $Cr-Al_2O_3$ dehydrogenation catalysts using propane and propene as the hydrocarbon feeds, Gorriz et al. [129] noted that as the chromia content was increased, the initial rate of coke formation increased, but the extent of coke deposited per unit mass of catalyst decreased. Also the initial rates of coke formation were much higher for propene than for propane [129].

The rate of carbon formation from $CO-H_2$ over Fe catalysts has been studied by Walker et al. [100]. Their results showed that as the H_2 content of the gas mixture increased, the temperature at which the maximum rate of carbon deposition occurred also increased. The deposition temperature was seen to affect the total amount of carbon which could be produced on a specific weight of catalyst. Change in the $H_2:CO$ ratio had a relatively minor effect on the maximum rate of carbon deposition at the lower temperatures (470–528°C) but had a major effect at

78

the higher temperatures. The authors [100] noted that extended periods of constant carbon deposition rates were found despite a probable build up of carbidic carbon. Their explanation for this was that, during these periods, disintegration of the catalyst into smaller particle sizes was occurring resulting in the total surface area of the iron remaining constant even though the percentage of the total surface which is iron continued to decrease. This idea fits in well with the growth of carbon filaments containing metal particles in their leading face. Lobo et al. [115] studied the temperature dependence of the rate of carbon deposition on nickel foil using light hydrocarbons in the C_1–C_4 range. It was found that after an initial acceleration period, the rate of carbon deposition achieved a steady state which did not show signs of slowing down, even for long deposition times. Agreeing with Walker et al. [100], a temperature of maximum deposition was found for each of the hydrocarbons. In a later paper, Lobo et al. [116] defined three periods in the formation of carbon. Initially there is an induction period during which virtually no carbon is formed and this period is particularly long at low pressures and/or temperatures [116]. This is followed by an acceleratory period and finally a steady state period during which the rate of deposition is constant. These stages of carbon deposition proposed by Lobo et al. [116] were seen to occur on industrial coal hydrogenation catalysts [98,144]. Lobo et al. [116] found evidence to suggest that the final rate of coke formation was independent of the Ni foil surface but instead catalysed by Ni crystallites. These Ni crystallites originated from the metal foil and were transported away with the growing carbon. This suggests that the carbon deposit contained quite large amounts of dispersed nickel. Here the carbon content reached an 'equilibrium' level of between 10 and 20% after a few days and then remained constant [116]. It has been shown by Barbier et al. [98] that on reforming catalysts, coking occurs in two stages i.e. attainment of a quasi-steady state by rapid deposition on metal sites with associated changes in metal activity and selectivity, followed by a slower deposition on acid sites. Querini et al. [118] in their study of hydrocarbon reforming Pt-Re-S/Al_2O_3-Cl catalysts found that coke formation on the metal increased with time and then remained constant while coke formation on acid sites increased during the entire run.

1.4.2. Characterisation of coke.

Wolf et al. [97] have reviewed the chemical and physical characteristics of coke deposits and report on C/H ratios for various forms of coke, obtained by combustion analysis. It was found that the C/H ratios vary in the range 0.76–2.78 depending on the reaction. Plank et al. [138] have found that the C/H ratio varies with time on stream, an effect referred to as 'coke' ageing. Therefore C/H ratios do not give detailed information on coke except that different 'coke' precursors produce different types of coke deposits [97]. The variations in C/H ratio also reflect the degree of aromatization, cross-linking, and other structural features which vary with feed composition, catalyst, etc.

Differential Thermal Analysis (DTA) of Pt/Al_2O_3–Cl catalysts coked during naphtha revealed several peaks and two zones, one corresponding to carbon which burns at 123–316°C and the second at 316–550°C [122]. Analysis of the effluent revealed that the high temperature coke had a higher C/H ratio suggesting that coke which burns at higher temperatures is more polymerised. IR and NMR analysis of the extracted coke revealed the presence of condensed aromatics, naphthenes and alkyl chains.

Basso et al. [149] using Temperature Programmed Oxidation (TPO) have detected low and high temperature peaks on coked samples. The low-temperature peak (<300°C) was associated with oxidation of coke occurring on or near the metal sites where it was efficiently catalysed e.g. by platinum oxide while peaks at high temperatures were associated with less efficiently catalysed oxidation, or in extreme cases, non-catalysed combustion of coke on the support, e.g. on acid sites [137]. Barbier et al. [137] have also observed low and high temperature peaks during TPO analysis of $Pt/\gamma\text{-}Al_2O_3$ coked with cyclohexane. All metallic activity of the coked $Pt/\gamma\text{-}Al_2O_3$ catalyst was recovered when the low temperature carbon was removed by oxidation, supporting the view that the low temperature peak is associated with the metal [137].

According to Basso et al. [149], differences in TPO peak positions reflect the kinetics of coke oxidation and do not necessarily imply that the chemical nature or the structure of the deposits on these sites are different which disagrees with the results of Figoli et at. [122]. However, the results of Figoli et al. [122] are bases on actual microanalysis of the effluent while those of Basso are bases on TPO peak positions.

Biswas et al. [144] have also found the existence of two distinct coke types on the Pt surface itself which they referred to as reversible and irreversible (graphitic). Removal of the irreversible coke by heating the sample in a H_2 stream was one thousand times slower than for the removal of reversible coke. The reversible coke was a hydrogenated surface species (H/C atomic ratio of 1.5– 2.0) and the irreversible coke a graphitic form (H/C ~ 0.2) [144]. Coke produced in catalytic reactors has been distinguished as soluble and insoluble [152]. Analysis of the soluble coke by Gas Chromatography (GC) showed it to consist of linear paraffins. This agrees well with Afonso et al. [134] who found that 55% of soluble extracted coke from industrial $Pt/Sn-Al_2O_3$ dehydrogenating catalysts revealed the characteristic two peak profile and it was discovered that after extraction of soluble coke the low temperature oxidation zone disappeared and the initial high temperature oxidation zone at approximately $350^{\circ}C$ diminished [134].

Infrared spectroscopy has been used by Eberly et al. [139] on extracted coke deposits obtained from cracking of paraffins and olefins over silica-alumina. Three adsorption bands at 3050, 2930–2860 and $1580–1590cm^{-1}$ were observed, which correspond to aromatic CH groups, methylene groups and aromatic rings respectively. Similar results were obtained by Eisenbach et al. [140] who found a band at $1585cm^{-1}$ typical of C=C stretching vibrations of microcrystalline graphite carbon structures. These are present in polycyclic aromatic compounds and make up the carbonaceous deposits of the type detected by Haldeman et al. [136]. It was noticed that a drastic increase in the intensity of the adsorption band at $1585cm^{-1}$ was always accompanied by darkening of the catalyst sample [136]. A concomitant decrease in intensity of the adsorption band at $3640cm^{-1}$, characteristic of OH

groups, suggests that OH groups act as active sites in coke formation and are irreversibly consumed [97]. When this is considered in conjunction with the infrared bands at 900 and 700cm^{-1}, it implies that polycyclic aromatic compounds are precursors of carbonaceous deposits. Wolf et al. [97] conclude that coke deposits consist of mono- and polycyclic aromatic rings connected by aliphatic and alicyclic fragments the relative proportions of which depend on the reaction-catalyst system used. Also, the groups are interconnected forming a crystalline pseudographitic structure and an amorphous phase. In addition to coke consisting of polyaromatic molecules, Espinat et al. [143] using laser raman spectroscopy has found that even at low carbon contents, coke is at least partly present as carbon and not only as adsorbed isolated polyaromatic molecules on reforming catalysts.

Transmission Electron Microscopy (TEM) has shown that any carbonaceous matter, even when it has a very poor crystalline organisation, produces scattered beams characteristic of aromatic structures [142]. Around the contours of Al_2O_3 single crystals, structures were found which were suggested to be aromatic planar ring structures consisting of less than twelve rings piled up two or three high. These are referred to as basic structural units (BSU) and were formed in the interface between Pt and Al_2O_3 [142]. Once formed these BSU were deposited indifferently on the Al_2O_3 as there was no special relationship between the platinum and the carbon deposit.

Pt/Al_2O_3 catalysts, used to decompose cyclopentane when examined by high resolution microscopy revealed that carbon on the catalyst was poorly organised or amorphous and varied in thickness from a few Å to several hundred Å [147]. The Pt was covered with coke and fairly well organised carbon structures could be seen in its vicinity. This was confirmed by Electron Energy Loss Spectroscopy (EELS) and X-Ray Diffraction analysis (XRD). Structure of the carbon was found to be strongly influenced by the H_2/HC ratio. According to Tracz et al. [148] who used high-resolution electron microscopy to study the morphology of coke deposits on Ni/Al_2O_3 and Ni/MgO, temperature exerts a greater influence on the kind of carbon deposit formed than the support material. Yan et al. [141]

however, found that coke formed on Ni/Al_2O_3 appeared more structurally disordered than that formed on silica-alumina and was less graphitic, more porous, higher in surface area and lower in density than that deposited on the silica alumina catalyst [141].

The location and structure of coke deposits on alumina supported Pt catalysts has been characterised by Gallezot et al. [146]. Using a combination of TEM and EELS coupled to High-Resolution Scanning Transmission Electron Microscopy (HRSTEM) they found that for coked Pt/Al_2O_3 catalysts, coke was always present on and around the platinum particles but no carbon was detected more than 20nm away from a given particle. It was observed that the coke was always associated with the support and there were no whiskers or filaments protruding from the support. The results showed that the coke produced by the decomposition of cyclopentane at 440°C was essentially amorphous [146]. The authors [146] proposed that a more organised coke structure and higher surface coverage could be achieved under more severe coking conditions such as higher temperature and pressure and longer periods of time. Espinat et al. [147] have also studied the location and structure of coke on alumina supported catalysts. When the coked catalyst was examined using electron microprobe, the concentration profile revealed two types of regions. one of which consisted of large zones about 60µm in diameter where the percentage of coke was higher than the average percentage of deposited coke. The other region consisted of smaller zones 10–20µm in diameter.

Light microscopy examination revealed that in catalysts of low metal content there were no apparent preferential locations for carbon deposits [136]. This suggested that all regions of the catalyst were capable of carbon formation and the carbon phase was normally well dispersed over the catalyst [136]. When metal contamination was present in the hydrocarbon feed, carbon deposition showed a preference for the periphery of catalyst granules. Nitrogen adsorption studies have shown that carbon does not occlude catalyst pore space and that considerable irregularity or roughness exists in the carbon phase packing. XRD

studies revealed that approximately 50% of the carbon phase existed in pseudographitic, or turbostratic structures.

Fung and Querini [150] used a method for TPO of coke deposits where CO_2 formed was converted to CH_4 on a Ru catalyst, for detection. This system however was limited to a maximum conversion of 3% CO_2 at any particular time during the run due to operating conditions of the methanator and problems associated with sintering of the Ru metal particles. According to Fung and Querini [150] this system offers advantages over conventional systems in terms of sensitivity and spectral resolution.

In a later paper Querini and Fung [151] discussed the kinetics of the coke-O_2 reaction on supported metal catalysts using the TPO technique. It was found that high heating rates shortened TPO analysis times and greatly increased the sensitivity but at too high a heating rate problems arise with both mass and heat transfer. The spectra for three TPO analysis of a coked catalyst under the same experimental conditions, varying only the heating rates: 25,13 and 7°C/min., are shown in Fig. 1.40. Using a high heating rate increased (25°C/min.) increased both the height and T_m of the peak [151]. Although sensitivity is decreased at the lower heating rate (7°C/min.), it was found that the areas of the three spectra were the same, when calculated as total amount of CO_2 vs. time. The temperature at which the signal returns to zero decreased as the heating rate decreased because the lower heating rate resulted in a lengthening of the time that the catalyst remained at a particular temperature and therefore provided more time for coke removal at that temperature.

Fig. 1.40 *{Ref. 151}* Influence of heating rate on TPO spectrum.
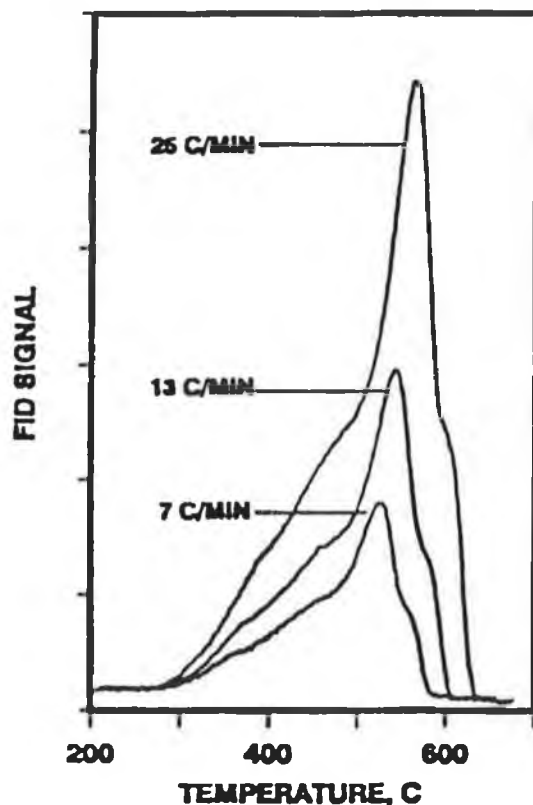
The effect of different coke contents on the TPO spectra of a catalyst have been investigated by Querini and Fung [151], Fig. 1.41. The two TPO spectra exhibit several distinct differences. In the case of the catalyst which had the lower level of coke (broken line), its peak position was shifted to a lower temperature. Also the analysis was completed at a lower temperature, and the shape of the peak became more symmetrical. These findings suggest that coke concentration and quantity (coke concentration times sample weight) effect the TPO spectrum. An increase in the carbon concentration of a coked catalyst generally leads to an increase in quantity and size of coke particles which affects T_m [151]. Catalyst mass also affects T_m since the greater the sample mass at a fixed initial carbon concentration, the more the oxygen concentration decreases along the bed. This leads to a decrease in reaction rate with increase in mass of the sample resulting in a shift of T_m toward higher temperature [151]. Increasing the inlet concentration of oxygen increases the rate of coke oxidation resulting in coke oxidation being

85

completed at lower temperatures and the peak height being increased. Oxygen for the oxidation process is used up mainly in three parallel or successive reactions : (i) coke carbons being converted to carbon dioxide, (ii) coke hydrogen atoms being converted to water, and (iii) metal atoms being converted into metal oxides [149].

Fig. 1.41 *{Ref. 151}* Influence of coke content on TPO spectrum.
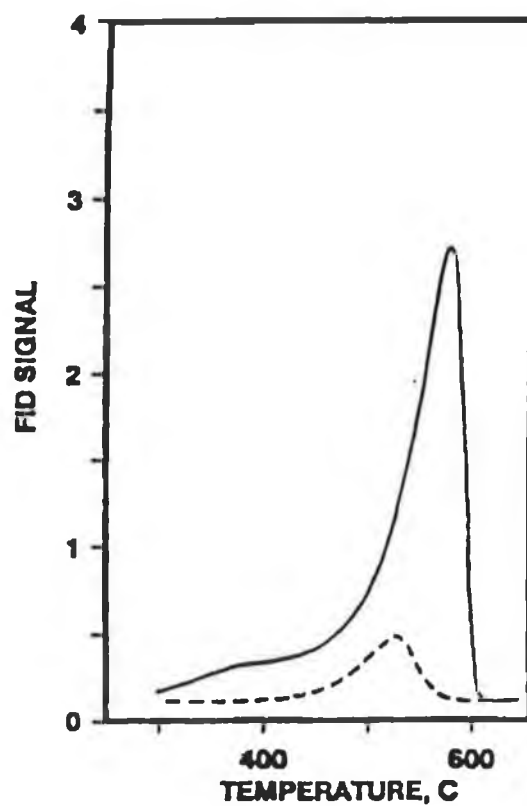
1.4.3 Effect of coke formation on catalyst activity

Barbier et al. [137] have found that coke can be a selective poison. In their experiments on Pt/Al_2O_3 catalysts, coke was observed to reduce the rate of hydrogenolysis of cyclopentane more than the hydrogenation of benzene. This suggests that coke formation on platinum occurred preferably on the hydrogenolysis sites. Also the side reactions by which coke is formed do not necessarily occur on the same active sites as the main reactions which has led to evidence in the literature showing that a direct relationship exists between catalyst activity and amount of coke formation as well as evidence demonstrating the opposite result [97].

Barbier [155] states that the effect of coke on catalytic activity can be measured as toxicity of the coke, defined as the number of surface metal atoms deactivated by the deposition of one atom of carbon or by the number of grams of catalyst deactivated by one gram of coke. Toxicity of coke varies according to the reaction taken into consideration [137]. In the case of hydrogenolysis reactions it is equal to 2.5 atoms of deactivated platinum per deposited carbon atom but is 0.6 for hydrogenation reactions and close to zero for exchange reactions [155]. Barbier [155] concludes that there are three variables on which toxicity of coke depend, (i) nature of the catalyst, (ii) nature of the coking agent and (iii) nature of the reaction taken into consideration which agrees with Wolf et al. [97]. By analysing industrial reforming $Pt-Re-S/Al_2O_3-Cl$ catalysts, coked in an industrial reactor Querini et al. [118] found that after four days the metallic catalytic activity reached a type of steady state. This was interpreted as meaning that not only the amount of coke but also its quality and toxicity for the reactions remained constant during most of the run in an industrial reactor. They also found that while the amount of coke on the metal increased with time and then remained constant, the quantity of coke on acid sites increased during the entire run. Therefore, long-term deactivation is controlled by the deactivation of the acid function [118].

Plank et al. [138] have obtained data for cracking of cumene and cumene-hydroperoxide mixtures over silica-alumina catalysts. From plots of reaction rate and coke deposition vs time on stream it was seen that after rapid activity decline, a steady activity was reached while carbon formation increased steadily with time. Based on the results of similar experiments, Prater et al. [154] deduced that two types of chemical species were present on the catalyst surface (i) harmless coke deposits and (ii) strongly chemisorbed inhibitors. Differences concerning the role of coke in catalyst deactivation reflect differences in coke precursors and catalyst used [97]. This suggests that effects associated with one type of feed and catalyst do not necessarily extrapolate to a different feed and catalyst even though coke may be cited as the culprit in each case.

Kooh et al. [158] have established that catalytic activity falls off rapidly with time because of carbon fouling the metal surface during heptane oxidation over supported platinum and palladium The authors [158] also found that the rate of carbon formation differed from the rate of deactivation which disagrees with Davis et al. [145] whose results showed that deactivation of platinum catalysts after reaction with n-hexane correlates with an increased coverage of surface carbon. Kooh et al. [158] justify their finding by proposing that the carbon formed on metal particles migrates slowly to the support and is not the carbon that fouls the metal particles. It appears that carbon which fouls the metal particle is a single adsorbed layer [158]. The rate of carbon accumulation normalised to the metal surface area has been found to correlate inversely with the rate of deactivation. A similar effect occurs in relation to the surface area of the support as it was found that equal platinum loadings on high surface area supports accumulated more carbon per surface platinum atom but deactivated much more slowly than on low surface area supports [158]. The amount of deactivation which occurred in the initial reactions increased with increasing reaction temperature [145]. In this case the carbonaceous deposit mainly functioned as a non selective poison, blocking platinum surface sites from incident reactant molecules.

It is proposed by Absi-Halabi et al. [156] that coke originating from several sources deposits on the surface of supported metal heterogeneous catalysts masking active sites or blocking pores that contain active sites. Both of these events result in the catalyst activity being reduced. In agreement Marin et al. [153] found that catalyst deactivation by coke deposition in butane dehydrogenation on Cr_2O_3/Al_2O_3 can be adequately described in terms of active site coverage and pore blockage. The initial coke deposit was found to inhibit acid catalysed reactions much more than other reactions. It is known that much of this initial coke is deposited in small pores [157]. This would suggest that the active sites of catalysts may be located in pores. During a study of coke deposition on $Pt-Al_2O_3$ supported reforming catalysts, Espinat et al. [147] found that pore volume and specific area decreased with increasing percentage of coke. Surface area decreased sharply at low coke content and then changed only slightly at higher carbon concentration suggesting that pore plugging without filling occurred on the catalyst as shown in Fig. 1.42 [147].

Fig. 1.42 *{Ref. 147}*   Coke localisation model.
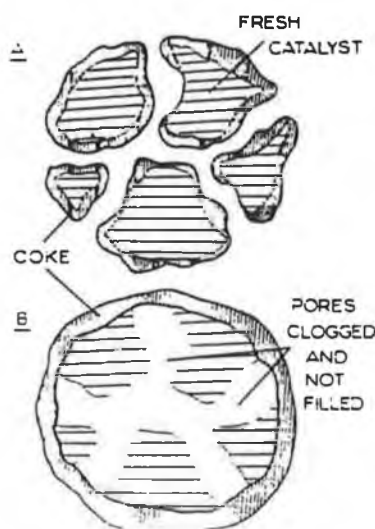
The pore distribution on the catalyst can also be affected by coke depositing resulting in an increase in the number of pores smaller than 50Å due to the filling of larger channels.

Tracz et al. [148] have found that filamentous carbon does not decrease the specific activity of catalysts but destroyed them mechanically and also increased resistance to flow through catalyst beds. The authors also found that carbon shells can completely encapsulate large metal particles (>100nm) resulting in deactivation. These shells show a high degree of graphitization and are mostly created on faceted particles at high temperatures ($\geq 500^{\circ}$C).

In addition to decreasing the activity of a catalyst, the formation and deposition of coke on a catalyst is a self destructive process as it also deactivates its own formation [153].

1.4.4 Coke inhibition and removal

Trimm [125] states that a catalytic reaction is desired but coking is not and it is often better to select a catalyst that is less active for the desired reaction if the extent of coking is also decreased. Also it may be preferable to use an additive that promotes the gasification of coke, even if the additive decreases the catalysts efficiency for the main reaction [159]. Many factors can influence the accumulation of coke on a catalyst and in order to minimise coke formation these factors must be controlled both individually and collectively [125].

Reacting coking intermediates with various gases can remove them before they combine to give coke [125]. Gases which can be used are outlined below with coke being represented as elemental carbon.

$$C + 2H_2 \rightarrow CH_4$$
$$C + O_2 \rightarrow CO_2$$
$$C + CO_2 \rightarrow 2CO$$
$$C + H_2O \rightarrow CO + H_2$$
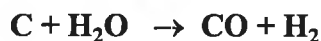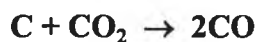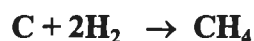
Tauster et al. [160] studied the removal of coke precursors using alternating pulses of propane and hydrogen over a $Cr-Al_2O_3$ supported catalyst. Results showed that 80% of the precursors formed during one second of development could be removed by the introduction of a one second hydrogen pulse while removal of coke precursors was reduced to 40% when five seconds of precursor development was followed by a five second hydrogen pulse.

An increase in the amount of time which a deposit remains on a catalyst surface decreases the rate and degree of its gasification. This is due to transformations which carbonaceous deposits undergo on the surface of transition metals at temperatures greater than $400^{o}C$ [148]. The chemical composition of the

support affects the rate of catalyst coking and decoking [180]. Also intermediate surface species undergo gasification much more easily than carbon deposits.

The effect of adding increasing amounts of hydrogen to an ethylene feed stream, on carbon deposition over Cu-Ni and Ni has been studied by Kim et al. [126]. For the bimetallic catalyst the weight of carbon decreased in a monotonic fashion as the hydrogen concentration in the feed was increased. In the case of pure Ni catalyst, the amount of carbon increased with increasing concentration of hydrogen in the feed gas up to 50% hydrogen but then steadily declined as the concentration of hydrogen was further increased. It was found that the rate of hydrogasification was much higher for the bimetallic catalyst than on pure Ni. Analysis of the gas composition at the exit of the flow reactor showed that for Cu-Ni catalysts methane was a major product while only a small amount of methane was produced by the pure Ni catalyst. These results suggest that the weight decrease of carbon produced on the Cu-Ni catalyst as hydrogen is added to the feed stream is a result of catalytic hydrogasification of carbon [126].

Conditions that favour the formation of coke are high concentrations of suitable intermediates held at high temperature and pressure while gasification is favoured by lower temperature and pressure [125]. By controlling mass and heat transfer in the catalytic bed it may be possible to establish conditions where no coking may occur [125]. Selection of a suitable support material, however, is seldom based on its mass and heat transfer qualities. One approach to controlling coke formation may be to coat a metallic alloy material with a washcoat containing the catalyst so that the heat transfer properties are controlled by the alloy while the chemical properties of the catalyst are dictated by the washcoat. In order for this technique to be successful the thermal expansion values of the metallic alloy and washcoat must be similar or else the washcoat will fall off the metallic alloy during operation [125].

In situations where formation of coke involves the reaction of large organic molecules the problem can be reduced by engineering specific pore shapes as shown in Fig. 1.43 [1].

Fig. 1.43 *{Ref. 1}* Pore shape control of deactivation due to coke formation on hydrotreating catalysts

Time on line
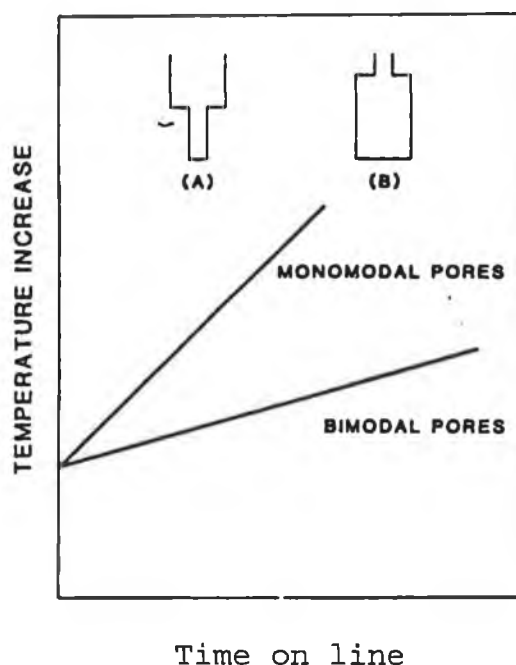
In situation (A) the small section of the bimodal pore is accessed through the larger section which gives a bimodal pore size distribution. In situation (B) bimodal 'ink bottle' structures with small neck openings allow reactants to pass but exclude large coke forming molecules.

Additives have been used to reduce the build up of coke. Baker [161] has found that formation of filamentous carbon from the Ni-Fe/C_2H_2 system varies with type of oxides added as shown in Table 1.6. Addition of W, Ta, Mo and Si oxides greatly reduced the rate of filament growth at 850°C. It was proposed that once oxides were incorporated within the metal catalyst they acted to reduce carbon solubility in the catalyst particle [161]. This results in reduced density of the metal catalyst's inner core region and the resultant build-up of excess carbon at the particle surface causes premature deactivation of the catalyst. Also the

93

diffusion of any carbon atoms which do dissolve in the metal catalyst is reduced since the temperature gradient, which is the driving force, is affected by the presence of the oxides [161].

Table 1.6 *{Adapted from Ref. 161}* Effect of various additives on the growth of filamentous carbon from Ni-Fe/C_2H_2

Additive	Onset Temperature (°C)	Rate of filament growth at 850°C (nm.sec^{-1})
None	480	413
Alumina	650	428
Titania	635	220
Tungsten oxide	700	12.6
Tantalum oxide	680	34.7
Molybdenum oxide	670	6.6
Boron oxide	475	204
Silica	620	2.1

The effect of sulphur addition on coking has been found to vary depending on the nature of the metal [162]. In the case of iron, stainless steel and Ni, pre-sulphiding was found to reduce the initial formation of carbon while it increased carbon deposition on Cu due to surface modification resulting in dissolution changes, encapsulation and gasification [162]. Somorjai et al. [112] stated that sulphur can selectively poison Pt surfaces as it first blocks the kink sites which have the highest binding energy on the heterogeneous surface. Gorriz et al. [129] have found that increasing the Cr content of Cr-Al_2O_3 catalysts resulted in an increase in the initial rate of coke formation, but conversely the extent of coke deposition per unit mass of catalyst decreased. Low levels of potassium in Al_2O_3–K catalysts lead to a large decrease in the amount of coke due to the fact that low amounts of potassium inhibit medium and strong acid sites [163]. The same authors found that chlorine addition on Al_2O_3 resulted in greater amounts of coke at

temperatures below 567°C. Papadopoulou et al. [164] discovered that fluorination of Ni-Mo/γ-Al$_2$O$_3$ catalysts decreased markedly the extent of coke formation on the surface with maximum inhibition observed for 0.3 wt.% F$^-$ ions.

Trimm [125] has reviewed minimisation of coking in terms of the ensemble effect. If the formation of methane from CO broken down to elemental carbon is taken as an example then an ensemble of five sites located in an appropriate symmetry on the catalyst surface would be necessary for the production of methane.

$$2 \underset{\times}{} + CO \rightarrow \underset{\times}{C} + \underset{\times}{O}$$

$$\underset{\times}{C} + 4 \underset{\times}{H} \rightarrow CH_4 + 5 \times$$

$\times$: surface site
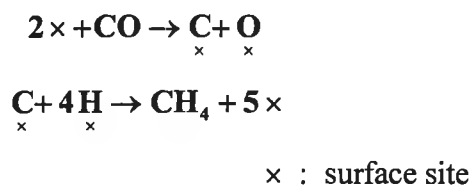
Assuming that coking involves the polymerisation of carbon, then the number of sites required in the ensemble should be large suggesting that coking could be minimised if the ensemble size was controlled to the point where the desired reaction could proceed but coking could not [125]. It may be possible to do this by blocking sites on the surface using methods such as adsorption or inclusion of a component in the catalyst which limits the ensemble size of the catalytically active species. The adsorbing species should be strongly adsorbed or be able to maintain an equilibrium over the catalyst and compounds containing sulphur and nitrogen can provide this function [125]. Addition of Pt [165] and Ir [166] to catalysts has been shown to limit ensemble size, thereby, reducing coking and catalysing coke gasification.

A major advance in coke inhibition came with the development of bi- and multi-metallic catalysts [167]. Wentrcek et al. [168] found that the addition of Ir to Ni on Al$_2$O$_3$ catalysts blocked ensembles containing 3– or 4– adsorption sites. It has also been shown by Ramaswamy et al. [166] that Pt-Ir catalysts reduce coking by enhancing gasification. Espinat et al. [143] have found

that bimetallic Pt-Ir and Pt-Re are more temperature stable than monometallic catalysts and that Ir or Re can destroy the strongly dehydrogenated hydrocarbon molecules which act as coke precursors. This destruction of coke precursors is usually catalysed by metal particles [155]. According to Parera et al. [169], the migration of hydrogen onto Al_2O_3 by spill-over would promote destruction of coke deposits on the support and additives such as Re and Ir would increase the rate of this migration. A comparison between Pt/Al_2O_3, $Re-Al_2O_3$ and $Pt-Re-Al_2O_3$ with regard to coking was made by Parera et al. [170]. They found that the level of coking was lower on the Re and Pt-Re catalysts due to their higher capacity to break H–H bonds. It was also found that in these catalysts sulphur decreased the number of large ensembles available for hydrogenolysis, increasing the concentration of coke precursors on the support. Increasing the H_2/HC ratio on a monometallic Pt/Al_2O_3 catalyst, gave a Raman spectrum quite similar to the one obtained on a Pt-Ir bimetallic catalyst suggesting to Espinat et al. [147] that addition of a second metal acts to reduce coke precursors in the same manner as an increase in hydrogen pressure. Barbier et al. [171] have discovered that the addition of Ir or Re to Pt acts to reduce coke formation in the same way as does increasing overall pressure for the coking reaction on Pt/Al_2O_3 catalysts.

Re addition to $Pt-Al_2O_3$ n-heptane reforming catalysts slowed down conversion of C_5 naphthenes to coke [172] and increased the hydrogenating capacity of the catalyst [173].

Interaction between catalyst components can minimise coke accumulation and is described in terms of the spillover effect by Neikam et al. [174]. The spillover concept involves adsorption of a gas on one catalyst component followed by adsorption of this species onto a second component [174]. This implies that if O or OH species were formed on the surface they could migrate to the metal where gasification of coke could occur. Trimm [175] has found that coking and deactivation of supported metal catalysts is significantly reduced by additives that favour adsorption of water on the support and spillover appears to be the only mechanism that can explain these observations. It has been found by Neikam et al.

[174] that spillover can be enhanced if the bonding between the catalyst and adsorbed fragments is weak allowing easy surface migration. Also the rate of spillover can be increased by the presence of certain molecules that appear to act as bridges (e.g. perylene) between the catalyst components.

Coke can be removed from supported metal catalysts by heating in air [176]. Parera et al. [176] have studied the influence of Pt on the burning temperature of coke produced on Pt-Al_2O_3 reforming catalysts. The Pt in Pt-Al_2O_3 catalysts is supported on the acid sites of Al_2O_3. Oxidation temperature of coke was reduced when the Pt-to-acid ratio was increased suggesting that Pt acts as a catalyst in coke oxidation [176]. The reason suggested for this was that at high concentrations of Pt the coke was less polymerised due to hydrogenation by Pt of coke precursors produced during reforming reactions. Less polymerised deposits would oxidise at lower temperatures [176]. After the initial 10–20% of coke has been burnt the rate of carbon removed by combustion is proportional to the BET surface area [136]. Haldeman et al. [136] also discovered that when combustion was started hydrogen-rich areas of the coke deposit are attacked preferentially. During coke combustion excessive heat can be generated resulting in possible irreversible catalyst sintering and permanent loss of activity [141]. It has been found by Holmen et al. [177] that gasification of the first coke deposit laid down on a new foil always resulted in higher rates of coke formation during subsequent runs. Evidence has been obtained by Pieck et al. [178] to suggest that during regeneration of Pt-Re-S/Al_2O_3–Cl catalysts, part of the coke on the support migrates to the metal where it is easily burnt. Further evidence has been offered by Basso et al. [149] who found that oxidation of some coke takes place on or near the metal sites and is efficiently catalysed by Pt oxide.

Hughes et al. [179] have removed coke, laid down under mild conditions, from hydrodesulphurization catalysts using hydrogen. After two hours H_2 gasification, the carbon levels on Co–Mo and Ni–Mo/γ-Al_2O_3 catalysts were reduced by 50% and after six hours by 90% which suggests that there may be at least two different forms of coke on the surface which are hydrogenated at different rates.

According to the authors this method provides a quick method of regenerating the activity of Mo/γ-Al$_2$O$_3$ catalysts, compared to a full oxidative regeneration and does not significantly affect the dispersion of molybdenum.

Chapter

Two

Experimental studies of coke deposition by TGA and TPO on alumina and modified alumina supported platinum

2   Introduction

Coke formation occurs on Pt/γ-Al$_2$O$_3$ oxidation catalysts leading to reduced activity and eventual deactivation of these catalysts. The coke formed can be deposited on the metal or on the support and even supports on their own can generate coke when exposed to air/hydrocarbon mixtures under similar oxidising conditions to those used for Pt/γ-Al$_2$O$_3$ catalysts. In this section, coke formation on Pt/γ-Al$_2$O$_3$, silica gel, α–, γ– and η–Al$_2$O$_3$ during oxidation of isobutane was examined along with conditions affecting coking such as fuel flow rate and temperature. The amount of coke deposited was determined using Thermogravimetric Analysis (TGA) and TPO which also gave details regarding where the coke was deposited. In an attempt to find ways of reducing coking, the catalysts were modified by physical and chemical means and the effect these modifications had on amount of coke formed was determined by TGA and/or TPO.

2.1   Experimental

2.1.1   Determination of coke formation using TGA.

A TGA (Stanton Redcroft TG–750/770) connected to a two pen Linseis L6510 chart recorder was used to determine the temperature of coke deposition, optimum flow rate for coke formation and amount of coke deposited, Fig. 2.01. Supports studied were (i) silica gel (60–120mesh, BDH Ltd. Poole England) (ii) α-Al$_2$O$_3$ (corundum, Aldrich chemical company Inc.) (iii) finely ground η-Al$_2$O$_3$ ('saffil mat' ICI) and (iv) γ-Al$_2$O$_3$ (puralox, condea), under a stoichiometric atmosphere of air/isobutane (32:1). To determine the optimum temperature of coke deposition ~5mg samples were heated to 500°C at a rate of 10°C/min. under an atmosphere of air/isobutane (32:1), flowing at 20cm^3/min.. Weight changes were monitored to within 0.05mg using a chart recorder. The temperature where the greatest increase in weight occurred was termed the optimum temperature for coke formation.

100

Flow of air isobutane was varied between 8cm^3/min. and 66cm^3/min. while the sample (2–2.5mg) was held at the optimum temperature for coke formation, to determine the effect of flow rate on coke formation. The sample was held for approximately 2 hours at each flow rate and weight changes measured with a detection limit of 0.005mg.

Finally using samples of <4mg, under conditions of optimum flow-rate and temperature, the amount of coke deposited on a selection of catalysts was determined to an accuracy of 0.005mg. Blank runs were performed on the silica gel, α-, η- and γ-Al$_2$O$_3$ under atmospheres of air and nitrogen to confirm that the weight increase was due to coke deposition caused by isobutane. TGA was also performed on an empty sample pan under each of the three atmospheres to act as a blank and again no weight increase was observed as the temperature was increased to 500°C.

A schematic diagram of the thermogravimetric analyser (TGA) used is given in Fig. 2.01.

Fig. 2.01 *{Ref. 181}*

TGA Apparatus
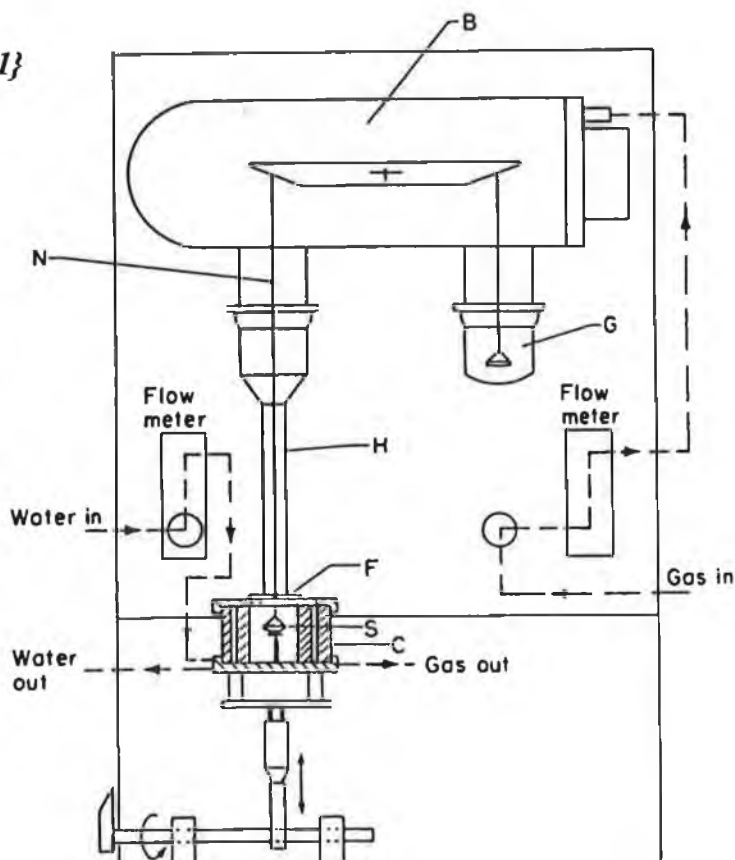
where

    S   : Platinum crucible for holding sample

    N   : Sample arm of balance

    B,H : Glass housing to protect from dust and draughts

    C   : Water cooled furnace assembly

    F   : Flange which forms gas tight seal with C

    G   : Reference balance pan

2.1.2 Quantification and characterisation of coke using Temperature Programmed Oxidation.

A schematic of the apparatus used is given in Fig. 2.02. Using gas flow controllers the volume of isobutane was regulated at $0.75cm^3$/min. and the flow of air regulated at $24cm^3$/min.. These two gases were then mixed and passed over the sample which was contained in a pyrex U–tube. Sample weights of $0.3000g(\pm0.0005g)$ were used in all analysis. The sample was heated to $400^{\circ}C$ by placing a 'Lenton Thermal Design' tube furnace, already at $400^{\circ}C$, around the U–tube. Samples were coked under flowing atmospheres of air/isobutane for three hours.

After coking, the furnace was removed from around the U–tube and the sample allowed to cool in a static air/isobutane gas mixture with the gas flow diverted to vent. When cool the sample was purged with air, at a flow rate of $24cm^3$/min for five minutes, and the air then passed to vent. After this period, the air passing over the sample was directed through the carbon dioxide analyser (The Analytical Development Co. Ltd., Hoddesdon, England). The CO_2 analyser, which used infra-red detection, was zeroed using the CO_2 content of the air. The furnace was then placed around the U–tube and the sample heated from room-temperature to $540^{\circ}C$ at a rate of $10^{\circ}C$/min, then maintained at $540^{\circ}C$ for sixty minutes.

Fig. 2.02 Schematic outline of TPO apparatus.

Air

Chart recorder

Vent

Vent

Infrared CO2 analyser

Vent

103

Iso-butane

Vent

Vent
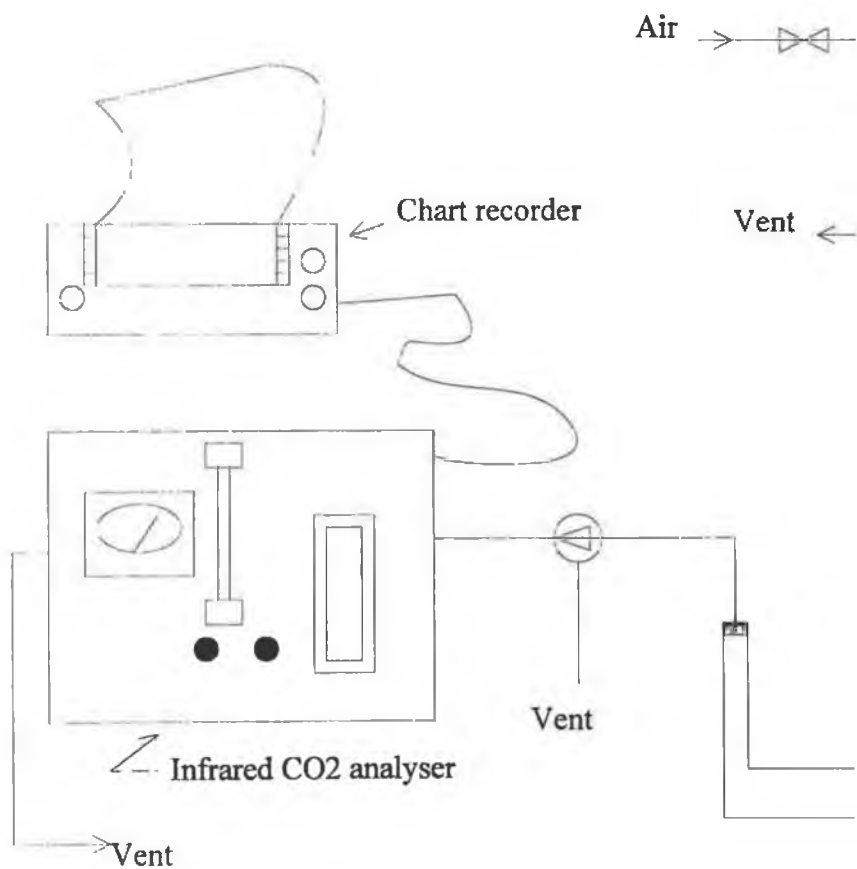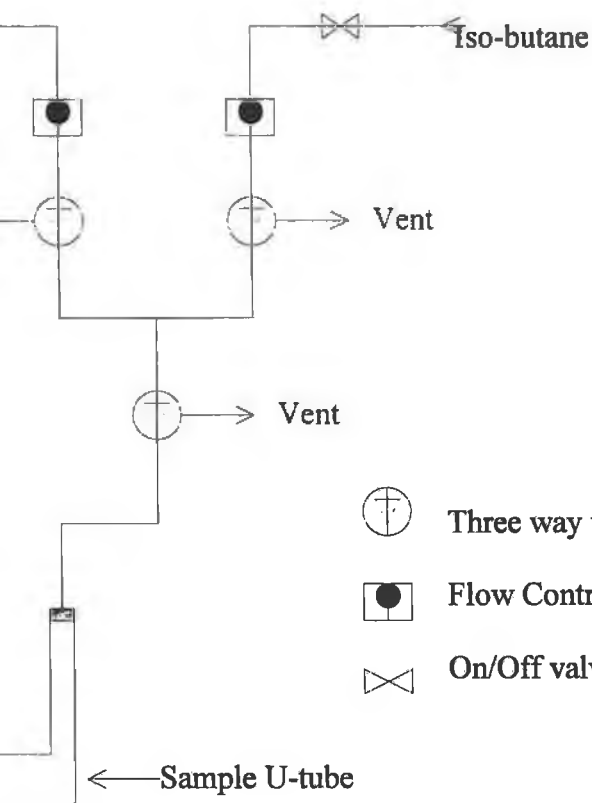
Three way valve

Flow Controller

On/Off valve

Sample U-tube

A maximum temperature of 540°C for TPO was chosen since the sample tubes used were made from pyrex which deformed above 550°C. Throughout the analysis a 'Viatron, multirange, module B' chart recorder was used to monitor the output from the CO_2 analyser.

A standard curve was prepared for the CO_2 analysis by injecting accurately measured volumes of CO_2 into the air carrier stream and measuring the area under the curves generated. The volumes of CO_2 used for the standard curve ranged from 200 to 3000µl and all injections were done in triplicate.

Area under each peak was calculated by counting the number of squares enclosed by each peak on the squared chart-recorder paper and using the calibration graph the amount of C removed was calculated (see Appendix 1). Where a peak took a long time to return to the baseline, the peak area was estimated between the start of the peak and thirty minutes after 540°C had been reached. The max of each peak was also noted. In each case the coke adsorption/desorption cycle was performed in duplicate on the same sample.

The gases used for this analysis were general purpose grade supplied by 'Irish Industrial Gases' and the flow rate of the air and isobutane were checked and recalibrated if necessary on a weakly basis.

2.1.3 Acid/base treatment of γ-Al_2O_3

For the acid treatment, approximately 2g of γ-Al_2O_3 was added to 100cm^3 ~0.1M HCl prepared by diluting 0.85cm^3 concentrated HCl to 100cm^3 in deionised water. The mixture was shaken vigorously to ensure thorough reaction, and then filtered through a sintered glass funnel (No. 4). Excess HCl was removed by washing the sample with 500cm^3 deionised water. The filtrate was confirmed to be chloride free using silver chloride TS (testing standard) solution. The sample was then dried at 110°C overnight and stored in a desiccator.

For base treatment, a solution of approximately 0.1M NaOH was prepared by dissolving 0.2048g solid NaOH in 50.0cm^3 deionised water. To this solution approximately 1g of γ-Al$_2$O$_3$ was added. The mixture was then shaken vigorously to ensure thorough reaction. Filtration was done under vacuum through a sintered glass funnel (No. 4) and the sample washed with deionised water until excess NaOH was removed. The sample was left to dry overnight in an oven at 110°C and then stored in a desiccator.

An alternative base treatment was to purge the sample with NH$_3$ gas. Ammonia gas can be produced by heating an ammonium salt with a strong solution of base. 10g of NH$_4$Cl was placed in a three neck round bottomed flask fitted with a pressure equalising separating funnel containing a concentrated solution of KOH. A tube connected the flask to a U-tube containing approximately 3g of γ-Al$_2$O$_3$ on a sintered disc, Fig 2.03. When heat was supplied to the reaction flask, using a heating mantle, ammonia gas was produced according to the equation.

$$NH_4Cl_{(S)} + KOH_{(aq)} \rightarrow NH_{3(g)} + H_2O_{(l)} + KCl_{(aq)}$$

This gas then passed over the Al$_2$O$_3$ in the U-tube before going through a scrubber containing water and then to vent. The flow of gas over the Al$_2$O$_3$ was indicated by generation of bubbles in the scrubber. By regulating the heat and quantity of KOH added to the reaction flask it was possible to pass a steady flow of ammonia gas over the sample of γ-Al$_2$O$_3$ for fifteen minutes at approximately 20cm^3/min..

Fig. 2.03 Apparatus used for Ammonia treatment of γ-Al_2O_3

Conc. KOH solution

Gamma alumina

Sintered glass disk

Ammonium chloride

Hot plate

Ammonia to vent

Dressner containing water
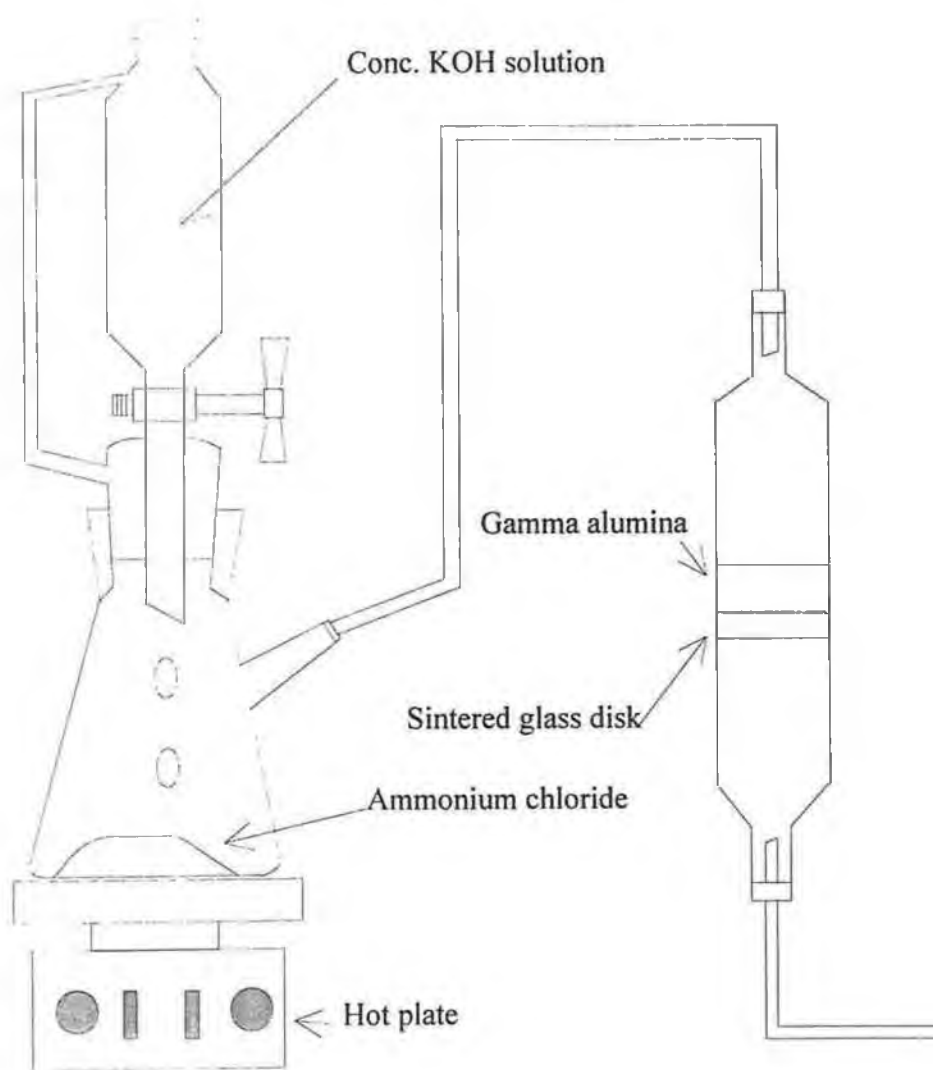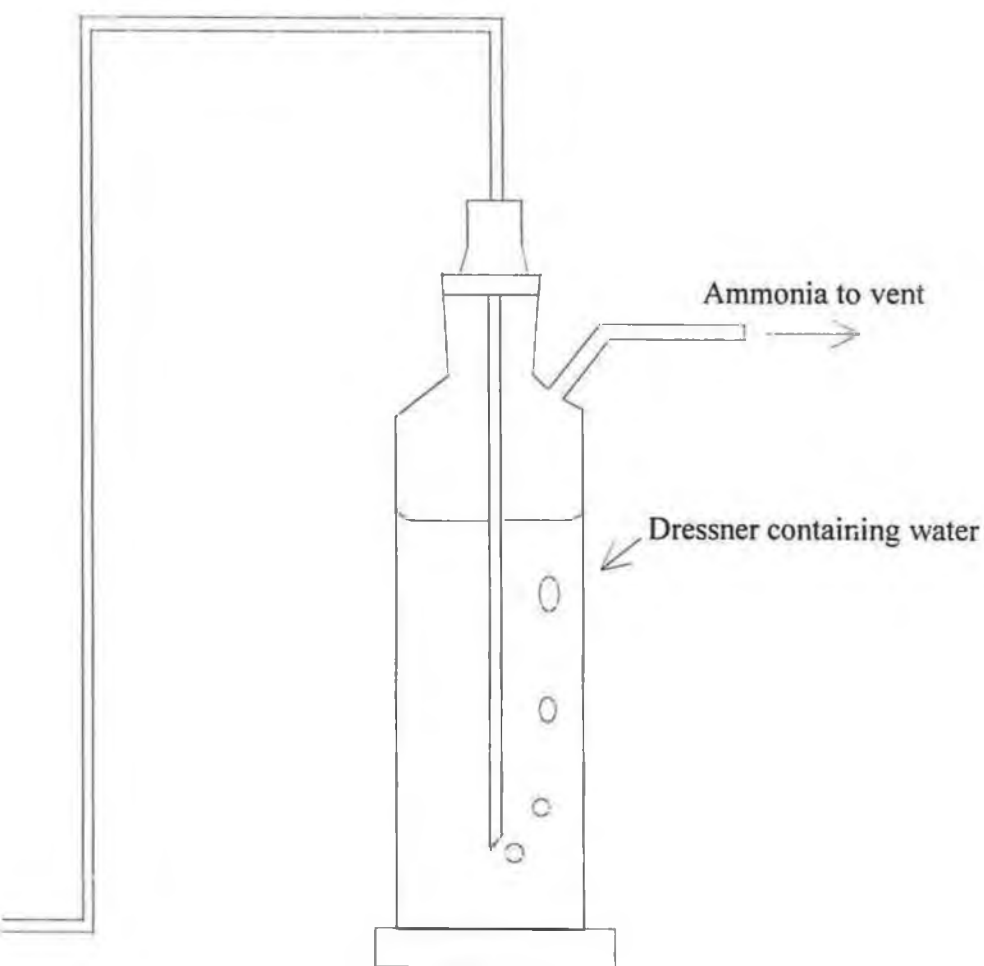
2.1.4 Impregnation of γ-Al$_2$O$_3$ with metal salts.

The required amount of metal salts were accurately weighed into a clean, dry, round-bottomed flask. Between 2.00 and 5.00cm^3 of ethanol were then added to dissolve the metal salts. A known amount of γ-Al$_2$O$_3$ was then weighed into the flask. If necessary more ethanol was added to achieve a suspension of the γ-Al$_2$O$_3$ and allow thorough mixing. The suspension was stirred for approximately five minutes and then the solvent removed by rotary evaporation. Samples were dried overnight in an oven at 55°C then placed in a clean ceramic crucible and heated in static air, using a muffle furnace, to a specified temperatures for a certain period of time i.e. calcination. Samples were then removed from the furnace and allowed to cool in a desiccator before being placed in airtight sample bottles.

Tin was impregnated on γ-Al$_2$O$_3$ at levels of 0.5 and 2.0% using SnCl$_4$.5H$_2$O. Normally the calcination procedure used in this laboratory entailed placing the sample in a furnace at 630°C for fifteen minutes and then allowing to cool in a desiccator. However, Burch [135] has recommended calcining Sn/γ-Al$_2$O$_3$ catalysts at 500°C for two hours to prevent volatilisation of Sn. In order to allow comparison, after impregnation the Sn/γ-Al$_2$O$_3$ catalysts were divided into two. One portion was calcined at 630°C for fifteen minutes while the other was calcined at 500°C for two hours. Bi-metallic Pt-Sn/γ-Al$_2$O$_3$ catalysts were also prepared by co-impregnation, with a 0.5% platinum content and 0.5% and 2.0% levels of tin. Again these were divided into two portions one of which was calcined at 630°C for fifteen minutes and the other at 500°C for two hours.

Using CeCl$_3$.7H$_2$O as the source of Ce, γ-Al$_2$O$_3$ was impregnated with 0.1, 0.5 and 2.0%Ce. Bimetallic Pt-Ce/γ-Al$_2$O$_3$ catalysts containing 0.5%Pt with 0.3%, 0.5%, and 3.0%Ce were prepared by co-impregnation and then calcined.

Zr/γ-Al$_2$O$_3$ and Pt-Zr/γ-Al$_2$O$_3$ catalysts were prepared which contained 0.5 or 2.0% Zr 0.5% Pt. The salt from which Zr was obtained was

ZrOCl$_2$.8H$_2$O. All samples were calcined in air at 630°C for fifteen minutes before analysis.

2.1.5 Step impregnation of γ-Al$_2$O$_3$ with metal salts.

Step impregnation was used to prepare a series of bi-metallic supported metal catalysts i.e., Pt–Ce/γ-Al$_2$O$_3$, Pt–Sn/γ-Al$_2$O$_3$, and Pt–Zr/γ-Al$_2$O$_3$. These contained a nominal Pt content of 0.5% and variable amounts of the other metals. In all cases Pt was the second metal impregnated.

As for 2.1.4 the required amount of metal salt was weighed into a clean dry, round-bottomed flask and dissolved in ~2.00 – 5.00cm^3 ethanol. The γ-Al$_2$O$_3$ support was then added and after mixing, the solvent removed by rotary evaporation, followed by drying and calcination.

Into another clean dry round-bottomed flask the amount of chloroplatonic acid required was accurately weighed and dissolved in ethanol. The monometallic sample already prepared was then added to the dissolved platinum solution and the suspension mixed thoroughly. Following this, the solvent was removed by rotary evaporation and the catalyst then dried and calcined as outlined in section 2.1.4.

Calcination entailed placing the catalysts in a muffle furnace, held at 630°C, for 15 minutes under an atmosphere of static air with the exception of Pt-Sn/γ-Al$_2$O$_3$ catalysts which were calcined in static air at 500°C for two hours.

2.1.6 Monitoring of gases evolved during the Temperature Programmed Oxidation of coke from γ-Al₂O₃

A Shimadzu 14A GC with a thermal conductivity detector (TCD) followed by a flame ionisation detector (FID) arranged in series was modified as shown in Fig. 2.04(i). A dual injection port led on one side to a carbosieve column which was connected to a TCD. The other side of the injection port led to a Poropak column connected to an FID detector. Each injection port was fitted with a Gas Sampling Valve (GSV) of loop volume 500µl. Helium was used as the carrier gas for each column. The flow of helium through the column connected to the FID detector was controlled by a gas flow controller. As the TCD is a mass flow detector and the flow rate of carrier gas through it must remain constant so as to prevent serious baseline drift, a combined mass flow controller and flow meter arrangement as shown in Fig. 2.04 provides a constant flow of helium to the carbosieve column and TCD detector even when temperature ramps are being run or there is a change in helium pressure at the cylinder. The gas sample line was connected to one of the GSVs and the vent from this valve connected to the sample inlet of the second gas sampling valve. This allowed the sample loop of each to be filled almost simultaneously by a single gas sample line.

Using a series of hydrocarbon gases (C1–C6 n-paraffins) and permanent gases (1%CH_4, CO, CO_2, H_2, & O_2 in N_2) conditions were optimised for their separation. The gas mixtures were high purity Scott speciality gases supplied by Supelco Inc.. Analysis conditions consisted of holding the columns at 35°C for four minutes after injecting from both GSVs and then heating the columns to 150°C at a rate of 40°C/min.. Temperature was held at 150°C for a further six minutes before cooling. Separation of the hydrocarbons occurred on the poropak column while the permanent gases separated on the carbosieve column.

Fig. 2.04(i) Schematic outline of modified GC system.

Helium

On/Off valve

Mass flow controler

Gas sample in

Vent

Flow controller

Helium

Molecular sieve

1.

2.

A

Six port gas sampling valve

Reference line

Injection port

TCD — Output

Output = FID

Air

Hydrogen

Carbosieve column

Poropak Column

A : See Enlargement in Fig. 2.04(ii)

110
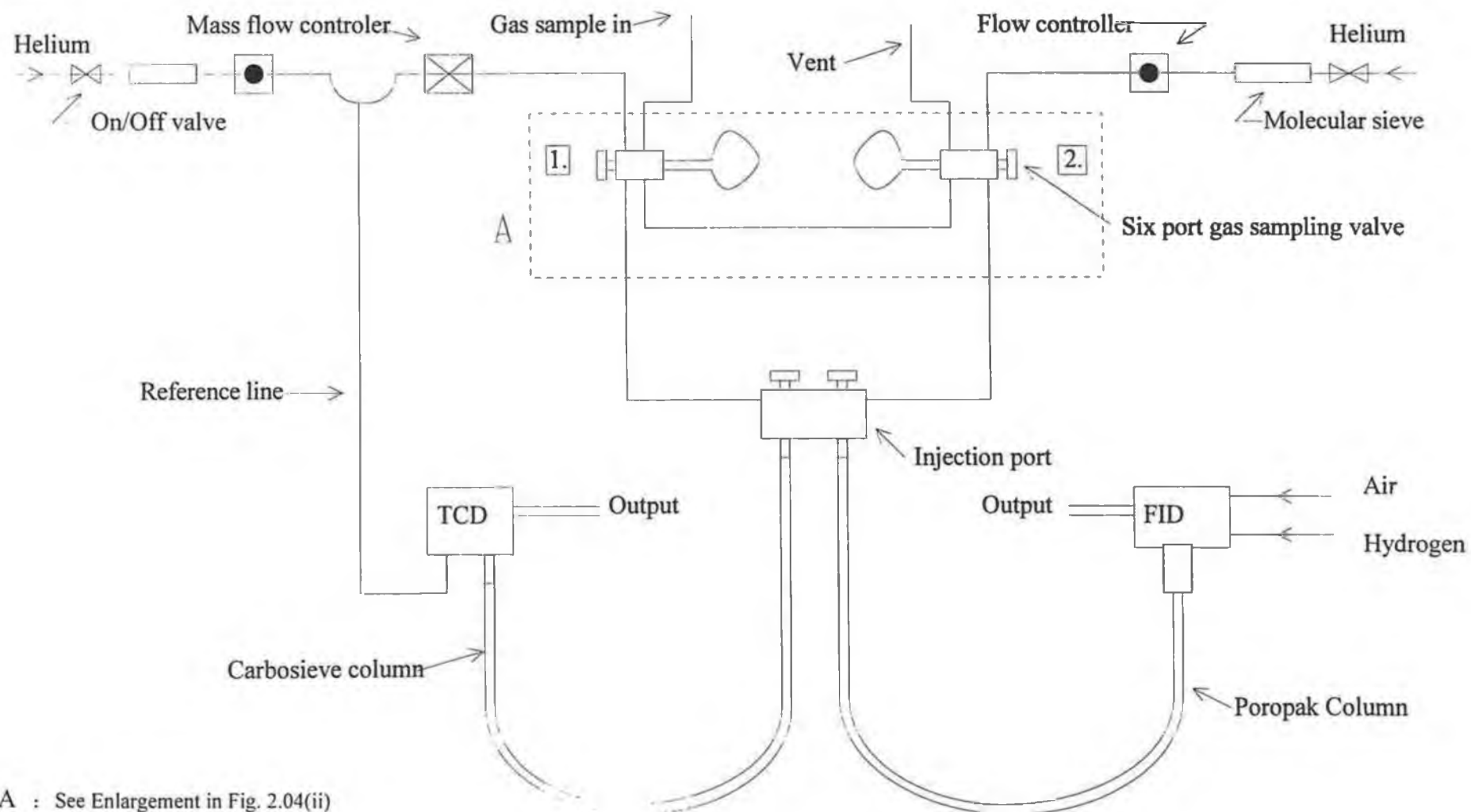
Fig 2.04(ii) Gas line arrangement for Gas Sampling Valves.

A.

Gas sample

Vent

1.

2.

Sample loops

He

To carbosieve column

He

To poropak column
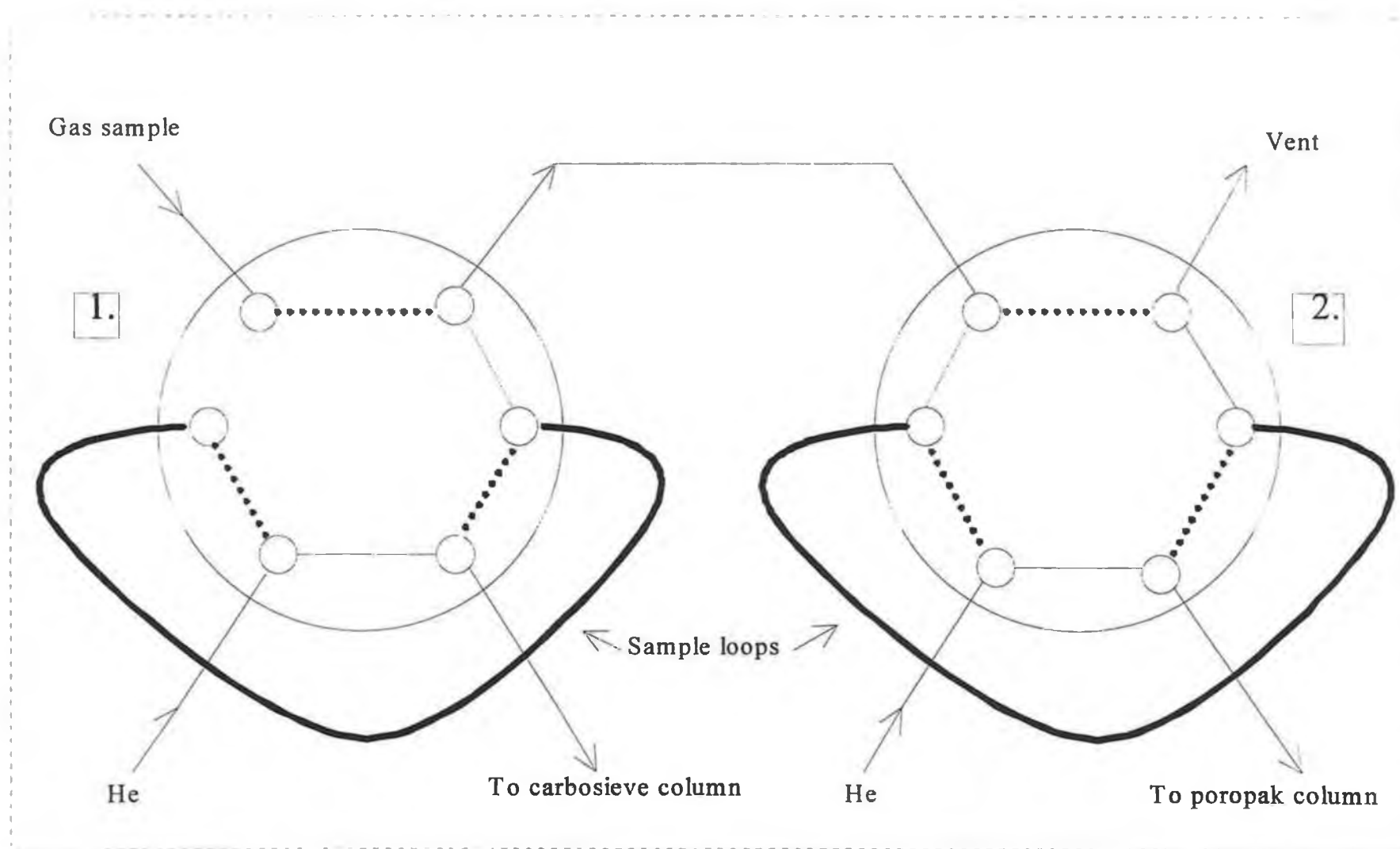
To determine the gases evolved when a coked sample of γ-Al_2O_3 was heated, the stream of air flowing over the sample was disconnected from the CO_2 analyser and connected to gas sampling valve no. 1, Fig. 2.04(i). The coked sample was heated from room-temperature to $540^{\circ}C$ at a rate of $2^{\circ}C/min$. and injections from each GSV performed simultaneously onto the GC at 40° intervals, starting at $20^{\circ}C$. A repeat of this experiment was performed using a sample heating rate of $10^{\circ}C/min$., and analysis injections were made at $100^{\circ}C$, $300^{\circ}C$, $500^{\circ}C$ and $540^{\circ}C$. Instrumental set up and a summary of the experimental conditions used for the GC analysis are presented in Table 2.01.

Table 2.01   Conditions used for GC analysis

GC		Shimadzu GC–14A	
TCD Line			
	Column packing	Carbosieve	
	Column size	Length : 1000mm Internal diameter : 3mm	
	Carrier gas	He	
	Flow controller		1.8Kkg/cm^2
	Mass flow controller		1.5kg/cm^2
	Current	100mA	
	Polarity	1	
	Recorder sensitivity	20mV	
FID Line			
	Column packing	Poropak 30	
	Column size	Length : 1000mm Internal diameter : 3mm	
	Carrier gas	He (0.8kg/cm^2)	
	Air	0.65kg/cm^2	
	Hydrogen	0.65kg/cm^2	
	Range	10^2	
	Polarity	1	
	Recorder sensitivity	10mV	
Instrumental parameters			
	Injector temperature	210^{0}C	
	Detector temperature	220^{0}C (FID & TCD)	
	Chart recorder speed	1 cm/min.	
Program			
	35^{0}C for four minutes		
	Ramp	40^{0}C/min.	
	Final temperature	150^{0}C	
	Time at final temperature	6 mins.	

In order to identify the compounds which may be eluted during TPO of coked γ-Al$_2$O$_3$ the retention times of the following compounds were determined.

Table 2.02 Compounds detected by the FID

Compound	Retention Time(mins)
Methane	0.20
Ethane	0.95
Propane	4.90
n-Butane	6.65
n-Pentane	7.85
n-Hexane	10.00
iso-Butane	7.80

Table 2.03 Compounds detected by the TCD

Compound	Retention Time(mins)
CO$_2$	6.80
CO	1.30
CH$_4$	4.10
H$_2$	0.70
O$_2$ + N$_2$	1.00
H$_2$O	8.60

2.1.7 Hydrogen chemisorption measurement

Hydrogen chemisorption measurements were performed on a Micrometrics Pulse Chemisorb 2700 instrument. This instrument is represented schematically in Fig 2.05.

Fig. 2.05 Schematic outline of Micrometrics Pulse Chemisorb 2700

FLOW READ SWITCHES FLOWMETER BETWEEN PREP & TEST CIRCUITS
DELAY ADDS EXTRA VOLUME BETWEEN SAMPLE UNDER TEST AND CELL B
INJECT MOVES LOOP BETWEEN TEST AND LOAD CIRCUITS
PATH SELECT REPLACES SAMPLE CELL WITH VOLUME APPROX. EQUAL TO EMPTY CELL
SAMPLE SELECT INTERCHANGES SAMPLES BETWEEN TEST AND PREP. CIRCUITS

115
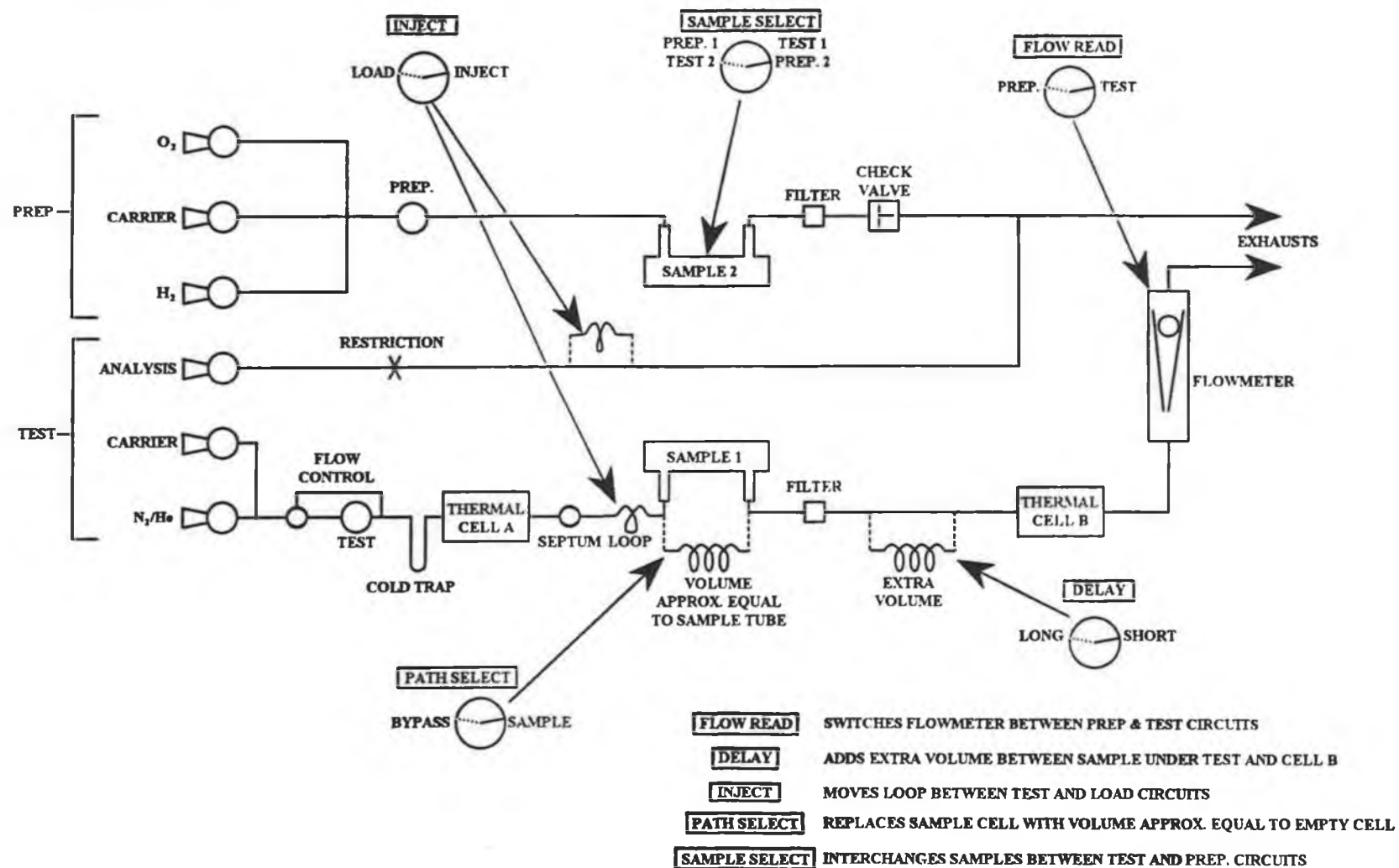
The gases used for catalyst pre-treatment and measurement were purified as they entered the instrument. The argon used (normal grade, Air Products Ltd.) was purified using a B.O.C. Rare Gas Purifier, which contained titanium granules held at 700°C to remove N_2 and O_2, a copper furnace to remove hydrocarbons, H_2 and CO, and a molecular sieve at ambient temperature to remove H_2O and CO_2. The hydrogen used (CP grade, Air Products Ltd.) was purified using a Johnson Matthey EP1 hydrogen purifier, which operated on the principle of hydrogen diffusion through a palladium alloy membrane that only allowed the passage of H_2. These purifiers gave specific purity of greater than 99.99% for both the argon and hydrogen.

Analysis of the sample involved weighing approximately 0.1g, accurately, into a clean dry, pre-weighed pyrex U-tube. The sample U-tube was then attached to the instrument. Pre-treatment of the sample was carried out on the prep. line of the instrument. Initially the sample was purged with argon at 15cm^3/min. for 25 minutes at room temperature. The sample was then heated to 100°C and held at this temperature for 30 minutes before being heated to 250°C and kept at this temperature for 60 minutes under flowing Ar. Reduction was done by passing hydrogen (15cm^3/min.) over the sample for 60mins. at 250°C followed by 400°C for two hours. After reduction the sample was purged in argon at 400°C for 25 minutes. The sample, once cooled to room temperature, was switched to the test line of the instrument via the four way switching valve and successive injections of 48µl hydrogen pulses were made into the Ar stream flowing over the sample. Non-adsorbed hydrogen was analysed by a thermal conductivity detector within the instrument. Desorption of the hydrogen involved heating the sample to 400°C for 15 minutes. Each analysis consisted of at least two adsorption/desorption cycles which gave the same or very similar results and after testing the sample tube was re-weighed in order to determine the dry sample weight.

This analysis method was examined by measurement of H_2 uptake by the silica supported platinum standard catalyst, Europt-1 [194]. Average

uptake was found to be 149µmol/g as opposed to between 160 and 190µmol/g as found by an international study [194].

2.2 Results and discussion.

TGA to determine the optimum temperature of coke formation on each of the supports revealed a slight increase in weight for the γ-Al_2O_3 sample as the temperature reached $350^{\circ}C$ which disappeared above $450^{\circ}C$. Using this procedure no weight increase was observed for α-Al_2O_3, η-Al_2O_3 or silica gel.

The optimum temperature for coke formation on γ-Al_2O_3 was $400^{\circ}C$. The amount of coke formed as a function of the air/isobutane flow rates are tabulated in Table 2.04 and represented graphically in Graph 2.01. A flow rate of $25cm^3$/min. air/isobutane was considered optimum for coke formation. This was the flow rate used for all subsequent coking experiments that had isobutane as the hydrocarbon source.

Table 2.04 Table of weight increases at various air/isobutane flow rates.

Flow rate (cm³/min.)	Wt. increase (mg)
8	0.01
16	0.02
25	0.04
35	0.03
45	0.01
55	0.00
66	0.00

118

Graph 2.01   Graph to determine the optimum flow rate for coke formation

Graph of Weight increase Vs Flow rate
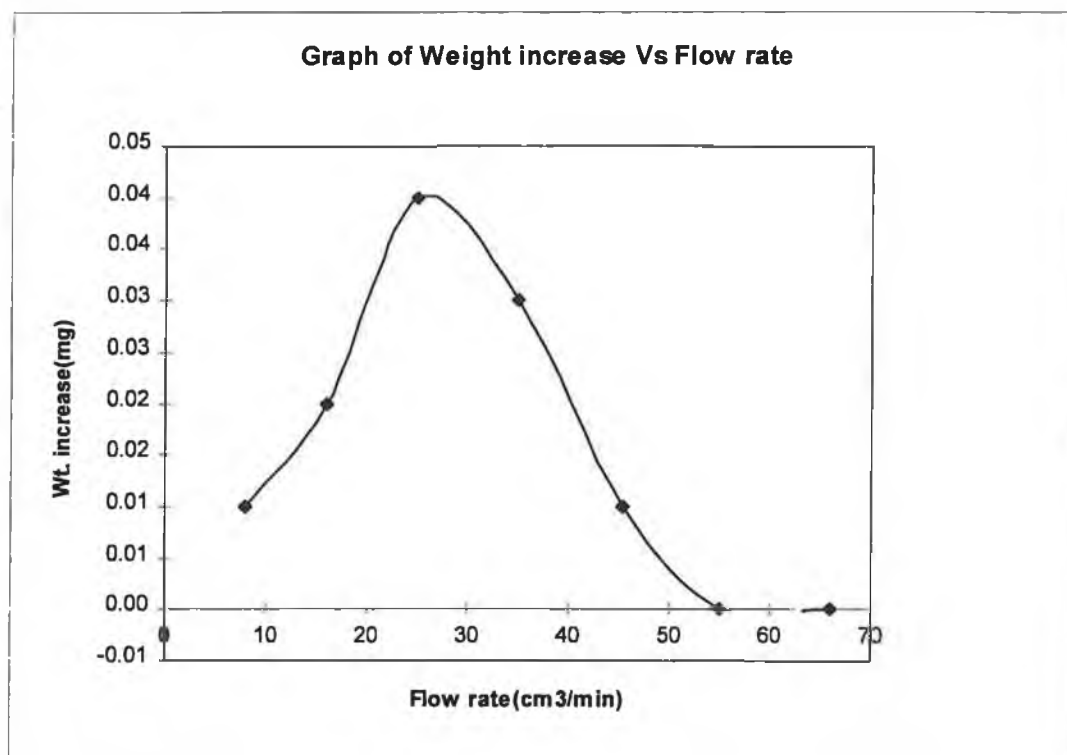
The amount of coke deposited at 400°C, on each of the support materials and $Pt/\gamma-Al_2O_3$ is given in Table 2.05. Weights quoted have an associated error of ±0.005mg. As each sample was heated to 400°C, initially a weight loss was recorded which was probably due to loss of H_2O. This is recorded in Table 2.05 as weight of volatiles. The actual weight taken was the original weight minus the weight loss due to volatiles. After 2 hours, the final weight was recorded and the percentage weight increase calculated relative to the actual weight recorded. Each sample was done in duplicate. From the results in Table 2.05 it can be seen that the highest weight gain as a result of coking was observed for $\gamma-Al_2O_3$. The η-Al_2O_3 and $0.5\%Pt/\gamma-Al_2O_3$ under these conditions showed an increase in weight of 0.5%.

Table 2.05 Weight gain from coking determined by TGA

Sample		Initial weight (mg)	Weight of volatiles (mg)	Actual weight (mg)	Final weight (mg)	% Weight increase
α-Al_2O_3	(1)	2.34	0.01	2.33	2.33	< 0.2%
	(2)	2.08	0.01	2.07	2.07	< 0.2%
η-Al_2O_3	(1)	2.30	0.14	2.16	2.17	0.5%
	(2)	2.23	0.15	2.08	2.24	0.5%
γ-Al_2O_3	(1)	2.20	0.16	2.04	2.08	2.0%
	(2)	2.20	0.21	1.99	2.02	1.5%
Silica gel	(1)	2.32	0.35	1.98	1.97	< 0.2%
	(2)	2.22	0.39	1.83	1.83	< 0.2%
0.5%Pt-Al_2O_3	(1)	2.08	0.12	1.96	1.97	0.5%
	(2)	2.35	0.11	2.24	2.25	0.5%

It is interesting to note that the temperature at which coke begins to form on γ-Al_2O_3 is just 50°C above the temperature at which Peri et al. [21] showed that water molecules not desorbed by heat during drying react to form surface hydroxyl groups. Later Maciver et al. [45] found that γ-Al_2O_3 did not develop appreciable acidity until 200–300°C which coincided with removal of 3.5wt.% of its 7wt.% water content. Lippens et al. [182] has shown that above 300°C Brönsted acid sites are gradually converted to Lewis acid sites, but it has also been stated that enough water is always present to generate Brönsted sites also [1]. This information suggests that the commencement of coking on γ-Al_2O_3, which we observed in our experiment, is associated with the removal of surface hydroxyl groups and the subsequent generation of Lewis acid sites.

The reduction in amount of coke formed on γ-Al_2O_3 after addition of platinum may be due to a reduction in the size of coke forming ensembles, caused by the platinum, as proposed by Olander et al. [165]. Since the number of sites required in the ensemble for coke formation is large, addition of any component which limits the size of the ensemble will consequently result in a

reduction in coking [125]. Platinum can also reduce coking by enhancing gasification [166]. Blank runs were performed on samples of γ-Al_2O_3 and empty sample pans under atmospheres of air, nitrogen and nitrogen/isobutane (32:1) gas mixtures. In each case no increase in weight was detected.

Fig. 2.06 shows the weight loss for γ-Al_2O_3 on initial heating. Lippens et al. [182] suggested removal of water molecules from the oxide surface originating from physically adsorbed surface water and/or the combination of adjacent hydroxyl groups to form water molecules, as the cause of weight loss. The percentage weight losses found for γ- and η-Al_2O_3 were 8.4 and 6.4% respectively. Maciver et al. [45] found that γ-Al_2O_3 contained 7wt.% water and η-Al_2O_3 4.5wt.%. These values are lower than those obtained in our study but Maciver et al. [45] based there values on Al_2O_3 which had weakly bound physically adsorbed water already removed by evacuation at 25°C. The observation that γ-Al_2O_3 lost 2% more weight than η-Al_2O_3 supports the view of Maciver et al. [45] that all the water present on η-Al_2O_3 is in the form of surface hydroxyl groups as opposed to γ-Al_2O_3 which in addition to surface hydroxyl groups also has molecular water strongly bonded to its surface even after evacuation at 25°C. This surface bound water can in addition to surface hydroxyl groups be removed by heating to 400°C and may account for the extra weight loss.

A weight loss of 16.3% was observed for silica gel when heated to 400°C. Based on the results of Curthoys et al. [68], a fully hydroxylated silica surface contains about $5OH/nm^2$ at 150°C which is reduced to $1OH/nm^2$ at 800°C, then at 400°C, the maximum temperature of this work, somewhat less than half of the hydroxyl groups have been removed. Dehydration involves the condensation of hydroxyl groups to form siloxane bonds with the subsequent evolution of water [63]. Work by Trouton [75] suggests that the dehydrated surface of silica is hydrophobic with the electrons of the siloxane oxygen atoms not free to enter into hydrogen bond formation. This inability of the oxygen atoms to allow their electrons enter into hydrogen bond formation may explain why no coke was formed on the partly dehydrated silica.

121

Fig. 2.06 Typical Chart for coke quantification by TGA.

Quantification of coke formation by TGA on γ-Al_2O_3
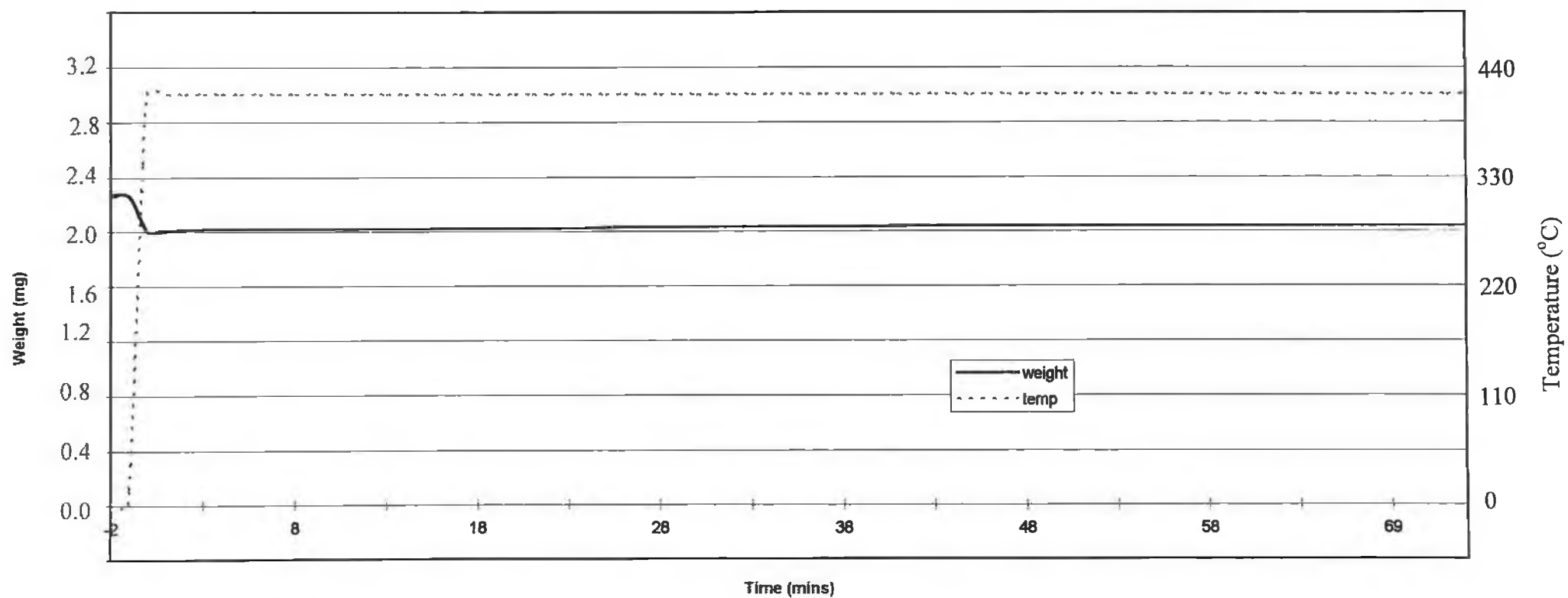
The α-Al_2O_3 only lost 0.5% weight on heating to 400°C and no increase in weight due to coking was detected. The dehydration of α-Al_2O_3 has been studied by Morterra et al. [183] who using infrared spectroscopy found that on α-Al_2O_3 all of the hydrogen bonded water was removed by heating to 250°C and at temperatures above 300°C free hydroxyl groups were the only species on the surface. At 400°C just over 75% of the surface water was found to be removed [183]. However, as Table 2.05 shows, this removal of surface water and hydroxyl groups does not lead to the deposition of coke.

All of the supports listed in Table 2.05 contain surface hydroxyl groups and can undergo dehydration by combination of adjacent hydroxyl groups. The difference in amount of coke deposited may be due to a difference in the polarity or arrangement of the surface hydroxyl groups. It has been shown by Peri et al. [21] that Al_2O_3 may contain several types of surface hydroxyl groups of varying degrees of polarity. The removal of these hydroxyl groups by heating exposes aluminium ions (Lewis acids) and adjacent O^{2-} ions (Lewis bases) [10] which may function as active sites for coke formation. Larson et al. [33] have found that not all Lewis acid and base sites created during dehydration are catalytically active for coke formation. Based on similar work Knözinger et al. [34] found that catalytic activity was only developed between 300°C and 400°C even though 3.7×10^{14} Lewis acid and Lewis base sites had been formed when the Al_2O_3 was heated to 300°C. The authors' [23] deductions based on these results are very interesting when considered in conjunction with the fact that from our study coke formation was seen to commence at 350°C reaching a peak at 400°C and then diminishing after 450°C. Knözinger et al. [23] conclusions were that between 300 and 400°C, special site configurations of low probability may begin to develop which posses the structural and energetic properties required for an active site. The fact that coke formation was seen to fall off after 450°C would suggest that the configurations required for coke formation can only exist within a particular temperature range and are deactivated by heating above this range.

To investigate how increased dehydration affected the level of coke formation on γ-Al_2O_3, a sample of γ-Al_2O_3 was heated in the TGA at 800°C under a 25cm³/min. flowing atmosphere of nitrogen for two hours. The temperature was then decreased to 400°C and the gas flow changed from nitrogen to an air/isobutane (32:1) gas mixture. The sample was held under these conditions for two hours. For comparison, a blank run was performed where the sample was first heated at 800°C, under nitrogen, for two hours and then the temperature held at 400°C under nitrogen. The results of this analysis are given in Table 2.06

Table 2.06   TGA results of coking on sample pre-treated at 800°C

	Run no. 1	Run no. 2	Blank
Initial sample weight at R.T. (mg)	2.30	2.60	2.30
Weight volatiles at 800°C (mg)	0.32	0.32	0.28
Actual weight at 800°C (mg)	1.98	2.28	2.02
Wt. increase after 2 hrs. at 400°C (mg)	0.05	0.04	0.01
% Weight increase based on actual wt.	2.53%	1.75%	0.50%
Average %Wt. increase	1.63%		

The results show that the percentage dehydration at 800°C is 13.1% as opposed to 8.4% at 400°C. Again our calculation of percentage coke deposition was calculated as a percentage of the actual weight which is the initial sample weight less the weight of volatiles. The results showed that the average percentage coke deposited on γ-Al_2O_3 decreased marginally from 1.75%(Table 2.02) to 1.63% after dehydration at 800°C. The difference however is very small and probably within experimental error. In this experiment the blank run showed an increase in weight of 0.01mg when the temperature was decreased from 800°C to 400°C. This is probably due to rehydration by trace amounts of moisture in the nitrogen supply.

Maciver et al. [45] have found that dehydration of γ-Al_2O_3 and η-Al_2O_3 was accompanied by the development of considerable acidity.

Measurement of this acidity by ammonia adsorption revealed that total acidity was about the same for both types of Al_2O_3 and that the average acid strength of the acid sites was greatest for η-Al_2O_3 [45]. If it is assumed that strength of acidity determines the amount of coke formed then it would be expected that η-Al_2O_3 should produce more coke than γ-Al_2O_3. Based on our results this does not appear to be the case. The way in which acidity is generated on dehydration is different for γ- and η-Al_2O_3 [45]. While η-Al_2O_3 develops acidity almost linearly with increased temperature, γ-Al_2O_3 displays very little acidity below 200°C and then develops acidity rapidly which may lead to its coke formation reactions above 350°C. Also it may be that the sites formed on γ-Al_2O_3 are more catalytically active for coke formation than those formed on η-Al_2O_3.

The effect of acid/base modification of γ-Al_2O_3 on the amount of coke deposited was monitored using the quantification of coking method described in Section 2.1.1. No weight increase was observed on NaOH modified γ-Al_2O_3 under air/isobutane (32:1) at 400°C while HCl treated γ-Al_2O_3 showed a decrease in weight of 0.75% over the duration of the run. These results suggest that treatment with NaOH reduces coking. It has been pointed out by Deo et al. [78] that doping of γ-Al_2O_3 with NaOH deactivates the least acidic surface hydroxyl group leaving the Al^{3+} ion (Lewis acid) free to participate in hydrogenation reactions. Fledorow et al. [80] concluded that alkali hydroxides eliminate Lewis acid centres on Al_2O_3. It has been shown by Ross et al. [77] that the sodium ions in NaOH exchange with protons from surface hydroxyl groups i.e. Brönsted acid sites. This suggests that NaOH is not selective for the type of acid site it reacts with and therefore prevents coking by destroying both Brönsted and Lewis acid sites.

The weight loss seen for HCl treated γ-Al_2O_3 may be due to volatilisation of chlorine on the surface of the γ-Al_2O_3. Melchor et al. [92] found that dechlorination of Cl treated γ-Al_2O_3 occurred during isomerisation reactions. This makes it impossible to quantify the amount of coke, if any, formed on the HCl treated γ-Al_2O_3 using the TGA apparatus.

Base pre-treatment of the γ-Al$_2$O$_3$ with NH$_3$ rather than NaOH followed by immediate testing showed no increase in weight of the sample due to coking. NaOH reacts with the least acidic sites [78] while NH$_3$ blocks all acidic sites [38]. However if the γ-Al$_2$O$_3$ was treated with NH$_3$ and tested the following day using TGA, a weight increase of 1.75% was observed. This suggests that NH$_3$ was desorbed with time. It can be concluded that treatment of γ-Al$_2$O$_3$ with NH$_3$ gas does neutralise the surface acidic sites. However, the ammonia desorbes with time and consequently acidity of these sites returns making this treatment of little practical use as a technique for preventing coking.

The effect of Sn, Ce or Zr ion addition on coking of γ-Al$_2$O$_3$ and Pt/γ-Al$_2$O$_3$ was studied.

TGA analysis was carried out to determine the level of coking on Sn/γ-Al$_2$O$_3$ and Pt-Sn/γ-Al$_2$O$_3$ samples and the results obtained are presented in Table 2.07.

Table 2.07 Results of TGA(coke) analysis on Sn/γ-Al$_2$O$_3$ and Pt-Sn/γ-Al$_2$O$_3$

Sample	Calcination treatment	Method of impregnation	Weight increase
γ-Al$_2$O$_3$	——	——	1.5–2.0%
0.5%Sn/γ-Al$_2$O$_3$	500°C/2hrs.	——	1.0%
2.0%Sn/γ-Al$_2$O$_3$	500°C/2hrs.	——	<0.5%
0.5%Sn/γ-Al$_2$O$_3$	630°C/15mins.	——	1.0%
2.0%Sn/γ-Al$_2$O$_3$	630°C/15mins.	——	<0.5%
0.5%Pt/γ-Al$_2$O$_3$	630°C/15mins.	——	0.5%
0.5%Pt-0.5%Sn/γ-Al$_2$O$_3$	630°C/15mins.	Co-impregnated	<0.5%
0.5%Pt-2.0%Sn/γ-Al$_2$O$_3$	630°C/15mins.	Co-impregnated	<0.5%
0.5%Pt-0.5%Sn/γ-Al$_2$O$_3$	500°C/2hrs.	Co-impregnated	<0.5%
0.5%Pt-2.0%Sn/γ-Al$_2$O$_3$	500°C/2hrs.	Co-impregnated	<0.5%
0.5%Pt-0.5%Sn/γ-Al$_2$O$_3$	500°C/2hrs.	Step-impregnated	<0.5%
0.5%Pt-2.0%Sn/γ-Al$_2$O$_3$	500°C/2hrs.	Step-impregnated	<0.5%

Addition of Sn(0.5% or 2.0%) to γ-Al_2O_3 resulted in a decrease in the amount of coke deposited relative to γ-Al_2O_3. A 2.0% Sn loading reduced the level of coking below the detection limit for both calcination temperatures. This may be due to tin acting to reduce the number of coke forming acid sites on γ-Al_2O_3. In the case of bi-metallic catalysts containing Pt and Sn the amount of coke was reduced to below the detection limit in comparison to Pt/γ-Al_2O_3. Burch [135] has found that Sn in Pt-Sn/γ-Al_2O_3 acts to increase the amount of hydrogen adsorbed by platinum. Based on this fact it is reasonable to suggest that any spillover of coke or coke precursors from the support to the platinum surface is likely to undergo hydrogasification if hydrogen is present on the platinum surface.

$$C + 2H_2 \rightarrow CH_4 \qquad [125]$$

The gaseous CH_4 then leaves the platinum surface and hence a process is set up which allows for coke removal. The amount of Sn present on the Pt-Sn/γ-Al_2O_3 surface did not affect the quantity of coke deposited; nor did the method of preparation.

The results for quantification of coke on Ce/γ-Al_2O_3 and Pt-Ce/γ-Al_2O_3 catalysts are presented in Table 2.08. Impregnation with levels of Ce as low as 0.1% were sufficient to reduce coking on γ-Al_2O_3 to below 0.5%(Wt. increase detection limit). Co-impregnated Pt-Ce/γ-Al_2O_3 catalysts containing 3.0% and 0.3% Ce produced 1.5 and 1.0% weight increases respectively while the 0.5%Pt–0.5%Ce/γ-Al_2O_3 catalyst did not form any detectable coke. In the case of step-impregnated Pt-Ce/γ-Al_2O_3 catalysts with either 0.5 or 0.1% Ce no coke was detected. A sample of 0.5%Pt-0.5%Ce/γ-Al_2O_3 (co-impregnated) was coked for a period of eight hours in an air/isobutane gas mixture and a gradual increase in weight of 2.0% was observed over the eight hours. From the results it would appear that the coke inhibitory effect of cerium is merely short term.

Table 2.08 Results of TGA analysis (coke) on Ce/γ-Al$_2$O$_3$ and Pt-Ce/γ-Al$_2$O$_3$.

Sample	Method of impregnation	Weight increase
γ-Al$_2$O$_3$	——	1.5–2.0%
0.1%Ce/γ-Al$_2$O$_3$	——	<0.5%
0.5%Ce/γ-Al$_2$O$_3$	——	<0.5%
2.0%Ce/γ-Al$_2$O$_3$	——	<0.5%
0.5%Pt/γ-Al$_2$O$_3$	——	0.5%
0.5%Pt–3.0%Ce/γ-Al$_2$O$_3$	Co-impregnated	1.5%
0.5%Pt–0.3%Ce/γ-Al$_2$O$_3$	Co-impregnated	1.0%
0.5%Pt–0.5%Ce/γ-Al$_2$O$_3$	Co-impregnated	<0.5%
0.5%Pt–0.5%Ce/γ-Al$_2$O$_3$	Step-impregnated	<0.5%
0.5%Pt–0.1%Ce/γ-Al$_2$O$_3$	Step-impregnated	<0.5%

Finally the Zr/γ-Al$_2$O$_3$ and Pt-Zr/γ-Al$_2$O$_3$ systems were analysed by TGA to determine their coke forming tendencies and the results obtained are summarised in Table 2.09.

Table 2.09 Results for TGA(coke) analysis of Zr/γ-Al$_2$O$_3$ and Pt-Zr/γ-Al$_2$O$_3$ samples.

Sample	Method of impregnation	Weight change
0.5%Zr/γ-Al$_2$O$_3$	——	<0.5%
2.0%Zr/γ-Al$_2$O$_3$	——	−1.0% (2 hr. run time) −2.0% (3 hr run time)
0.5%Pt–0.5%Zr/γ-Al$_2$O$_3$	Co-impregnation	+0.5%
0.5%Pt–2.0%Zr/γ-Al$_2$O$_3$	Co-impregnation	<0.5%
0.5%Pt–0.5%Zr/γ-Al$_2$O$_3$	Step-impregnation	+0.5%
0.5%Pt–2.0%Zr/γ-Al$_2$O$_3$	Step-impregnation	−2.0%

Unlike the results for other systems tested the Zr containing samples showed weight loss for some samples. The weight loss was not due to inadequate calcination as a $2.0\%Zr/\gamma-Al_2O_3$ sample after calcination at $630^{\circ}C$ for two hours as opposed to fifteen minutes gave a weight loss of 1.5%. Volatilisation of Zr is unlikely because of zirconium's high melting temperature, i.e. $1855^{\circ}C$ [184]. A possible explanation however for the weight loss is the conversion of $ZrOCl_2.8H_2O$ to $ZrCl_4$ when heated. $ZrCl_4$ is a white solid which sublimes at $331^{\circ}C$ [184]. Indeed a white deposit was seen on the sample arm of the TGA balance Fig. 2.01 after analysis of samples that contained Zr.

Quantification of coke on the Zr containing samples was therefore difficult as the build-up of coke (wt. increase) could be masked by loss of Zr as a result of sublimation (wt. decrease). Therefore an alternative technique to quantify coke formation on the catalysts systems was used i.e. TPO.

As has been outlined in section 2.1.2 the technique involved coking the sample at $400^{\circ}C$ for three hours under an air/isobutane (32:1) gas flow. After cooling the coke was removed from the catalyst by heating the sample from room-temperature to $540^{\circ}C$ in a flow of air. The coke reacts with O_2 to form CO_2 and water and the quantity of CO_2 formed is directly related to the amount of C present on the sample. By controlling the temperature ramp , the nature of coke on the surface can be examined.

A standard curve was prepared relating the volume of CO_2 to the peak area obtained on the CO_2 analyser (Table 2.10 and Graph 2.02). Blank runs on $\gamma-Al_2O_3$ which had suspended in ethanol, then calcined and $\gamma-Al_2O_3$ not exposed to air/isobutane were carried out. A typical trace for $\gamma-Al_2O_3$ is given in Fig. 2.07 and a worked example for calculating the amount carbon present is given in Appendix 1.

Table 2.10 Area of graphs for specified volumes of CO_2

Volume CO_2 (μl)	Peak area (units^2)
200	248
400	349
600	610
800	840
1000	1250
2000	1962
3000	3490

Graph. 2.02 Standard curve for CO_2

Graph of Peak Area Vs Vol. CO2

$y = 1.1099x$

$R^2 = 0.9863$

Area (units2)

Vol. CO2(ul)
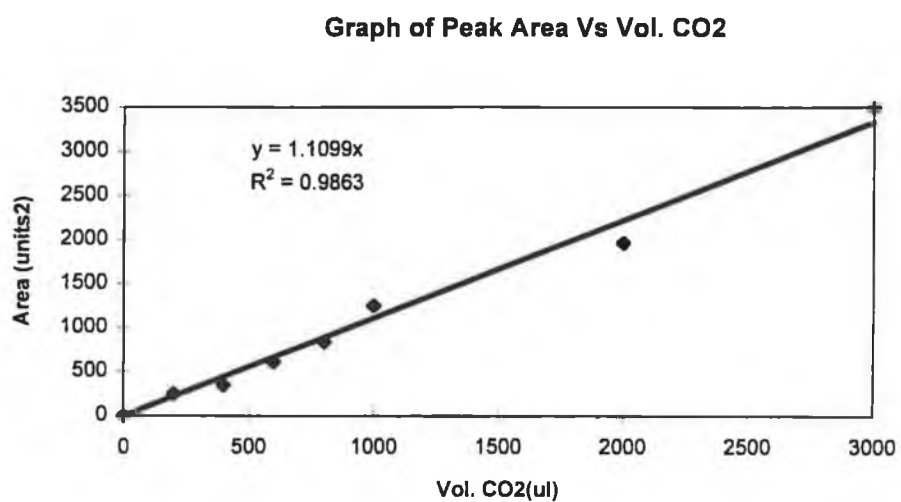
Fig. 2.07   Typical TPO chart for γ-Al$_2$O$_3$

131
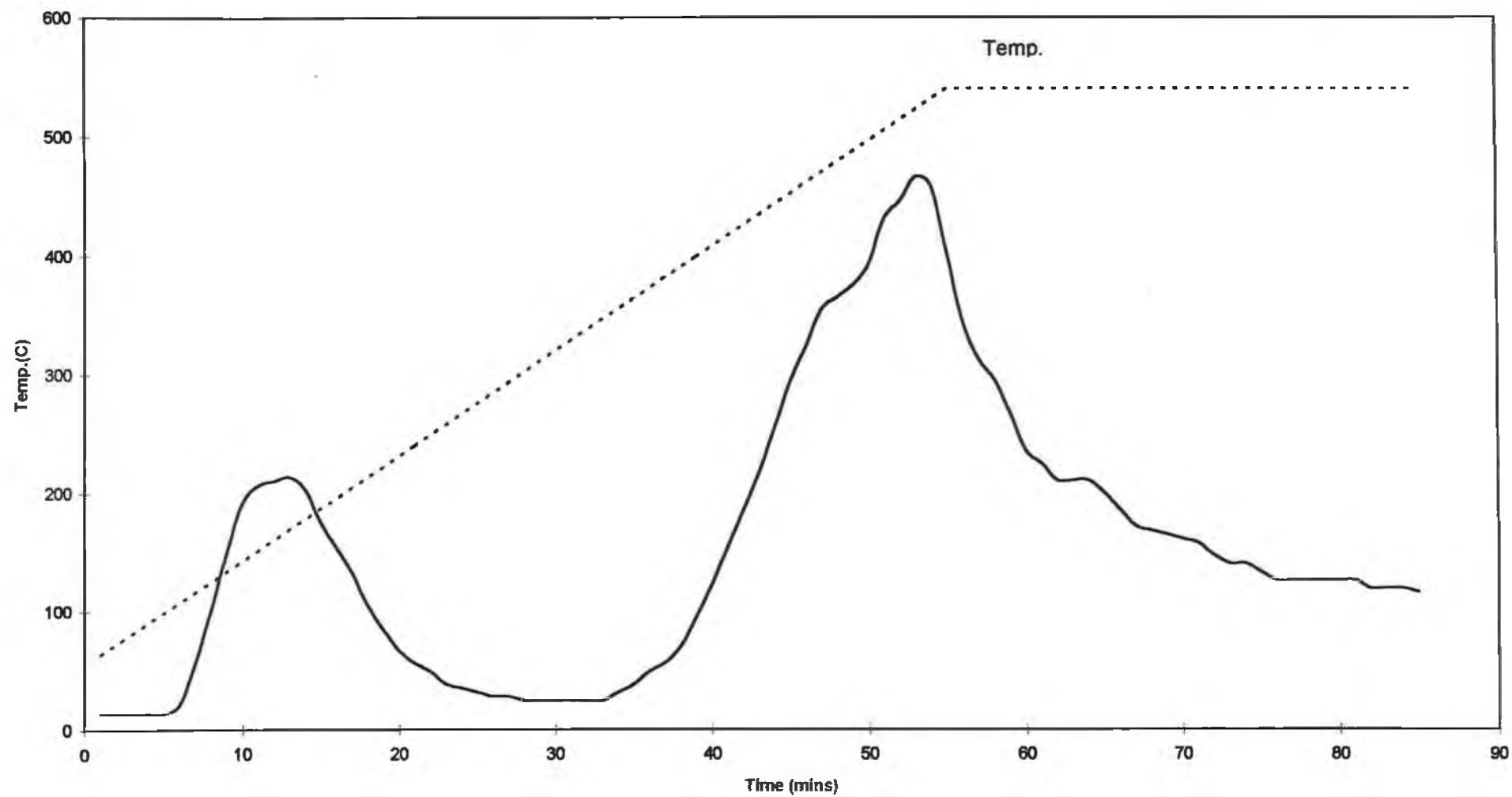
Table 2.11 summarises the results obtained on γ-Al$_2$O$_3$ samples and on Pt/γ-Al$_2$O$_3$. The temperature range of the peak(s) are noted as well as the peak maximum temperature and the % C that the peak corresponds to. T_x indicates the number of minutes that the catalyst is held at the maximum temperature, i.e. 540°C.

Two peaks were observed for 0.5%Pt/γ-Al$_2$O$_3$, one at 170°C and the other at 505°C. In a similar study Barbier et al. [137] found two peaks in the TPO spectrum of Pt–Al$_2$O$_3$ catalysts after use for hydrogenolysis of cyclopentane with maxima at 200°C and 380°C. Exact peak maxima values cannot be compared as different heating rates were used. The authors [137] attributed the low temperature peak to carbon deposited onto the metal and the high temperature peak to carbon deposited on the support. Based on results from Table 2.11 it is felt that the low temperature peak at 170°C on Pt/γ-Al$_2$O$_3$ is not entirely due to carbon deposited onto the platinum. The blank sample of γ-Al$_2$O$_3$, which was never exposed to an air/isobutane gas mixture and does not contain a metal component gave a peak between 60 and 220°C, of comparable area to the low temperature peak of 0.5%Pt/γ-Al$_2$O$_3$. In view of the relatively low temperature at which this carbon is removed it is unlikely to be due to carbon on the support [149,151]. Also since the blank γ-Al$_2$O$_3$ sample was never exposed to a hydrocarbon source the only place it could have obtained the carbon from is the atmosphere in the form of CO_2. Evidence which supports this is to be found in the work of Auroux et al. [44] who found that the O^{2-} ions on Al$_2$O$_3$ acted as bases and were capable of chemisorbing the acidic CO_2 molecules. The CO_2 was removed at approximately 130°C which agrees well with our peak maximum of 130°C for the low temperature peak. It is not possible to compare our peak maxima for combustion of surface coke with those of Barbier et al. [137] since different heating rates were used and it has been found that heating rates affect position of the peak maxima [151]. Comparing the low temperature peak maxima of Pt/γ-Al$_2$O$_3$ and blank γ-Al$_2$O$_3$ suggests that a more strongly bound C exists on the Pt/γ-Al$_2$O$_3$ requiring higher temperature for removal. This is probably coke associated with the Pt metal as opposed to chemisorbed CO_2 found on the blank γ-Al$_2$O$_3$.

Table 2.11 C content of γ-Al_2O_3 samples and Pt/γ-Al_2O_3 calculated by TPO.

Sample	Treatment	Peak Position	Peak Max (^{o}C)	%Carbon	Total C (%)	Area count (units)
γ-Al_2O_3	Blank (Not coked)	(1)60–220°C	130	0.05	0.08	301
		(2)470–T_{30}	T_4	0.03		179
γ-Al_2O_3	Untreated	(1)55–280°C	120	0.05	0.25	291
		(2)300–T_{29}	$T_{3.5}$	0.20		1266
γ-Al_2O_3	HCl treated	(1)65–T_{30}	$T_{4.5}$	0.17	0.17	1080
γ-Al_2O_3	NaOH treated	(1)70–310°C	150	0.04	0.42	260
		(2)360–T_{30}	T_3	0.38		2364
γ-Al_2O_3	NH$_3$ treated	(1)75–300°C	145	0.05	0.25	329
		(2)350–T_{30}	T_4	0.20		1270
γ-Al_2O_3	ethanol washed Cal. @ 630°C/15mins.	(1)65–253°C	110	0.07		432
		(2)300–350°C	325	0.01	0.11	35
		(3)357–T_7	480	0.03		204
0.5%Pt/γ-Al_2O_3	Cal. @630°C/15mins	(1)65–170°C	170	0.04	0.16	265
		(2)380–T_{30}	505	0.12		724

However, the total amount of C associated with the low temperature peak on Pt/γ-Al_2O_3 is less than on the blank sample of γ-Al_2O_3 which suggests that Pt is deposited on the acidic sites of γ-Al_2O_3 and hence displaces the CO_2.

The blank Al_2O_3 sample also gave a small high temperature peak between 470°C and T_{30} which was probably due to trace amounts of carbonaceous impurities on the support [195]. This high temperature peak was seen on all traces but differed in size, suggesting that C formation on the support occurred on all the samples, including 0.5%Pt/γ-Al_2O_3. Figoli et al. [122] has attributed the different TPO peaks to differences in the C/H ratio of the coke giving rise to them with the high temperature peak containing a higher C/H ratio than the low temperature peak.

The coked sample of γ-Al_2O_3 gave two peaks in TPO, the low temperature peak accredited to chemisorbed CO_2 while the high temperature peak was considered to be due to coke on the Al_2O_3 surface.

HCl treatment of γ-Al_2O_3 changed the shape of the TPO curve to a single broad peak starting with a hip at 65°C, climbing rapidly after 425°C, peaking at $T_{4.5}$ and then dropping slowly to T_{30}. This is not surprising since the HCl being an acid would compete with the acidic CO_2 molecules, associated with the low temperature peak, for the Lewis basic sites. It has been found by Garbowski et al. [90] that treatment of Al_2O_3 with HCl produces a big increase in the number of strong sites. Since the treatment of Al_2O_3 with 0.1M HCl in our study brought about a decrease in the total amount of coking it would suggest that these strong sites are not the ones predominantly responsible for coking.

Treatment of γ-Al_2O_3 with NaOH did not greatly alter the area or temperature of the low temperature peak; however, the high temperature peak was almost twice the area of that of the untreated γ-Al_2O_3. Saad et al. [84] found that sodium in concentrations greater than 1000ppm can create new basic sites on γ-Al_2O_3. As the sodium concentration used in this study was 2300ppm it is possible

that more basic groups, including OH groups, were produced, thus explaining the increase in coking. This would also agree with the work of Eisenbach et al. [140] who using infrared found that the formation of coke deposits was accompanied by a decrease in the intensity of the band at $3640cm^{-1}$ characteristic of surface OH groups, suggesting that surface OH groups can act as sites for coke formation and are consequently used up. Wolf et al. [97] have also suggested that OH groups act as active sites in coke formation.

Treatment of γ-Al_2O_3 with NH_3 had virtually no effect on the amount of coke deposited (Table 2.11) relative to untreated γ-Al_2O_3. Treating γ-Al_2O_3 with ethanol had little effect on the low and high temperature peaks but a small intermediate peak was seen, possibly due to ethanolic C.

In order to determine how TPO of adsorbed coke affected coking characteristics of the catalysts tested a repeat of the coking/TPO procedure (section 2.1.2) was performed on 0.5%Pt/γ-Al_2O_3 and the modified aluminas. The results from these analyses are presented in Table 2.12. Comparing Table 2.11 and Table 2.12, it is notable that the total C deposited on the second coking was similar on all γ-Al_2O_3 samples but was more than doubled on 0.5%Pt/γ-Al_2O_3.

The TPO of HCl (Table 2.12) showed two peaks as seen for untreated γ-Al_2O_3. Since it is likely that the single peak for the first spectra was due to the acidic HCl affecting the Lewis basic sites, the return of a two peak spectra for the second analysis implies that HCl is removed by the coking and subsequent TPO. However, since the low temperature peak on second Coking/TPO is smaller than that for untreated γ-Al_2O_3 suggests that some HCl still remains. The high temperature peak for the HCl treated γ-Al_2O_3 is smaller than that of untreated γ-Al_2O_3. The coke inhibitory effect of HCl has been attributed to the ability of chlorine to increase spillover of hydrogen and so keep the support surface relatively free of coke precursors [185]. Total amount of coke removed on first and second TPO was the same for the HCl treated γ-Al_2O_3.

135

Table 2.12 Results for second Coking/TPO

Sample	Treatment	Peak position	Peak max. ($^{\circ}$C)	Qty. Carbon (%)	Total Qty. Carbon (%)	Area count (units^2)
γ-Al$_2$O$_3$	Untreated	(1) 55 – 290°C	130	0.07	0.30	426
		(2) 335 – T$_{30}$	T$_3$	0.23		1432
γ-Al$_2$O$_3$	HCl treated	(1) 60 – 270°C	145	0.03	0.17	196
		(2) 360 – T$_{30}$	T$_4$	0.14		885
γ-Al$_2$O$_3$	NaOH treated	(1) 65 – 310°C	145	0.06	0.40	402
		(2) 350 – T$_{30}$	T$_3$	0.34		2134
γ-Al$_2$O$_3$	NH$_3$ treated	(1) 75 – 360°C	200	0.06	0.30	358
		(2) 405 – T$_{30}$	T$_4$	0.24		1500
0.5%Pt/γ-Al$_2$O$_3$	Cal@630°C/15 mins.	(1) 75 – 270°C	230	0.03	0.40	199
		(2) 280 – T$_{30}$	500	0.37		2313

In the case of NaOH treated γ-Al$_2$O$_3$ a decrease in the amount of carbon associated with the high temperature peak is most likely due to sodium loss during the TPO coking steps. Peña et al. [133] also found that NaOH was relatively volatile and could be lost during combustion of coke. The increase in amount of carbon associated with the low temperature peak would suggest an increase in Lewis basicity of the catalyst as a result of the coking and TPO analysis. Again the total amount of carbon removed on first and second TPO was very similar for NaOH treated γ-Al$_2$O$_3$.

The second TPO spectra for the NH$_3$ treated γ-Al$_2$O$_3$ sample was very similar to that of the untreated sample with regard to amount of coke deposited and high temperature peak maxima, however the low temperature peak is increased. It appears that even after coking and TPO analysis the NH$_3$ treatment is still exerting an inhibitory effect on coke forming Lewis basic sites.

The total carbon deposited on 0.5%Pt/γ-Al$_2$O$_3$ during the second coking was more than double that deposited during the first coking with this increase in the high temperature peak suggesting that the increased quantity of coke is deposited on the support material. A possible explanation for what has happened may be offered by one of Barbier et al. [98] results. In a study into coke formation on Pt-Al$_2$O$_3$ catalysts of different dispersion they found that the number of carbon atoms per surface site on Al$_2$O$_3$ decreased as platinum dispersion increased. Therefore a decrease in dispersion of the platinum after the coking/TPO steps may be the reason for increased coke deposition.

A decrease in platinum dispersion could be caused by sintering at the high temperatures produced during coke burning associated with TPO analysis. Platinum sintering can occur due to platinum particle mobility and collisions between particles [124]. The effect of coking/TPO on Pt surface area was determined by selective H$_2$ chemisorption on a freshly prepared sample of (i) 0.5%Pt/γ-Al$_2$O$_3$ (ii) a sample of 0.5%Pt/γ-Al$_2$O$_3$ after one coking/TPO cycle and (iii)

a sample of $0.5\%Pt/\gamma-Al_2O_3$ after two coking/TPO cycles. The results from this analysis are given in Table 2.13 and the calculation procedure in Appendix II.

Table 2.13 Results for chemisorption analysis of $Pt/\gamma-Al_2O_3$

Sample	Treatment	Platinum surface area (m²/g)	Dispersion
$0.5\%Pt/\gamma-Al_2O_3$	None (fresh sample)	0.99	80%
$0.5\%Pt/\gamma-Al_2O_3$	One coking/TPO cycle	0.62	50%
$0.5\%Pt/\gamma-Al_2O_3$	Two coking/TPO cycles	0.11	9%

As shown, the Pt surface area decreased after each coking/TPO cycle and was associated with an increase in coking. From these results it can be seen that for $0.5\%Pt/\gamma-Al_2O_3$ a decrease in dispersion corresponds with an increase in coke deposition. This agrees with the findings of Barbier et al. [98] and implies that coke formation on $0.5\%Pt/\gamma-Al_2O_3$ catalysts will increase after each regeneration step that involves removal of coke by burning it in an oxidising environment.

The next part of this section examines the results obtained by TPO on the effect of second metal addition to $Pt/\gamma-Al_2O_3$ to gauge the effect on reducing coke formation. Comparison will be made between levels of coking determined on first and second coking/TPO cycles to determine the long term effect, if any, of second metal addition on the rate of coking.

The effect of Sn on coking of $Sn/\gamma-Al_2O_3$ and $Pt-Sn/\gamma-Al_2O_3$ as determined by TPO (section 2.1.2) is given in Table 2.14.

Table 2.14 First TPO analysis results for $Sn/\gamma-Al_2O_3$ and $Pt-Sn/\gamma-Al_2O_3$ catalysts.

Sample	Treatment	Peak position	Peak max. ($^\circ$C)	Amt. Carbon (%)	Total Carbon (%)	Area count (units^2)
$\gamma-Al_2O_3$	Untreated	(1) 55 – 280°C	120	0.05	0.25	291
		(2) 300 – T_{30}	$T_{3.5}$	0.20		1266
$0.5\%Sn/\gamma-Al_2O_3$	500°C/2 hours	(1) 70 – 333°C	155	0.03	0.26	196
		(2) 420 – T_{30}	$T_{4.5}$	0.23		1449
$2.0\%Sn/\gamma-Al_2O_3$	500°C/2 hours	(1) 95 – 230°C	140	0.00	0.06	21
		(2) 450 – T_{30}	T_5	0.06		394
$0.5\%Sn/\gamma-Al_2O_3$	630°C/15mins.	(1) 50 – 275°C	140	0.04	0.14	254
		(2) 290 – T_{30}	370	0.10		606
$2.0\%Sn/\gamma-Al_2O_3$	630°C/15mins.	(1) 90 – 285°C	(shoulder)	0.01	0.15	40
		(2) 367 – T_{24}	$T_{3.5}$	0.14		880
$0.5\%Pt/\gamma-Al_2O_3$	630°C/15 mins.	(1) 65 – 170°C	170	0.04	0.16	265
		(2) 380°C – T_{30}	505	0.12		724
$0.5\%Pt-0.5\%Sn/\gamma-Al_2O_3$	630°C/15mins., co-imp.	(1) 60 – 230°C	140	0.02	0.11	148
		(2) 350 – T_{30}	490	0.09		540
$0.5\%Pt-2.0\%Sn/\gamma-Al_2O_3$	630°C/15mins., co-imp.	(1) 70 – 170°C	120	0.01	0.04	45
		(2) 190 – 300°C	210	0.00		10
		(3) 330 – T_{30}	470	0.03		179
$0.5\%Pt-0.5\%Sn/\gamma-Al_2O_3$	500°C/2 hrs., co-imp.	(1) 50 – 230°C	130	0.02	0.12	232
		(2) 320 – T_{30}	485	0.10		604
$0.5\%Pt-2.0\%Sn/\gamma-Al_2O_3$	500°C/2 hrs., co-imp.	(1) 65 – 180°C	120	0.00	0.13	10
		(2) 200 – 230°C	210	0.00		4
		(3) 330 – T_{30}	500	0.13		785
$0.5\%Pt-0.5\%Sn/\gamma-Al_2O_3$	500°C/2 hrs., step-imp.	(1) 60 – 220°C	135	0.04	0.13	240
		(2) 250 – T_{30}	490	0.09		550
$0.5\%Pt-2.0\%Sn/\gamma-Al_2O_3$	500°C/2 hrs., step-imp.	(1) 70 – 170°C	130	0.02	0.10	45
		(2) 310 – T_{30}	510	0.08		611

TGA results (Table 2.07) suggested that addition of Sn to Al_2O_3 resulted in a decrease in coke formation. The results of TPO (Table 2.14) agree with this. Comparing the TPO results of Sn addition to γ-Al_2O_3 relative to γ-Al_2O_3, the low temperature peaks remained more or less unchanged while the high temperature peaks decreased in size except for 0.5%Sn/γ-Al_2O_3 (Cal.@500/2hrs).

Incorporation of Sn into Pt/γ-Al_2O_3 resulted in decreased coke deposition except for the Pt–2.0%Sn/γ-Al_2O_3 (co-imp.,500°C/2hrs) sample. The greatest decrease in coking was seen for 2.0%Sn addition with calcination at 630°C. The most effective systems for coke inhibition were the Pt–2.0%Sn/γ-Al_2O_3 (co-imp./Cal.@630°C) sample and the Pt–2.0%Sn/γ-Al_2O_3 (step-imp./Cal.@500°C) sample.

A second cycle of coking was carried out on these samples to determine the effect of regeneration on the catalysts. Results are given in Table 2.15. In agreement with first coking results, the γ-Al_2O_3 impregnated with 2% Sn and calcined at 500°C was the most effective at minimising coking. The bimetallic Pt–Sn catalysts Pt–2.0%Sn/γ-Al_2O_3 (co-imp.,cal.@630°C) and Pt–0.5%Sn/γ-Al_2O_3 (step-imp.,cal.@500°C) produced quantities of coke on second coking that were as low as for first coking, suggesting good coke inhibition. The Pt–0.5%Sn/γ-Al_2O_3 (co-imp.,cal.@500°C) and Pt–2.0%Sn/γ-Al_2O_3 (step-imp.,cal.@500°C) showed reduced coking on second analysis. The Pt–0.5%Sn/γ-Al_2O_3 (co-imp.,cal.@630°C) displayed a higher coke content on second coking.

A possible explanation for this reduction in coking may be the effect of Pt dispersion as discussed earlier. Barbier et al. [98] and Kooh [158] have stated that carbon deposition is lower on catalysts where the platinum dispersion is high and the metal particles are small. Meitzner et al. [187] found that Pt clusters in Pt–Sn/Al_2O_3 were smaller than in monometallic systems. Sn maintains Pt dispersion and prevents sintering by anchoring Pt clusters to the Al_2O_3 support via the bonding of a few Pt atoms to Sn^{2+} ions at the surface of the Al_2O_3 [187]. This should help maintain the initial high dispersion of Pt on Al_2O_3 and consequently

reduce coking. Dautzenberg et al. [186] have found that addition of Sn to Al_2O_3 supported platinum catalysts drastically lowered the rates of reaction leading to carbonaceous catalyst poisons produced by polymerisation of extensively dehydrogenated surface species. The authors' results were based on the conversion of n-hexane to benzene or lower hydrocarbons [186].

Table 2.15 Results for second coking of Sn/γ-Al$_2$O$_3$ and Pt–Sn/γ-Al$_2$O$_3$ samples

Sample	Treatment	Peak position	Peak max. ($^{\circ}$C)	Amt. Carbon (%)	Total Carbon (%)	Area count (units^2)
γ-Al$_2$O$_3$	Untreated	(1) 55 – 290°C	130	0.07	0.30	426
		(2) 335 – T$_{30}$	T$_3$	0.23		1432
0.5%Sn/γ-Al$_2$O$_3$	500°C/2 hours	(1) 20 – 345°C	150	0.05		321
		(2) 375 – 415°C	Shoulder	0.00	0.18	8
		(3) 428 – T$_{30}$	T$_{4.5}$	0.13		813
2.0%Sn/γ-Al$_2$O$_3$	500°C/2 hours	(1) 65 – 150°C	100	0.00	0.10	8
		(2) 400 – T$_{30}$	T$_5$	0.10		638
0.5%Sn/γ-Al$_2$O$_3$	630°C/15mins.	(1) 40 – 320°C	230	0.02		102
		(2) 390 – T$_{30}$	T$_5$	0.24		1482
2.0%Sn/γ-Al$_2$O$_3$	630°C/15mins.	(1) 65 – 325°C	Shoulder	0.01	0.20	90
		(2) 400 – T$_{30}$	T$_{3.5}$	0.19		1187
0.5%Pt/γ-Al$_2$O$_3$	630°C/15mins.	(1) 75 – 270°C	230	0.03	0.40	199
		(2) 280 – T$_{30}$	500	0.37		2313
0.5%Pt–0.5%Sn/γ-Al$_2$O$_3$	630°C/15mins., co-imp.	(1) 30 – 240°C	140	0.05	0.35	322
		(2) 290 – T$_{30}$	500	0.30		1871
0.5%Pt–2.0%Sn/γ-Al$_2$O$_3$	630°C/15mins., co-imp.	(1) 70 – 280°C	140	0.02	0.05	111
		(2) 350 – T$_9$	485	0.03		205
0.5%Pt–0.5%Sn/γ-Al$_2$O$_3$	500°C/2 hrs., co-imp.	(1) 80 – 190°C	130	0.01	0.05	50
		(2) 260 – T$_{30}$	350	0.04		226
0.5%Pt–2.0%Sn/γ-Al$_2$O$_3$	500°C/2 hrs., co-imp.	(1) 85 – 165°C	120	0.00	0.14	11
		(2) 195 – T$_{30}$	220	0.14		879
0.5%Pt–0.5%Sn/γ-Al$_2$O$_3$	500°C/2 hrs., step-imp.	(1) 60 – 210°C	13	0.01	0.10	74
		(2) 315 – T$_{30}$	510	0.09		557
0.5%Pt–2.0%Sn/γ-Al$_2$O$_3$	500°C/2 hrs., step-imp.	(1) 80 – 200°C	140	0.01	0.04	51
		(2) 230 – T$_{19}$	470	0.03		179

142

With regard to differences seen in the coking characteristics of Pt–Sn/γ-Al$_2$O$_3$ catalysts prepared by step- and co-impregnation Baronetti et al. [188] have found that co-impregnation resulted in a strong metal–metal interaction while step-impregnation, where first Sn and then Pt was added, resulted in a weak metal–metal interaction between the Sn and Pt. In another study Srinivasan et al. [189] found that for co-impregnated Pt–Sn/γ-Al$_2$O$_3$ catalysts the dominant Pt:Sn ratio of interaction was 1:1. From the results of this study it appears that for Pt–Sn/γ-Al$_2$O$_3$ catalysts (co-imp., cal. @ 500°C/2hrs.) the best coke inhibition is achieved when the quantity of Pt and Sn are almost equal and an excess of Sn appears to result in a higher level of coking. The step-impregnated Pt–Sn/γ-Al$_2$O$_3$ samples (Cal.@500°C/2hrs.) however display the opposite trend for Sn concentration vs level of coking. This information suggests that when the metal–metal interaction between Pt and Sn is strong, as is the case when the catalyst is prepared by co-impregnation, low levels of Sn are most effective at coke prevention and when the metal–metal interaction is weak as for catalysts prepared by step-impregnation of Sn followed by Pt, minimisation of coking is achieved with higher levels of Sn.

Following from TGA results on Zr/γ-Al$_2$O$_3$ and Pt–Zr/γ-Al$_2$O$_3$ these samples were studied using TPO. The TGA results were unclear due to weight increases and decreases being observed. Results for the TPO of these catalysts are given in Table 2.16.

Table 2.16 Results of first coking/TPO analysis on $Zr/\gamma\text{-}Al_2O_3$ and $Pt\text{–}Zr/\gamma\text{-}Al_2O_3$ samples.

Sample	Treatment	Peak position	Peak max. (^{o}C)	Amt. Carbon (%)	Total carbon (%)	Area count (units^2)
$\gamma\text{-}Al_2O_3$	Untreated	(1) 55 – 280°C	120	0.05	0.25	291
		(2) 300 – T_{29}	$T_{3.5}$	0.20		1266
$0.5\%Zr/\gamma\text{-}Al_2O_3$	Cal. @ 630°C/15mins.	(1) 40 – 80°C	60	0.00	0.01	3
		(2) 195 – 235°C	215	0.00		3
		(3) 360 – T_{29}	shoulder	0.01		47
$2.0\%Zr/\gamma\text{-}Al_2O_3$		(1) 30 – 53°C	40	0.00	0.01	3
		(2) 70 – 95°C	85	0.00		3
		(3) 117 – 141°C	130	0.00		3
		(4) 158 – 178°C	167	0.00		1
		(5) 260 – T_{30}	410	0.01		65
$0.5\%Pt/\gamma\text{-}Al_2O_3$	Cal. @ 630°C/15mins.	(1) 65 – 170°C	170	0.04	0.16	265
		(2) 380 – T_{30}	505	0.12		724
$0.5\%Pt\text{–}0.5\%Zr/\gamma\text{-}Al_2O_3$	630°C/15 mins., co-imp.	(1) 40 – 95°C	50	0.00	0.07	5
		(2) 190 – T_{30}	520	0.07		418
$0.5\%Pt\text{–}2.0\%Zr/\gamma\text{-}Al_2O_3$	630°C/15 mins., co-imp.	(1) 58 – 82°C	70	0.00	0.11	3
		(2) 170 – 360°C	260	0.01		33
		(3) 390 – T_{30}	540	0.10		649
$0.5\%Pt\text{–}0.5\%Zr/\gamma\text{-}Al_2O_3$	630°C/15 mins., step-imp.	(1) 30 – 70°C	50	0.00	0.22	7
		(2) 190 – T_{30}	T_2	0.22		1359
$0.5\%Pt\text{–}2.0\%Zr/\gamma\text{-}Al_2O_3$	630°C/15 mins., step-imp.	(1) 65 – 230°C	110	0.01	0.18	76
		(2) 295 – T_{30}	405	0.17		1082

Addition of Zr to Al_2O_3, at either 0.5% or 2.0%, decreased the level of coke significantly. A possible reason for this large reduction in coke deposition has already been given to explain the weight loss observed during TGA experiments. It was proposed that the weight loss was due to formation of $ZrCl_4$ from $ZrOCl_2.8H_2O$, which undergoes sublimation at 331^oC. The $ZrCl_4$ on the surface of γ-Al_2O_3 may interfere with the coke forming sites, which have been found to be both Lewis acid sites [137] and Brönsted acidic sites [190], and hence lead to a decrease in coke formation. The bimetallic Pt–Zr/γ-Al_2O_3 catalysts at both 0.5% and 2.0%Zr (co-imp.) also gave reduced quantities of coke relative to Pt/γ-Al_2O_3, while step impregnation increased the quantity of coke. These results suggest that co-impregnation with Zr at low levels (0.5wt.% Zr) is most efficient at reducing coking during oxidation of isobutane. To determine the effect of repeated cokings on the inhibitory effect of Zr, a second coking and regeneration cycle was carried out and results are given in Table 2.17.

Table 2.17   Results from second coking/TPO analysis of Zr/γ-Al$_2$O$_3$ and Pt–Zr/γ-Al$_2$O$_3$ samples.

Sample	Treatment	Peak position	Peak max. ($^\circ$C)	Amt. Carbon (%)	Total carbon (%)	Area count (units^2)
γ-Al$_2$O$_3$	Untreated	(1) 55 – 290°C	130	0.07	0.30	426
		(2) 335 – T$_{30}$	T$_3$	0.23		1432
0.5%Zr/γ-Al$_2$O$_3$	Cal. @ 630°C/15mins.	(1) 40 – 70°C	55	0.00	0.02	4
		(2) 137 – T$_6$	350	0.02		125
2.0%Zr/γ-Al$_2$O$_3$	Cal. @ 630°C/15mins.	(1) 70 – 115°C	90	0.00	0.06	4
		(2) 193 – 240°C	220	0.00		7
		(3) 315 – T$_{30}$	T$_{10}$	0.06		374
0.5%Pt/γ-Al$_2$O$_3$	Cal. @ 630°C/15mins.	(1) 75 – 270°C	230	0.03	0.40	199
		(2) 280 – T$_{30}$	500	0.37		2313
0.5%Pt–0.5%Zr/γ-Al$_2$O$_3$	630°C/15 mins., co-imp.	(1) 30 – 65°C	45	0.00	0.14	4
		(2) 110 – 130°C	120	0.00		2
		(3) 157 – T$_{30}$	T$_2$	0.14		862
0.5%Pt–2.0%Zr/γ-Al$_2$O$_3$	630°C/15 mins., co-imp.	(1) 35 – 70°C	60	0.00	0.22	3
		(2) 150 – 400°C	280	0.02		115
		(3) 405 – T$_{30}$	520	0.20		1231
0.5%Pt–0.5%Zr/γ-Al$_2$O$_3$	630°C/15 mins., step-imp.	(1) 30 – 75°C	60	0.00	0.25	14
		(2) 210 – T$_{30}$	T$_2$	0.25		1600
0.5%Pt–2.0%Zr/γ-Al$_2$O$_3$	630°C/15 mins., step-imp.	(1) 65 – 230°C	135	0.04	0.16	250
		(2) 250 – 530°C	420	0.12		722

After the second coking cycle, all the $Zr/\gamma\text{-}Al_2O_3$ and $Pt\text{-}Zr/\gamma\text{-}Al_2O_3$ catalysts showed similar or increased coking except for $Pt\text{-}2.0\%Zr$ (step-imp.) which displayed reduced coking. The $Pt\text{-}Zr/\gamma\text{-}Al_2O_3$ (co-imp.) catalyst produced almost twice the amount of coke it produced during first coking.

Of particular interest is the trend in level of coking on second TPO analysis of the co-impregnated $Pt\text{-}Sn/\gamma\text{-}Al_2O_3$ (cal.@500°C/2hrs.) and the $Pt\text{-}Zr/\gamma\text{-}Al_2O_3$ catalysts. For both bimetallic systems the amount of coking is lowest at the 0.5% level of additive. Higher levels of additives were more effective at reducing coking in $Pt\text{-}Sn/\gamma\text{-}Al_2O_3$ catalysts where the interaction between the Pt and Sn was weak, and this trend was also seen for step-impregnated $Pt\text{-}Zr/\gamma\text{-}Al_2O_3$ catalysts suggesting that the strength of interaction between Pt and Zr is less in step-impregnated catalysts. Although the level of coking is much higher for the $Pt\text{-}Zr/\gamma\text{-}Al_2O_3$ systems the fact that the trends are so similar may imply a similar mode of coke inhibition. The reduction in coking being less on addition of Zr may indicate that the Zr is less efficient at 'anchoring' the Pt clusters to the $\gamma\text{-}Al_2O_3$ support via bonding between Pt atoms and Zr at the support thereby allowing Pt cluster growth through sintering.

TPO results on $Ce/\gamma\text{-}Al_2O_3$ and $Pt\text{-}Ce/\gamma\text{-}Al_2O_3$ after one and two coking/regeneration cycles are given in Tables 2.18 and 2.19 respectively. Addition of Ce alone to $\gamma\text{-}Al_2O_3$ led to a reduction in the level of coke deposited for all Ce loadings tested between 0.1 and 2.0%. The level of coke deposited did not vary significantly between catalysts containing 0.1 and 0.5% Ce but it did increase for the $2.0\%Ce/\gamma\text{-}Al_2O_3$ sample. It is worth noting the increase in area of the low temperature peak for the $2.0\%Ce/\gamma\text{-}Al_2O_3$ sample, assumed to be associated with chemisorbed CO_2 and coke deposited on the Ce, as the concentration of Ce was increased. Also the high temperature peak position changed when the Ce concentration was above 0.1% with T_{max} being raised to a higher temperature.

Table 2.18 Results for first coking/TPO analysis of Ce/γ-Al$_2$O$_3$ and Pt–Ce/γ-Al$_2$O$_3$ samples.

Sample	Treatment	Peak position	Peak max.	Amt. Carbon (%)	Total carbon (%)	Area count (units^2)
γ-Al$_2$O$_3$	Untreated	(1) 55 – 280°C	120	0.05	0.25	291
		(2) 300 – T$_{29}$	T$_{3.5}$	0.20		724
0.1%Ce/γ-Al$_2$O$_3$	630°C/15mins.	(1) 70 – 260°C	140	0.02	0.07	152
		(2) 370 – T$_5$	530	0.05		295
0.5%Ce/γ-Al$_2$O$_3$	630°C/15mins.	(1) 60 – 310°C	135	0.04	0.08	263
		(2) 360 – T$_{30}$	T$_2$	0.04		269
2.0%Ce/γ-Al$_2$O$_3$	630°C/15mins.	(1) 60 – 300°C	140	0.09	0.15	575
		(2) 380 – T$_{22}$	T$_3$	0.06		357
0.5%Pt/γ-Al$_2$O$_3$	630°C/15mins.	(1) 65 – 170°C	170	0.04	0.16	265
		(2) 380 – T$_{30}$	505	0.12		724
0.5%Pt–0.3%Ce/γ-Al$_2$O$_3$	Co-imp., 630°C/15mins.	(1) 70 – 170°C	120	0.01	0.23	34
		(2) 200 – T$_{34}$	225, 410, 500	0.22		1355
0.5%Pt–0.5%Ce/γ-Al$_2$O$_3$	Co-imp., 630°C/15mins.	(1) 60 – T$_{30}$	375, 485	0.36	0.36	2243
0.5%Pt–3.0%Ce/γ-Al$_2$O$_3$	Co-imp., 630°C/15mins.	(1) 82 – T$_5$	410	0.23	0.23	1447
0.5%Pt–0.1%Ce/γ-Al$_2$O$_3$	Step-imp., 630°C/15mins.	(1) 63 – 250°C	125	0.02	0.11	126
		(2) 330 – T$_{15}$	515	0.09		530
0.5%Pt–0.5%Ce/γ-Al$_2$O$_3$	Step-imp., 630°C/15mins.	(1) 60 – 270°C	150	0.03	0.08	184
		(2) 325 – T$_{30}$	490	0.05		339

The level of coking on Pt–Ce/γ-Al$_2$O$_3$ (co-imp.) was similar at 0.3 and 3.0% Ce addition and very much larger at 0.5%Ce. Even at 0.3% and 3.0% levels of Ce, the amount of coke formed is approximately twice that formed by the monometallic Pt/γ-Al$_2$O$_3$ system. Step impregnation of Pt–Ce/γ-Al$_2$O$_3$ with 0.5%Ce resulted in a greater reduction in coking than did 0.1% Ce. Summers et al. [191] have found that on fresh step-impregnated Pt–Ce/γ-Al$_2$O$_3$ samples containing between 4 and 13% Ce the Pt dispersion decreased as the Ce concentration increased. After ageing in air at 900°C the particle size for non ceria containing samples was seen to increase dramatically while at low levels of Ce it was found that upon ageing the Pt particle size increased more than the non Ce containing sample resulting in an even greater apparent loss in Pt dispersion [191]. The apparent Pt dispersion, after ageing in air, was seen to increase at the higher levels of Ce. When our results are assessed in light of those established by Summers et al. [191] the difference in Pt particle size as a result of various Ce loadings may explain why the level of coke deposited was higher for the step-impregnated Pt–0.1%Ce/γ-Al$_2$O$_3$ catalyst. The Pt–Ce/γ-Al$_2$O$_3$ (step-imp.) catalyst containing 0.5% Ce would have higher apparent dispersion [191] and as has already been stated by Barbier et al. [98] high Pt dispersion results in reduced coking.

To access how coking levels on Ce/γ-Al$_2$O$_3$ and Pt–Ce/γ-Al$_2$O$_3$ catalysts are affected by regeneration the results following a second coking and TPO cycle are presented in Table 2.19.

Table 2.19   Results from second coking/TPO cycle on Ce/γ-Al$_2$O$_3$ and Pt–Ce/γ-Al$_2$O$_3$ samples.

Sample	Treatment	Peak position	Peak max.	Amt. Carbon (%)	Total carbon (%)	Area count (units^2)
γ-Al$_2$O$_3$	Untreated	(1) 55 – 290°C	130	0.07	0.30	426
		(2) 335 – T$_{30}$	T$_3$	0.23		1432
0.1%Ce/γ-Al$_2$O$_3$	630°C/15mins.	(1) 20 – 330°C	105°C	0.02	0.08	154
		(2) 370 – T$_{30}$	535°C	0.06		392
0.5%Ce/γ-Al$_2$O$_3$	630°C/15mins.	(1) 50 – 350°C	200°C	0.07	0.11	433
		(2) 417 – T$_{30}$	T$_1$	0.04		262
2.0%Ce/γ-Al$_2$O$_3$	630°C/15mins.	(1) 70 – 360°C	190°C	0.09	0.17	562
		(2) 405 – T$_{30}$	T$_3$	0.08		504
0.5%Pt/γ-Al$_2$O$_3$	630°C/15mins.	(1) 75 – 270°C	230	0.03	0.40	199
		(2) 280 – T$_{30}$	500	0.37		2313
0.5%Pt–0.3%Ce/γ-Al$_2$O$_3$	Co-imp., 630°C/15mins.	(1) 60 – 220°C	125°C	0.03	0.17	163
		(2) 310 – T$_{30}$	425°C, 518°C	0.14		893
0.5%Pt–0.5%Ce/γ-Al$_2$O$_3$	Co-imp., 630°C/15mins.	(1) 60 – T$_{30}$	110°C	0.00		26
		(2) 185 – 240	220°C	0.01	0.30	39
		(3) 285 – T$_{30}$	385°C	0.29		1801
0.5%Pt–3.0%Ce/γ-Al$_2$O$_3$	Co-imp., 630°C/15mins.	(1) 75 – T$_{30}$	410°C	0.31	0.31	1918
0.5%Pt–0.1%Ce/γ-Al$_2$O$_3$	Step-imp., 630°C/15mins.	(1) 205 – 260°C	235°C	0.01	0.32	38
		(2) 280 – T$_{12}$	515°C	0.31		1914
0.5%Pt–0.5%Ce/γ-Al$_2$O$_3$	Step-imp., 630°C/15mins.	(1) 75 – 260°C	225°C	0.03	0.39	76
		(2) 270 – T$_{14}$	390°C, 495°C	0.36		2216

After second coking a small increase in amount of coke produced was found on Ce/γ-Al$_2$O$_3$ at each loading (Table 2.19). The least amount of coking occurred on the Pt–Ce/γ-Al$_2$O$_3$ (co-imp.) catalyst containing 0.3wt.% Ce. Step-impregnation of Pt and Ce resulted in increased amounts of coke being deposited at both Ce loadings. When compared to the amount of coke detected for the second cycle of TPO analysis on Pt/γ-Al$_2$O$_3$ the addition of 0.3%Ce has reduced coking by approximately 60%. The results on Pt–Ce/γ-Al$_2$O$_3$ suggest that 0.3wt.% Ce (co-imp.) is effective at reducing coking; this corresponds to a Pt:Ce atomic ratio of 1:1. A possible explanation for the reduced level of coking may have to do with oxygen storage capacity (OSC). Su et al. [192] have shown that addition of Ce to precious metal catalysts significantly enhanced the catalysts OSC after ageing in an oxidising environment under reaction temperatures. Also, the OSC of catalysts containing both Ce and Pt was notably greater than the sum of the OSCs for the samples containing Pt and Ce separately, after similar thermal treatments [192]. Possibly this stored oxygen results in gasification of coke and/or coke precursors during reaction, hence preventing its deposition in the first instance. Further to this the OSC may be greater and gasification higher when the atomic ratio of Pt to Ce is 1:1 resulting in the lowest level of coke with this combination.

So far the quantity of coke formed by each of the systems mentioned has been examined but very little reference has been made to the type of coke being formed. Coke characterisation by TPO has been discussed by Basso et al. [149] who suggest that low temperature peaks (T_{max} <300°C) indicate oxidation of coke on or near the metal sites while high temperature peaks represent less efficiently catalysed coke oxidation or non-catalysed combustion of coke on the support. Our results however suggest that the low temperature peak may also be contributed to by CO$_2$ adsorbed on the surface of the catalyst. Auroux et al. [44] have found that the occurrence of peaks at different temperatures does not necessarily imply that the chemical nature or structure of the deposits on these sites are different. Indeed it has been found by Fung and Querini [150,151] that factors such as heating rate, coke content, catalyst mass and oxygen concentration can affect the temperature at which peaks emerge and also the peak maximum. This would

imply that comparison of TPO data between different research groups may be difficult.

If the peak-max.(P_{max}) temperatures for 0.5%Pt/γ-Al$_2$O$_3$ are compared to those of γ-Al$_2$O$_3$ it can be seen from both first and second TPO curves that addition of Pt acts to increase P_{max} of the low temperature peak. This is probably due to the oxidation of coke on the Pt metal which is not formed on γ-Al$_2$O$_3$ due to the absence of a metal component. The P_{max} of the high temperature peak was seen to decrease slightly after addition of Pt, most likely a result of the Pt acting to catalyse the combustion of coke. These results for the high temperature peaks agree with those of Parera et al. [176] who also found that Pt catalysed the oxidation of coke leading to a reduction in oxidation temperature of the high temperature peak. A possible reason for the reduction in T_{max} is that Pt addition results in the formation of less polymerised coke which is more easily oxidised [176]. From second coking/TPO results it is seen that chemical modification of γ-Al$_2$O$_3$ with acid and bases did not significantly affect the P_{maxs} of either the high or low temperature peaks except in the case of NH$_3$ treatment. Here T_{max} of the low temperature peak increased from 130°C to 200°C suggesting that NH$_3$ increases the strength of Lewis basic sites and therefore higher temperatures are required to remove surface bound CO$_2$ molecules.

Addition of Sn to γ-Al$_2$O$_3$ did effect P_{maxs} of the low temperature peaks. These peaks were often low and broad making it difficult to measure P_{max} accurately. Concerning the high-temperature peaks, Sn addition was seen to have little effect on the P_{maxs} except for the first cycle analysis of 0.5%Sn/γ-Al$_2$O$_3$ (cal. @630°C/15 mins.) where a modest decrease in P_{max} occurred. The Pt–2.0%Sn/γ-Al$_2$O$_3$(step-imp.) catalyst had a higher P_{max} than that of Pt/γ-Al$_2$O$_3$. Also, T_{max} for the Pt–0.5%Sn/γ-Al$_2$O$_3$(step-imp.) catalyst was higher for the second TPO cycle than the first. The main point to note is that for all the Pt–Sn/γ-Al$_2$O$_3$ catalysts the P_{maxs} of the high-temperature peaks are lower than for γ-Al$_2$O$_3$ alone.

Area of the low-temperature peaks for $Zr/\gamma-Al_2O_3$ catalysts were essentially insignificant. With reference to the high-temperature peaks for $Zr/\gamma-Al_2O_3$ catalysts only the second TPO spectra gave peaks of sizeable area. A P_{max} of 350°C was seen for the 0.5%$Zr/\gamma-Al_2O_3$ catalyst and T_{10} for the 2.0%$Zr/\gamma-Al_2O_3$ catalyst indicating that low levels of Zr on Al_2O_3 can greatly increase gasification of carbon. The P_{maxs} for the $Pt-Zr/\gamma-Al_2O_3$ high-temperature peaks are similar to those of $\gamma-Al_2O_3$ and higher than for $Pt/\gamma-Al_2O_3$ except in the case of 0.5%$Pt-2.0$%$Zr/\gamma-Al_2O_3$, prepared by step-impregnation which revealed a P_{max} of 405°C for the first TPO analysis and 420°C for the second. What is particularly interesting is that this catalyst also produced the least amount of coke on second analysis. Based on these results for $Zr/\gamma-Al_2O_3$ and $Pt-Zr/\gamma-Al_2O_3$ catalysts it would appear that high gasification rates correspond to low carbon deposition.

In the case of $Ce/\gamma-Al_2O_3$ the high-temperature P_{maxs} were similar to $\gamma-Al_2O_3$ on both first and second TPO analysis as were the low-temperature P_{maxs} for the first TPO and then increased for the 0.5% and 2.0%$Ce/\gamma-Al_2O_3$ samples on second TPO analysis. With regard to the first TPO spectra for $Pt-Ce/\gamma-Al_2O_3$ catalysts, prepared by co-impregnation, multiple high-temperature peak maxima were obtained for catalysts containing the lower 0.5% and 0.1% levels of Ce. The TPO spectra for first analysis of $Pt-Ce/\gamma-Al_2O_3$ catalysts prepared by step-impregnation revealed peaks with maxima very similar to those of 0.5%$Pt/\gamma-Al_2O_3$. It is interesting to note that multiple maxima occurred during second TPO analysis on the samples of step- and co-impregnated catalysts containing the lowest level of ceria. This suggests that under certain circumstances $Pt-Ce/\gamma-Al_2O_3$ can posses high temperature coke which has different oxidation kinetics. A possible explanation for the multiple maxima may have to do with the oxygen storage capacity of $Pt-Ce/\gamma-Al_2O_3$ catalysts discussed earlier. If variations in binding energy existed for the stored oxygen such as may exist if the oxygen was stored in layers, then the removal of various layers would require different quantities of energy. In this study energy is supplied in the form of heat and if it is assumed that the removal of the most loosely bound outer layer of oxygen occurs at the lower temperature then this oxygen may be able to combine with coke to form CO_2 and hence produce a peak. Removal of

the next oxygen layer would require more energy, due to it being closer to the positively charged metal, and hence occur at a higher temperature. Again this oxygen could combine with coke to give another CO_2 peak. It is assumed that one layer of oxygen is completely removed before the next layer is started on. Based on this theory a monolayer of oxygen would result in a single CO_2 peak while double or triple layers of oxygen would produce two and three CO_2 maxima respectively. Our results for TPO of coke on Pt–Ce/γ-Al_2O_3 have shown all three such CO_2 peak conformations.

Differences in the percentage coke deposited have been determined by coking quantified by the TPO and TGA methods. Taking γ-Al_2O_3 as an example it can be seen that the amount of coke as determined by the TGA method was 1.75% while percentage coke determined by coking followed by TPO was 0.20%. While the thermogravimetric method detects total weight increase, the TPO method only detects coke which has been converted to CO_2. Therefore, coke which is converted to volatile hydrocarbons or CO will not be detected by the CO_2 analyser. Since the concentration of H_2 in air passing over the sample is only ~0.03% it is unlikely that much of the coke will be converted to volatile hydrocarbons. In the case of CO formation from C and O it is known that ΔG is − 394.36kj/mol^{-1} for CO_2 and -137.15kj/mol^{-1} for CO [193]. This suggests that CO_2 would be formed in preference to CO where O_2 concentration was not a limiting factor. With the sample size and flow rate of air which was passing over the sample in our TPO analysis procedure it is theoretically possible to remove 0.81% carbon in one minute (Appendix III). This, in conjunction with the fact that Querini and Fung [150,151] used an O_2 concentration of 3.0% for their TPO work as compared to our 20% O_2 concentration, would indicate that O_2 was not a limiting factor in the system used. Further evidence for the preferential formation of CO_2 over CO can be found in the work of Boehm [101]. The author [101] found that at temperatures below 700°C, in the presence of a catalyst, equilibrium for the following reaction favours the right hand side.

$$2CO \Leftrightarrow C + CO_2$$
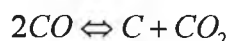
This suggests that any CO formed at temperatures below 700^0C would most likely combine with other CO molecules to form C and CO_2. The C left on the surface could then react to form CO_2 which can be detected using the CO_2 analyser.

Despite this evidence for the preferential formation of CO_2, it was decided to analyse the effluent air stream from the TPO apparatus during a run for hydrocarbons and permanent gases by GC.

Results for a sample of $\gamma-Al_2O_3$, heated at $2^oC/min.$, indicated the presence of CO_2 only at 20^oC and 60^oC, suggesting CO_2 adsorbed on the surface. At 100^oC water was also detected. The FID peak detected at 140^oC and 180^oC did not correspond to a straight chain saturated hydrocarbon and was probably an unsaturated C_5. No further peaks were detected with FID and at 420^oC, 500^oC, and 540^oC CO_2 was detected by the TCD.

The experiment was then repeated on another coked $\gamma-Al_2O_3$ sample where the sample heating rate used was $10^oC/min.$and the results for this analysis along with those obtained using a heating rate of $2^oC/min$ are presented in Tables 2.20 and 2.21.

Table 2.20   GC analysis of TPO effluent from coked $\gamma-Al_2O_3$, heating rate $2^oC/min.$

Temperature (^0C)	FID	TCD
20	——	CO_2
60	——	CO_2
100	——	H_2O
140	unsat. HC (possibly C_5)	——
180	unsat. HC (possibly C_5)	——
420	——	CO_2
500	——	CO_2
540	——	CO_2

Table 2.21 GC analysis of coked γ-Al$_2$O$_3$ sample, heating rate 10°C/min.

Temperature (°C)	FID	TCD
100	unsat. $C_3 - C_4$ HC	CO_2 & possible H_2O
300	4 peaks HC $< C_6$	No peaks
500	HC $< C_4$	CO_2
540	HC $< C_4$	no peaks

The multitude of peaks seen with FID above 300°C, while all being quite small would suggest that a host of volatile hydrocarbons are produced during TPO of coked catalysts, especially when 10°C/min is used as the heating rate, and this may explain the variation in quantities of coke determined by TPO and TGA. It should be noted that all the TCD traces gave a peak at 1.0mins which was due to O_2 and N_2 in the air being passed over the coked γ-Al$_2$O$_3$ catalyst. None of the injections indicated the presence of CO under our operating conditions which allowed detection of CO at levels as low as 1ppm.

Chapter

Three

Titrimetric estimation of the acidity of Alumina, Silica and Modified Alumina supported Platinum.

3 Introduction

The ability to determine the acidity of catalysts is of particular relevance in view of the fact that acidic sites on surfaces have been associated with coke formation [125,196]. The coke produced on acidic sites normally arises from polymerisation reactions involving carbonium ions [125] and can be distinguished from coke deposits on metals by TPO as it forms a peak at higher temperatures than coke deposited on or around metals [122]. Also infrared studies on coke formation seem to indicate that the OH groups can act as active sites in coke formation [97]. Therefore quantification of acidic and basic groups is important for estimating the tendency of a catalyst to accumulate coke.

In Sections 1.1.4 and 1.1.5, various ways of measuring the surface acidity and basicity of solid acids and bases are reviewed. Tanabe et al. [29] have outlined a method for quantifying acid sites by suspending the solid acid in benzene and titrating with n-butylamine. Using a series of indicators with different pK_a values, the amount of acid sites at various acid strengths can be determined [29]. Determination of basic sites involved suspending the solid base in benzene and titrating with benzoic acid suspended in benzene [29]. Again, by using a range of indicators with different pK_a values, it is possible to calculate the number of basic sites present on the solid base at various basic strengths [29]. While this method is commonly used it does have associated with it certain faults, one being that the large size of the indicator molecules present steric problems meaning that the technique cannot detect sites which are within narrow pores [96]. This seriously limits the usefulness of the technique especially considering that Tiernan et al. [157] have found evidence to indicate that the acidic function of catalysts may be located in pores since much of the initial coke is deposited in pores. Also there are problems when coloured catalysts are being analysed as the coloured compound can mask the indicator colour change [29].

In this study potentiometric titrations were used to determine the number of acidic and basic sites present on silica and alumina. The effect of

chemical modification and metal addition on the quantities of acidic and basic sites was also determined by performing titrations on the modified and supported metal catalysts. The amount of acidic or basic sites on a solid acid or base can be expressed as mMoles/g and also as mMoles per unit surface area.

While it has been seen from Section 2.2 that some acid/base treatments and addition of Sn, Ce, or Zr can bring about a reduction in coking, it is important to investigate how these modifications affect the operation of the catalyst. In order to determine the effect of these modifications, the ability of each catalyst to oxidise isobutane is used as a test reaction to measure activity.

3.1 Experimental Section

3.1.1 Titration of acid and base sites on solid samples

Forward titration of basic sites

Approximately 0.1g of the sample to be titrated was weighed accurately into a clean dry 100cm^3 beaker. To this was added 50.0cm^3 of glacial acetic acid and a stirring rod. The beaker was then placed on a stirring mantle and stirred vigorously. Using 0.50cm^3 increments, 5.00cm^3 of 0.0977M perchloric acid in glacial acetic acid was then added. The end-point was determined potentiometrically using a digital pH meter (Philips PW9421) with a glass single sensor electrode (type No. GSFC11) and a glass reference electrode (R2-glass double junction reference). Each reading was taken two minutes after addition of the perchloric acid solution. Calculation of the end-point was done by taking the point where the second derivative curve of potential vs volume cuts the x-axis of the graph. The procedure for calculating an end point by this technique was obtained from ref. [197] and for clarity a worked example is included in Appendix *IV*. Manipulation of data and plotting of graphs was done using *EXCEL 5.0*. Titration of each sample was performed in duplicate and calculations done using each end-point and sample weight, with the result being taken as the average of the two final values.

Back titration of basic sites

Back titration of basic sites was performed by suspending approximately 0.1g of the sample, accurately weighed, in a clean dry 100cm^3 beaker and then adding 5.00cm^3 of 0.0098M perchloric acid in glacial acetic acid followed by 50.0cm^3 2-methoxy-ethanol and a stirring rod. The mixture was then set stirring on a stirring mantle and titrated with 0.0109M n-butylamine in 2-methoxy-ethanol. Titration involved addition of the titrant in 1.00cm^3 increments with the potential reading being taken two minutes later using the pH meter and electrodes as stated

above. The end-point was determined from a second derivative plot of potential vs volume.

The perchloric acid was standardised using a procedure outlined in the literature [200] which involved titrating the perchloric acid against dried potassium hydrogen phthalate. In this work the potassium hydrogen phthalate was suspended in glacial acetic acid and the end-point determined potentiometrically. Based on the fact that $1.00cm^3$ 0.1M $HClO_4$ is equivalent to 20.42mg $C_8H_5KO_4$ [200] molarity of the stock solution was calculated to be 0.0977M ($\pm$0.0079M). Knowing the concentration of the stock solution allowed calculation of the concentration of dilutions prepared from this solution. Therefore the ~0.01M solution which was prepared from the stock solution actually had a concentration of 0.0098M.

Molarity of n-butylamine was determined by titrating $5.00cm^3$ 0.0098M perchloric acid in $50.0cm^3$ 2-methoxy-ethanol with the n-butylamine solution of unknown molarity. The titrant was added in $1.00cm^3$ increments and the potential reading taken after two minutes. Using the mean of end points from three titrations, the molarity of the n-butylamine solution was calculated to be 0.0109M ($\pm$0.0005M).

Forward titration of acidic sites

The sample (~0.1g accurately weighed) was placed in a clean, dry $100cm^3$ beaker to which was added $50.0cm^3$ of 2-methoxy-ethanol. The titrant used was 0.0109M n-butylamine which was added in $0.50cm^3$ increments. The potential was measured two minutes after each addition while the suspended sample was stirred vigorously. Determination of the end-point was from a second derivative plot of potential vs volume.

Back titration of acidic sites

For this procedure, ~0.1g samples were accurately weighed into clean, dry, 100cm^3 beakers to which 5.00cm^3 0.0109M n-butylamine was added followed by 50.0cm^3 glacial acetic acid. A stirring rod was placed in the beaker and the solution set stirring on a magnetic stirring mantle to ensure interaction between the n-butylamine and the surface acidic sites of the sample. The titrant, (0.0098M perchloric acid in glacial acetic acid) was added in 1.00cm^3 increments up to a final volume of 10.00cm^3. Potential readings were taken two minutes after each addition and the end-point again calculated from a second derivative plot of potential vs volume.

For each of the back titrations, blank titrations were performed which involved performing the titrations as outlined above without any solid sample present. Details of the calculations for each of the titrimetric techniques used are given in Appendix *VI*.

3.1.2 Surface area determination

Surface area determination was carried out on a Micrometrics Pulse Chemisorb 2700. A schematic diagram of the instrument has already being given in Fig. 2.05. The instrument consists of a preparation line, for sample treatment prior to analysis, and a test line connected to a TCD. Specific surface areas were determined using a single point method, results being obtained by calculating the amount of N$_2$ adsorption at liquid nitrogen temperatures from a specialist gas mixture that consisted of 30%N$_2$/70%He (supplied by Air Products Ltd., Special Gases Group).

Calibration of the instrument was done prior to analysis. by injecting 1.00cm^3 volumes of nitrogen using a precision syringe, filled with the gas immediately above the level of liquid nitrogen in a dewar. The evaporating liquid nitrogen from a dewar flask provided an atmosphere of nitrogen from which 1.00cm^3 of nitrogen was injected into the N$_2$/He carrier stream which flowed through the

TCD. The increase in peak area due to the N_2 was measured by the instruments integrator and converted to a surface area value. The actual surface area of a 1.00cm^3 sample of nitrogen at the temperature and atmospheric pressure on the day of operation was calculated using the BET equation as outlined in Appendix *V*. The instrument was then adjusted to the calculated value and the calibration repeated to check that the instrument was giving the correct reading for the surface area.

Analysis of the samples first entailed accurately weighing them into a clean, dry, preweighed pyrex U-tube. For high surface area samples e.g. γ- and η-alumina, approximately 0.1g samples were used while samples of approximately 0.3g were used for the lower surface area sample i.e. α-alumina. The U-tube was fitted onto the Micrometrics instrument and the sample outgased by first leaving at room temperature for five minutes, then at 100°C for thirty minutes and 250°C for ninety minutes, with the gas mixture flowing over the sample at a rate of 16–20cm^3/min. After outgassing, the sample was cooled to room temperature by surrounding the U-tube with water. Adsorption was achieved by placing liquid nitrogen about the sample U-tube. The surface area reading on the instrument was then zeroed and desorption induced by replacing the dewar of liquid nitrogen with a beaker of water, which brought the sample back up to room temperature. The amount of N_2 desorbed was monitored and the surface area of the sample calculated. Adsorption/desorption cycles were performed until there was close agreement between results from three consecutive analysis. After analysis, the sample tube was reweighed to determine the actual sample weight after adsorbed water had been removed. The surface area based on the actual sample weight was taken as the mean of three desorption peaks.
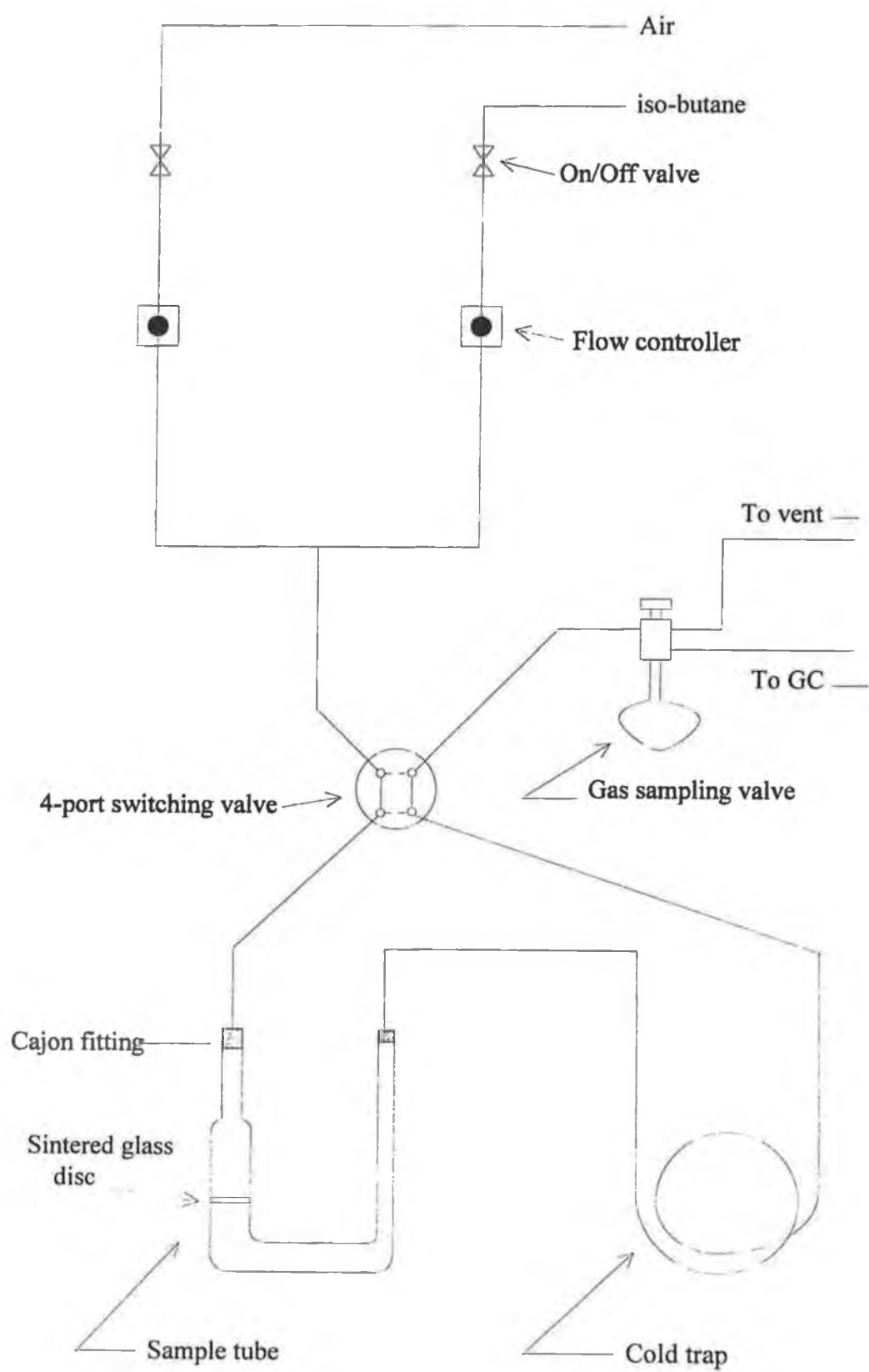
3.1.3 Activity measurements

Activity of the catalysts was assessed by monitoring combustion of isobutane as a function of temperature in a continuous flow apparatus. A schematic diagram of the activity unit used for this purpose is given in Fig. 3.01. Using flow controllers the flow of isobutane could be varied between 0–

5cm^3/min and air between 0–100cm^3/min. The flow of isobutane was set at 0.5cm^3/min while that of air was set at 16cm^3/min. producing a stoichiometric mixture of (32:1) air : isobutane. The air used was normal grade supplied by Air Products Ltd. and the isobutane had a specification of 99.6% isobutane, 0.3% methane 0.03% ethane and 0.01% propane (manufacturers specification). Design of the activity unit allowed for the air/isobutane gas mixture to be passed directly to the gas chromatograph (GC) by way of a 4-port switching valve. This meant that the sample could be bypassed to check hydrocarbon content of the gas mixture before passing over the catalyst. Concentration of hydrocarbon was determined using an FID on the GC. In order to prevent the water produced during reaction reaching the gas sampling loop, a cold trap at 0°C was placed on the gas line downstream of the sample. Flow-rates of the air and isobutane were checked with a bubble flow meter prior to each test. For introduction of samples onto the GC a gas sampling valve of volume 1.00cm^3 was used and the actual GC instrumental conditions used are given in Table 3.1.

Table 3.1   Instrumental conditions for GC analysis

Instrument	Pye Unicam 4550
Detector	Flame Ionisation Detector
Column	2m, 6mm (i.d.), packed
Column packing	Poropak Q
Carrier gas	He (normal grade, Air Products) Flow rate : 40cm^{3}min^{-1}
Temperatures	Column : 200°C Injector : 225°C Detector : 225°C

Fig. 3.01 Schematic diagram of Activity Unit.

Air

iso-butane

On/Off valve

Flow controller

To vent —

To GC —

Gas sampling valve

4-port switching valve →

Cajon fitting

Sintered glass
disc

Sample tube

Cold trap

The sample tested was weighed into a pyrex sample holder where it was supported on a sintered glass disc. Sample weights of 0.3000g (±0.0005g) were used for each test. The reaction mixture was passed through the sample which was heated from room temperature to 350°C using a programmable furnace (Lenton Thermal Design Systems Ltd.). At particular temperatures, the amount of unreacted isobutane was determined by GC over a period of at least 15mins (Run 1). The sample was then allowed to cool to room temperature in a static atmosphere of the air/isobutane gas mixture and a repeat run performed under the same conditions (Run 2). For each of the systems i.e. $Pt/\gamma\text{-}Al_2O_3$, $Sn/\gamma\text{-}Al_2O_3$, $Pt\text{--}Sn/\gamma\text{-}Al_2O_3$, $Zr/\gamma\text{-}Al_2O_3$, $Pt\text{--}Zr/\gamma\text{-}Al_2O_3$, $Ce/\gamma\text{-}Al_2O_3$ and $Pt\text{--}Ce/\gamma\text{-}Al_2O_3$ at least one activity analysis was performed at temperatures between 20°C and 350°C. The results from these analysis were plotted as percentage conversion vs reaction temperature using *EXCEL 5.0.*

3.2 Results and Discussion

3.2.1 Titrimetric method development

Earlier titrimetric work done by the DCU group utilised aqueous acids and bases to determine the concentration of surface acidic and basic sites [198]. Tanabe et al. [29] has stated that CO_2 is an acidic molecule and therefore its presence in the suspending solvent would act as an interferent. Removal of CO_2 was achieved by purging the suspension with nitrogen before the titration. The titrants used were CH_3COOH, NH_2OH and $NaOH$ [198].

Results from the aqueous titrations performed by the DCU group were difficult to reproduce due to severe drifting in the potential readings. Some improvement in stability was achieved by performing the titrations under CO_2 free conditions achieved by bubbling nitrogen gas through the suspension as the titration was been carried out and taking the average of several potential readings within a particular time interval. Despite these efforts the aqueous titration results were very irreproducible. Non-aqueous conditions had already been used on solid acids and bases [29,51,52]. A non-aqueous procedure was tried which used perchloric acid (0.025M) in glacial acetic acid as the titrant and a (1:1v/v) toluene/chloroform mixture as the suspending solvent with the end-point being determined potentiometrically [199]. When this system was used very unstable potential readings were encountered. Different solvent systems were tried such as chloroform, methanol and toluene but again none of these gave a stable electrode response. Since the perchloric acid was made up in glacial acetic acid it was decided to try glacial acetic acid as the suspending solvent. The electrode response was very stable in the glacial acetic acid and when this system was used to titrate ~0.1g of γ-Al_2O_3 a clear end-point was detected. Concentration of perchloric acid was however reduced to ~0.01M for subsequent titrations.

A method for titration of weak acids which used tetrabutylammonium hydroxide as the titrant and a mixture of propan–2–ol/benzene

167

as the solvent system was found in the literature [201]. A solution of ~0.1M tetrabutylammonium hydroxide in anhydrous methanol/toluene (1:4v/v) was prepared using a procedure outlined in the United States Pharmacopoeia [202]. Due to the carcinogenic nature of benzene the suspending solvent was prepared from anhydrous methanol/toluene(1:4v/v) rather than methanol/benzene(1:4v/v). Problems arose with this system due to the instability of the pH and reference electrodes in the suspending solvent. Other solvent systems were tried namely acetonitrile, methanol, toluene, cyclohexane, pyridine and 2-methoxy-ethanol with the latter being the only one to give good electrode stability. Tetrabutylammonium hydroxide while a good base is however sensitive to light and moisture [202]. In view of this it was decided to use n-butylamine instead which has been used by Tanabe [59] as a base for non-aqueous titration of solid acids.

Despite the stability and reproducibility of this system no acid sites could be detected on any of the Al_2O_3 or SiO_2 materials using sample sizes of approximately 0.1g and n-butylamine titrant concentrations of 0.1M, 0.01M, 0.001M and 0.0001M. This was unexpected since it is known from the literature that for example γ-Al_2O_3 possesses both Brönsted [41] and Lewis acid sites [38,35]. Also, Tanabe et al. [29] states that titration with n-butylamine gives the sum of the amounts of both Brönsted and Lewis acids since both proton donors and electron pair acceptors on the surface will react with the electron pair of the amine ($\equiv$N:) to form a co-ordination bond. However when the work of Parry [38] is examined it is seen that the Brönsted acid sites on Al_2O_3 are very weak and it is not possible to detect them by the adsorption of pyridine. In this work n-butylamine (pK_b=3.38), which is a much stronger base than pyridine (pK_b = 8.75) and should therefore react with the weak acid sites, was used [39]. Morimoto et al. [39] has used n-butylamine in conjunction with infrared in an effort to detect the presence of aprotic and Brönsted acidic sites on γ-Al_2O_3. It was found that when this technique was applied to γ-Al_2O_3 which had been pre-treated at 500°C *in vacuo,* only aprotic acid sites were found. Adsorption of n-butylamine on γ-Al_2O_3, which had been pre-treated at 100°C and therefore still contained a lot of physisorbed water, did not reveal the existence of Brönsted acid sites [39]. Based on these results, both Morimoto et al.

[39] and Parry [38] have concluded that part of the Lewis acid sites are converted to Brönsted acid sites through reaction with water. Since our titrations were carried out on untreated γ-Al_2O_3 it would be expected to find both aprotic and Brönsted acid sites. Our results nonetheless did not reveal the presence of either. The reason for this is unlikely to be a result of steric problems since n-butylamine is quite a small molecule i.e. 4–5Å [46]. A possible reason for the failure of our titration procedure to detect acid sites may have to do with the slow rate at which n-butylamine achieves adsorption equilibrium as noted by Take et al. [53].

In order to try and increase the amount of time which the acid sites have to react with the n-butylamine it was decided to try a back titration procedure. Dowden [167] has stated that when solid acids are suspended in an excess of alkali, their acidic sites are converted to basic ones. This would suggest that if the catalysts were reacted with an excess of n-butylamine their acidic sites would be converted to basic ones and could therefore be quantified by titration with perchloric acid. Details of the back titration procedure used for determination of acidic sites have been discussed in Section 3.1.2.

3.2.2 Results of titrimetric measurements

The surface area values quoted have associated with them an error of $\pm 5m^2$/g. Because of the wide variation in surface area values (e.g. α-Al_2O_3 = $10m^2$/g and γ-Al_2O_3 = $220m^2$/g) an actual figure was chosen for the error as opposed to a percentage error which may suggest unrealistic levels of accuracy on samples of low surface area. All results for acidic and basic site concentrations are the average of two titrations and have the associated error quoted alongside. This error value was obtained by calculating an error for each of the titration results and then averaging these values.

The results for titrations performed on samples of α-Al_2O_3, γ-Al_2O_3, η-Al_2O_3 and silica gel are presented in Table 3.2. Limit of detection for this analysis was calculated based on a $0.50cm^3$ volume of 0.0098M perchloric acid

169

which is the smallest addition of titrant. Therefore if the end-point for a titration was below 0.50cm^3 it would not be detected using this system. Using a value of 0.50cm^3 as an end-point gives a limit of detection value of 2.33×10^{-7}moles/m^2 and 0.49×10^{-4}moles/g.

The results in Table 3.2 show that the methods of forward titration and back titration of basic sites gave similar results for each of the samples tested. The back titration method was capable of detecting the weaker basic sites on silica that could not be detected by forward titration suggesting that it was more sensitive than forward titration.

As can be seen from Table 3.2, γ-Al$_2$O$_3$ possesses roughly 2.5 times more Brönsted basic sites than η-Al$_2$O$_3$ and over three times as many per gram as α-Al$_2$O$_3$. With regard to the concentration of Brönsted basic sites per m^2, the density of sites is approximately six times higher on α-Al$_2$O$_3$ than on γ-Al$_2$O$_3$ and approximately ten times higher than on η-Al$_2$O$_3$. It is known that the surface of silica gel consists of silanol groups [62]. The OH groups attached to the silicon atoms on the surface of silica vary in distance from each other, they vary in their behaviour for adsorption or chemical reactions [63]. The OH groups may therefore possess acidic or basic character depending on their chemical environment. The surface Brönsted basic sites on silica gel could only be detected by back titration, suggesting that the hydroxyl groups, mentioned by Iler [63], which cover the surface of silica are either very few in number or are very weak Brönsted bases.

Table 3.2   Concentration of acidic/basic sites as determined by titration analysis

Sample	Surface area	Forward titration of basic sites		Back titration of basic sites		Back titration of acidic sites	
	(m^2/g)	$moles/m^2 \times 10^{-7}$	$moles/g \times 10^{-4}$	$moles/m^2 \times 10^{-7}$	$moles/g \times 10^{-4}$	$moles/m^2 \times 10^{-7}$	$moles/g \times 10^{-4}$
γ-Al_2O_3	220	7.46 (±0.82)	1.68 (±0.10)	6.92 (±1.53)	1.52 (±0.27)	12.2 (±3.15)	2.68 (±0.57)
η-Al_2O_3	134	4.74 (±1.09)	0.63 (±0.10)	4.03 (±1.85)	0.54 (±0.21)	7.31 (±2.74)	0.98 (±0.29)
α-Al_2O_3	10	50.7 (±80.9)	0.51 (±0.10)	37.7 (±76.2)	0.38 (±0.18)	94.7 (±165.7)	0.95 (±0.29)
Silica gel	144	T.L.T.M. < 2.33	T.L.T.M. < 0.48	2.05 (±1.41)	0.32 (±0.18)	1.50 (±1.40)	0.22 (±0.19)

T.L.T.M.   :   To Low To Measure

The number of Brönsted basic sites on Al_2O_3 has been determined by Yamanaka et al. [60] who used trichloroacetic acid to titrate samples in benzene. Indicators were used to determine the end-point and it was found that basicity existed on aluminas at $H_0 \geq 1.5$. Yamanaka et al. [60] also found the basicity of γ-Al_2O_3 to be higher than the results quoted in this work. The value determined was 0.43×10^{-4} moles/g which is much lower than that determined by either our forward or back titration procedures. A possible explanation for this may be that the technique used in this study detects all Brönsted sites capable of reacting with perchloric acid whereas the value quoted by Yamanaka et al. [60] applies to basicity detected when $H_0 \geq 1.5$. In addition to this the potentiometric mode of detection does not have the steric problems associated with use of large indicator molecules. This would allow even Brönsted basic sites in small pores to be detected and hence may explain the higher concentration of Brönsted basic sites detected by the potentiometric technique. The presence of strong basic sites on both γ- and η-Al_2O_3 have been found by Scokart & Rouxhet [57].

As has been mentioned, no acidic sites could be detected on any of the support materials by forward titration using n-butylamine. Results were however obtained for acid site concentration using the back titration procedure outlined in Section 3.1.1 (Table 3.2). The trend for concentration of acidic sites (moles/g) was as for basic sites with the highest concentration existing on γ-Al_2O_3 and the lowest on silica gel. The highest density of acidic sites per m^2 was found on α-Al_2O_3 followed by γ-Al_2O_3, η-Al_2O_3 and silica gel. Richardson [1] and Trimm [125] have found that coke may be formed on acidic oxides and that the tendency for coke formation is directly related to surface acidity. Comparing the results obtained to coking tests using TGA (Table 2.05) it is seen than the highest level of coking was observed for γ- and η-Al_2O_3 which also possess the highest number of acidic sites. Maciver et al. [45] however found that total acidity was about the same for both γ- and η-Al_2O_3 and that the average strength of the sites was greatest for η-Al_2O_3. It should be noted however that these results were obtained using ammonia adsorption, a technique criticised by Parry [38] who found that the ammonia band used to determine the co-ordinately bonded ammonia was subject to interferences.

172

From TPO data already discussed in Chapter Two, it was seen that modification of Pt/γ-Al_2O_3 with other metals could reduce the amount of coking observed. The effect of these treatments on the acidic/basic nature of the catalyst was investigated by titration.

The titrimetric results for chemically treated samples of γ-Al_2O_3 and 0.5%Pt/γ-Al_2O_3 are given in Table 3.3. Again, the back titration method appeared to be more sensitive in detecting basic sites.

Treatment of γ-Al_2O_3 with HCl (0.1M) slightly reduced the concentration of Brönsted basic sites (Table 3.3). Williams et al. [94] have described the adsorption of mineral acids on Al_2O_3 as the exchange of aqueous electrolytes with H^+ and OH^- ions at the surface. Since the acid in this case is HCl the reaction on the surface would be the exchange of a Brönsted basic group (i.e. the hydroxyl group) with the Cl^- of HCl. This exchange of OH^- groups for Cl^- ion may explain the decrease in basicity of γ-Al_2O_3 after treatment with HCl. Treatment with HCl led to a decrease in number of acidic sites by approximately half. This was unexpected since the electronegative Cl after replacing a surface OH group would be expected to polarise the Al_2O_3 lattice more than the OH and therefore increase both protonic and aprotonic acidities. A possible explanation to this anomaly could be that treatment of γ-Al_2O_3 with HCl may result in an increase in number of strong acid sites as proposed by Melchor et al. [92] but may also cause an overall decrease in total number of acid sites as indicated by the results of this study.

Table 3.3 Results of acid/base titrations on modified γ-Al$_2$O$_3$

| Sample	Treatment	Surface Area	Forward titration of Basic Sites		Back titration of Basic Sites		Back titration of Acidic Sites		%C for High Temp. Peak
		(m^2/g)	mols$\times10^{-7}/m^2$	mols$\times10^{-4}/g$	mols$\times10^{-7}/m^2$	mols$\times10^{-4}/g$	mols$\times10^{-7}/m^2$	mols$\times10^{-4}/g$	
0.5%Pt/γ-Al$_2$O$_3$	Cal @ 630°C, 15 mins.	205	T.L.T.M. < 2.33	T.L.T.M. < 0.48	5.36 ($\pm$1.49)	1.10 ($\pm$0.25)	4.85 ($\pm$1.67)	0.99 ($\pm$0.30)	0.12
γ-Al$_2$O$_3$	——	220	7.46 ($\pm$0.82)	1.68 ($\pm$0.10)	6.92 ($\pm$1.53)	1.52 ($\pm$0.27)	12.2 ($\pm$3.15)	2.68 ($\pm$0.57)	0.20
γ-Al$_2$O$_3$	HCl treated	211	4.56 ($\pm$0.68)	0.96 ($\pm$0.10)	5.93 ($\pm$1.54)	1.25 ($\pm$0.26)	6.58 ($\pm$2.04)	1.39 ($\pm$0.37)	0.17
γ-Al$_2$O$_3$	NaOH treated	223	15.4 ($\pm$1.20)	3.44 ($\pm$0.01)	11.2 ($\pm$2.22)	2.50 ($\pm$0.38)	17.2 ($\pm$4.21)	3.84 ($\pm$0.37)	0.38
γ-Al$_2$O$_3$	NH$_3$ treated	201	9.84 ($\pm$0.98)	1.98 ($\pm$0.10)	11.2 ($\pm$2.28)	2.24 ($\pm$0.36)	13.8 ($\pm$3.68)	2.78 ($\pm$0.59)	0.20

Treatment of γ-Al$_2$O$_3$ with 0.1M NaOH resulted in a near doubling of the basic site concentration and a 1.5 times increase in acidic site concentration (Table 3.3). This could be due to the formation of new hydroxyl groups and agrees with the results obtained by Saad et al. [84] who found that sodium in concentrations greater than 1000ppm could create new basic sites. The sodium concentration used in this study was 2300ppm. The increase in acidic sites suggests that some of the hydroxyl groups, produced by sodium, have Brönsted acid character. This may be due to the electropositive nature of Na which on addition to Al$_2$O$_3$, would pull electrons away from O in the OH group and consequently increase acidity of the H.

As in the case of NaOH addition, treatment of Al$_2$O$_3$ with NH$_3$ resulted in an increase in total basicity; however the level of increase was less than for NaOH. Treatment with NH$_3$ had little effect on the acidic sites. This indicates that NH$_3$ increased the number or strength of Brönsted basic sites on Al$_2$O$_3$ and had very little effect on acidic sites. These findings appear to disagree with those of Tanabe et al. [29] and Malinowski et al. [96] who found that NH$_3$ interacted with acidic sites on the surface of Al$_2$O$_3$. However these researchers used samples of Al$_2$O$_3$ which had loosely bound surface water removed prior to analysis. In this study the Al$_2$O$_3$ used possessed surface water which may have been attached to the acidic sites and hence blocked interaction between these sites and the NH$_3$.

Impregnation of γ-Al$_2$O$_3$ with 0.5%Pt resulted in a decrease in basic and acidic site concentration. The basic sites could only be detected by back titration. Impregnation of γ-Al$_2$O$_3$ with aqueous H$_2$PtCl$_6$ is thought to proceed via adsorption of the acid onto the Al$_2$O$_3$ surface as shown in Fig. 3.02. A decrease in acidity was noted by Garbowski et al. [204] when γ-Al$_2$O$_3$ was impregnated with chloroplatinic acid and they concluded that Pt on Al$_2$O$_3$ inhibited strong Lewis acid sites. From Fig. 3.02 it can be seen that the impregnation procedure is accompanied by the production of HCl. The results from HCl treatment of γ-Al$_2$O$_3$ (Table 3.3) show that HCl reduces the number of acid sites on γ-Al$_2$O$_3$; therefore the HCl produced during impregnation with Pt may be the cause of decreased acidity. Parera

175

et al. [176] also found that Pt was supported on the acid function of Al_2O_3. The agreement of our results, for decrease in acidity on addition of Pt, with both Garbowski and Primet [204] and Parera et al. [176] helps to confirm that the titration procedure developed in this lab does in fact detect acidity on Al_2O_3 and Al_2O_3 supported catalysts.

Fig. 3.02 *{Ref. 203}*   Impregnation of γ-Al_2O_3 with H_2PtCl_6
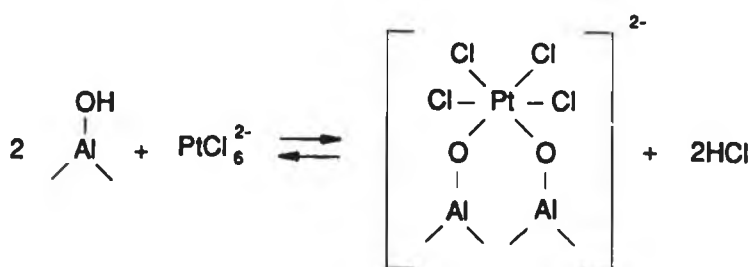
In order to determine if a correlation exists between concentration of acidic or basic sites and coking the results from Table 3.3 must be compared to those in Table 2.11. Since the titrations were performed on fresh samples of catalyst the coking results used for comparison are those from the first cycle TPO analysis. The high temperature TPO peak for γ-Al_2O_3 and NH_3 treated γ-Al_2O_3 showed that both samples has accumulated 0.20% coke during coking analysis (Table 2.11). When the concentration of acidic and basic sites on these samples are compared it is seen that the level of basicity is slightly higher for the NH_3 treated sample and that the level of acidity is essentially the same suggesting that the increased number of basic sites are not responsible for coking. NaOH treated γ-Al_2O_3 showed an increase in concentration of both acidic and Brönsted basic sites and a coking level of 0.38%. Al_2O_3 treated with HCl showed a decrease in concentration of both Brönsted basic sites and acidic sites which corresponded with a decrease in the level of coking to 0.17%. Treatment with chloroplatinic acid to produce 0.5%Pt/γ-Al_2O_3 also gave a reduction in the concentration of acidic and

176

Brönsted basic sites and a reduction in the level of coking down to 0.12%. Based on these results it would appear that concentration of acidic sites has an effect on coking. The lowest level of coke was detected for 0.5%Pt/γ-Al$_2$O$_3$ which also had the smallest concentration of acidic and Brönsted basic sites. However other factors, such as platinum's ability to catalyse coke and coke precursors [176], may have also contributed to this reduction in coking.

The effect of Sn addition to γ-Al$_2$O$_3$ and Pt/γ-Al$_2$O$_3$ catalysts are presented in Table 3.4. The surface area of γ-Al$_2$O$_3$ impregnated with Sn is slightly reduced compared to γ-Al$_2$O$_3$; however the surface areas are similar for all Sn/γ-Al$_2$O$_3$ samples.

From Table 3.4 it can be seen that addition of 0.5% Sn has little effect on the Brönsted basic sites and acidic sites as measured by back titration (small decrease in number of basic sites determined by forward titration). Addition of 2.0% Sn (cal.@500°C/2hrs.) resulted in reduction by half in the number of Brönsted basic sites determined by back titration (values below detection limit for forward titration) and reduction by quarter in number of acidic sites. The largest reduction in coking was seen for 2.0%Sn/γ-Al$_2$O$_3$ calcined at 500°C. Results from the titrations, however, show that the lowest levels of acidic and Brönsted basic sites are found on 2.0%Sn/γ-Al$_2$O$_3$ calcined at 630°C. This sample however, while giving less coke than γ-Al$_2$O$_3$, gave almost twice that of the 2.0%Sn/γ-Al$_2$O$_3$(500°C) sample. These results indicate that the effect of Sn on coking levels cannot be explained solely in terms of acidic or Brönsted basic site concentration.

Again for the Pt–Sn/γ-Al$_2$O$_3$ catalysts, the lowest level of coking did not occur on the catalyst containing the smallest concentration of acidic and Brönsted basic sites. Indeed the analysis reveals that the Pt–Sn/γ-Al$_2$O$_3$ sample, which possessed the lowest level of acidic and Brönsted basic sites, produced the greatest amount of coke. Pt addition appeared to decrease the number of Brönsted basic sites and, depending on the catalyst increased or decreased the number of

Table 3.4 Results for Acid/Base titrations on Sn/γ-Al$_2$O$_3$ and Pt–Sn/γ-Al$_2$O$_3$ catalysts.

Sample	Treatment	Surface area	Forward titration of Basic Sites		Back titration of Basic Sites		Back titration of Acidic Sites		% C in High Temp. peak
		(m^2/g)	moles×10^{-7}/m^2	moles×10^{-4}/g	moles×10^{-7}/m^2	moles×10^{-4}/g	moles×10^{-7}/m^2	moles×10^{-4}/g	
γ-Al$_2$O$_3$	None	220	7.46 (±0.82)	1.68 (±0.10)	6.92 (±1.53)	1.52 (±0.27)	12.2 (±3.15)	2.68 (±0.57)	0.20
0.5%Sn/γ-Al$_2$O$_3$	500°C/2hrs.	208	5.26 (±0.68)	1.10 (±0.09)	8.32 (±1.93)	1.73 (±0.31)	8.84 (±2.54)	1.84 (±0.44)	0.23
2.0%Sn/γ-Al$_2$O$_3$	500°C/2hrs.	201	T.L.T.M. (<2.33)	T.L.T.M. (<.48)	3.92 (±1.32)	0.79 (±0.23)	2.90 (±1.30)	0.58 (±0.23)	0.06
0.5%Sn/γ-Al$_2$O$_3$	630°C/15mins.	211	5.88 (±0.76)	1.24 (±0.10)	7.18 (±1.71)	1.51 (±0.29)	9.66 (±2.67)	2.04 (±0.46)	0.10
2.0%Sn/γ-Al$_2$O$_3$	630°C/15mins.	194	T.L.T.M. (<2.33)	T.L.T.M. (<.48)	1.52 (±1.01)	0.30 (±0.18)	0.87 (±0.90)	0.17 (±0.16)	0.14
0.5%Pt/γ-Al$_2$O$_3$	630°C/15mins.	205	T.L.T.M (<2.33)	T.L.T.M. (<0.48)	5.36 (±1.49)	1.10 (±0.25)	4.85 (±1.67)	0.99 (±0.30)	0.12
0.5%Pt– 0.5%Sn /γ-Al$_2$O$_3$	630°C/15mins, co-imp.	206	4.98 (±0.75)	1.03 (±0.10)	6.41 (±1.64)	1.32 (±0.27)	9.02 (±2.60)	1.86 (±0.44)	0.09
0.5%Pt– 2.0%Sn /γ-Al$_2$O$_3$	630°C/15mins, co-imp.	207	T.L.T.M. (<2.33)	T.L.T.M. (<.48)	3.61 (±1.47)	0.75 (±0.27)	5.58 (±1.84)	1.16 (±0.32)	0.03
0.5%Pt– 0.5%Sn /γ-Al$_2$O$_3$	500°C/2hrs., co-imp.	215	T.L.T.M. (<2.33)	T.L.T.M. (<.48)	5.03 (±1.40)	1.08 (±0.25)	5.03 (±1.70)	2.17 (±0.62)	0.10
0.5%Pt– 2.0%Sn /γ-Al$_2$O$_3$	500°C/2hrs., co-imp.	190	T.L.T.M. (<2.33)	T.L.T.M. (<.48)	1.26 (±0.98)	0.24 (±0.17)	1.05 (±1.21)	0.20 (±0.22)	0.13
0.5%Pt– 0.5%Sn /γ-Al$_2$O$_3$	500°C/2hrs., step-imp.	198	T.L.T.M. (<2.33)	T.L.T.M. (<.48)	5.36 (±1.54)	1.06 (±0.25)	5.40 (±1.84)	1.07 (±0.31)	0.09
0.5%Pt– 2.0%Sn /γ-Al$_2$O$_3$	500°C/2hrs., step-imp.	203	T.L.T.M. (<2.33)	T.L.T.M. (<.48)	2.38 (±)1.17	0.49 (±0.22)	1.30 (±)1.00	0.27 (±0.19)	0.02

acidic sites. The general trend for these Pt–Sn/γ-Al$_2$O$_3$ bimetallic catalysts was that increasing the level of Sn brought about a reduction in both acidic and Brönsted basic sites, regardless of calcination temperature or method of preparation, and also reduced the extent of coking.

The concentration of acidic and Brönsted basic sites was determined for Zr/γ-Al$_2$O$_3$ and Pt–Zr/γ-Al$_2$O$_3$ catalysts and the results are given in Table 3.5. Addition of Zr to γ-Al$_2$O$_3$ had little effect on surface area. As with Sn addition, Zr addition to γ-Al$_2$O$_3$ decreased the number of Brönsted basic and acidic sites, with the samples containing 2.0% Zr showing the greatest decrease. Back titration showed the decrease to be similar for 0.5% and 2.0% Zr. Very little coking was detected on the samples (~ 0.01%), regardless of the amount of Zr added (Table 3.4). When Pt was added to Zr/γ-Al$_2$O$_3$ at the low level, regardless of preparation conditions, an increase in the number of Brönsted basic sites was seen; however at the highest level of Zr (2%) a decrease was noted. Interestingly, the basic sites and acidic sites either both increase or both decrease. Also, at each level of Zr, the concentration of Brönsted basic sites and acidic sites was lower for the samples prepared by step-impregnation. The quantity of coke deposited on Pt–Zr/γ-Al$_2$O$_3$ catalysts appears to depend more on the method of impregnation than the concentration of acidic or Brönsted basic sites. The lowest level of coking occurred on the co-impregnated 0.5%Pt–0.5%Zr/γ-Al$_2$O$_3$ sample which was the one that showed the highest number of acidic sites and Brönsted basic sites. It should also be noted that this sample was the only one which possessed any Brönsted basic sites detectable by forward titration with perchloric acid. Even though the number of acidic and Brönsted basic sites on step-impregnated Pt–Zr/γ-Al$_2$O$_3$ are lower than on corresponding catalysts prepared by co-impregnation, levels of coke are higher on the step-impregnated samples.

Table 3.5 Results from Acid/Base titrations on Zr/γ-Al$_2$O$_3$ and Pt–Zr/γ-Al$_2$O$_3$

Sample	Treatment	Surface area	Forward titration of Basic Sites		Back titration of Basic Sites		Back titration of Acidic Sites		%C in High Temp. Peak
		(m^2/g)	mol.×10^{-7}/m^2	mol.×10^{-4}/g	mol.×10^{-7}/m^2	mol.×10^{-4}/g	mol.×10^{-7}/m^2	mol.×10^{-4}/g	
γ-Al$_2$O$_3$	None	220	7.46 (±0.82)	1.68 (±0.10)	6.92 (±1.53)	1.52 (±0.27)	12.2 (±3.15)	2.68 (±0.57)	0.20
0.5%Zr/γ-Al$_2$O$_3$	630°C/15 min	212	5.64 (±0.73)	1.20 (±0.11)	6.25 (±1.59)	1.33 (±0.27)	9.61 (±2.67)	2.04 (±0.47)	0.01
2.0%Zr/γ-Al$_2$O$_3$	630°C/15 min	205	T.L.T.M. (< 2.33)	T.L.T.M. (< 0.48)	6.41 (±1.63)	1.31 (±0.27)	4.08 (±1.52)	0.84 (±0.27)	0.01
0.5%Pt/γ-Al$_2$O$_3$	630°C/15 min	205	T.L.T.M. (< 2.33)	T.L.T.M. (< 0.48)	5.36 (±1.49)	1.10 (±0.25)	4.85 (±1.67)	0.99 (±0.30)	0.12
0.5%Pt–0.5%Zr /γ-Al$_2$O$_3$	630°C/15 min co-imp.	208	5.08 (±0.71)	1.06 (±0.09)	6.50 (±1.64)	1.36 (±0.28)	7.18 (±2.18)	1.49 (±0.38)	0.07
0.5%Pt–2.0%Zr /γ-Al$_2$O$_3$	630°C/15 min co-imp.	190	T.L.T.M. (< 2.33)	T.L.T.M. (< 0.48)	2.54 (±1.16)	0.49 (±0.20)	1.14 (±1.08)	0.22 (±0.19)	0.11
0.5%Pt–0.5%Zr /γ-Al$_2$O$_3$	630°C/15 min step-imp.	213	T.L.T.M. (< 2.33)	T.L.T.M. (< 0.48)	5.18 (±1.43)	1.10 (±0.25)	5.79 (±1.84)	1.24 (±0.34)	0.22
0.5%Pt–2.0%Zr /γ-Al$_2$O$_3$	630°C/15 min step-imp.	202	T.L.T.M. (< 2.33)	T.L.T.M. (< 0.48)	1.32 (±0.95)	0.27 (±0.18)	0.47 (±0.76)	0.10 (±0.15)	0.17

From the results of Table 3.5 it would appear that, as for Pt–Sn/γ-Al$_2$O$_3$ the effect of Zr on coking of Pt–Zr/γ-Al$_2$O$_3$ catalysts cannot be explained solely in terms of acidic or basic sites. As was proposed in Section 2.2 the type of preparation procedure used exerts an important effect on the level of coking due to the strength of interaction between the Pt and the second metal. It was decided, based on the findings of Baronetti et al. [188] and the results in section 2.2, that for bimetallic catalysts strongest interaction between Pt and the second metal occurred for samples prepared by co-impregnation and when the atomic loading of the two metals was similar. If this was the case then the amount of acidic or Brönsted basic sites affected by the metals should be lowest when the interaction is highest and the metals are closest together. Our results show this to be the case with the highest concentration of acidic and Brönsted basic sites on samples of Pt–Zr/γ-Al$_2$O$_3$ where the metal levels are both 0.5wt.% for each. In addition to this, of the two 0.5%Pt–0.5%Zr/γ-Al$_2$O$_3$ catalysts, the one prepared by co-impregnation had the highest level of sites. A similar trend was seen for 0.5%Pt–2.0%Zr/γ-Al$_2$O$_3$ catalysts where those prepared by co-impregnation did not destroy as many sites as those prepared by step-impregnation.

The last system to be analysed for number of acid/base sites was the Ce/γ-Al$_2$O$_3$ and the Pt–Ce/γ-Al$_2$O$_3$. Results are given in Table 3.6. On Ce addition to γ-Al$_2$O$_3$, the number of Brönsted basic sites and acidic sites decreased, with 0.1% loading having the greatest effect followed by 0.3% and finally 2.0%. The limit of detection for Brönsted basic sites by back titration was taken to be 0.11×10^{-4}mols/g or 0.55×10^{-7}mols/m^2 which was calculated using an end point of 0.10cm^3. In the case of acidic sites the 0.1%Ce/γ-Al$_2$O$_3$ sample did not indicate the presence of any detectable acidic sites. The limit of detection for acidic sites was 0.10×10^{-4}moles/g or 0.50×10^{-7}moles/m^2 which was calculated for an end-point of 0.10cm^3. A possible explanation for the presence of Brönsted basic sites and acidic sites at concentrations above 0.1wt.% Ce may be that at higher Ce concentration, dispersion is decreased resulting in larger Ce particles and less of the acidic and Brönsted basic sites on γ-Al$_2$O$_3$ are affected.

Table 3.6 Results from Acid/Base titrations on Ce/γ-Al$_2$O$_3$ and Pt–Ce/γ-Al$_2$O$_3$ catalysts.

Sample	Treatment	Surface Area	Forward titration of Basic Sites		Back titration of Basic Sites		Back titration of Acidic Sites		%C in High Temp. Peak
		(m^2/g)	mols×10^{-7}/m^2	mols×10^{-4}/g	mols×10^{-7}/m^2	mols×10^{-4}/g	mols×10^{-7}/m^2	mols×10^{-4}/g	
γ-Al$_2$O$_3$	None	220	7.46 (±0.82)	1.68 (±0.10)	6.92 (±1.53)	1.52 (±0.27)	12.2 (±3.15)	2.68 (±0.57)	0.20
0.1%Ce/γ-Al$_2$O$_3$	630°C/15mins	215	T.L.T.M. (<2.33)	T.L.T.M. (<0.48)	T.L.T.M (<0.55)	T.L.T.M. (<0.11)	T.L.T.M. (<0.50)	T.L.T.M. (<0.10)	0.05
0.5%Ce/γ-Al$_2$O$_3$	630°C/15mins	200	T.L.T.M. (<2.33)	T.L.T.M. (<0.48)	5.64 (±1.56)	1.13 (±0.24)	5.69 (±1.89)	1.14 (±0.32)	0.08
2.0%Ce/γ-Al$_2$O$_3$	630°C/15mins	215	5.68 (±0.74)	1.22 (±0.10)	6.21 (±1.56)	1.34 (±0.27)	9.41 (±2.54)	1.98 (±0.46)	0.06
0.5%Pt/γ-Al$_2$O$_3$	630°C/15mins	205	T.L.T.M. (<2.33)	T.L.T.M. (<0.48)	5.36 (±1.49)	1.10 (±0.25)	4.85 (±1.67)	0.99 (±0.30)	0.12
0.5%Pt–0.3%Ce /γ-Al$_2$O$_3$	630°C/15mins co-imp.	211	T.L.T.M. (<2.33)	T.L.T.M. (<0.48)	1.78 (±0.94)	0.38 (±0.19)	1.90 (±1.03)	0.40 (±0.20)	0.22
0.5%Pt–0.5%Ce /γ-Al$_2$O$_3$	630°C/15mins co-imp.	208	T.L.T.M. (<2.33)	T.L.T.M. (<0.48)	4.89 (±1.42)	1.02 (±0.24)	3.92 (±1.48)	0.82 (±0.27)	0.36
0.5%Pt–3.0%Ce /γ-Al$_2$O$_3$	630°C/15mins co-imp.	205	T.L.T.M. (<2.33)	T.L.T.M. (<0.48)	T.L.T.M. (<0.55)	T.L.T.M. (<0.11)	T.L.T.M. (<0.50)	T.L.T.M. (<0.10)	0.23
0.5%Pt–0.1%Ce /γ-Al$_2$O$_3$	630°C/15mins step-imp.	207	3.86 (±0.69)	0.80 (±0.10)	5.78 (±1.55)	1.20 (±0.26)	4.80 (±1.68)	1.00 (±0.30)	0.09
0.5%Pt–0.5%Ce /γ-Al$_2$O$_3$	630°C/15mins step-imp.	210	5.09 (±0.71)	1.08 (±0.11)	5.80 (±1.54)	1.22 (±0.27)	4.95 (±1.69)	1.04 (±0.31)	0.05

The amount of coke formed on each of the $Ce/\gamma-Al_2O_3$ samples was very similar regardless of the Ce concentration (Table 3.6). In comparison the level of coke formed on $Ce/\gamma-Al_2O_3$ catalysts was 75% less than that formed on $\gamma-Al_2O_3$ itself. It is worth noting that coking occurred on the $0.1\%Ce/\gamma-Al_2O_3$ sample even though it did not possess any detectable acidic or basic sites.

Titration of the $Pt-Ce/\gamma-Al_2O_3$ catalysts showed that concentration of acidic and Brönsted basic sites varied depending on the level of Ce and method of preparation (Table 3.6). Forward titration of Brönsted basic sites with perchloric acid did not detect any Brönsted basic sites on the $Pt-Ce/\gamma-Al_2O_3$(co-imp.) samples containing 0.3%, 0.5% or 3.0%Ce. In fact the $0.5\%Pt-3.0\%Ce/\gamma-Al_2O_3$(co-imp.) revealed no detectable acidic or basic sites. This is probably due to the large Ce loading (i.e. 3.0%) which may act to block acidic and basic sites on the surface of $\gamma-Al_2O_3$. As was seen for $Ce/\gamma-Al_2O_3$, low levels of Ce in $Pt-Ce/\gamma-Al_2O_3$ can affect the concentration of Brönsted basic sites and acidic sites as determined by back titration. Addition of Ce at all concentrations reduced the number of basic sites relative to $Pt/\gamma-Al_2O_3$. The effect on acid sites was not as clear with decreased concentration observed only for the co-impregnated samples at the levels examined. The number of Brönsted basic sites and acidic sites on $Pt-Ce/\gamma-Al_2O_3$ catalysts prepared by step-impregnation were found to be higher than the co-impregnated samples and were less sensitive to Ce concentration than those prepared by co-impregnation. It can be seen from Table 3.6 that the levels of Brönsted basic sites were 0.122mMoles/g and 0.120mMoles/g for step-impregnated catalysts containing 0.5% and 0.1% Ce respectively. Values obtained for acid site concentration on step-impregnated $Pt-Ce/\gamma-Al_2O_3$ samples are similar to $Pt/\gamma-Al_2O_3$. No acidic or Brönsted basic sites could be detected on the $0.1\%Ce/\gamma-Al_2O_3$ yet the step-impregnated $0.5\%Pt-0.1\%Ce/\gamma-Al_2O_3$, which had Ce added first during preparation, displayed levels of acidic and Brönsted basic site concentrations comparable with those of $0.5\%Pt/\gamma-Al_2O_3$. Also the step-impregnated $0.5\%Pt-0.1\%Ce/\gamma-Al_2O_3$ sample possessed Brönsted basic sites which were strong enough to be detected by forward titration with perchloric acid. This suggests that addition of 0.5%Pt to samples of $0.1\%Ce/\gamma-Al_2O_3$ and $0.5\%Ce/\gamma-Al_2O_3$ brings about the

formation of Brönsted basic sites. A possible explanation for this may be that addition of Pt reduces the Ce–Al$_2$O$_3$ interaction and hence exposes the acidic and Brönsted basic sites previously blocked or covered over by Ce.

With regard to levels of coke formed on these Pt–Ce/γ-Al$_2$O$_3$ catalysts a large variation was seen between catalysts prepared by co-impregnation and step-impregnation (Table 3.6). When this is considered in conjunction with acidic and Brönsted basic site concentration it is seen that the quantities of coke are much lower on the step-impregnated samples which also have a higher concentration of Brönsted basic and acidic sites. The co-impregnated samples, while having less acidic and Brönsted basic sites than γ-Al2O$_3$, formed more coke, regardless of the amount of Ce added. Therefore again, there does not appear to be a direct relationship between the number of Brönsted basic sites and degree of coking for Pt–Ce/γ-Al$_2$O$_3$ systems.

3.2.3 Activity analysis results

In Chapter Two, the effect of Sn, Zr, and Ce on the coking of Pt/γ-Al$_2$O$_3$ has been investigated. The effect of these additives on the activity of Pt/γ-Al$_2$O$_3$ is now investigated as it has been found that modifications which bring about reductions in coking can also have detrimental effects on catalyst activity [125]. The activity of these catalysts was determined as detailed in Section 3.1.3. The extent of isobutane-butane conversion is given as a percentage of the overall amount present prior to reaction. In order to compare activities of the various catalysts the temperatures at which 10%, 50% and 90% conversion occurred (referred to as T_{10}, T_{50}, and T_{90} respectively) were determined.

Graph 3.1 and Table 3.7 show the results obtained for first and second activity analysis on 0.5%Pt/γ-Al$_2$O$_3$ and on γ-Al$_2$O$_3$.

Graph 3.1 Activity analysis of Pt/γ-Al$_2$O$_3$ and γ-Al$_2$O$_3$

185
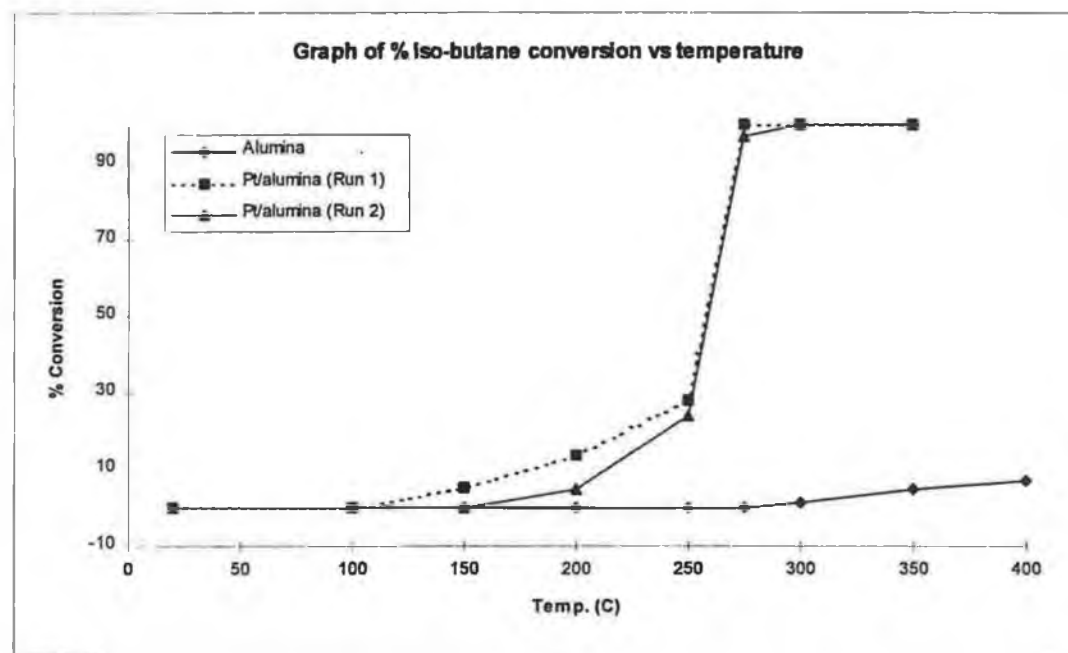
Table 3.7 Activity test results for Pt/γ-Al$_2$O$_3$ and γ-Al$_2$O$_3$.

Sample	Treatment	Activity Test 1			Activity Test 2		
		T$_{10}$ (°C)	T$_{50}$ (°C)	T$_{90}$ (°C)	T$_{10}$ (°C)	T$_{50}$ (°C)	T$_{90}$ (°C)
0.5%Pt/γ-Al$_2$O$_3$	Cal. @630°C /15mins	185	265	270	225	270	275
γ-Al$_2$O$_3$	None	>400	——	——	——	——	——

The T_{50} and T_{90} values for Pt/γ-Al$_2$O$_3$ in Table 3.7 indicate that isobutane conversion occur at lower temperatures on the fresh catalyst. It may be recalled from Section 2.2 that 0.12% coke was formed on a fresh sample of Pt/γ-Al$_2$O$_3$ while re-coking of this catalyst followed by TPO revealed the presence of 0.37% coke. Based on these results and those of analysis by chemisorption it was proposed that the increase in coking and consequent reduction in Pt surface area was due to sintering of Pt particles during TPO of coke. Sintering of Pt particles produces larger Pt crystallites and reduced dispersion which in this case resulted in the catalyst having a lower activity overall, for isobutane conversion. Kooh et al. [158] found that for oxidation of heptane over Pt/Al$_2$O$_3$ large Pt crystallites were more active than small ones. A possible explanation for the anomaly in results may have to do with the types of Al$_2$O$_3$ used. In this study high surface area γ-Al$_2$O$_3$ was used whose surface area was calculated to be 220m^2/g while the Al$_2$O$_3$ used by Kooh et al. [158] was calcined at 1000°C for 24 hours prior to analysis. According to Fig. 1.1 this would result in the production of either θ-, δ- or κ-Al$_2$O$_3$ which have relatively low surface areas. The surface area of the Al$_2$O$_3$ used by Kooh et al. [158] was determined to be 83m^2/g and Pt loadings of 0.8 and 5.0% were used. These factors would result in a much higher Pt density on Kooh et al [158] catalysts compared to those used in this study and may explain the differences in results.
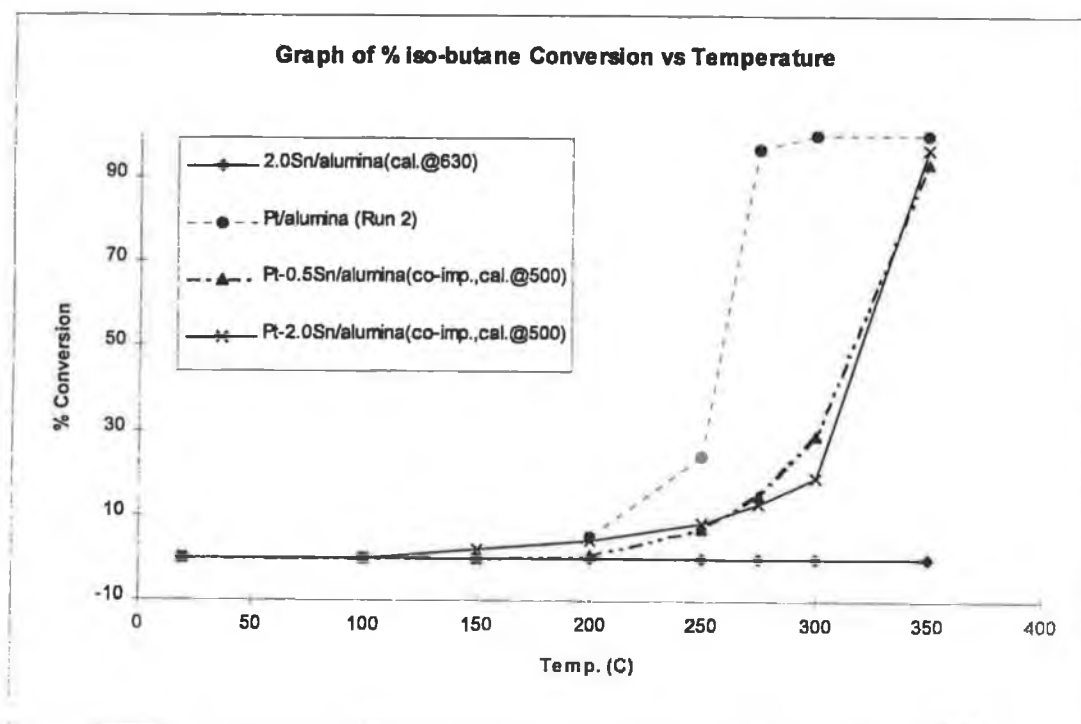
With regard to γ-Al$_2$O$_3$ it can be seen that almost no activity for conversion of isobutane was detected even when the sample was heated to 400°C. At temperatures above 350°C a small decrease in the isobutane peaks was observed which could be due to non catalytic combustion of isobutane. The level of this decrease in the isobutane peak was approximately 3% at 400°C.

The effect of Sn addition on the activity of γ-Al$_2$O$_3$ and Pt/γ-Al$_2$O$_3$ is given in Graphs 3.2, 3.3 and 3.4 and summarised in Table 3.8.

Graph 3.2 Activity analysis on Sn/γ-Al₂O₃ and Pt–Sn/γ-Al₂O₃ catalysts.

Graph of % iso-butane Conversion vs Temperature

Legend:
- 2.0Sn/alumina(cal.@500)
- Pt/alumina (Run 2)
- Pt-0.5Sn/alumina(co-imp.,cal.@630)
- Pt-2.0Sn/alumina(co-imp.,cal.@630)
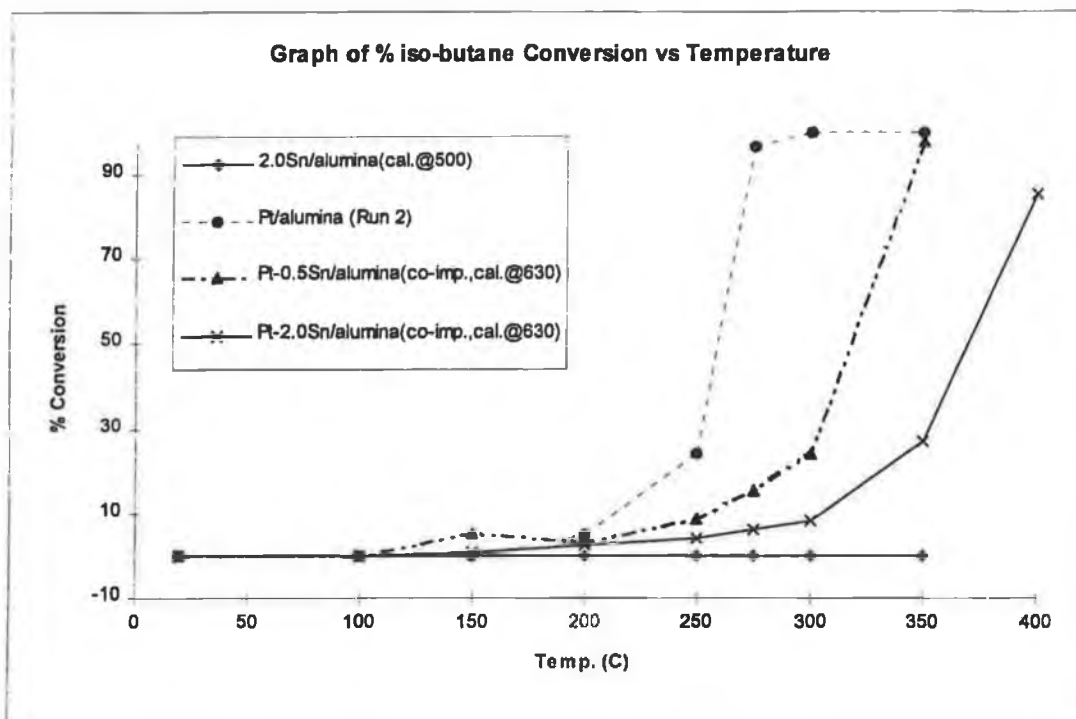
Graph 3.3 Activity analysis on Sn/γ-Al₂O₃ and Pt–Sn/γ-Al₂O₃ catalysts.

Graph of % iso-butane Conversion vs Temperature

Legend:
- 2.0Sn/alumina(cal.@630)
- Pt/alumina (Run 2)
- Pt-0.5Sn/alumina(co-imp.,cal.@500)
- Pt-2.0Sn/alumina(co-imp.,cal.@500)

188

Graph 3.4   Activity analysis on Pt–Sn/γ-Al$_2$O$_3$ catalysts.

189
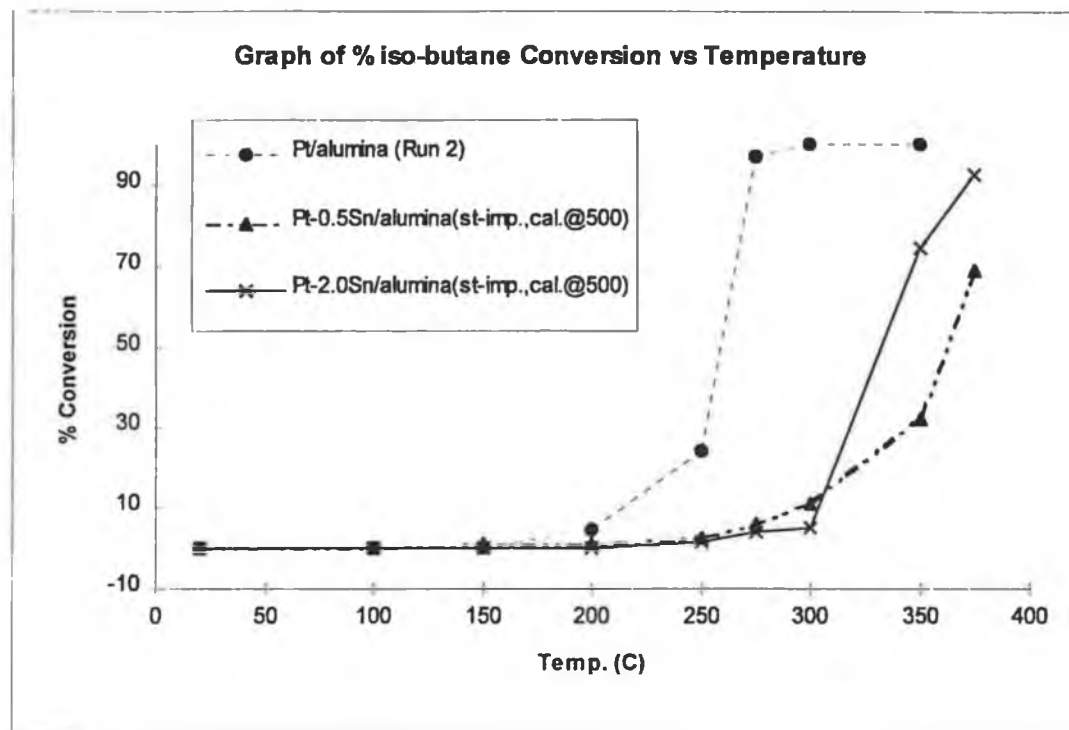
Table 3.8 Table of conversion values for $Sn/\gamma-Al_2O_3$ and $Pt-Sn/\gamma-Al_2O_3$

Sample	Treatment	Activity Analysis		
		T_{10} (°C)	T_{50} (°C)	T_{90} (°C)
2.0%Sn/γ-Al$_2$O$_3$	630°C/15 mins	>400	——	——
2.0%Sn/γ-Al$_2$O$_3$	500°C/2 hrs.	>400	——	——
0.5%Pt/γ-Al$_2$O$_3$	630°C/15 mins	225	265	270
0.5%Pt–0.5%Sn/γ-Al$_2$O$_3$	630°C/15 mins, Co-imp.	257	320	346
0.5%Pt–2.0%Sn/γ-Al$_2$O$_3$	630°C/15 mins, Co-imp.	353	382	>400
0.5%Pt–0.5%Sn/γ-Al$_2$O$_3$	500°C/2 hrs, Co-imp.	260	316	344
0.5%Pt–2.0%Sn/γ-Al$_2$O$_3$	500°C/2 hrs, Co-imp.	260	320	344
0.5%Pt–0.5%Sn/γ-Al$_2$O$_3$	500°C/2 hrs, Step-imp.	245	366	>400
0.5%Pt–2.0%Sn/γ-Al$_2$O$_3$	500°C/2 hrs, Step-imp.	298	330	363

The results show that addition of Sn to γ-Al$_2$O$_3$ does not bring about any activity for oxidation of isobutane-butane. Sn addition to Pt/γ-Al$_2$O$_3$ results in reduced activity. For all the Pt–Sn/γ-Al$_2$O$_3$ catalysts, temperatures at which the various levels of conversion occur are higher than for Pt/γ-Al$_2$O$_3$ itself. The lowest T_{10} value was seen for Pt–0.5%Sn/γ-Al$_2$O$_3$ (step-imp.,cal.@500°C/2hrs) but the T_{90} value for this catalyst was above 400°C suggesting that the catalyst is not very active. The Pt–2.0%Sn/γ-Al$_2$O$_3$ (co-imp.,cal.@630°C/15mins) catalyst had the highest T_{10} value and also had a T_{90} value in excess of 400°C. In generally, activity of Pt–Sn/γ-Al$_2$O$_3$ catalysts was low with all of them possessing T_{50} values in excess of 300°C while the T_{90} value was below 280°C for the Pt/γ-Al$_2$O$_3$ sample. Of the better Pt–Sn/γ-Al$_2$O$_3$ catalysts were the two prepared by co-impregnation and calcined at 500°C for two hours and the Pt–0.5%Sn/γ-Al$_2$O$_3$ (co-imp.,cal.@630°C/15mins). The activity of equivalent catalysts prepared by step-impregnation were lower than those prepared using co-impregnation.

In section 2.2 the Pt–2.0%Sn/γ-Al$_2$O$_3$ (cal.@500°C/2hrs., step-imp.) and Pt–2.0%Sn/γ-Al$_2$O$_3$ (cal.@630°C/15mins.,co-imp.) catalysts were found to be best at reducing coking. To determine which Pt–Sn/γ-Al$_2$O$_3$ catalyst is best overall requires assessment on the basic of activity and level of coking. With regard to the two catalysts mentioned in this paragraph the co-impregnated one was found to have very poor activity and only gave an isobutane-butane conversion of 85% at 400°C. Activity of the step-impregnated sample was better achieving T_{90} at 363°C. The Pt–0.5%Sn/γ-Al$_2$O$_3$ (co-imp.,cal.@500°C/2 hrs) yielded 0.04% coke, during second TPO analysis, which is only 0.01% higher than that found for the two catalysts mentioned at the beginning of the paragraph. From Table 3.8 it can be seen that activity of the Pt–0.5%Sn/γ-Al$_2$O$_3$ catalyst (cal.@500°C/2hrs,co-imp.) was among the highest and since it also combines good coke prevention characteristics it can be considered best overall of the Pt–Sn/γ-Al$_2$O$_3$ catalysts.

The activity of Zr/γ-Al$_2$O$_3$ and Pt–Zr/γ-Al$_2$O$_3$ was analysed by the activity procedure outlined in Section 3.1.6 and the data obtained was plotted in Graphs 3.5 to 3.8 and tabulated in Table 3.9. Addition of Zr to γ-Al$_2$O$_3$ results in the

191

production of a catalyst with increased activity for conversion of isobutane-butane. The amount of activity was however quite low and only evident at 2.0%Zr loading where a 10% conversion was achieved at 339°C. Again for all Pt–Zr/γ-Al$_2$O$_3$ catalysts the activity was lower than for 0.5%Pt/γ-Al$_2$O$_3$. For the co-impregnated samples, the activity was greatest at the lower Zr content.
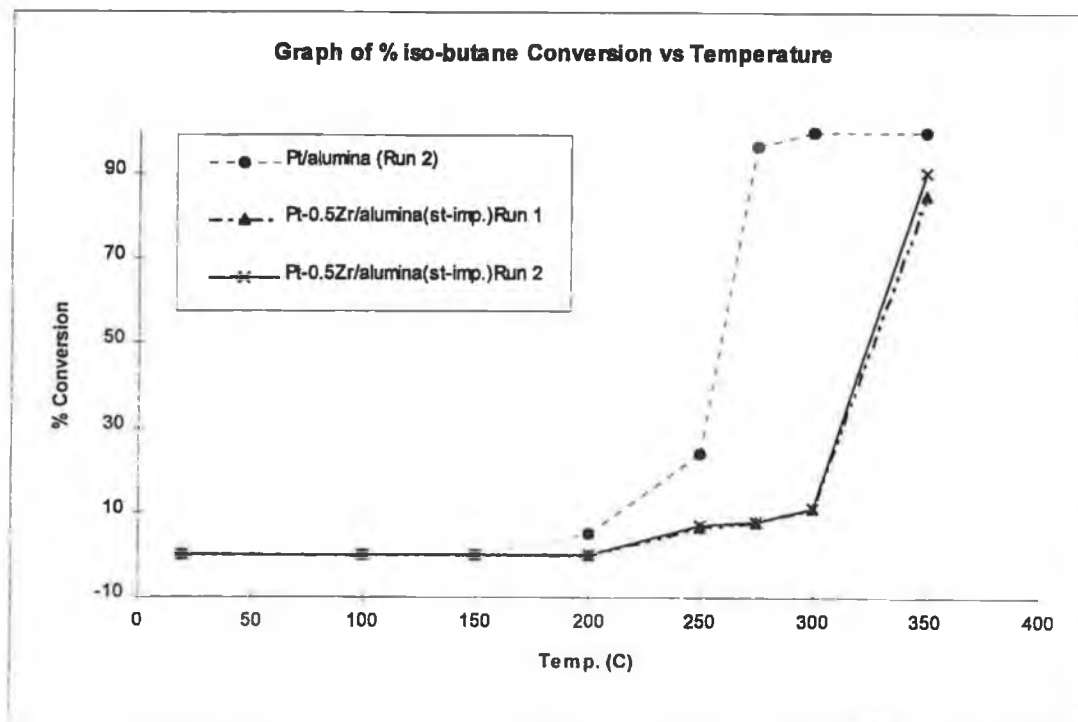
Graph 3.5 Activity analysis of Zr/γ-Al$_2$O$_3$ and Pt/γ-Al$_2$O$_3$
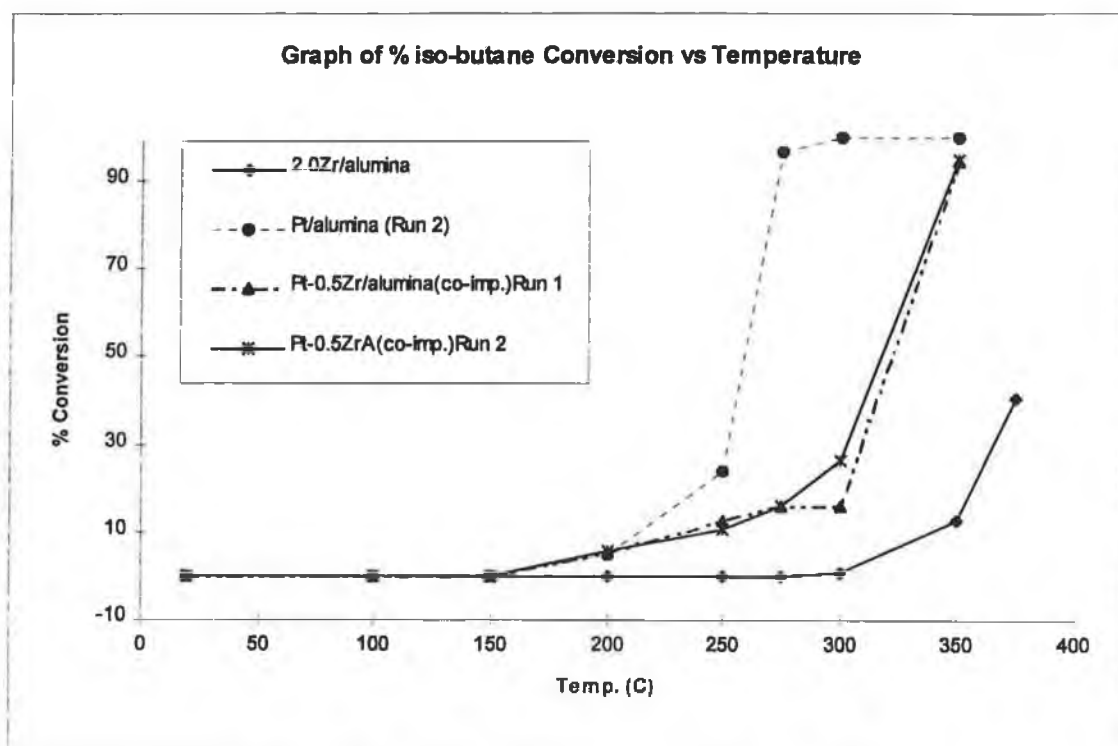
Graph 3.6 Activity analysis of Pt/γ-Al$_2$O$_3$ and Pt–Zr/γ-Al$_2$O$_3$ catalysts.
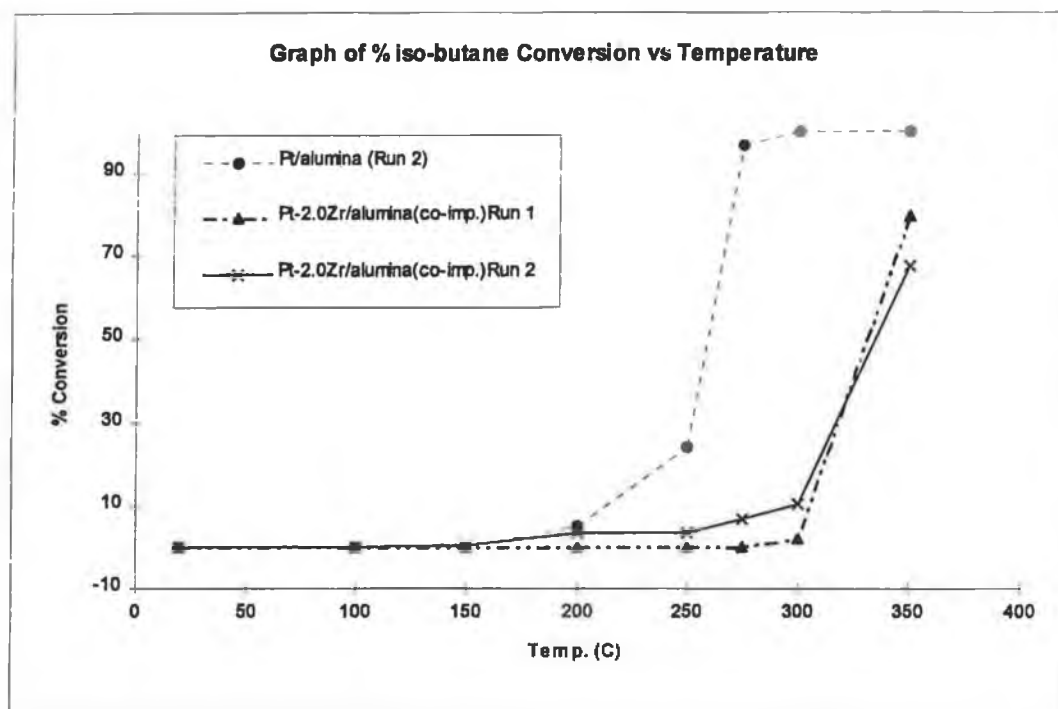
Graph 3.7 Activity analysis of Pt/γ-Al$_2$O$_3$ and Pt–Zr/γ-Al$_2$O$_3$ catalysts.

Graph 3.8 Activity analysis of Pt/γ-Al$_2$O$_3$ and Pt–Zr/γ-Al$_2$O$_3$ catalysts.

Graph of % Iso-butane Conversion vs Temperature

Legend:
- Pt/alumina (Run 2)
- Pt-2.0Zr/alumina(st-imp.)Run 1
- Pt-2.0Zr/alumina(st-imp.)Run 2

Y-axis: % Conversion (-10, 10, 30, 50, 70, 90)
X-axis: Temp. (C) (0, 50, 100, 150, 200, 250, 300, 350, 400)
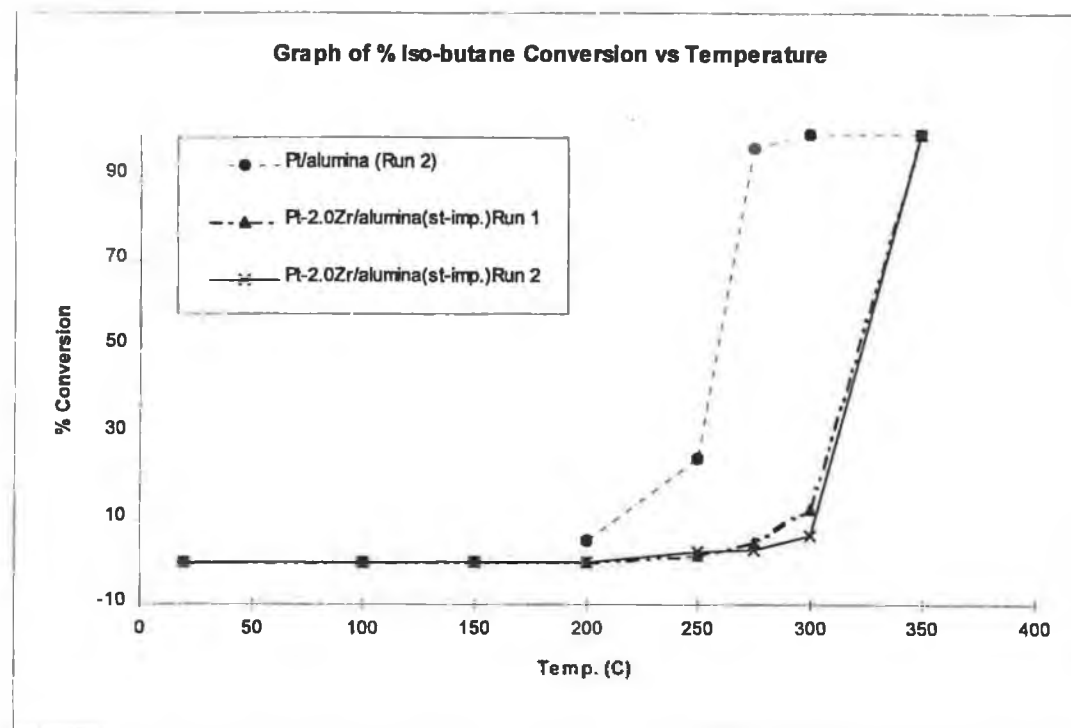
Table 3.9 Data from activity analysis of Zr/γ-Al$_2$O$_3$ and Pt–Zr/γ-Al$_2$O$_3$ catalysts.

Sample	Treatment	Activity Test 1			Activity Test 2		
		T_{10} (^{o}C)	T_{50} (^{o}C)	T_{90} (^{o}C)	T_{10} (^{o}C)	T_{50} (^{o}C)	T_{90} (^{o}C)
0.5%Zr/γ-Al$_2$O$_3$	630°C/15 mins	>350	——	——	——	——	——
2.0%Zr/γ-Al$_2$O$_3$	630°C/15 mins	339	>400	——	——	——	——
0.5%Pt–0.5%Zr/γAl$_2$O$_3$	630°C/15 mins, Co-imp.	228	321	346	240	316	346
0.5%Pt–2.0%Zr/γAl$_2$O$_3$	630°C/15 mins, Co-imp.	300	325	>350	300	330	>350
0.5%Pt–0.5%Zr/γAl$_2$O$_3$	630°C/15 mins, Step-imp.	291	325	>350	290	324	350
0.5%Pt–2.0%Zr/γAl$_2$O$_3$	630°C/15 mins, Step-imp.	291	322	339	301	322	339

Comparison of the activity curves for both co- and step-impregnated Pt–Zr/γ-Al$_2$O$_3$ catalysts revealed very little difference in activity between first and second analysis for either system. For co-impregnated Pt–Zr/γ-Al$_2$O$_3$ samples addition of 0.5% Zr resulted in higher activity than addition of 2.0%Zr while the opposite was seen for step-impregnated Pt–Zr/γ-Al$_2$O$_3$ samples.

Based on these results it appears that the most active catalysts are Pt–0.5Zr/γAl$_2$O$_3$(co-imp.) and Pt–2.0Zr/γ-Al$_2$O$_3$(step-imp.). From second TPO analysis of these Pt–Zr/γ-Al$_2$O$_3$ catalysts the amount of coke deposited on each was 0.14% and 0.16% respectively (Table 2.17). As can be seen from the T$_{10}$, T$_{50}$ and T$_{90}$ values, activities for the two Pt–Zr/γ-Al$_2$O$_3$ catalysts mentioned are quite similar.

The final systems to be analysed for isobutane conversion activity were Ce–Al$_2$O$_3$ and Pt–Ce/γ-Al$_2$O$_3$ catalysts and results are given in Graphs 3.9 to 3.13 and Table 3.10.

Graph 3.9 Activity analysis of Ce/γ-Al$_2$O$_3$ and Pt–Ce/γ-Al$_2$O$_3$ catalysts.

196

Graph 3.10 Activity analysis of Ce/γ-Al₂O₃ and Pt–Ce/γ-Al₂O₃ catalysts.

Graph of % iso-butane Conversion vs Temperature

Graph 3.11 Activity analysis of Pt–Ce/γ-Al₂O₃ catalysts.

Graph of % iso-butane Conversion vs Temperature

Graph 3.12 Activity analysis of Pt–Ce/γ-Al₂O₃ catalysts.

Graph of % iso-butane Conversion vs Temperature

Legend:
- Pt/alumina (Run 2)
- Pt-0.1Ce/alumina(st-imp.)Run 1
- Pt-0.1Ce/alumina(st-imp.)Run 2

Graph 3.13 Activity analysis of Pt–Ce/γ-Al₂O₃ catalysts.

Graph of % iso-butane Conversion vs Temperature

Legend:
- Pt/alumina (Run 2)
- Pt-0.5Ce/alumina(st-imp.)Run 1
- Pt-0.5Ce/alumina(st-imp.)Run 2

198
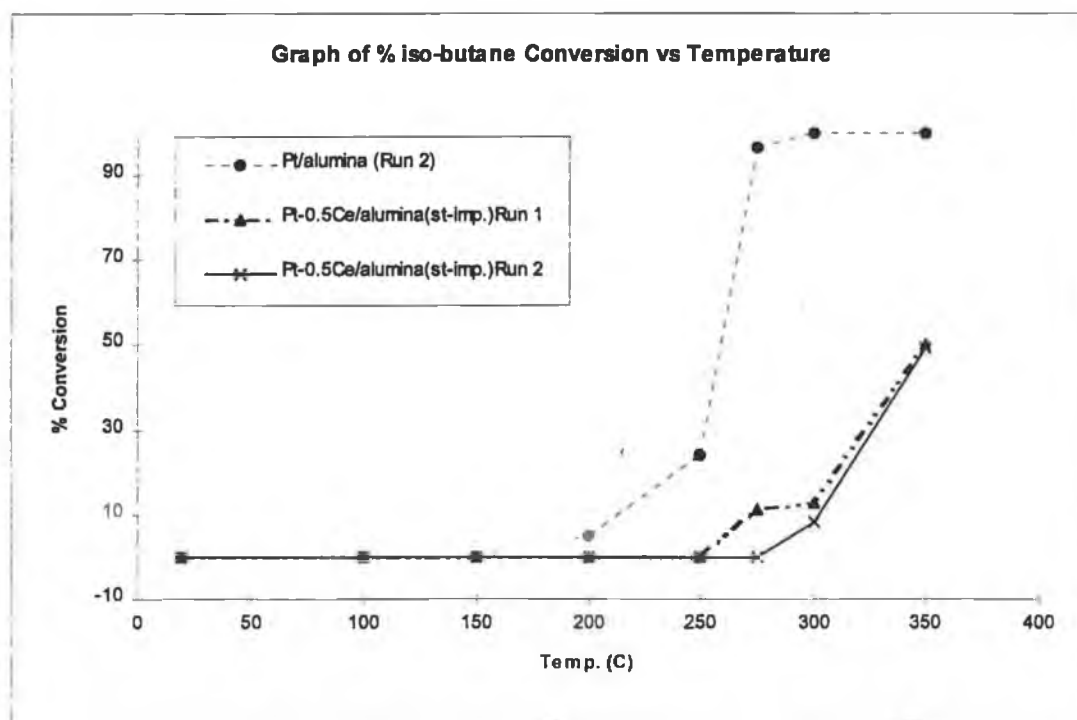
Table 3.10 Activity analysis results for Ce/γ-Al$_2$O$_3$ and Pt–Ce/γ-Al$_2$O$_3$.

Sample	Treatment	Activity Test 1			Activity Test 2		
		T_{10} (^{o}C)	T_{50} (^{o}C)	T_{90} (^{o}C)	T_{10} (^{o}C)	T_{50} (^{o}C)	T_{90} (^{o}C)
2.0%Ce/γ-Al$_2$O$_3$	630°C/15 mins	355	>400	>400	355	>400	>400
0.5%Pt–0.3%Ce/γ-Al$_2$O$_3$	630°C/15 mins, Co-imp.	160	225	245	145	240	290
0.5%Pt–0.5%Ce/γ-Al$_2$O$_3$	630°C/15 mins, Co-imp.	239	313	>350	275	347	>350
0.5%Pt–3.0%Ce/γ-Al$_2$O$_3$	630°C/15 mins, Co-imp.	270	290	390	100	235	285
0.5%Pt–0.1%Ce/γ-Al$_2$O$_3$	630°C/15 mins, Step-imp.	263	317	350	239	335	>350
0.5%Pt–0.5%Ce/γ-Al$_2$O$_3$	630°C/15 mins, Step-imp.	272	350	>350	305	350	>350

As in the case of 2.0%Zr/γ-Al$_2$O$_3$, 2.0%Ce/γ-Al$_2$O$_3$ revealed a slight amount of activity for conversion of isobutane-butane with T$_{10}$ at 355°C. The activity results for Pt–Ce/γ-Al$_2$O$_3$ showed that when Ce was added at 3.0% or 0.3% loading (co-imp.) the activity of the catalyst increased to a level higher than that seen for 0.5%Pt/γ-Al$_2$O$_3$. After the second activity analysis, activity of Pt–3.0%Ce/γ-Al$_2$O$_3$ (co-imp.) improved further while that of Pt–0.3Ce/γ-Al$_2$O$_3$ decreased. The step-impregnated Pt–Ce/γ-Al$_2$O$_3$ catalysts were not as active as the co-impregnated samples and both required temperatures >350°C for 90% conversion of isobutane-butane.

From Tables 2.18 and 2.19 the level of coking associated with the active catalysts Pt–3.0%Ce/γ-Al$_2$O$_3$ (co-imp.) and Pt–0.3%Ce (co-imp.) were 0.23% and 0.22% respectively (1st coking cycle) and 0.3% and 0.14% respectively (2nd coking cycle), suggesting that Pt–0.3%Ce/γ-Al$_2$O$_3$ (co-imp.) is the better system for activity and coke minimisation

This study showed that when the number of acid/base sites on γ-Al$_2$O$_3$ were modified chemically the level of coke formation was directly related to number of acid sites. In the case of γ-Al$_2$O$_3$ which had been impregnated with Pt, Sn, Zr, or Ce it was found that the amount of coke formed was more dependent on (i) type of metal (ii) amount of metal and (iii) method of preparation. When the coking results from chapter two were considered in light of the activity results from chapter 3, it was found that the best catalyst overall on the basis of high activity and low coke formation rates was Pt–0.5%Sn/γ-Al$_2$O$_3$ (co-imp.,cal.@500/2hrs). Best of the Pt–Zr/γ-Al$_2$O$_3$ was Pt–2.0%Zr/γ-Al$_2$O$_3$ (step-imp.) while Pt–0.3%Ce/γ-Al$_2$O$_3$ (co-imp.) was best of the Pt–Ce/γ-Al$_2$O$_3$ catalysts.

3.3 Discussion of results from Chapters Two and Three

The main objective of this project was to develop ways of reducing the amount of coke formed and hence extend the working life of supported metal oxidation catalysts. In order to approach this task chapter one reviewed literature concerning support material manufacture and surface composition. A section on coking was also included.

The amount of coke formed on silica gel, α-, η-, and γ-Al_2O_3, which are commonly used catalyst support materials, was determined using a 32:1 air/isobutane fuel mixture and a modified thermo-gravimetric analyser. It was found that the highest level of coke was formed on γ-Al_2O_3. By varying the operating conditions it was found that for this system a maximum rate of coke formation was achieved at 400°C using an air/isobutane (32:1) flow rate of $25cm^3$/min. Since the problem of coking was greatest on γ-Al_2O_3 subsequent work attempted to find ways of reducing coking on this material. It was found that treating γ-Al_2O_3 with 0.1M HCl reduced the level of coking while treatment with 0.1M NaOH led to an increase in the level of coke deposited. Non-aqueous titration of these samples revealed that treatment with 0.1M HCl reduced the concentration of titratable acidic sites by about 15%. Treatment with 0.1M NaOH increased the concentration of titratable acidic sites by over 40% and titratable Brönsted basic sites by approximately 60%. Based on these results it would appear that the concentration of Brönsted basic and especially acidic sites is directly related to the level of coke deposited on γ-Al_2O_3.

When the temperature programmed oxidation (TPO) technique was used to quantify the amount of coke deposited on γ-Al_2O_3 impregnated with Sn, Zr, or Ce it was seen that addition of these metals resulted in reduced coking on these catalysts. The greatest reduction in coking was seen for γ-Al_2O_3 impregnated with Zr. When these results for coking are viewed in conjunction with titration results it can be seen that there is no apparent correlation between the levels of coking and concentrations of acidic and Brönsted basic sites.

This was also observed for the bimetallic catalysts containing Pt and either Sn, Zr or Ce supported on γ-Al$_2$O$_3$. These results would suggest that when Sn, Zr or Ce, either on their own or in conjunction with Pt, are impregnated on γ-Al$_2$O$_3$ at the levels examined the influence which they exert on coking is much more pronounced than that exerted by acidic or Brönsted basic sites. In the absence of these metals on γ-Al$_2$O$_3$ the concentration of acidic and Brönsted basic sites appear to be directly related to coking.

The titrimetric procedure used to determine the concentration of acidic and Brönsted basic sites utilised non-aqueous acidic and basic molecules that are small and highly mobile with the end-point being determined potentiometrically. This offers advantages over conventional indicator based titrimetric techniques that are unable to detect acidic and basic sites contained in small pores due to the steric problems associated with large bulky indicator molecules. In addition to this the fact that the end-point is determined potentiometrically makes this system more applicable to coloured samples. The titrations themselves showed a high level of electrode stability for the potential readings and were also very reproducible.

The activity of each bimetallic catalyst for conversion of isobutane was compared to Pt/γ-Al$_2$O$_3$. Results for this analysis showed that addition of Sn and Zr to Pt/γ-Al$_2$O$_3$ at the levels tested resulted in a loss of activity. Addition of 0.3% Ce by co-impregnation did however result in an increased level of activity but the repeat activity analysis done revealed a level of activity that was marginally lower than for the second activity performed on Pt/γ-Al$_2$O$_3$.

Based on the combined activity and coking data it is seen that the best catalyst overall with regard to activity and tendency to form low levels of coke is 0.5%Pt–0.5%Sn/γ-Al$_2$O$_3$, prepared by co-impregnation and calcined at 500°C for two hours. Best of the Pt–Zr/γ-Al$_2$O$_3$ catalysts was a step-impregnated 0.5%Pt–2.0%Zr/γ-Al$_2$O$_3$ catalyst which had been calcined at 630°C for fifteen minutes. With regard to the Pt–Ce/γ-Al$_2$O$_3$ system a 0.5%Pt–0.3%Ce/γ-Al$_2$O$_3$

catalyst prepared by co-impregnation and calcined at 630°C for fifteen minutes was found to be the best for conversion of isobutane while at the same time minimising coking.

In addition to identifying the best overall catalyst of the systems tested this thesis in the broader sense has outlined criteria, with suitable methods, for the testing of other catalyst systems not looked at in this study but which may be looked at in further studies by other researchers. Indeed the methods outlined could be used to study activity, coke forming tendency and titratable acid/base concentrations on catalysts containing different metals and supported on different oxides. In developing these techniques it is hoped that this study will allow for further research into the area of coke inhibition on supported metal catalysts.

Supplementary Study

Chapter

Four

Tests of the efficiency of catalytic burners as

sources of heat for an industrial application

4.0 Introduction

This chapter details work done for an industrial company to assist in their development of a gas powered catalytic heat exchanger. The company presented a prior electrical instrument which could rapidly vaporise a liquid stored in a pressurised canister. Due to confidentiality agreements the exact function of this instrument cannot be given. The project was to investigate the construction of a gas powered catalytic system which was capable of operating as effectively as the electrical instrument. Initial work determined the operating temperature and power rating of the electrical instrument and the boiling point and flow-rate of the liquid.

A short review of relevant literature on catalytic combustion is given in 4.1.

4.1 Catalytic Combustion

Hanby [209] defines combustion as a chemical reaction between a fuel and oxygen which is accompanied by the production of a considerable amount of heat. In engineering terms the combustion of a fuel can be divided into several processes;

a. bringing together the fuel and air (the reactants) in the correct proportions
b. igniting the reactants
c. ensuring that the flame burns in a stable manner and that combustion is complete
d. extracting useful heat from the process, and
e. arranging for the safe disposal of the products of combustion.

The simplest example of where the above mentioned processes occur is thermal combustion in a flame. In the flame gas-phase radicals are initiated thermally after which oxidation reactions proceed rapidly [210]. Temperature of the flame can

easily reach 1500–2000°C. Since nitrogen and oxygen can react together at approximately 1650°C, flame combustion can lead to the production of nitrogen oxides which can give rise to smog. As an alternative to this conventional form of combustion, catalytic combustion has received significant attention in recent times [210]. By using a heterogeneous catalyst, better control of oxidation over wider fuel:air ratios can be achieved and since catalytic combustion occurs at lower temperatures, nitrogen oxides are not formed. In addition to this, if the catalyst is well designed the efficiency of heat recovery from combustion can be improved.

The principle of catalytic combustion is simple but the mechanisms involved are complex and influenced by the atmosphere, temperature and type of catalyst [210, 211]. Mixtures of fuel and air are passed over a catalyst maintained at a temperature high enough to favour total oxidation and activation of oxygen and/or fuel molecules occurs at the catalyst surface [210]. This leads to reaction occurring with the consequent liberation of energy and oxidised products which are CO_2 and H_2O when hydrocarbons are used as the fuel source.

A performance plot for a typical combustion catalyst is presented in Fig. 4.1 [Ref. 210].

Fig. 4.1 *{Ref. 210}* Typical rate curve for catalytic combustion. A: ignition; B: light off; C : mass transfer limitation; D: homogeneous reactions.
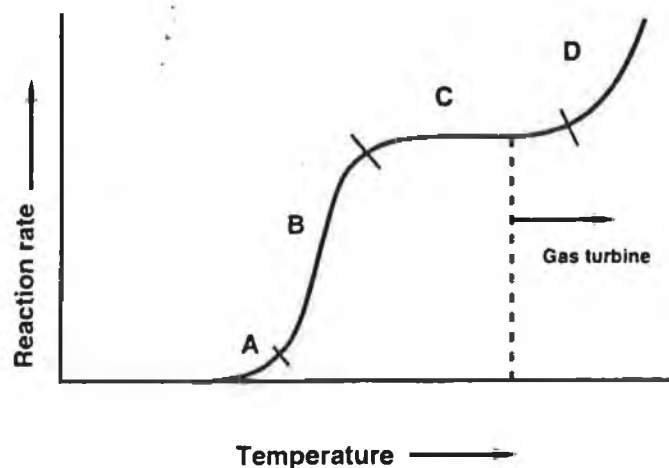
The rate of combustion in region 'A' is controlled by kinetics of the chemical reaction. In region 'B' catalyst light-off occurs due to a build-up of heat caused by an increase in rate of reaction. The rate of reaction plateaus off in region 'C' as the amount of air and fuel being transported to the catalyst becomes a limiting factor. In region 'D' at still higher temperatures homogeneous combustion may come into play and the catalyst may accelerate the reaction by generating radicals [210].

The required properties of suitable combustion catalysts have been summarised by Prasad et al. [212] as follows;

a. Ignition of fuel/air mixtures should be possible at as low a temperature as possible;
b. The catalyst activity should be sufficiently high to maintain complete combustion at the lowest inlet temperature and the highest values of mass throughput;
c. The support should have a large geometric surface area, low pressure drop, good thermal shock resistance, and it should allow high working temperatures;
d. The support should maintain moderately high surface area under high temperature combustion conditions (above 1300°C);
e. The catalyst system should be sufficiently stable to allow prolonged use at operating temperatures up to 1300°C.

Catalytic combustors are easier to operate than flame combustors and are not severely affected by fluctuating feed composition and temperature which can cause unstable flames in conventional combustion [210]. It is possible to combust all gaseous and gasifable organic compounds catalytically over a wide range of fuel/air ratios, even at fuel concentrations too low to support flame combustion. Also the temperature distribution across a catalytic combustion rector is more even than for conventional combustors.

There are however problems associated with catalytic combustors. The catalyst itself can be expensive and has a finite life [211]. Ageing and poisoning limit the lifetime of the catalyst and bring about a gradual drop in

performance [210]. If it has to be operated at high temperatures problems can arise with sintering of the metal or the support. In addition to this the presence of a catalyst in the combustion chamber causes a technical complication and introduces an additional failure possibility. This necessitates special combustion chamber design.

The mechanism of complete catalytic oxidation depends on the type of catalyst used [213]. The two main types of catalyst used for oxidation reactions are metal oxides and noble metals (supported or unsupported). The noble metals will be discussed first.

The noble metals Pt, Pd, Ag, and Au are frequently alloyed with the closely related metals Ru, Rh, Os and Ir, and supported on an oxide support such as γ-Al_2O_3 or SiO_2. In practice though only Pt, Pd and a few alloys are used as oxidation catalysts because the generally high temperatures employed for most oxidation catalyst applications can cause sintering, volatility loss, and irreversible oxidation of the other metals [213].

Noble metals do not form very stable bulk oxides and hence remain as reduced metals during oxidation reactions at moderate temperatures [213]. Based on this, Spivey [213] proposed that the mechanism of oxidation, even when the noble metals are supported on oxides such as SiO_2 or Al_2O_3, may involve only molecular O_2 in the incoming gas stream. In the case of metals which form stable oxides it is known that the lattice oxygen is involved in the oxidation of hydrocarbons in O_2–containing gas streams [213]. It has been suggested by Volter et al. [215] that even at moderate temperatures there may be a complex interaction between the Pt and oxygen which affects the hydrocarbon conversion. A direct relationship between the oxygen adsorption capacity of Pd and Pt on a variety of oxide supports and the catalytic oxidation activity has been observed for the oxidation of methane [215].

Pt/Al$_2$O$_3$ and Pd/Al$_2$O$_3$ catalysts with high initial metal dispersion, i.e. small metal crystallites, undergo extensive oxidation of the metal under operation in a small excess of oxygen and temperatures below 370°C resulting in a catalyst which behaves as a noble metal oxide supported on an oxide carrier [210]. Larger metal particles on catalysts with lower initial dispersion are only partially oxidised. The authors [210] assumed that in all cases the noble metals were covered with oxygen under reaction conditions. Using the oxidation of methane as a test reaction it was found that chemisorbed oxygen covering the crystallites was far more reactive toward methane oxidation than the noble metal oxide from the highly dispersed supported metal. This structure sensitivity was found to be higher for Pd than Pt and Pd also showed more complete oxidation and much higher activity than Pt. It has however been found by Cullis et al. [214] that at temperatures above 450°C prolonged exposure of supported Pd and Pt to oxygen causes structural changes in both metals which results in a loss of catalytic activity for the oxidation of methane.

Metal oxide catalysts consist of oxides of metals occurring in groups IIIB through II–B of the periodic table and are characterised by high electron mobility and positive oxidation states [213]. In general these catalysts are less active than supported noble metal catalysts for complete oxidation of hydrocarbons. Their main advantage over noble metal catalysts is the lower cost of raw materials and greater resistance to poisoning. It has been suggested by Spivey [213] that this resistance to poisoning may be due to the high active surface area of metal oxides as compared to supported noble metals. In addition to this, by choosing the proper metal oxide composition, higher thermal stability can be achieved. However, the lower specific activity results in higher ignition temperatures for metal oxides.

In relation to catalytic oxidation metal oxide catalysts can be generally divided into three groups [213]. These consist of n-type semiconductors, p-type semiconductors and insulators. Electrical conductivity is used as a basis for classification and is also related to their catalytic properties. In the case of n-type metal oxides the excess of electrons present in the lattice give rise to electrical

conductivity. Generally n-type oxides are not active oxidation catalysts. The p-type metal oxides are electron-deficient in the lattice and conduct electrons by means of positive 'holes'. P-type oxides are usually active as oxidation catalysts. The electrical conductivity of insulators are low because of the strictly stoichiometric metal-oxygen ratio in the lattice and very low mobility of electrons or positive holes [213]. For this reason insulators are generally not active catalysts but are often used as catalyst supports.

On heating in air n-type oxides loose oxygen whereas p-type oxides gain oxygen. It has been shown by Fierro et al. [220] that the less stable a metal oxide is, as measured by the heat of formation per oxygen atom, the more easily the surface is reduced to form oxygen adsorption sites. This is an important characteristic of metal oxides because differences in their catalytic properties are directly related to their respective strength of interaction with oxygen at reaction conditions [213]. The adsorption of oxygen occurs far more readily on p-type oxides as electrons can easily be removed from the metal cations to form active species such as O^-, whereas no such mechanism is available on an n-type oxide.

The oxygen required for oxidation can be activated by interacting with oxide surfaces. According to Zwinkels et al. [210] co-ordination, dissociation and incorporation into the oxide lattice may be steps in the activation process. The two possible states of activated oxygen that can be recognised are:

a. Highly reactive surface states of adsorbed oxygen; and
b. Less active, lattice-incorporated oxygen species.

Since the lattice-incorporated species is more strongly bound than the adsorbed species, it is generally believed to be involved in selective partial oxidation [210]. The surface adsorbed species has been found by Arakawa et al. [216] to be the important species in complete oxidation reactions. Spivey [213] has found that there is an optimum level of metal oxygen interaction in an oxide catalyst. The rates of oxidation for hydrocarbons have been correlated by Moro-oka et al. [217,218]. In

their discussions Moro-oka et al. [217,218] used the term 'ΔH_0' which is the heat of formation for an oxide divided by the number of oxygen atoms in the oxide molecule. It was found that the rate of oxidation increased as ΔH_0 decreased. Bond [219] has found that the catalytic activity of a metal oxide catalyst is inversely related to the strength of chemisorption of the hydrocarbon and oxygen, provided that adsorption is sufficiently strong for the hydrocarbon and oxygen to achieve a high surface coverage. This can be represented graphically by what is often referred to as the 'volcano' plot as shown in Fig. 4.2. If the chemisorption of the hydrocarbon is too strong, the catalyst will be quickly deactivated as active sites are irreversibly covered. On the other hand if chemisorption is too weak, only a small fraction of the surface is covered and the catalytic activity is very low.

Fig. 4.2 *{Ref. 210}* Volcano plot showing relationship between activity of metal oxide catalysts and strength of chemisorption of the hydrocarbon.
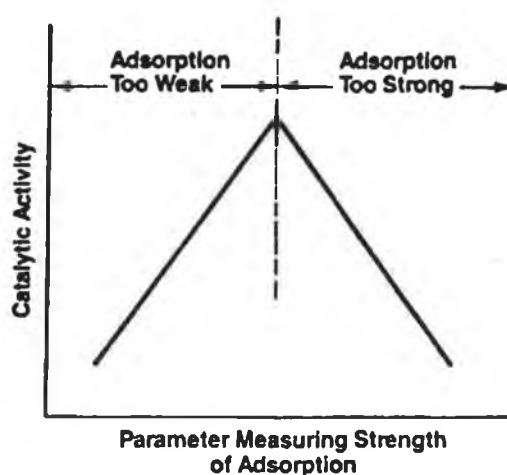
Partial oxidation of hydrocarbons depends on metal–oxygen bond strength and hence oxygen mobility [223]. To achieve complete oxidation of reactants the metal-oxygen bond must be weak. On n-type oxides oxidation is thought to involve lattice oxygen while on p-type oxides the reaction involves an

211

adsorbed oxygen [219]. Satterfield [3] states that 'highly mobile' oxygen should result in a highly active non selective catalyst but he also points out that oxygen mobility as a sole criterion for catalyst activity and selectivity is of limited use.

If the oxygen supply is discontinued over a metal oxide catalyst that has been brought to steady state, for many reactions the metal oxide catalyst will continue to oxidise the reactants at the same selectivity but with a decrease in activity [221]. The original activity is restored once the O_2 supply is started again. Margolis [222] has found the existence of O_2^-, atomic O^- and O^{2-} in the oxide lattice. Fierro et al. [220] concludes that complete oxidation of hydrocarbons to CO_2 over a metal oxide catalyst is possible even when no oxygen is present in the gas stream since both chemisorbed and lattice oxygen can participate in complete oxidation but selective oxidation involves lattice oxygen.

The actual design and operation of a catalytic heater has been studied by Radcliffe et al. [224]. In Fig 4.3 a schematic diagram of the diffusive catalytic heater is given.

Fig. 4.3 *{Ref. 224}* Schematic construction of a diffusive catalytic heater.
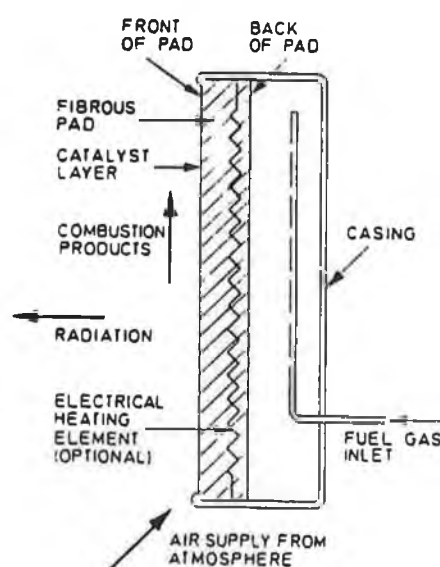
The fuel gas flows into the chamber behind the catalyst pad and then passes through the catalyst to the atmosphere. The 5% Pt catalytic pads used in the study by Radcliffe et al. [224] were constructed on supports of asbestos wool, ceramic wool and fibreglass. The Pt lay in globules on the supporting fibres [224]. Porosity and surface area of the catalyst pads are high which should make interchange of precious metal catalysts with cheaper and more plentiful base metal catalysts of lower specific activity possible.

Radcliffe et al. [224] recognised that the most important practical difficulty in igniting the catalytic heater is initial heating of the pad. In some designs an electrical element is placed within the pad to heat it to a certain threshold temperature (normally around $250^{o}C$), but because of the low thermal conductivity associated with the fibrous support materials, ten minutes or more can elapse before the catalyst temperature is high enough for natural gas oxidation to be sustained [224]. Other systems utilise a temporary pilot flame which is burnt close to the front surface of the pad. After the main gas supply is switched on, an unsteady flame is seen to flicker across the surface of the pad, heating it, and within one or two minutes the flickering vanishes and catalytic combustion takes over. In other cases no flickering may be seen but the area of catalytic activity spreads gradually outwards from the vicinity of the pilot flame. A disadvantage here is that during the ignition period a significant amount of fuel can escape through the section of pad where no combustion is taking place [224].

After combustion has begun on the catalyst pad, the reaction becomes self sustaining and there is no further need for the catalyst pad to be heated by the electrical heating element. The energy generated is transported to the surroundings by thermal radiation, convection and conduction through the metal frame of the heater [225]. Under normal operation the outer surface of the pad is about $425^{o}C$ so there is no visible sign of combustion. This temperature is insufficient to cause an explosion involving either unburned reactants or organic vapours in the atmosphere, this makes the heaters very suitable for drying paint etc. [211].

A disadvantage of this type of catalytic combustion is that the flue gases inevitably contain small quantities of fuel that have passed unburned through the pad. Such emissions may be a hazard and also results in a loss of combustion efficiency [226]. In fact fuel emission appears to be the major disadvantage of most diffusive catalytic burners. The problem is more prevalent with natural gas than with LPG since methane is the most difficult hydrocarbon to burn catalytically. It is laid down by European standards [227] that no more than 4% of the volatile hydrocarbon fuel passes unburned, at any setting, through LPG heaters. Dilution of the flue gas mixtures with combustion products usually reduces it to below the lower limit of inflamability.

Using methane fuel, Radcliffe et al. [224] found that during combustion tests the flue gases contained mostly air, carbon dioxide, water vapour and methane. In addition to these, carbon monoxide(CO) was produced, but at levels much lower than would be seen for flame combustion. Even when the O_2 concentration was decreased to 15% of stoichiometry the amount of CO produced was much lower than for flame systems. For most practical thermal burners the flames would be extremely unstable at O_2 levels as low as 15% stoichiometry and would most likely have extinguished. Measurement of NO_x levels were also found to be very low in the catalytic combustor.

The combustion of methane over platinum supported on porous and non-porous Al_2O_3 fibre has been studied by Trimm et al. [225]. It was found that on porous Al_2O_3, methane was oxidised to CO_2 while on non-porous alumina, CO was a major product. The selectivity of non-porous fibre for CO formation is believed to be due to its higher acidity but the authors [225] also acknowledge that the difference in selectivity for CO and CO_2 formation could be a result of differences in porosity of the two fibres. On the porous Al_2O_3 supported catalyst the catalytic oxidation of methane was found to be very dependent on temperature [225]. Although the only products formed were CO_2 and CO, selectivity for the latter increased with increasing temperature when the $O_2 : CH_4$ ratio was less then unity. This appears to reflect only the depletion of O_2 e.g. with

this system when the O_2 : CH_4 ratio was less than 0.8 at a temperature in excess of 540°C, carbon monoxide was produced [225]. The authors [225] conclude that the selectivity of CH_4 combustion to CO formation probably reflects the degree of coverage of the surface by CH_4, with CO being favoured at high O_2 coverage and CO becoming more important as the CH_4 coverage increases. Temperature can change the reaction mechanism from one in which O_2 adsorption is predominant to one in which CH_4 adsorption is most important.

The role of the catalyst in diffusive catalytic combustion applications with methane and propane as fuels has been examined by Dongworth et al. [226]. For the purpose of their work a loosely-packed bed of a 5% platinum on γ-alumina catalyst was used. Gas chromatographic analysis of components within the catalyst bed of the diffusive heater revealed a relatively large concentration of hydrogen on the fuel feed side of the temperature maximum within the catalyst pad. This is important since hydrogen can ignite on the catalyst at room temperature. It is believed that the hydrogen is produced in a methane-cracking process and evidence to support this view is provided by the simultaneous deposition of carbon on the catalyst [226]. The deposition of this carbon would be expected to lead to catalyst deactivation. Since it was found that the combustion catalyst could still operate with a carbon content of 0.8% by weight it would appear that long-term deactivation is probably associated with pore blocking by carbon. The reasoning behind this is that 0.8% carbon would be more than sufficient to block all the active sites present [226].

The surface temperatures of the catalyst pads were found to range between 325 and 475°C and were dependent on heat input, type of pad and location on the pad [224]. Using an infrared camera to inspect the pad during combustion the temperature pattern was found to be non uniform across the front surface and local hot and cold regions were continuously changing in size. The authors [224] also investigated the effect which varying the air to fuel ratio had on combustion. Methane combustion efficiency increased when air was added up to 20% stoichiometry but subsequent addition of air reduced efficiency. It was concluded that improvement in efficiency caused by having a small amount of extra

215

oxygen in the combustion reaction was offset by the convective cooling effect of nitrogen in the air stream.

In a later paper, Trimm et al. [228] used a convective-diffusive catalytic combustor to study the total oxidation of methane over a platinum on alumina fibre catalyst. The type of heater used was very similar to that shown in Fig. 4.3. Arrangement of the experiment allowed for temperature profiles across the catalytic pad to be measured along with the gas composition in front of and behind the pad. Only the rate of fuel input was open to control in this system. It was found that the position of maximum temperature in the bed varied with fuel input. Maximum temperature moved toward the front of the catalyst pad when flow rate was increased but this also coincided with a decrease in temperature. This is because high input rates cause the reaction zone to move to the front of the catalyst bed but also decrease contact time resulting in less reaction and less heat generation [228]. At low fuel input rates reaction occurred at the back of the pad and at a reduced rate, due to the low amount of methane. Heat was transferred to the front of the pad where it could radiate to the surroundings. Thickness of the catalyst pad also affects the temperature within but does not affect radiation efficiency. The efficiency of combustion decreased with increasing fuel input and efficiency of emitted radiation passes through a maximum [228]. No carbon monoxide was detected during this study.

Laboratory tests of small scale catalytic combustion systems have been carried out by Krill et al. [229] including a radiative catalyst/watertube system for applications such as a watertube boiler. A schematic diagram of the system is presented in Fig. 4.4 [229]. Because of material temperature limitations, monolithic substrate catalysts cannot function at near stoichiometric conditions and in order to limit the maximum temperature reached during operation they are normally operated under very fuel-lean (or rich) conditions. The radiative catalyst/watertube system however, can allow stoichiometric operation since it actively cools the catalyst surfaces during operation.

Fig. 4.4 *{Ref. 229}* Schematic diagram of a radiative catalyst/watertube boiler
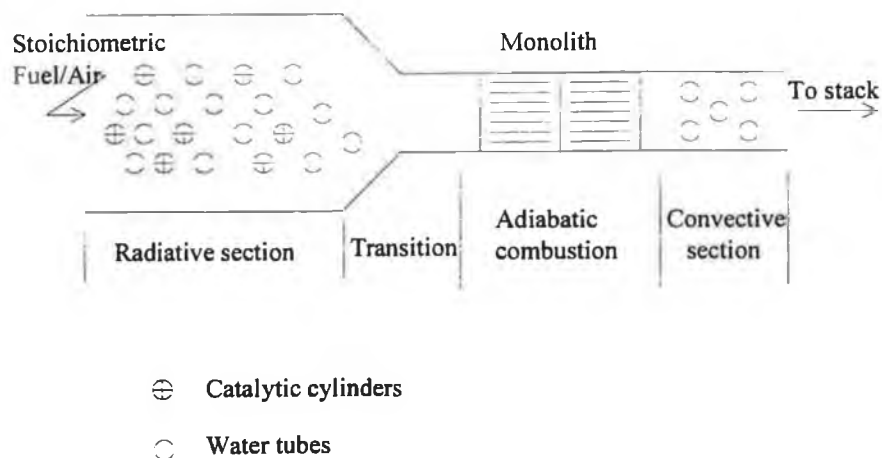
A stoichiometric fuel/air mixture is fed to the radiative section containing ceramic catalyst tubes and metal watertubes. Partial combustion of the fuel occurs on the catalyst which is kept cool by radiation heat loss to the watertubes. Following this the combustion products, air and remaining unburned fuel are passed downstream to a catalytic adiabatic combustor for completion of combustion. Here a convective section extracts energy from the fully combusted gases.

In the system tested by Krill et al. [229] only the radiative section was examined. Heat transfer was evaluated from energy extracted by the cooling tubes. The adiabatic flame temperature of the fuel/air mixture controls thermal input to the catalyst cylinders and this temperature was found to peak near unit stoichiometry corresponding with a maximum in tube temperature. Increasing air concentration in the fuel mix to above unit stoichiometry resulted in decreased surface temperature and consequently decreased radiant exchange to the watertubes. Levels of CO were seen to increase under fuel-rich conditions and nitrogen oxide levels were less than 2ppm for all test conditions. Over the range of air concentrations tested (40% to 219% stoichiometry), levels of unburned hydrocarbon were fairly constant at approximately 2.5%. Catalyst surface temperature decreased in the flow direction because of increased convective cooling of the combustion mixture [229]. Surface temperature of the catalyst also increased with throughput

because of increased convective heating to the catalyst cylinders. Although the radiative catalyst/watertube section was found to perform extremely well at stoichiometric conditions, combustion was less than 50% which would make it unsuitable for use with a downstream adiabatic catalytic combustor.

Catalytic pad heaters are attractive to the combustion industries due to their potential for low emissions of carbon monoxide and nitrogen oxides [229]. The efficiency of catalytic combustion cannot be increased by improvements in catalyst performance since the catalysts in use are already highly active [226]. However, addition of a second component to facilitate the oxidation of any carbon monoxide that is produced would probably be beneficial [228].

4.2 Design, Construction and Testing of prototype catalytic heat exchanger

The basis of this work was to construct and test a prototype catalytic heat exchanger which would hopefully match the performance of an already existing electrical instrument that converted a liquid, contained in a pressurised canister, to a gas as it passed through an electrically heated coil. In order to make a catalytic heat exchanger which could perform the same task, the electrical instrument had to be 'reverse engineered'. The specifications of the electrical instrument were measured. The electrical instrument consisted of copper coil tubing and an electrical stove heating ring. These were sandwiched between three steel plates and held together with bolts. Temperature of this block was regulated by a *'set point bang bang controller'* which switched off the power going to the heating coil once a specific temperature had been reached. The operating parameters of the unit were determined and are given in Table 4.1.

Table 4.1 Operating parameters of electrical instrument.

Cut–out temperature	290^{0}C
Overshoot temperature	400^{0}C
Warm up time from cold to cut–out temperature	6 mins 50 seconds
Operating temperature	350–400^{0}C
Resistance of coil	54Ω $\equiv$ 0.893kW (appendix VII)
Flow rate of liquid	Approximately 10cm^3/sec.
Boiling point of liquid	107.5^{0}C

Several catalytic systems were devised. The first attempt consisted of a cone shaped coil made from ⅛" copper tubing. One end of this tubing was connected to the fluid containing canister via an on/off valve while the

219

other end was crumpled so as to restrict the flow of emerging gas. Catalytic heating was achieved by packing a Pt/γ-Al$_2$O$_3$ mat around the inside of the cone shaped tubing arrangement. The fuel gas was introduced to the catalyst via a Bunsen burner. Ignition of the catalyst mat was done by first heating it using the Bunsen flame and then momentarily switching off the gas to extinguish the flame. When the isobutane supply was again continued it burnt without a flame on the catalyst mat, Fig 4.5. A thermocouple draped around the coil showed that temperature of the coil rose to approximately 320°C in less than two minutes after ignition of the catalyst. When the valve for the liquid was opened a stream of gas emerged from the crimpled end of the copper tube. However, the temperature of the heating coil quickly fell to approximately 60°C and then the liquid itself was seen emerging from the crimpled end of the coil. To improve the efficiency of this system, tin-foil was wrapped around the outside of the coil to act as insulation, but this did not result in any noticeable improvement in the operation of the system. To increase the amount of heat being supplied to the system, a second cone-shaped heating coil was placed in series with the first and both of them heated as previously described. This system was much more efficient than the single coil arrangement but again under continuous use, was not powerful enough to generate a constant stream of gas.

These designs showed that catalytic heating was capable of reaching the required temperatures to convert the pressurised liquid to a gas but the systems tried could not maintain high enough temperatures during continuous use. What was required was a system which had enough stored energy to maintain its temperature above the liquid's boiling point during continuous use. The electrical device had a 30sec. continual use time requirement.

The design was changed to a metal block which had a coil of tubing running through it and was heated by Pt on wire gauze catalysts. Because of its high thermal conductivity (386 Wm^{-1}K^{-1} at 20°C and 1 bar) [230] and relative softness which makes it easy to drill, copper was chosen as the metal most suitable for constructing the heat exchanger. A diagram of the block is given in Fig. 4.6.

**Fig. 4.5** Prototype cone shaped copper coil catalytic heater
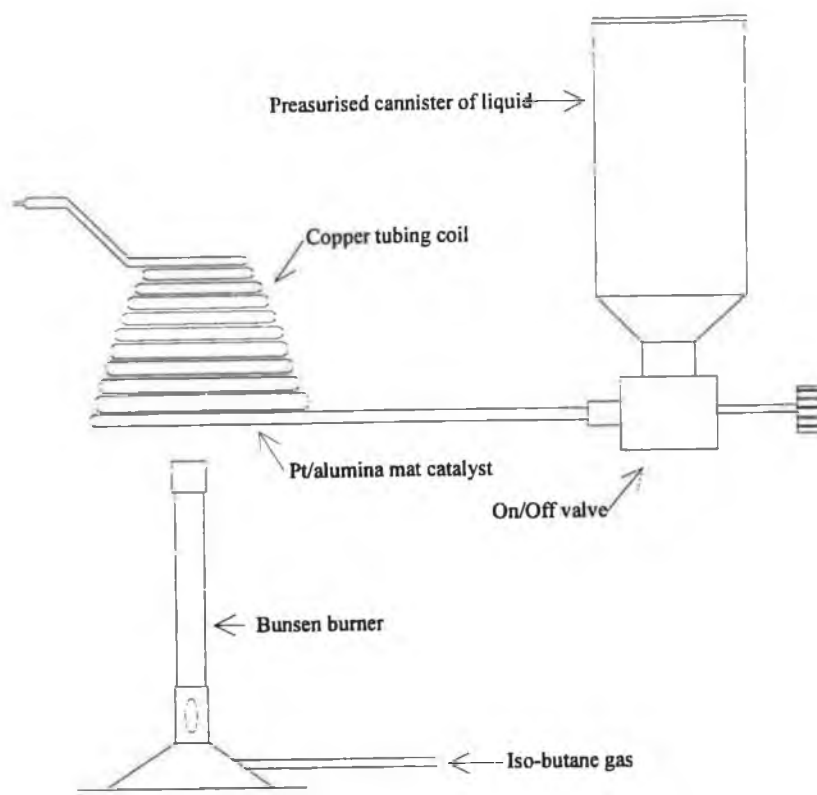
The arrangement consisted of a series of 4mm holes drilled along both sides of the copper block as shown in the cross section at 'B'. By 'threading' these holes with $\frac{1}{8}$" copper tubing as outlined in the plan and front elevation a continuous coil was formed through which the liquid could pass. One end of the copper tube was crimpled slightly while the other was connected to the pressurised liquid canister via an on/off valve. Flow of liquid through the block was from bottom to top. In order to heat the copper block, three separate combustion chambers were incorporated in the copper block. These consisted of 12.5mm $\varnothing$ blind holes drilled into the copper block that all led to a 10mm $\varnothing$ hole drilled perpendicular which acted as a vent. This arrangement is outlined in Fig. 4.6 as the cross-section at 'A'. Strips of Pt on metal gauze catalyst were cut whose width was equal to the circumference of the 12.5mm $\varnothing$ holes and whose length was equal to the depth of the 12.5mm $\varnothing$ holes. These were then rolled along their lengths so that they could fit into the 12.5 mm $\varnothing$ holes.

For the purpose of testing operation of the copper block heat exchanger an air/isobutane fuel mix was supplied to each of the catalyst chambers. Difficulty was experienced trying to get the catalyst to light so in an attempt to improve efficiency of ignition some platinum on alumina mat was packed loosely around the entrance to the catalyst containing chambers. By heating these mats with a Bunsen flame and then switching on the air/isobutane supply to the catalysts, ignition of the platinum gauze catalyst was achieved. After the copper block had been allowed to heat up, the pressurised liquid was passed through the coil and this time a continuous stream of gas emerged from the crimpled end of the tube, even with continuous use.

A thermocouple was inserted into one of the 4mm $\varnothing$ holes and it was found that the temperature of the copper block rose to $200^{\circ}C$ approximately five minutes after ignition and then appeared to stabilise at ~$310^{\circ}C$ seven minutes after ignition. The liquid was vaporised at ~$150^{\circ}C$ but most effective operation was attained after $200^{\circ}C$ had been reached. It was also seen that even under continuous use the temperature drop of the copper block was only $20^{\circ}C$ at most and this temperature drop recovered quickly once the flow of pressurised liquid through the coil was stopped. The values given for warm up times and operating temperatures were all obtained without the use of thermal insulation around the copper block. Addition of a layer of suitable thermal insulation would reduce the warm up time and increase the maximum temperature.

While the operation of the copper block catalytic heat exchanger compared well with that of the electric model its power rating and consumption of isobutane had to be calculated in order to determine efficiency of the unit. The first parameter to be measured was flow of air and isobutane during operation. Initial attempts to measure the flow rate of these gases involved the use of a bubble meter but this proved unsuitable due to the high flow rates. A search of the literature [230] revealed a device referred to as an orifice meter which appeared suitable for measurement of gases in this study.

**Fig. 4.6** Diagram showing copper block catalytic heater

Cross section at B

Cross section at A

4mm holes

B

Front Elevation

A
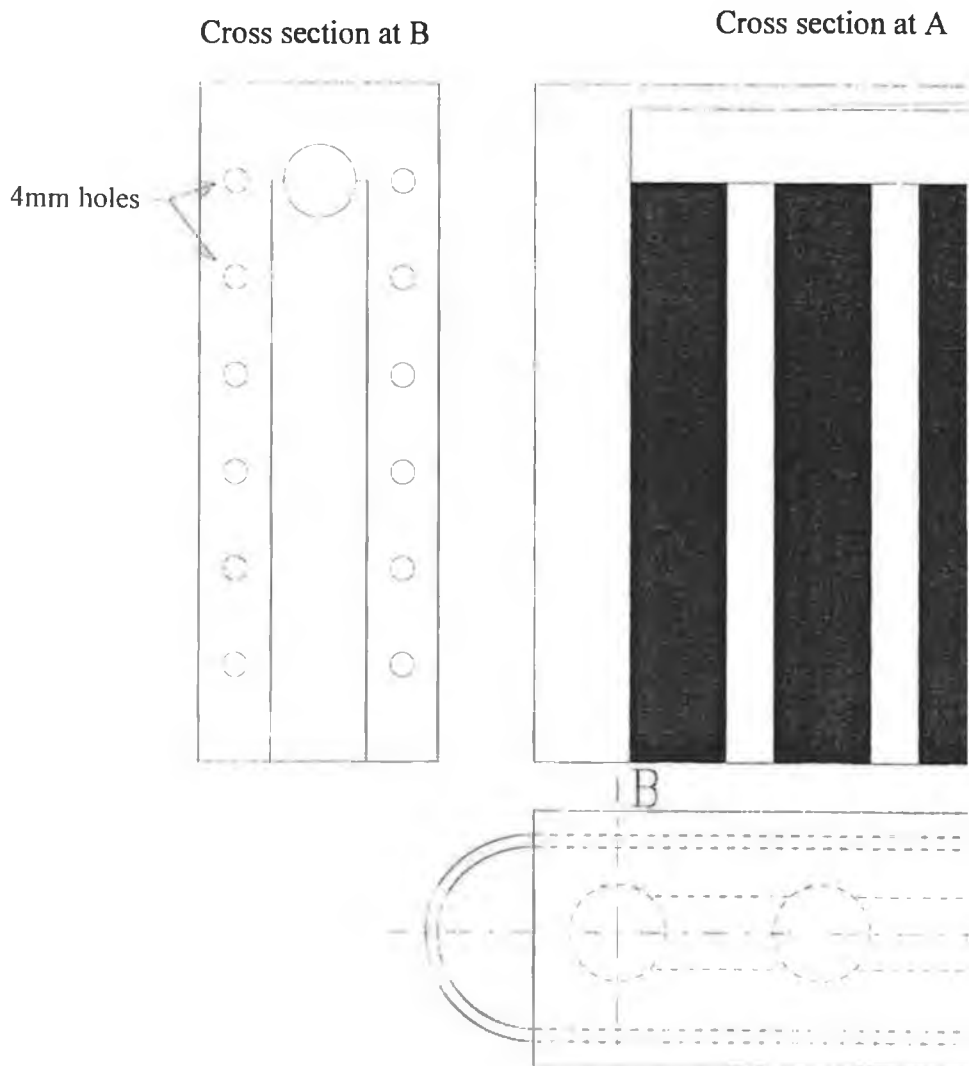
Plan
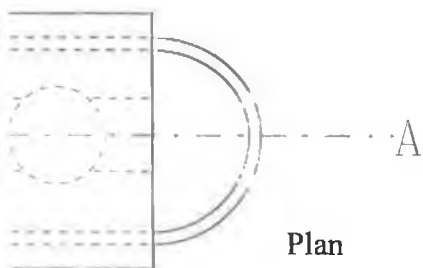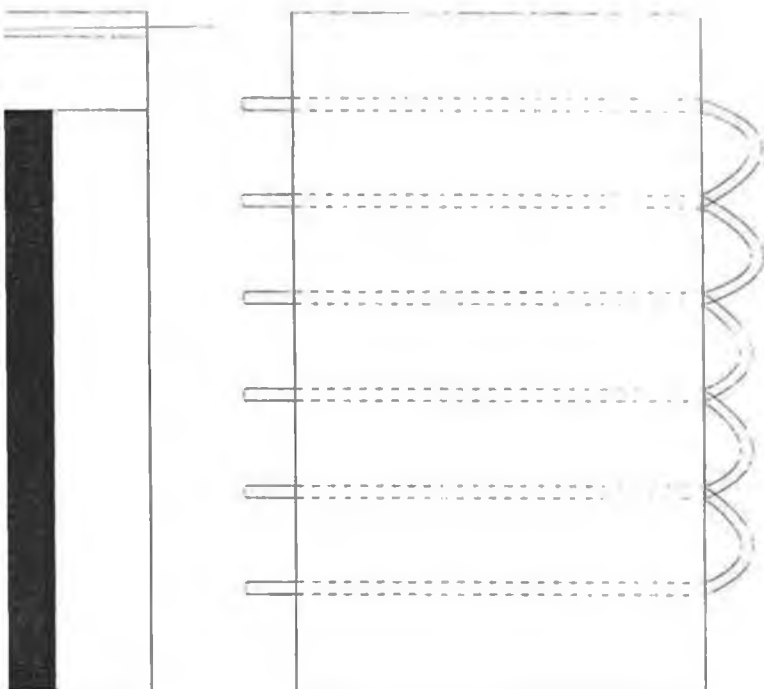
The schematic outline of a typical orifice meter is given in Fig. 4.7 [230]. During operation, gas flows through the orifice meter from left to right. The decrease in diameter from 'D' to 'd' restricts the flow of gas and creates a pressure difference between P_1 and P_2. This difference in pressure results in height of the liquid in the manometer changing and this difference in height 'h' between the inlet and outlet sides of the orifice allows the flow of gas through the orifice to be calculated.

Fig. 4.7 *[Adapted from Ref. 230]* Schematic outline of orifice meter
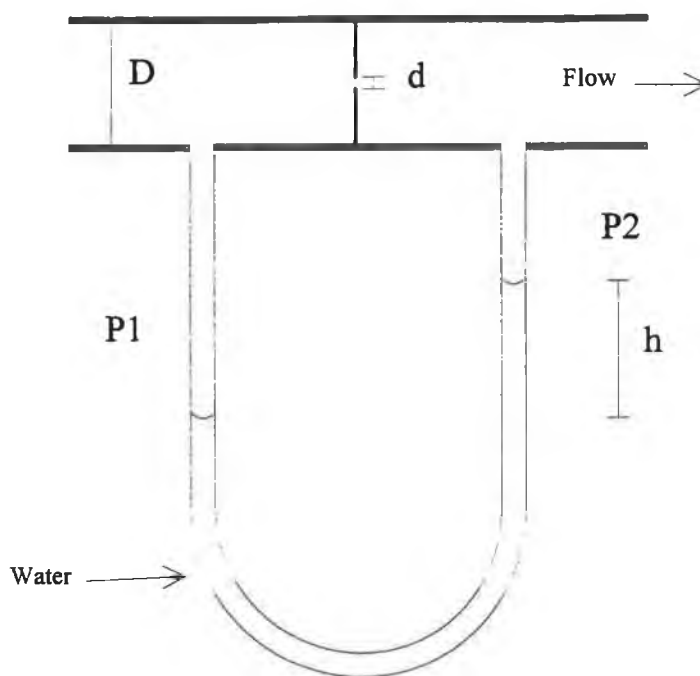
For the purpose of this work two orifice meters were built, one for the air line and the other for the isobutane line. The fluid used in the manometer was water and the most suitable orifice diameter was determined empirically to be 4.5 mm. Difference in height 'h' of the water in the manometers, while the gases were flowing, was measured using sliding callipers. These values when inserted into the formula in appendix *VIII* allowed the flow rates for air and isobutane to be calculated at 7604cm^3/min and 358cm^3/min respectively.

Based on the consumption of 358cm^3/min isobutane a power rating of 0.764 kW was calculated for the heat exchanger. Details of this calculation are given in Appendix *IX*. This however assumes 100% combustion of the isobutane which is unlikely especially in view of the fact that the air:isobutane fuel mix used was 21:1 while chemical stoichiometry requires 32 : 1.

It was seen that when the catalysts were ignited the temperature of the block increased but a steady state was reached at 310°C after which the temperature did not increase suggesting that at this temperature the rate of heat loss through radiation is equal to the amount of heat being supplied to the copper block from combustion of isobutane. By determining the amount of heat being lost by radiation at 310°C (Appendix X) the actual rating of the heat exchanger was calculated to be 0.118kW giving a combustion efficiency of only 15%. It is likely however, that a better heat exchanger design and thermal insulation of the copper block would bring about a decrease in warm-up time and increase general efficiency.

4.3 Discussion

In section 4.2 the prototype catalytic heat exchanger constructed has been seen to match the operating performance of the original electrical instrument.

The principle of using a copper block was that it had sufficient stored energy capable of converting the liquid to a gas without itself dropping significantly in temperature. The copper block used had a mass of 3.66 Kg which at a temperature of 310°C contains 407kJ of energy (based on a specific heat capacity of 0.384 kJ Kg^{-1} K^{-1} for copper [230]). This stored energy is used to heat the liquid as it flows quickly through the coil. Once the flow of liquid ceases, the temperature of the block again rises to 310°C. Since the metal used in construction of the heat exchanger was copper which has a high thermal conductivity, stored

energy can flow quickly through the block to around the coil where it is used to vaporise the liquid.

A more practical design is proposed for the catalytic block. Although copper is a suitable material for the block due to its thermal properties, cost makes its use prohibitive. The coil arrangement in the copper block heat exchanger required a series of 4mm $\varnothing$ holes to be drilled through the copper block. This was an extremely delicate and difficult operation which would be totally impractical in an industrial situation so another system for forming a coil would have to be developed. Lastly, combustion on the wire mesh catalyst could probably be increased if the supply of air/isobutane fuel mixture reaching it was improved by optimising the position of the catalyst within the chamber.

The design shown in Fig. 4.8 has been proposed. Catalytic combustion occurs in hexagonal holes formed through the copper block. The copper block itself is composed of two separate plates and the hexagonal slots are formed from matching dovetail slots that are milled out of each copper plate. These slots form the chambers into which the Pt on wire gauze catalyst is inserted. Placing a cylindrical catalyst in a hexagonal hole should increase the surface area of catalyst exposed to the air/isobutane fuel mixture and hence increase combustion efficiency. To form the coil a ¼" copper tube is wrapped around the copper block. A steel plate is fixed on either side of the copper block and holes drilled through the assembly to allow it to be bolted together. By placing washers on the bolts between the copper and steel plates and then tightening the assembly it is possible to flatten slightly the ¼" tubing thus increasing the surface area of coil in contact with the copper plate, without greatly restricting the flow of liquid through the coil. Since flattening ⅛" copper tubing, even slightly, would greatly affect the flow of liquid ¼" tubing is suggested instead. The steel plates either side of the copper block would hold the coil close to the copper block, insulate the copper block due to the lower thermal conductivity of steel and also store heat which could be used to vaporise liquid flowing through the coil during use. Further efficiency could be achieved by placing

226

a suitable insulating material around the sides of the copper block which would reduce warm up time.

While this proposed design would appear to be more suitable for industrial manufacture it is quite likely that modifications would have to be made to optimise the unit. Also it is possible that problems could arise with bending due to different rates of expansion for copper and steel. This problem may however be overcome by using steel spring washers and punching slots in the steel plates as opposed to drilling holes for inserting the bolts, to allow for unequal expansion.

This work did not focus on any control mechanisms such as ignition or temperature regulation of the heat exchanger. The objective of this project was solely to determine if it was possible to manufacture a gas powered catalytic heat exchanger which was capable of performing equally as well as the already commercially available electrical version. In probing this we have found that it is indeed possible to make a catalytic heat exchanger of comparable capacity and size to the electrical instrument and a design for such a heat-exchanger has been proposed. Relative costings have not been considered at all.

Fig. 4.8 Schematic diagram of proposed Catalytic Heat exchanger.

Catalyst slot

Copper tube
coil

Steel plates
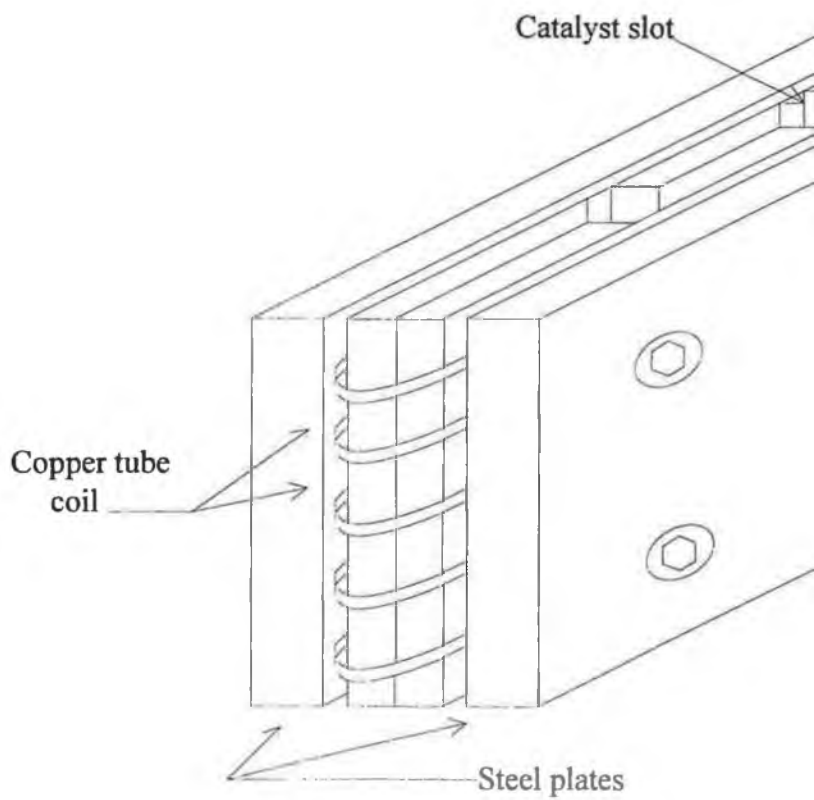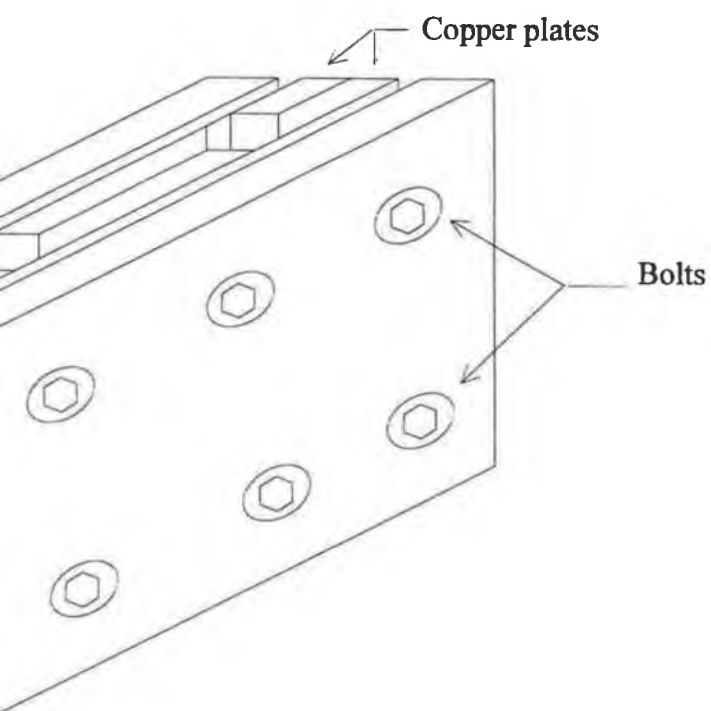
References

1. Richardson, J.T., *Principles of Catalyst Development,* (eds. Twigg, M.V. & Spencer, M.S.), Plenum Press, New York & London (1989)

2. Delanny, F., *Characterisation of Heterogeneous Catalysts,* M. Dekker, New York, (1984)

3. Satterfield, C.N., *Heterogeneous Catalysis in Practice*, McGraw-Hill Book Company, (1980)

4. Adadurov, I.J., in *Metal-support Iinteractions in Catalysis, Sintering and Redispersion,* (eds. Stevenson, S.A., Dumesic, I.A., Baker, R.T.K., & Ruckenstein, E.), Van Nostrand Reinhold Co., New York, (1987)

5. Gates, B.C., Katzer, J.R., & Schuit, G.C.A., *Chemistry of Catalytic Processes,* McGraw-Hill Book Company, (1979)

6. Lippens B.C. & Steggerda, J.J., *Physical and Chemical Aspects of Adsorbents and Catalysts,* (ed. Linsen, B.G.) Academic Press, New York (1970)

7. Greenwood, N.N. and Earnshaw, A., *Chemistry of the Elements,* Pergamon Press, New York (1986)

8. Cotton, F.A. & Wilkinson, G., *Basic Inorganic Chemistry,* Wiley, New York, (1976)

9. Cotton, F.A. & Wilkinson, G., *Advanced Inorganic Chemistry,* (4th ed.) Wiley, New York, (1980)

10. Peri, J.B., *The Journal of Physical Cemistry,* **69(1),** 20 (1965)

11. Verway, E.J.B., *Z. Kristallogr,* **91,** 17 (1935)

12. Jagodzinski, H. & Satterfeld, H., *Z. Kristallogr,* **110,** 97 (1958)

13. Leonard, A.J., Semaille, P.N. & Fripiat, J.J., *Proceedings of the British Ceramic Society.,* **103,** 103 (1969)

14. Stumpf, H.C., Russell, A.S., Newsome, J.W. & Tucker, C.M., *Industrial Engineering Chemistry,* **42,** 1398 (1950)

15. Lippens, B.C. & de Boer, J.H., *Acta. Cryst.,* **17,** 1312 (1964)

16. Soled, S., *Journal of Catalysis,* **81,** 252 (1983)

17. Tamale, M. W., *Discussions of the Faraday Society,* **8,** 270 (1950)

18. Dabrowski, J.E., Butt, J.B., & Bliss, H., *Journal of Catalysis,* **18,** 297 (1970)

19. Cornelius, E. B., Milliken, T.H., Mills, G.A., & Oblad, A.G., *The Journal of Physical Chemistry,* **59,** 809 (1955)

20. Cook, M.A., & Oblad, A.G., *Industrial and Engineering Chemistry,* **45(7),** 1456 (1953)

21. Peri, J.B. & Hannan, R.B., *The Journal of Physical Chemistry,* **64,** 1256 (1960)

22. Pines, H., & Hagg, W.O., *Journal of the American Chemical Society,* **82,** 2471 (1960)

23. Knözinger, H. & Ratnasamy, P., *Cataysis Review - Science & Engineering,* **17(1),** 31 (1978)

24. Bond, G.C. & Webb, G., *Catalysis,* **vol. 6,** (p.109–113), A specialist periodical report, The Royal Society of Chemistry, London (1983)

25. Boehm, H.P., *Advanced Catalysis,* **16,** 179 (1966)

26. Pauling, L., *The Nature of the Chemical Bond,* (3rd ed.), Cornell University Press, New York, p.548 (1960)

27. Van Cauwelaert, F.H. & Hall, W.K., *Transactions of the Faraday Society,* **66,** 454 (1970)

28. Knözinger, H., *Catalysis by Acids and Bases,* Elsevier Science Publishers, p.115, (1985)

29. Tanabe, K., Misono, M., Ono, Y., & Hattori, H., *New Solid Acids and Bases,* (eds. Delmon, B. & Yates, J.T.) Studies in Surface Science and Catalysis, Vol. 51, Academic Press, New York (1989)

30. Boehm, H.P., *Discussions of the Faraday Society,* **52,** 264 (1971)

31. Morterra, C., Coluccia, S., Garrone, E. & Ghiotti, G., *Transactions of the Faraday Society I.,* **75,** 289 (1979)

32. Pines, H. & Ravoire, J., *The Journal of Physical Chemistry,* **65,** 1859 (1961)

33. Larson, J.G. & Hall, W.K., *The Journal of Physical Chemistry* **69(9),** 3080 (1965)

34. Knözinger, H., *Advances in Catalysis,* **25,** 184 (1976)

35. Peri, J.B., *The Journal of Physical Chemistry,* **69(1),** 231 (1965)

36. Barth, R.T. & Ballou, E.V., *Analytical Chemistry,* **33(8),** 1080 (1961)

37. Malinowski, S. & Marczewski, M., in *Catalysis,* **(vol. 8)** chapter 4, A specialist periodical report, The Royal Society of Chemistry, Chambridge (1989)

38. Parry, E.P., *Journal of Catalysis*, **2**, 371 (1963)

39. Morimoto, T., Imai, J. & Nagao, M., *The Journal of Physical Chemistry*, **78(7)**, 704 (1974)

40. Hair, M.L. & Hertl, W., *The Journal of Physical Chemistry*, **74(1)**, 91 (1970)

41. Pearson, R.M., *Journal of Catalysis*, **46**, 279 (1977)

42. Gay, I.D. & Liang, S., *Journal of Catalysis*, **44**, 306 (1976)

43. Knözinger, H. & Müller, H.D., *Journal of the Chem. Soc., Faraday Transactions I*, **72**, 2703 (1976)

44. Auroux, A. & Verdine, J.C., in *Catalysis by Acids and Bases*, (eds. Imelik, C., Naccache, G., Coudurier, Y., Taarit, B., and Verdine, J.C.), Studies in Surface Science and Catalysis, Elsevier Science Publishers B.V., Amsterdam (1985) p.311

45. Maciver, D.S., Tobin, H.H. & Barth, R.T., *Journal of Catalysis*, **2**, 485 (1963)

46. Taniguchi, H., Masuda, T., Tsutsumi, K. & Takahashi, H., *Bulletin of the Chemical Society of Japan*, **51(7)**, 1970 (1978)

47. Taniguchi, H., Masuda, T., Tsutsumi, K. & Takahashi, H., *Bulletin of the Chemical Society of Japan*, **53(9)**, 2463 (1980)

48. Nelson, H.C., Lussier, R.J. & Still, M.E., *Applied Catalysis*, **7(1)**, 113 (1983)

49. Aboul-Gheit, A.K. & Summon, A.M., *Advances in Hydrotreating Catalysts*, (eds. Occelli M.L. & Anthony, R.G.), Elsevier Science Publishers B.V., Amsterdam (1989) p.181

50. Benesi, H.A., *Journal of Catalysis*, **28**, 176 (1973)

51. Benesi, H.A., *Journal of the American Chemical Society*, **78(5)**, 5490 (1956)

52. Benesi, H.A., *The Journal of Physical Chemistry*, **61**, 970 (1957)

53. Take, J–I., Nomizo, Y. & Yoneda, Y., *Bulletin of the Chemical Society of Japan*, **46(11)**, 3568 (1973)

54. Barthomeuf, D., *The Journal of Physical Chemistry*, **83(6)**, 767 (1979)

55. Knözinger, H., in *Catalysis by Acids and Bases*, (eds. Imelik, C., Naccache, G., Coudurier, Y., Taarit, B., & Verdine, J.C.), Elsevier Science Publishers B.V., Amsterdam (1985) p.111

56. Che, M. & Tench, A.J., *Characterisation and Reactivity of Oxygen on Oxide Surfaces*, Chemistry Division, AERE Harwell, Oxfordshire, pp. 27–37 (1980)

57. Scokart, P.O. & Rouxhet, P.G., *Journal of the Chemical Society, Faraday I,* **76**, 1476 (1980)

58. Paukshits, E.A., Kotsarenko, N.S., & Karakchiev, L.G., *Reat. Kinet. Catal. Letters,* **12(3)**, 315 (1979)

59. Tanabe, K., *Solid Acids and Bases,* Academic Press, New York/London (1970)

60. Yamanaka, T. & Tanabe, K., *The Journal of Physical Chemistry,* **79(22)**, 2409 (1975)

61. Esumi, K. & Meguro, K., *Shikizai Kyokaishi,* **58**, 9 (1985)

62. Carman, P.C., *Transactions of the Faraday Society,* **36**, 964 (1940)

63. Iler, R.K., *The Chemistry of Silica,* Wiley, New York (1979)

64. Vysotskii Z.Z., Galinskaya, V.I., Kolychev, I.I., Strelko, V.V. & Strazhesko, D.N., in *Adsorption and Adsorbents,* (ed. Strazhesko, D.N.), **Vol.1,** Wiley, New York, p.75 (1974)

65. Klier, K. & Zettlemoyer, A.C., *Journal of Colloid and Interface Science,* **58**, 216 (1977)

66. Iler, R.K. & Dalton, R.L., *The Journal of Physical Chemistry* **60**, 955 (1956)

67. Lange, K.R., *Journal of Colloid Science,* **20**, 231 (1965)

68. Curthoys, G., Davydov, V. Ya., Kiselev, A.V., Kiselev, S.A. & Kuznetsov, B.V., *Journal of Colloid and Interface Science,* **48(1)**, 58 (1974)

69. Vit, Z., Nondek, L. & Maleck, J., *Applied Catalysis,* **2**, 107 (1982)

70. Thorp, J.M., *Transactions of the Faraday Society,* **55**, 442 (1959)

71. Brunauer, S., Kantro, D.L. & Weise, C.H., *Canadian Journal of Chemistry,* **34**, 1483 (1956)

72. Whalen, J.W., *The Journal of Physical Chemistry,* **71**, 1557 (1967)

73. McDonald, R.S., *Journal of the American Chemical Society,* **79**, 850 (1957)

74. Shapiro, I. & Kolthoff, I.M., *Journal of the American Chemical Society,* **72**, 776 (1950)

75. Trouton, F.T., *Proceedings of the Royal Society London Ser. A.,* **79**, 383 (1907)

76. Vordonis, L., Koutsoukos, P.G. & Lycourghiotis, A., *Journal of Catalysis,* **98**, 296 (1986)

77. Ross, R.A. & Bennett, D.E.R., *Journal of Catalysis,* **8**, 289 (1967)

78. Deo, A.V. & Dalla Lana, I.G., *The Journal of Physical Chemistry,* **73(3)**, 716 (1969)

79. Chuang, T.T. & Dalla Lana, I.G., *Journal of the Chemical Soc., Faraday Transactions I,* **68**, 773 (1972)

80. Fledorow, R. & Dalla Lana, I.G., *The Journal of Physical Chemistry,* **84(21)**, 2779 (1980)

81. Marczewski, M. & Malinowski, S., *Bull. Acad. Polon. Sci., Ser. Sci. Chim.,* **24**, 1 (1976)

82. Paukshits, E.A., Solianov, P.I., Yurchenko, E.N. & Jiratova. K., *Collection Czechoslovak Chem. Commun.,* **47**, 2044 (1982)

83. Huang, C.P. & Stumm, W., *Journal of Colloid and Interface Science,* **43(2)**, 409 (1973)

84. Saad, A.B., Ivanov, V.A. & Lavalley, J.C., *Applied Catalysis A: General,* **94**, 71 (1993)

85. Shen, J., Cotright, R.D., Chen, Y. & Dumesic, J.A., *Journal of Physical Chemistry,* **98(33)**, 8067 (1994)

86. Berteau, P., Kellens, M.A. & Delmon, B., *Journal Chem. Soc., Faraday Transactions,* **87(9)**, 1425 (1991)

87. Malinowski, S., in *Catalysis by Acids and Bases,* (eds. Imelik, C., Naccache, G., Coudurier, Y., Taarit, B., & Verdine, J.C.), Studies in Surface Science and Catalysis, Elsevier Science Publishers B.V., Amsterdam, (1985) p.107

88. Contescu, A., Schramm, C., Sato, R. & Schwartz, J.A., *Journal of Colloid and Interface Science,* **165**, 66 (1994)

89. Corma, A., Fornés, V. & Ortega, E., *Journal of Catalysis,* **92**, 284 (1985)

90. Garbowski, E., Candy, J.P. & Primet, M., *Journal Chem. Soc., Faraday Trans. I.,* **79**, 835 (1983)

91. Basset. J., Mathieu, M.V. & Prettre, M., *Journal Chimical Physics,* **66**, 1264 (1969)

92. Melchor, A., Garbowski, E., Mathieu, M.V. & Primet, M., *Journal Chemical Society, Faraday Transactions I,* **82**, 1893 (1986)

93. Jacimovic, L. J., Stevoic, J. & Veljkovic, S., *The Journal of Physical Chemistry,* **76(24),** 3625 (1972)

94. Williams, K.C., Daniel, J.L., Thomson, W.J., Kaplan, R.I. & Maatman, R.W., *The Journal of Physical Chemistry,* **69(1),** 250 (1965)

95. Boorman, P.M., Kydd, R.A., Sarbak, Z. & Somogyvari, A., *Journal of Catalysis,* **96,** 115 (1985)

96. Malinowski, S. & Marczewski, M., in *Catalysis by Acids and Bases,* (eds. Imelik, C., Naccache, G., Coudurier, Y., Taarit, B. & Verdine, J.C.), Studies in Surface Science and Catalysis, Elsevier Science Publishers B.V., Amsterdam (1985) p.107

97. Wolf, E.E. & Alfani, F., C*atalysis Review, - Science and Engineering,* **24(3),** 329 (1982)

98. Barbier, J., Corro, G. & Zhang, Y., *Applied Catalysis,* **13,** 245 (1985)

99. Baker, R.T.K., Barber, M.A., Harris, P.S., Feates, F.S. & Waite, R.J., *Journal of Catalysis,* **26,** 51 (1972)

100. Walker, P.L., Rakszawski, J.F. & Imperial, G.R., *The Journal of Physical Chemistry,* **63,** 140 (1959)

101. Boehm, H.P., *Carbon,* **11,** 583 (1973)

102. Ruston, W.R., Warzee, M., Hennaut, J. & Watty, J., *Carbon,* **7,** 47 (1969)

103. Derbyshire, F.J., Presland, A.E.B. & Trimm, D.L., *Carbon,* **10,** 114 (1972)

104. Baird, T., Fryer, J.R. & Grant, B., *Carbon,* **12,** 591 (1974)

105. Baker, R.T.K. & Waite, R.J., *Journal of Catalysis,* **37,** 101 (1975)

106. Baird, T., in *Catalysis* **vol. 5.** chapter 5, The Royal Society of Chemistry, London (1981)

107. Rostrup-Nielsen, J. & Trimm, D.L., *Journal of Catalysis,* **48,** 155 (1977)

108. Grenga, H.E. & Lawless, K.R., *Journal of Applied Physics,* **43(4),** 1508 (1972)

109. Massaro, T.A. & Petersen, E.E., *Journal of Applied Physics,* **42(13),** 5534 (1971)

110. Yang, R.T. & Yang, K.L., *Journal of Catalysis,* **93,** 182 (1985)

111. Cooper, B.J. & Trimm, D.L., in *Catalyst Deactivation,* (eds. Delmon, B. & Froment, G.F.), Studies in Surface Science and Catalysis, Elsevier Scientific Publishing Company, Amsterdam (1980) p.63

112. Somorjai, G.A. & Blakely, D.W., *Nature,* **258**, 580 (1975)

113. Rivera-Latas, F.J., Dalla Betta, R.A. & Boudart, M., *AIChE Journal,* **38(5)**, 771 (1992)

114. Alstrup, I. & Rostrup-Nielsen, J.R., *Journal of Catalysis* **100**, 545 (1986)

115. Lobo, L.S. & Trimm, D.L., *Nature, Physical Science,* **234**, 15 (1971)

116. Lobo, L.S. & Trimm, D.L., *Journal of Catalysis,* **29**, 15 (1973)

117. Gavin, D.G., in *Catalysis,* **Vol. 5.,** The Royal Society of Chemistry, Cambridge (1982)

118. Querini, C.A., Figoli, N.S. & Parera, J.M., *Applied Catalysis,* **52**, 249 (1989)

119. Blakely, D.W. & Somorjai, G.A., *Journal of Catalysis,* **42**, 181 (1976)

120. Weinberg, W.H., Deans, H.A. & Merill, R.P., *Surface Science,* **41**, 312 (1974)

121. Brown, A.M., & Hill, M.P., in *Coke Formation on Metal Surfaces,* Chapter 10, (ed. Albright, L.F.) ACS Symposium Series no. 202, American Chem. Soc. Washington D.C., (1982)

122. Figoli, N.S., Beltramini, J.N., Martinelli, E.E. & Parera, J.M., *Journal of Chemical Technology and Biotechnology,* **32**, 445 (1982)

123. Voorhies, A., *Industrial and Engineering Chemistry,* **37(4)**, 318 (1945)

124. Chang, T.S., Rodriguez, N.M. & Baker, R.T.K., *Journal of Catalysis,* **123**, 486 (1990)

125. Trimm, D.L., *Applied Catalysis,* **5**, 263 (1983)

126. Kim, M.S., Rodriguez, N.M. & Baker, R.T.K., *Journal of Catalysis,* **131**, 60 (1991)

127. Nishiyama, Y. & Tami, Y., *Journal of Catalysis,* **45**, 1 (1976)

128. Kim, M.S., Rodriguez, N.M., & Baker, R.T.K., *Journal of Catalysis,* **134**, 253 (1992)

129. Gorriz, O.F., Corberan, V.C. & Fierro, J.L.G., *Industrial and Engineering Chemistry Research,* **31(12)**, 2670 (1992)

130. Billaud, F., Broutin, P., Busson, C. & Gueret, C., *Revue de l'Institut Francais de Pétrole,* **48(2)**, 115 (1993)

131. Scelza, O.A., Baronetti, G.T., de Miguel, S.R., Silber, P. & Costro, A.A., *Journal of Chemical Technology and Biotechnology,* **58**, 135 (1993)

132. Magnoux, P., & Guisnet, M., *Applied Catalysis,* **38**, 341 (1988)

133. Peña, J.A., Monzón, A. & Santamaría, J., *Applied Catalysis A: General*, **101**, 185 (1993)

134. Afonso, J.C., Schmal, M. & Fréty, R., *Fuel Processing Technology*, **41**, 13 (1994)

135. Burch, R., *Journal of Catalysis*, **71**, 348 (1981)

136. Haldeman, R.,G. & Botty, M.C., *The Journal of Physical Chemistry*, **63**, 489 (1959)

137. Barbier, J., Marecot, P., Martin, N., Elassal, L. & Maurel., R., in *Catalyst Deactivation*, (eds. Delmon, B. & Froment, G.F.), Studies in Surface Science and Catalysis, Elsevier Scientific Publishing Company, Amsterdam (1980) p.53

138. Plank, C.J. & Nace, D.M., *Industrial Engineering Chemistry*, **47**, 2374 (1955)

139. Eberly, P.E., Kimberlin, C.N., Miller, W.H. & Drushel, H.V., *Industrial Engineering Chemistry Process Design and Development*, **5**, 193 (1966)

140. Eisenbach, D. & Gallei, E., *Journal of Catalysis*, **56**, 377 (1979)

141. Yan, T.Y. & Rosynek, M.P., in *Coke Formation on Metal Surfaces*, Chapter 14, American Chem. Soc. Washington D.C., (ed. Albright, L.F), A.C.S. Symposium series no.202, (1982)

142. Cabrol, R.A. & Oberlin, A., *Journal of Catalysis*, **89**, 256 (1984)

143. Espinat, D., Dexpert, H., Freund, E. & Martino, G., *Applied Catalysis*, **16**, 343 (1985)

144. Biswas, J., Gray, P.G. & Do, D.D., *Applied Catalysis*, **32**, 249 (1987)

145. Davis, S.M., Zaera, F. & Somorjai, G.A., *Journal of Catalysis*, **77**, 439 (1982)

146. Gallezot, P., Leclercq, C., Barbier, J. & Marecot, P., *Journal of Catalysis*, **116**, 164 (1989)

147. Espinat, D., Freund, E., Dexpert, H. & Martino, G., *Journal of Catalysis*, **126**, 496 (1990)

148. Tracz, E. & Scholz, R., *Applied Catalysis*, **66**, 133 (1990)

149. Basso, T.C., Zhang, Z. & Sachtler, W.M.H., *Applied Catalysis A: General*, **79**, 227 (1991)

150. Fung, S.C. & Querini, C.A., *Journal of Catalysis*, **138**, 240 (1992)

151. Querini, C.A. & Fung, S.C., *Applied Catalysis A: General*, **117**, 53 (1994)

152. Turlier, P., Forissier, M., Rivault, P., Pitault, I. & Bernard, J.R., *Fluid Catalytic Cracking III, Materials and Processes*, **571**, 98 (1994)

153. Marin, G.B., Beckman, J.W. & Froment, C.F., *Journal of Catalysis*, **97**, 416 (1986)

154. Prater, C.D. & Logo, R.M., *Advances in Catalysis*, **8**, 329 (1956)

155. Barbier, J., *Applied Catalysis*, **23**, 225 (1986)

156. Absi-Halabi, M. & Stainislaus, A., *Applied Catalysis*, **72**, 193 (1991)

157. Tiernan, M. & Kriz, J.F., in *Catalyst Deactivation*, (eds. Delman, B. & Froment, G.F.), Studies in Surface Science and Catalysis, Elsevier Scientific Publishing Company, Amsterdam, p.283 (1980)

158. Kooh, A.B., Han, W.-J., Lee, R.G. & Hicks, R.F., *Journal of Catalysis*, **130**, 374 (1991)

159. Ross, J.R.H., in *Catalysis*, **Vol. 4.**, Specialist Periodical Report of the Chemical Society, chapter 2 (1975)

160. Tauster, S.J.& Koros, R.M., *Journal of Catalysis* **27**, 307 (1972)

161. Baker, R.T.K., in *Microstructure and Properties of Catalysts*, (eds. Tracy, M.M.J., Thomas, J.M. & White, J.M.), Materials Research Society, **Vol. III**, p. 41 (1988)

162. Trimm, D.L. & Turner, C.J., *Journal of Chemical Technology and Biotechnology*, **31**, 285 (1981)

163. Marécot, P., Martinez, H. & Barbier, J., *Journal of Catalysis*, **138**, 474 (1992)

164. Papadopoulou, Ch., Matralis, H. & Lycoughiotis, A., *Journal of the Chemical Society, Faraday Transactions*, **89(16)**, 3157 (1993)

165. Olander, D.R. & Balooch, M., *Journal of Catalysis*, **60**, 41 (1979)

166. Ramaswamy, A.V., Ramaswamy, P., Sivasanker, S. & Leonard, A.J., *Proceedings of the 6th International Congress of Catalysis*, **2**, 855 (1977)

167. Dowden, D.A., in *Catalysis*, **Vol. 2.**, Specialist Periodical Reports, The Chemical Society, London, p.1 (1978)

168. Wentrcek, P.W., McCarthy, J.G., Ablow, C.M. & Wise, H., *Journal of Catalysis*, **61**, 232 (1980)

169. Parera, J.M., Figoli, N.S., Jablonski, E.L., Sad, M.R. & Beltramini, J.N., in *Catalyst Deactivation,* (eds. Delmon, B. & Froment, G.F.), Studies in Surface Science and Catalysis, Elsevier, Amsterdam, p. 571 (1980)

170. Parera, J.M., Verderone, R.J., Pieck, C.L. & Traffano, E.M. *Applied Catalysis,* **23**, 15 (1986)

171. Barbier, J., Churin, E. & Marecot, P., *Journal of Catalysis,* **126**, 228 (1990)

172. Querini, C.A. & Fung, S.C., *Journal of Catalysis,* **141**, 389 (1993)

173. Burch, R. & Mitchell, A.J., *Applied Catalysis,* **6**, 121 (1983)

174. Neikam, W.C. & Vannice, M.A., *Journal of Catalysis,* **27**, 207 (1972)

175. Trimm, D.L., *Design of Industrial Catalysts,* Elsevier Scientific, Amsterdam, (1980)

176. Parera, J.M., Figoli, N.S. & Traffano, E.M., *Journal of Catalysis,* **79**, 481 (1983)

177. Holmen, A., & Lindvaag, O.A., in *American Chemical Society Symposium,* series no.202, Albright, L.L.(ed.) , Washington D.C. p.45 (1982)

178. Pieck, C.L., Jablonski, E.L., Verderone, R.J. & Parera, J.M., *Applied Catalysis,* **56**, 1 (1989)

179. Hughes, A.E. & Pratt, K.C., *Applied Catalysis A: General,* **90**, 117 (1992)

180. Borowiecki, T., *Polish Journal of Chemistry,* **67**, 1755 (1993)

181. Dodd, J.W., & Tonga, K.H., *Thermal Methods,* Analytical Chemistry by Open Learning, (ed. Currell, B.R.), Wiley and Sons, p.49 (1987)

182. Lippens, B.C. & Steggerada, J.J., *Physical and Chemical Aspects of Adsorbents and Catalysts,* (ed. Linsen, B.G.), Academic Press, New York, (1970)

183. Morterra, C., Giovanna, G., Garrone, E. & Boccuzzi, F., *Journal of the Chemical Soc., Faraday Transactions I,* **72**, 2722 (1976)

184. Cotton, F.A. & Wilkinson, G., *Advanced Inorganic Chemistry,* Chapter 19, Fifth edition, Wiley-Interscience, New York, (1988)

185. Parera, J.M., Figoli, N.S., Jablonski, E.L., Sad, M.R. & Beltramini, J.N., in *Catalyst Deactivation,* (eds. Delmon, B. & Froment, G.F.), Studies in Surface Science and Catalysis, Elsevier Scientific Publishing, Amsterdam, p. 571(1980)

186. Dautzenberg, F.M., Helle, J.N., Biloen, P. & Sachtler, W.M.H., *Journal of Catalysis*, **63**, 119 (1980)

187. Meitzner, G., Via, G., Lytle, F.W., Fung, S.C. & Sinfelt, J., *Journal of Physical Chemistry*, **92**, 2925 (1988)

188. Baronetti, G.T., de Miguel, S.R., Scelza, O.A., Fritzler, M.A. & Castro, A.A., *Applied Catalysis*, **19**, 77 (1985)

189. Srinivasan, R., Rice, L.A. & Davis, G.H., *Journal of Catalysis*, **129**, 257 (1991)

190. Gates, B.C., Katzer, J.R. & Schuit, G.C.A., *Chemistry of Catalytic Processes*, McGraw-Hill, New York, p.259 (1979)

191. Summers, J.C. & Ausen, S.A., *Journal of Catalysis*, **58**, 131 (1979)

192. Su, E.C., Montreuil, C.N. & Rothschild, W.G., *Applied Catalysis*, **17**, 75 (1985)

193. Adamson, A.W., *A Textbook of Physical Chemistry*, Academic Press, New York, 2nd edition (1979)

194. Bond, G.C. & Hui, L., *Journal of Catalysis*, **147**, 346 (1994)

195. Baldwin, T.R. & Burch, R., *Applied Catalysis*, **66**, 359 (1990)

196. Augustine, S.M., Adameddin, G.N. & Sachtler, W.M.H., *Journal of Catalysis*, **115**, 217 (1989)

197. Christian, G.D., *Analytical Chemistry*, Wiley, New York, 3rd edition (1980)

198. Escandon Chantres, M., *M.Sc. Disertation*, Dublin City University, (1992)

199. Determination of alkaloids in tobacco by potentiometric and conductimetric non-aqueous titrations, in *Third year analytical science laboratory manual*, Dublin City University.

200. *United Stated Pharmacopoeia*, Twentieth revision, p.1111 (1979)

201. *United Stated Pharmacopoeia*, Twentieth revision, pp.929–931 (1979)

202. *United Stated Pharmacopoeia*, Twentieth revision, p. 1054 (1979)

203. Gens, J.W. & van Veen, J.A.R. in *Catalysis*, (eds. Moulijn, J.A., van Leeuwen, P.W.N.M. & van Santen, R.A.), Studies in Surface Science and Catalysis, Elsevier Scientific Publishing, Amsterdam, **Vol. 79**, chapter 9 (1993)

204. Garbowski, E. & Primet, M., *Journal of the Chemical Society, Faraday Transactions I*, **83**, 1469 (1983)

205. Anderson, J.R. & Pratt, K.C., *Introduction to Characterisation and Testing of Catalysts,* Academic Press, Australia (1985)

206. Scholten, J.J.F., Pÿpers, A.P. & Hustings, A.M.L., *Catalysis Reviews - Science and Engineering,* **27(1),** 151 (1985)

207. Scholten, J.J.F., in *Catalysis,* Moulijn, J.A. van Leeuwen, P.W.N.M. & van Santen, R.A. (eds.), Studies in Surface Science and Catalysis, **Vol. 79,** Elsevier, Amsterdam, pp. 419–438 (1993)

208. Curley, J.W., *Oxidation Studies on Supported Metal Catalysts,* Ph.D. Thesis, Dublin City University, March 1995.

209. Hanby, V.I., *Combustion and Pollution Control in Heating Systems,* Springer-Velay London Ltd. (1994)

210. Zwinkels, M.F.M., Järås, S.G. & Menton, P.G., *Catalyst Reviews - Science and Engineering,* **35(3),** 319 (1993)

211. Trimm, D.L., *Applied Catalysis,* **7,** 249 (1983)

212. Prasad, R., Kennedy, L.A. & Ruckenstein, E., *Catalyst Reviews - Science and Engineering,* **26(1),** 1 (1994)

213. Spivey, J.J., in *Catalysis,* **(vol. 8)** chapter 5, A Specialist Periodical Report, Royal Society of Chemistry, Cambridge (1989)

214. Cullis, C.F. & Willatt, B.M., *Journal of Catalysis,* **83,** 267 (1983)

215. Volter, J., Lietz, G., Spindler, H. & Lieske, H., *Journal of Catalysis,* **104,** 375 (1987)

216. Arakawa, T., Tsuchi-Ya, S. & Schiokawa, J., *Journal of Catalysis,* **74,** 317 (1982)

217. Moro-oka, Y. & Ozaki, A., *Journal of Catalysis,* **5,** 116 (1966)

218. Moro-oka, Y., Morikakawa, K. & Ozaki, A., *Journal of Catalysis,* **7,** 23 (1967)

219. Bond, G.C., *Heterogeneous Catalysis : Principles & Applications,* Clarendon Press, Oxford (1979)

220. Fierro, J.L.G. & de la Banda, J.F.G., *Catalysis Reviews - Science & Engineering,* **28(2,3),** 310 (1986)

221. Pearce, R. & Patterson, W.R., *Catalysis and Chemical Processes,* Wiley, J., New York, (1981)

222. Margolis, L.Ya., *Catalysis Reviews - Science & Egineering,* **8(2)**,241(1973)

223. Simons, T.G.J., Verhijen, E.J.M., Batist, P.A. & Schuit, G.C.A., *Advanced Chemistry Series,* no. 76, p.261 (1968)

224. Radcliffe, S.W. & Hickman, R.G., *Journal of the Institute of Fuel,* December, 228 (1975)

225. Trimm, D.L. & Lam, C.-W., *Chemical Engineering Science,* **35**, 1405 (1980)

226. Dongworth, M.R., & Melvin, A., in *Proceedings of the 16th International Symposium on Combustion,* p.225 (1977)

227. French standard NF D35-352 (February 1969)

228. Trimm, D.L. & Lam, C.-W., *Chemical Engineering Science,* **35**, 1731 (1980)

229. Krill, W.V., Kesselring, J.P., Chu, E.K. & Kendall, R.M., *Mechanical Engineering,* **28**, 102 (1980)

230. Cravill, J., *Mechanical Engineers Data Handbook,* Butterworth–Heinemann Ltd., Oxford (1983)

231. Powder Diffraction Files (1987), International Centre for Diffraction Data, Inorganic phases

Appendices

Appendix I

Calculation for percentage carbon content

Let

Peak area = 1500 units^2

Wt. sample = 0.3000g

From Graph 2.2, $Y = 1.1099X$

$\Rightarrow$ For $Y = 1500$, $X = 1352$

$\therefore$ 1500 units $\equiv$ 1352 µl CO_2

1 mole CO_2 gas @STP $\equiv$ 22.414L

$\Rightarrow$ 1352µL $CO_2 = \dfrac{1352 \times 10^{-6}\,L}{22.414\,L/mole} = 6.04 \times 10^{-5}\,moles$

Molecular Wt. CO_2 = 44.01g/mol.

$\Rightarrow 6.04 \times 10^{-5}$ moles $CO_2 = 2.66 \times 10^{-3}$g

Weight of which is carbon

$$\frac{2.66 \times 10^{-3}\,g \times 12.01g}{44.01g} = 7.25 \times 10^{-4}\,g$$

$$\% \text{ C} = \frac{7.25 \times 10^{-4}\,g}{0.3000g} \times 100\%$$

$$= \underline{0.24\%}$$

Appendix II

Calculation of Pt surface area and dispersion from H_2 chemisorption measurement.

Using the following equations and assuming that one hydrogen atom is adsorbed by each surface Pt atom it is possible to calculate free metal surface area and percentage metal dispersion. It is also necessary to assume the number of Pt surface atoms per unit of the polycrystalline surface being investigated. If the surface consists of equal proportions of (111), (110) and (100) planes then there are 1.25×10^{19} Pt atoms per m^2 [205,206]. Scholten et al. [206] have postulated that the morphology of face-centred cubic metals of small crystalline size corresponds to the exposure of 70% (111) planes, 25% (100) planes and 5% (110) planes. This would result in 1.42×10^{19} Pt surface atoms per m^2 of the polycrystalline surface. In this study a value of 1.25×10^{19} Pt atoms per m^2 was assumed for calculation of Pt surface areas.

Pt Surface Area

The Pt surface area was calculated using the relationship

$$S_{P_t} = \frac{n_m . x_m . A}{n_s} \qquad \{1\}$$

where

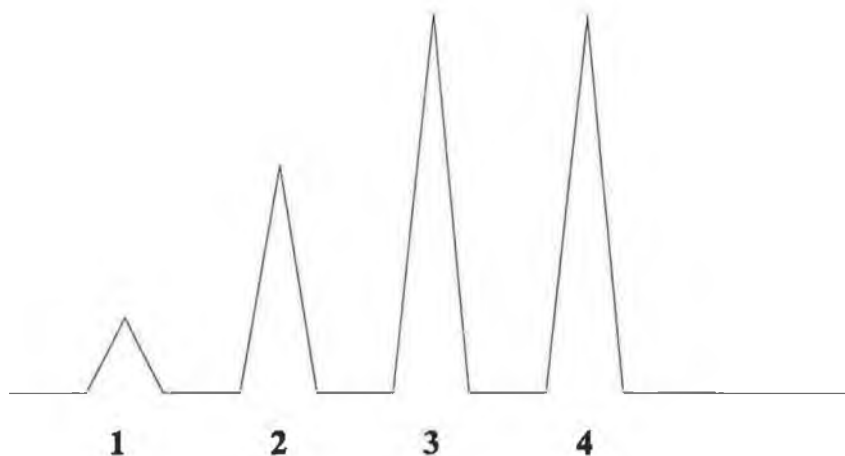$\quad S_{Pt}$: Pt surface area

$\quad n_m$: Number of moles of H_2 adsorbed

$\quad x_m$: Average number of surface Pt atoms associated with
$\qquad$ adsorption of each molecule of H_2 i.e. $x_m = 2$

$\quad A$: Avagado's number $= 6.023 \times 10^{23}$ atoms/mole of Pt

$\quad n_s$: Number of Pt atoms per unit area of surface $=$
$\qquad 1.25 \times 10^{19}$ atoms/m^2

In order to calculate n_m, the volume of H_2 adsorbed i.e. V_{ads} must firstly be calculated.

Typical chemisorb Trace

$$V_{ads}(cm^3) = \left[\frac{I.L.V. \times (Area3 - Area1)}{Area3}\right] + \left[\frac{I.L.V. \times (Area3 - Area2)}{Area3}\right] \quad \{2\}$$

where

     I.L.V. = Injection loop volume, i.e. $(0.050cm^3)$

As the measurements were performed at room temperature and pressure,

$$V_{ads}\, g^{-1} \text{ s.t.p. } (cm^3 g^{-1}) = \left(\frac{V_{ads}}{W}\right) \times \left(\frac{273}{RT}\right) \times \left(\frac{R.P.}{760}\right) \quad \{3\}$$

where

     $V_{ads}\, g^{-1}$ stp $(cm^3 g^{-1})$: Volume of H_2 adsorbed per gram of catalyst sample at standard temperature & pressure

     W   : Final sample weight (g)

     R.T.   : Room temperature (K)

     R.P.   : Atmospheric pressure (mmHg)

The number of moles of H_2 adsorbed, n_m, is then given by

$$n_m \text{ (moles/g)} = \frac{V_{ads}g^{-1}stp}{22414} \qquad \{4\}$$

where

$22414 cm^3$ = volume occupied by one mole of gas at s.t.p.

Substituting for n_m into equation $\{1\}$ yields

$$S_{Pt} \text{ (m}^2 \text{ Pt/g catalyst)} = \left(\frac{V_{ads} \, g^{-1} stp}{22414} \right) \times \left(\frac{2 \times 6.023 \times 10^{23}}{1.25 \times 10^{19}} \right) \qquad \{5\}$$

Equation 5 was used to calculate the Pt surface areas in this study

Percentage dispersion

The state of subdivision of a supported metal catalyst is often defined in terms of the ratio between number of surface metal atoms and the total number of metal atoms present. This is referred to as metal dispersion (DM)

$$D_m = \frac{Pt_s}{Pt_t} \qquad \{6\}$$

$$\% D_m = \left[\frac{Pt_s}{Pt_t} \right] \times 100 \qquad \{7\}$$

where

Pt_S = number of Pt surface atoms

Pt_t = total number of Pt atoms present

Using the relationship described above, Pt_S can be calculated as follows

$$Pt_S \text{ (atoms/g catalyst)} = \left(\frac{V_{ads}g^{-1}stp}{22414} \right) \cdot X_m \cdot A$$

$$= \frac{V_{ads}g^{-1}stp \times 2 \times 6.023 \times 10^{23}}{22414} \qquad \{8\}$$

247

The number of grams of Pt per gram of catalyst is given by

$$\left(\frac{1g}{100}\right) \times \% Pt \qquad \{9\}$$

The number of Pt atoms in one gram of Pt is equal to,

$$= \frac{6.023 \times 10^{23}}{M} \qquad \{10\}$$

where

$$M \;=\; \text{molecular weight of Pt} \;=\; 195.09 g/mole$$

Combining {9} and {10} gives

$$Pt_t \text{ (atoms/g catalyst)} \;=\; (0.01 \times \% Pt) \cdot \left(\frac{6.023 \times 10^{23}}{195.09}\right) \qquad \{11\}$$

Substituting for Pt_t and Pt_S into equation {7} yields

$$\% D_m = \left(\frac{V_{ads}\, g^{-1} stp \times 2 \times 6.023 \times 10^{23}}{22414}\right) \cdot \left(\frac{0.01 \times \% Pt \times 6.023 \times 10^{23}}{195.09}\right) \times 100 \quad \{12\}$$

Equation {12} was used to calculate the dispersion of Pt in catalyst samples

Appendix III

Calculation of amount C that can theoretically be removed in one minute, using the TPO unit.

Flow rate of air over catalyst = 24 cm^3/min

$$\text{Vol. } O_2 \text{ flowing over catalyst} = \frac{24\text{cm}^3 \times 20\%}{100\%}$$

$$= 4.8 \text{ cm}^3/\text{min.}$$

$$\text{No. moles } O_2 = \frac{4.8\text{cm}^3}{22.414\text{cm}^3} = 0.0002 \text{ mol/min}$$

$$C + O_2 \rightarrow CO_2$$
$$1 \ : \ 1 \ : \ 1$$
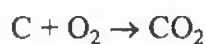
$\therefore$ possible to form 0.0002 mols CO_2

No. grams C in 0.0002 mols CO_2

$$= 0.0024\text{g}$$

Sample weights used were 0.3005g ($\pm$0.0005g)

$$\% \text{ C removable in one min} = \frac{0.0024 \times 100\%}{0.3005g}$$

$$= \underline{0.81\%}$$

Worked example for calculation of end-point from data obtained during a potentiometric titration.

In this example the data accumulated during a typical potentiometric titrations is analysed to show how using *Excel 5.0* the end-point was calculated. The titration consisted of adding $10.00cm^3$ of titrant in $1.00cm^3$ increments and taking the potential reading two minutes after each addition.

| Col. 1	Col. 2	Col. 3	Col. 4	Col. 5	Col. 6`
Vol.(cm^3)	E.(mV)	$V_{av}1$	dE/dV	$V_{av}2$	d^2E/d^2V
0.00	513	0.5	2	1	8
1.00	511	1.5	10	2	7
2.00	501	2.5	17	3	43
3.00	484	3.5	60	4	71
4.00	424	4.5	131	5	-101
5.00	293	5.5	30	6	-15
6.00	263	6.5	15	7	-4
7.00	248	7.5	11	8	-3
8.00	237	8.5	8	9	-3
9.00	229	9.5	5		
10.00	224				

Column one shows the volume of titrant used while the corresponding potential is given in column 2. Plotting Col. 2 vs Col. 1 gives the typical sigmoid shaped graph as shown in graph I. From this it can be seen that the end-point is around $4cm^3$ but it is not possible to determine it accurately.

To improve on this it is necessary to plot dE/dV vs the average volume (V_{av}) [197]. To determine V_{av} the first volume was subtracted from the second and then divided by two with the result being placed in Col. 3. This process was continued down through Col. 1 with the results of the calculations being placed in Col. 3. In the case of potential readings, each value was subtracted from the one above it and the results tabulated in Col. 4. Plotting Col. 4 vs Col. 3 produced graph II where the end-point is calculated by bringing a line from the peak-max. perpendicular to the x-axis and then noting where the line cuts the x-axis.

Graph I   Graph of E vs Vol.
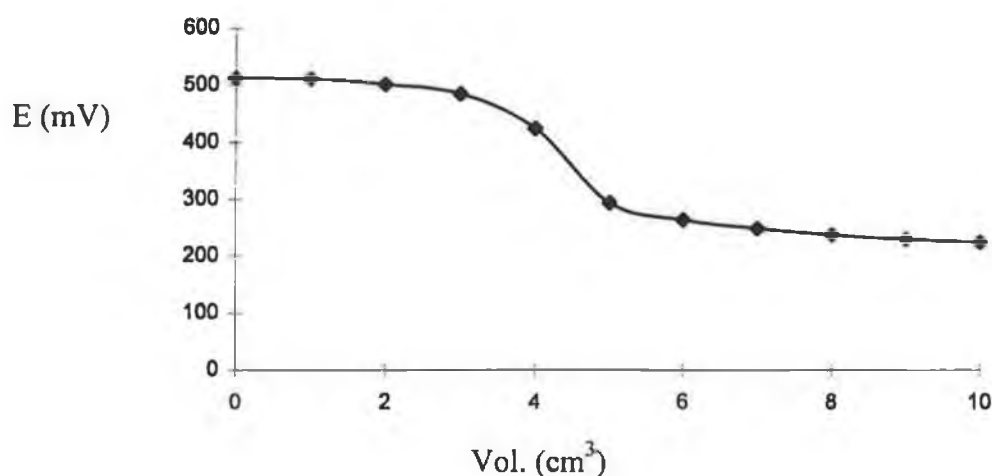
Graph II   Graph of dE/dV vs $V_{av}1$

251
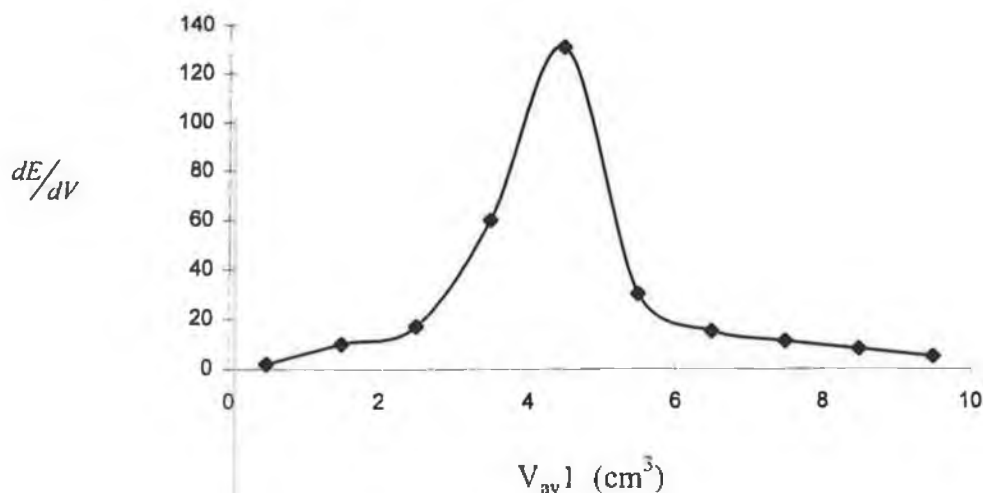
The accuracy in determining end-point can be further improved by plotting a second derivative of the data in Cols. 1 and 2. This requires calculating average volumes from the figures in Col. 3. The first volume was subtracted from the second and the value obtained tabulated in Col. 5. This was continued down through the figures in Col. 3. With regard to potential values in col. 4, each one was subtracted from the one below it and the values tabulated in Col. 6. When the data in Col. 6 is plotted against that in Col. 5 the end-point can easily be determined from where the graph cuts the x-axis as shown in graph III.

Graph III *Graph of $\dfrac{d^2 E}{d^2 V}$ vs $V_{av}2$*

$V_{av}2$
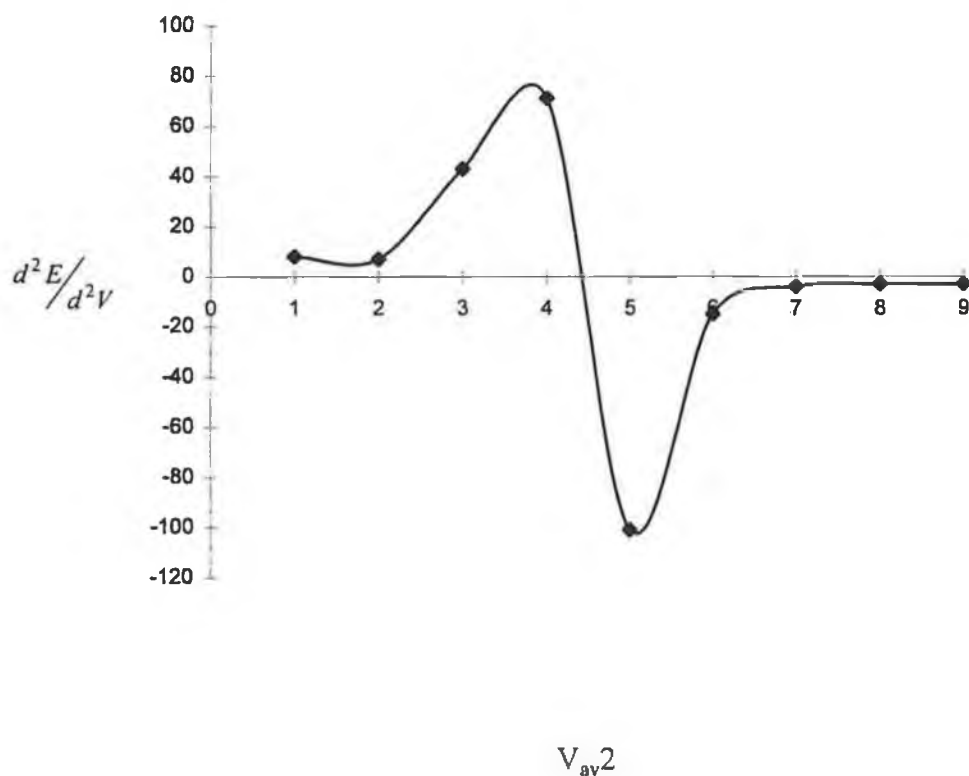
Appendix V

Basis of surface area determination by N_2 physisorption.

The BET equation describes the physical adsorption of a gas on a solid surface. One form of the BET equation is

$$\frac{\left(P/P_0\right)}{V\left[1-\left(P/P_0\right)\right]} = \left[\frac{1}{(V_m C)}\right] + \left[\frac{(C-1)}{V_m C}\right] \times P/P_0 \qquad \{1\}$$

where

    V : volume of gas adsorbed at STP

    P : gas pressure

    P_0 : saturated vapour pressure of liquefied gas at the adsorbing temperature

    V_m : volume of gas (@ stp) required to form an adsorbed monolayer

    C : a constant related to the energy of adsorption

The surface area, S, of a sample which has a monolayer of adsorbed gas of volume, V_m, can be calculated from

$$S = \frac{V_m\, A\, N}{M} \qquad \{2\}$$

where

    A : Avagado's number = 6.023×10^{23} molecules/mole of gas.

    N : area of each adsorbed gas molecule = 16.2×10^{-20} m^2/molecule for N_2

    M : molar volume of gas = 22414

Multipoint surface area determination

From equation 1, it can be seen that by plotting values for $\left(P/P_0\right)/ V\left[1-\left(P/P_0\right)\right]$ on the ordinate against P/P_0 on the abscissa, the slope and intercept

of the resulting straight line, gives values for $(C-1)/(V_mC)$ and $1/(V_mC)$ respectively. The surface area, S_1, can be obtained using equation {2}

$$S_1 = \frac{6.023 \times 10^{23} \times 16.2 \times 10^{-20}}{22414 \times (\text{slope} + \text{intercept})}$$

This allows multipoint surface area determination from physisorption data.

Single point surface area determination

Work done previously in this laboratory has shown that single point physisorption measurements give results for surface area that are in good agreement with values obtained by multipoint measurements [208]. Since the single point procedure is much less laborious, it was employed for surface area determination in this study.

The constant C in equation 1 is typically a relatively large number, i.e. $C \gg 1$: using this assumption equation 1 approximates to :

$$\frac{\left(P/P_0\right)}{V\left[1-\left(P/P_0\right)\right]} = \left(1/V_m\right) \cdot \left[\left(1/C\right) + \left(P/P_0\right)\right]$$

If $P/P_0 \gg 1/C$, this equation reduces to :

$$\frac{\left(P/P_0\right)}{V\left[1-\left(P/P_0\right)\right]} = \left(1/V_m\right) \cdot \left(P/P_0\right)$$

Rearranging for V_m leads to :

$$V_m = V\left[1 - \left(\frac{P}{P_0}\right)\right]$$

Substituting this equation for V_m into equation {2} leads to

$$S = \frac{V\,A\,N\left[1 - \left(\frac{P}{P_0}\right)\right]}{M}$$

Taking into account standard temperature and pressure, the surface area of a given volume of N_2, V, can be calculated as follows

$$S = \frac{V \times 273.2 \times Atm.\ Pres. \times 6.023 \times 10^{23} \times 16.2 \times 10^{-20} \times \left[1 - \%N_2 / 100\right]}{Room\ temp \times 760 \times 22414 \times standard\ pressure}$$

$$= V \times \textbf{constant}$$

Appendix VI

(A) Calculation of Brönsted basic site concentration [B.B.S.] from data obtained using the procedure outlined in section 3.1.1.

$$[\text{Brönsted basic sites}] = \frac{\text{End} - \text{point} \times \text{molarity of perchloric acid}}{1000 \text{cm}^3}$$

$$[\textbf{B.B.S.}]/\textbf{g} = \frac{[\text{B.B.S.}]}{\text{Wt. sample}}$$

$$[\textbf{B.B.S.}]/\textbf{m}^2 = \frac{[\text{B.B.S.}]/\text{g}}{\text{Surface area of sample}}$$

(B) Calculation of Brönsted basic site concentration from data obtained using the procedure outlined in section 3.1.2.

$$[\text{B.B.S.}] = \frac{(\textit{Blank end point} - \textit{End point}) \times \textit{molarity of } n-\textit{butylamine}}{1000 cm^3}$$

$$[\textbf{B.B.S.}]/\textbf{g} = \frac{[\text{B.B.S.}]}{\text{Wt. sample}}$$

$$[\textbf{B.B.S.}]/\textbf{m}^2 = \frac{[\text{B.B.S.}]/\text{g}}{\text{sample surface area}}$$

(C) Calculation of <u>acid site concentration</u> [A.S.] from data obtained using the procedure outlined in section 3.1.4.

$$[A.S.] = \frac{(Blank\ end\ point - End\ point) \times molarity\ of\ perchloric\ acid}{1000cm^3}$$

$$[A.S.]/g = \frac{[B.B.S.]}{Wt.\ sample}$$

$$[A.S.]/m^2 = \frac{[B.B.S.]/g}{sample\ surface\ area}$$

Appendix VII

Calculations to determine power rating of electrical heat exchanger.

Resistance of heating coil $=$ 54Ω

Power supply $=$ 220V (A.C.)

$$\frac{V}{I} = R \quad \text{(Ohm's law)}$$

where

V : voltage

I : current

R : resistance

$$\Rightarrow \quad I = \frac{V}{R} = \frac{220V}{54\Omega}$$

$$= 4.07 \text{ Amps.}$$

$$H = I^2 R T$$

where

H : heat (watts)

I : current (amps)

R : resistance (ohms)

T : time (seconds)
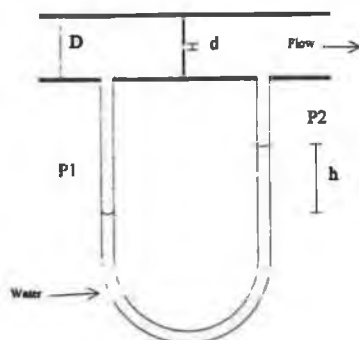
V : voltage (volts)

(For 1 kilowatt hour (kWhr))

$$H = (4.07)^2 \, 54 \, (60)^2$$

$$= 3110400J \qquad (1 \text{ kWhr} = 3.6 \times 10^6 J)$$

$$\Rightarrow \text{Rating} = \underline{0.893 \text{ kW}}$$

Appendix VIII

Calculation of gas flow rate for Catalytic Heat Exchanger.

Diagram of Orifice Meter

Formula for flow rate

$$\text{Flow rate } Q \;=\; C_d \; E \; \frac{\Pi d^2}{4} \sqrt{\frac{2(P_1 - P)}{\rho}}$$

$$\text{Approach factor } E \;=\; \frac{1}{\sqrt{1 - \left(\dfrac{d}{D}\right)^4}}$$

$$(P_1 - P_2) \;=\; (\rho_m - \rho) g \, h$$

where

D : pipe diameter

d : throat diameter

ρ : fluid density

ρ_m : density of manometer fluid

P_1 : upstream pressure

P : throat pressure

C_d : coefficient of discharge

h : manometer reading

Note : For the type of orifice meter used in this work $C_d = 0.60$ *[Ref. 230]*

259

Appendix IX

Calculation of heat output from combustion of iso-butane

Note : It is assumed for this calculation that all of the iso-butane is totally combusted in the catalytic heat exchanger..

358 cm^3/min i–C$_4$H$_{10}$ = 21,400cm^3/hr.

1 mole i–C$_4$H$_{10}$ = 22,400cm^3 at S.T.P.

$$\Rightarrow \frac{21,400\text{cm}^3 \,/\, \text{hr}}{22,400\text{cm}^3 \,/\, \text{mol}} = 0.955\text{mol/hr.}$$

ΔH_c^0 (i–C$_4$H$_{10}$) = -2878 kJ/mol

$\Rightarrow$ 2878 kJ/mol × 0.955 mol/hr = 2748.5 kJ/hr

1 kWhr = 3.6×10^{6}J

$$\Rightarrow \text{Heat output} = \frac{2.7485 \times 10^6 \, J}{3.6 \times 10^6 \, J}$$

$$= \underline{0.764 \text{ kW}}$$

Appendix X

Calculation of heat radiated from a body to surroundings

$$q = \sigma e_1 \left(T_1^4 - T_2^4 \right) A_1 \qquad \text{[Ref. 230]}$$

where

q : radiated energy flow (watts)

T_1 : temperature of radiating body (K)

T_2 : temperature of surroundings (K)

A_1 : area of radiating body (m^2)

e_1 : emissivity of radiating body

σ : Stefan-Boltzmann constant

$(= 5.67 \times 10^{-8} \text{ Wm}^{-2}\text{K}^{-4})$

Note : For the purpose of this calculation the room-temperature i.e. T_2 was taken
to be 20°C (293K)

Emissivity of copper surface (oxidised)

$0 - 50°C$: 0.87

$250°C$: 0.083

Note : Emissivity value of copper used in this calculation was 0.85
(i.e. average of above values).